LEABHARLANN CHOLÁISTE NA TRÍONÓIDE, BAILE ÁTHA CLIATH | TRINITY COLLEGE LIBRARY DUBLIN
Ollscoil Átha Cliath | The University of Dublin

Terms and Conditions of Use of Digitised Theses from Trinity College Library Dublin

Copyright statement

All material supplied by Trinity College Library is protected by copyright (under the Copyright and Related Rights Act, 2000 as amended) and other relevant Intellectual Property Rights. By accessing and using a Digitised Thesis from Trinity College Library you acknowledge that all Intellectual Property Rights in any Works supplied are the sole and exclusive property of the copyright and/or other IPR holder. Specific copyright holders may not be explicitly identified. Use of materials from other sources within a thesis should not be construed as a claim over them.

A non-exclusive, non-transferable licence is hereby granted to those using or reproducing, in whole or in part, the material for valid purposes, providing the copyright owners are acknowledged using the normal conventions. Where specific permission to use material is required, this is identified and such permission must be sought from the copyright holder or agency cited.

Liability statement

By using a Digitised Thesis, I accept that Trinity College Dublin bears no legal responsibility for the accuracy, legality or comprehensiveness of materials contained within the thesis, and that Trinity College Dublin accepts no liability for indirect, consequential, or incidental, damages or losses arising from use of the thesis for whatever reason. Information located in a thesis may be subject to specific use constraints, details of which may not be explicitly described. It is the responsibility of potential and actual users to be aware of such constraints and to abide by them. By making use of material from a digitised thesis, you accept these copyright and disclaimer provisions. Where it is brought to the attention of Trinity College Library that there may be a breach of copyright or other restraint, it is the policy to withdraw or take down access to a thesis while the issue is being resolved.

Access Agreement

By using a Digitised Thesis from Trinity College Library you are bound by the following Terms & Conditions. Please read them carefully.

I have read and I understand the following statement: All material supplied via a Digitised Thesis from Trinity College Library is protected by copyright and other intellectual property rights, and duplication or sale of all or part of any of a thesis is not permitted, except that material may be duplicated by you for your research use or for educational purposes in electronic or print form providing the copyright owners are acknowledged using the normal conventions. You must obtain permission for any other use. Electronic or print copies may not be offered, whether for sale or otherwise to anyone. This copy has been supplied on the understanding that it is copyright material and that no quotation from the thesis may be published without proper acknowledgement.

Trinity College Dublin
Coláiste na Tríonóide, Baile Átha Cliath
The University of Dublin

The role of phagocytosis and circadian entrainment in regulating innate immunity

Sarah Sofia Geiger

M. Sc.

Under the supervision of Prof. Luke O'Neill Ph.D. (Trinity College Dublin)
and Dr. Richard Siegel MD, Ph.D. (National Institutes of Health)
on the NIH-Wellcome Trust Ph.D. Programme

THESIS

11388

A dissertation submitted to the University of Dublin for the degree of Doctor of Philosophy

December, 2016

TRINITY COLLEGE DUBLIN
10 MAY 2017
ACADEMIC REGISTRY

50735191
5073519 1

PhD
BIOCHEMISTRY
& IMMUNOLOGY

TRINITY LIBRARY
0 8 AUG 2017
DUBLIN

Thesis 11388

Declaration

The University of Dublin

School of Biochemistry and Immunology

I declare that this thesis has not been submitted as an exercise for a degree at this or any other university and it is entirely my own work.

I agree to deposit this thesis in the University's open access institutional repository or allow the library to do so on my behalf, subject to Irish Copyright Legislation and Trinity College Library conditions of use and acknowledgement.

I declare that parts of this work have been previously published in Immunology, 2016, "Chrono-Immunology: progress and challenges in understanding links between the circadian and immune systems" by Geiger, Fagundes and Siegel.

Dublin, 21.12.20

Sarah Sofia Geig

Abstract

Lifestyles in wide parts of the world have changed. Exposure to artificial light at night, intermittent meals, night-/ shift-work is part of the everyday life for many people, leading to chronic disruption of their internal 24h timing system, the circadian clock. Only now are we beginning to understand the consequences circadian disruption may have on health and wellbeing. Obesity, cancer and incidences of other inflammatory and metabolic diseases have equally increased and association with circadian disruption has been made. Besides chronic diseases, daily rhythms in acute inflammation following an infection have been observed in mice. The integration of the immune and the circadian system has been the focus of many studies, and although much progress has been made, our understanding is still lacking. In the course of this study we investigated two aspects of daily oscillations in the immune response in mouse models. In a first project the diurnal nature of phagocytosis of bacterial particles by macrophages was tested in an *in vivo* and *ex vivo* system. While cells harvested from the animal at the beginning of the active phase displayed increased uptake - correlating to the time of enhanced inflammatory response - this effect was not recapitulated *in vivo*. In a second project a more fundamental aspect of the origin of rhythmic susceptibility to endotoxin challenge was addressed. Circadian research often focuses on the role of light, as the strongest signal known to influence the circadian system. In the present work we provide evidence that circadian oscillations in food intake, govern susceptibility to the lethal effects of bacterial LPS. While the mechanisms underlying food-entrained oscillations in innate immunity have not yet been fully unravelled, we substantiate a central role for the liver and possibly fluctuations in metabolism in this phenotype. This work describes a previously unknown level of regulation and will help to improve our understanding of the crosstalk between the circadian and the immune systems. These studies may allow new opportunities to manipulate the clock to manage and treat inflammatory diseases in individuals at risk.

Acknowledgements

There are many people that affected me personally and scientifically over the past years. It's hard to put down in words what every single one meant to me on one little piece of paper, and I can only acknowledge a tiny aspect here, but I'm sure everyone knows the impact they had on me.

My supervisors, Luke and Richard, as different as you two are, you both taught me a great deal about what kind of scientist I can be, and want to be. I thank you both for giving me the opportunity to work in your labs and be part of this wonderful Wellcome Trust/NIH Ph.D. programme. I certainly grew as a person and as a scientist in this time.

Annie, who introduced me to the circadian world, and who helped me along the way in many ways. I wouldn't have applied for the Wellcome fellowship if it wasn't for you.

Nathan, for always offering a hand when I was doing crazy 32 h experiments with only 1 h of nap time at 04:00 in the morning. For staying up to help me process organs in the middle of the night, and for helping me change cages every 12 h. You were a great help in an intense project.

John, for being the best lab mate and pub partner/chatter box; Paulina, for giving me a place to stay, and for always having a sympathetic ear; Mustafa, for just being the way you are; Moritz for handing in this thesis for me; Taylor, for helping with some big experiments and for not complaining about gross tasks; Franzi and Jürgen for bringing a bit of home to the US and for being the most fun couple to spend time with; Alejandro, the only other scientist that comes to the lab at 7AM, for being an excellent sweets supplier. Sinead, Arianne, Caio, Tom, Lia, Anthony, Alex, Nick F, Fei, Kelly, Claudia, Francoise, Johnny, Erika, Stacy, Michelle, Beth, Evanna, Nick B, Gilly, Raquel, Niamh, Sylvia, Danny, Eva, Anne, Kathy, Cait, Becca, Dympna, Xu, really everyone on the 4th floor in TBSI and the 13th floor NIAMS people, you all helped me in one way or another and it was a privilege to work with you.

The Wellcome Trust gang for being a blast! I will miss you guys a lot!

I also want to thank my family for always having my back, and last but most importantly, Christian, my husband, who supports me every single day in all kinds of ways. Who agreed to move every two years, who constantly had to listen to the bureaucratic madness of animal research committees that I had to continuously deal with (which also almost made me lose my sanity), and who gave me strength whenever I struggled.

I am fortunate to know all of you, and I'm happy to say that I found good friends along the way.

Index

Declaration I
Abstract II
Acknowledgements III
Index IV
Table of Figures VIII
Abbreviations XIII
1 Introduction 1
1.1 Immunology 2
1.1.1 Adaptive and Innate Immunity 2
1.1.2 Macrophages 3
1.1.3 Cytokine Response 4
1.1.4 Sepsis 6
1.1.5 Uptake of Extracellular Material 7
1.1.5.1 Efferocytosis 8
1.1.5.2 Endocytosis 9
1.1.5.3 Phagocytosis 9
1.1.5.4 Macropinocytosis 9
1.1.5.5 Autophagy 9
1.1.6 Immuno-Metabolism 10
1.2 The Circadian Clock 12
1.2.1 The Circuitry of the Mammalian Circadian Clock 12
1.2.2 The Clock at the Molecular Level 14
1.3 Chrono-Immunology 17
1.3.1 "Sleep will Heal": Immunological Memory and Immune Activity during Sleep 17
1.3.2 Rhythmic Cytokine Production and Cytotoxic Activities 19
1.3.3 Shift work 25
1.4 The Role of Chrono-Nutrition 27
1.5 Research Models used Throughout our Studies 32
1.5.1 Serum Shock 32
1.5.2 Entrainment 32

1.5.3 Selection of Time Points 35
1.5.4 Models of Lethality 36
1.6 Aims 37
2 Materials and Methods 39
2.1 Mice 39
2.1.1 Bmal1 LyzM-Cre colony 39
2.1.2 Cd36 knockout colony 39
2.1.3 WT C57bl6/J mice 39
2.2 Animal entrainment schedules and *in vivo* protocols 39
2.2.1 General animal holding 39
2.2.2 Time restricted feeding (TRF) 40
2.2.3 Time restricted feeding in Constant light 41
2.2.4 LPS mortality 41
2.2.5 CLAMS, Comprehensive Lab Animal Monitoring System 44
2.3 Primary cell isolation and cell culture 44
2.3.1 Peritoneal lavage 44
2.3.2 Magnetic Purification of Peritoneal Macrophages 44
2.3.3 Bone marrow derived macrophages 45
2.3.4 L929 conditioned medium 46
2.3.5 Immortalized BMDMs 46
2.3.6 Serum Shock 46
2.4 Uptake protocols 46
2.4.1 *In vivo* uptake 46
2.4.2 *Ex vivo* uptake 47
2.4.3 Colony Formation Assay 47
2.4.4 *E. coli* culture for uptake studies with living bacteria 48
2.4.5 Phagocytic Index 49
2.5 Fluorescence measurement 49
2.5.1 Flow cytometry 49
2.5.2 Fluorescence plate reader 51
2.5.3 Confocal microscopy 52
2.5.4 FACS purification 52
2.6 RNA protocols 52

2.6.1 RNAlater 52
2.6.2 TRIzol isolation 52
2.6.3 RNeasy Mini Kit 53
2.6.4 Reverse Transcription PCR (RT-PCR) 54
2.6.5 qPCR 55
2.6.6 NanoString 55
2.6.7 RT^2 Profiler Plates 56
2.6.8 Quantification via Nanodrop 57
2.7 Other protocols 57
2.7.1 Genotyping 57
2.7.2 Cytokine measurement 60
2.7.3 Corticosterone measurement 61
2.7.4 Beta-Hydroxybutyrate measurement 61
2.7.5 Liver enzymes 61
2.7.6 CD36 blocking studies 61
2.7.7 Transfection 62
2.8 Statistics 62
2.9 Materials 63
2.9.1 Taq man probes 63
2.9.2 General 63
2.9.3 Particles 65
2.9.4 RNA 65
2.9.5 Blocking Antibodies and inhibitors 66
2.9.6 Magnetic bead separation Antibodies 66
2.9.7 Staining Antibodies and Dyes 66
2.9.8 Equipment 66
3 Diurnal particle uptake by immune cells is limited to *ex vivo* settings and is independent of the scavenger receptor CD36 68
3.1 Introduction 68
3.2 Results 73
3.2.1 Phagocytosis and oxidative stress pathways display daily rhythmicity in macrophages 73
3.2.2 *Ex vivo* uptake capacity in macrophages is diurnal 75

3.2.3 The fluorescence signal detected in uptake studies originates from ingested, not surface bound particles 82
3.2.4 Serum shock is not a reliable method to investigate rhythmic uptake85
3.2.5 The cell intrinsic clock is dispensable for diurnal oscillations in particle uptake 92
3.2.6 Rhythmicity of CD36 and its role in bacterial uptake..... 95
3.2.7 Particle uptake by macrophages is not diurnal *in vivo* 115
3.3 Discussion 119
4 Food entrainment determines oscillations in the susceptibility to LPS 125
4.1 Introduction 125
4.2 Results 127
4.2.1 LPS induced mortality is a function of feeding time 127
4.2.2 Feeding time determines the clock phase in the liver, but not in other peripheral organs or the brain 130
4.2.3 Cytokines and liver enzymes, measured basally or 6h post stimulation, are not predictive of LPS induced morbidity 153
4.2.4 The immune modulators β-Hydroxybutyrate and corticosterone are diurnal and food regulated, however do not appear indicative of mortality 159
4.2.5 Time restricted feeding alters oscillations in metabolism 163
4.3 Discussion and Future Studies 174
5 Conclusions and Future Work 182
6 References..... 189
7 Appendix..... 207

Table of Figures

Figure 1.1.5.1: Overview of selected ingestion mechanisms 10
Figure 1.2.1.1: Light entrainment of the SCN and peripheral organs. 14
Figure 1.2.2.1 The Molecular Clock 16
Figure 1.3.2.1 Circadian Oscillations of Immune Factors 22
Figure 1.3.2.1 The Body Clock 31
Figure 1.5.3.1: A phase shift can falsely be interpreted as absence of oscillation when only two time-points are being used. 36
Figure 2.2.2.1: Time restricted feeding schedule. 40
Figure 2.2.3.1: Feeding schedule of TRF in constant light. 41
Figure 2.2.4.1: LPS mortality schedule with continued TRF post stimulation. ..42
Figure 2.2.4.2: LPS mortality schedule with ad libitum feeding post stimulation. 42
Figure 2.2.4.3: Mortality study scoring sheet. 43
Figure 2.4.4.1: *E. coli* growth curve. 49
Figure 2.5.1.1: Gating strategy of uptake positive peritoneal macrophages following particle uptake. 51
Figure 2.6.6.1: Schematic illustration of RNA quantification via NanoString technology. 56
Figure 2.7.1.1: Genotyping Primer Sequences. 60
Figure 3.2.1.1: Peritoneal macrophages differentially express phagocytic and oxidative stress genes dependent on the time of the day. 74
Figure 3.2.2.1: Efficiency of *E. coli* and *S. aureus* bioparticle uptake in peritoneal macrophages is increased at ZT12. 76
Figure 3.2.2.2: F4/80$^-$ cells do not impact on uptake measurements. 77
Figure 3.2.2.3: Peritoneal macrophages show diurnal uptake of various particles. 79
Figure 3.2.2.4: Ingestion of living and heat-inactivated *E. coli* bacteria is increased at ZT12 as measured by various methods. 80
Figure 3.2.2.5: Acidification of phagosomes is not diurnal. 81
Figure 3.2.3.1: Confocal microscopy verifies ingestion, rather than surface binding of particles. 83

Figure 3.2.3.2: Latrunculin A inhibition dose dependently decreases bacterial uptake and cytokine secretion. 84
Figure 3.2.4.1: Uptake in serum shocked and control BMDMs. 86
Figure 3.2.4.2: The clock in peritoneal cells is functional and can be ablated in $BMAL1^{fl/fl}LyzMCre^{+/+}$ animals. 88
Figure 3.2.4.3: Serum shock appears to induce clock gene oscillation in WT, but not in *Bmal1* knockout macrophages. 89
Figure 3.2.4.4: Cells lacking *Bmal1* have similar uptake properties to wild type cells. 91
Figure 3.2.5.1: *Bmal1* deletion does not alter bacterial particle uptake in macrophages. 93
Figure 3.2.5.2: *Bmal1* and *Clock* overexpression does not affect particle uptake. 94
Figure 3.2.6.2: *Cd36* mRNA is not rhythmic in $F4/80^{+}$ or $F4/80^{-}$ peritoneal macrophages. 96
Figure 3.2.6.5: Restricted feeding schedules for 5 days do not alter uptake capacity of peritoneal macrophages *ex vivo*. 100
Figure 3.2.6.6: Prolonged restricted feeding schedules do not affect uptake capacity and CD36 surface expression in peritoneal macrophages at ZT6. 102
Figure 3.2.6.7: 12 days of time restricted feeding does not affect *ex vivo* particle uptake in peritoneal macrophages at ZT0. 103
Figure 3.2.6.8: High fat diet does not induce CD36 expression. 104
Figure 3.2.6.9: Particle uptake by iBMDMs seemingly cannot be inhibited with an antibody directed against CD36. 105
Figure 3.2.6.10: CD36 surface blockage does not appear to inhibit uptake of fluorescent latex particles. 107
Figure 3.2.6.11: Uptake of latex particles by peritoneal cells does not seem to be inhibited by CD36 blockage. 108
Figure 3.2.6.12: *Ex vivo* bacterial particle uptake is not CD36 dependent. 109
Figure 3.2.6.13: Uptake of oxLDL, a known CD36 ligand, is not impaired in *Cd36* knockout macrophages *ex vivo*. 110

Figure 3.2.6.14: Serum and Oleic acid do not affect oxLDL and *S. aureus* uptake. 111
Figure 3.2.6.15: *Ex vivo* oxLDL uptake does not follow a diurnal rhythm. 112
Figure 3.2.6.16: *S. aureus* uptake is not impaired in *Cd36* knockout mice *in vivo*. 113
Figure 3.2.6.17: *In vivo* oxLDL uptake is dose dependent, but CD36 independent. 114
Figure 3.2.7.1: *S. aureus* ingestion by peritoneal macrophages is not rhythmic *in vivo*. 116
Figure 3.2.7.2: The macrophage intrinsic biological clock does not affect *S. aureus* ingestion *in vivo*. 117
Figure 3.2.7.3: pHrodo uptake *in vivo* is dose dependent. 118
Figure 4.2.1.1: LPS induced, rhythmic mortality is a function of food availability. 128
Figure 4.2.1.2: The effect of food availability following LPS stimulation. 129
Figure 4.2.2.1: Day-time restricted feeding induces a 12 h period shift in the liver, but not in the spleen, adipose tissue and peritoneal macrophages. 131
Figure 4.2.2.2: The liver clock, but not *Tnfa* and *Il1b* expression, is reversed in day-time fed animals. 133
Figure 4.2.2.3: TRF does not reverse the spleen clock, but causes a mild attenuation of diurnal cycling, while *Tnfa* expression appears to follow the feeding cycle. 134
Figure 4.2.2.4: Metabolic and clock gene expression, but not basal inflammatory gene expression in the liver is a function of food availability. 137
Figure 4.2.2.5: Gene expression oscillations in the spleen are less pronounced, and amplitudes are further reduced upon day-time feeding. 140
Figure 4.2.2.6: Rhythmicity of clock gene expression in adipose samples is diminished in day-time fed animals. 143
Figure 4.2.2.7: Expression of circadian genes appears diurnal, but food independent in peritoneal macrophages, while inflammatory genes do not oscillate strongly and metabolic genes exhibit food dependent rhythmicity. 146

Figure 4.2.2.8: Magnetic, negative selection of peritoneal macrophages results in purity of approximately 50%. 147
Figure 4.2.2.9: Ad libitum fed and TRF mice display widely congruent gene expression profiles under constant light conditions in peritoneal macrophages. 149
Figure 4.2.2.10: Magnetic, negative selection of peritoneal macrophages from TRF mice in constant light results in purity levels of approximately 50%. 150
Figure 4.2.2.11: Clock gene expression in the liver, but not in SCN and other peripheral tissues is rhythmic in TRF animals under constant light conditions. 152
Figure 4.2.3.1: Basal serum cytokines are neither diurnal, nor affected by time restricted access to food. 154
Figure 4.2.3.2: Time restricted feeding under constant light conditions does not affect basal cytokine level or absence of rhythmicity. 155
Figure 4.2.3.3: Serum cytokines are uniformly induced in day- and night-time fed animals, and are unaffected by the feeding regimen following LPS stimulation. 157
Figure 4.2.3.4: Liver damage as measured by liberation of liver enzymes into the circulation is absent early after LPS stimulation. 158
Figure 4.2.4.1: Basal Corticosterone levels are a function of food and are highly induced following LPS stimulation irrespective of feeding time. 160
Figure 4.2.4.2: β-Hydroxybutyrate patterns are sustained upon LPS stimulation with increased overall levels. 162
Figure 4.2.5.1: RER is a function of food availability, independent of the time of the day. 164
Figure 4.2.5.2: Food dependent oscillations in RER are sustained over the course of two weeks. 165
Figure 4.2.5.3: Activity is regulated by the light, not the feeding schedule. 167
Figure 4.2.5.4: Light dependency of activity patterns is sustained over the course of two weeks. 168
Figure 4.2.5.5: Dietary intake patterns in day and night-time fed animals are comparable. 170

Figure 4.2.5.6: Feeding patterns adjust rapidly and are sustained over the course of two weeks. 171
Figure 4.2.5.7: Overall metabolism and activity is unaffected by TRF. 172
Figure 4.2.5.8: Body composition is unaffected by time restricted feeding up to two weeks. 173
Figure 4.2.5.1: Graphic summary: Food entrainment determines oscillations in the susceptibility to LPS. 181

Appendix 1: NanoString CodeSets 207
Appendix 2: RT Profiler Gene Sets 208

Abbreviations

ACK	Ammonium-Chloride-Potassium
BMDM	Bone marrow derived macrophages
DAMP	Damage Associated Molecular Patterns
d	Day
FSC	Forward Scatter
h	Hour
HBSS	Hank's Balanced Salt Solution
IFN	Interferon
Ig	Immunoglobulin
IL	Interleukin
KC	Kupffer Cells
LPS	Lipopolysaccharide
MHC	Major Histocompatibility Complex
min	Minutes
mRNA	messenger RNA
NOD	Nucleotide-binding Oligomerization Domain
oxLDL	oxidized Low-Density Lipoprotein
PAMP	Pathogen Associated Molecular Patterns
PBS	Phosphate-Buffered Saline
PenStrep	Penicillin/Streptomycin
PEC	Peritoneal Exudate Cells
PM	Peritoneal Macrophages
RER	Respiratory Exchange Ratio
RNA	Ribonucleic acid
RT	Room temperature
SCN	Suprachiasmatic Nucleus
SSC	Side Scatter
TLR	Toll Like Receptor
TNF	Tumor Necrosis Factor
TRF	Time Restricted Feeding
ZT	Zeitgeber Time

1 Introduction

The immune system is a complex machinery which continuously protects organisms against pathogens and malignancies (Sukari et al., 2016); and just as immunological responses themselves can be localized or systemic, the immune system itself is regulated both, locally and systemically.

The immune system is largely protective, however, over-reactivity of the immune system can occur which can be detrimental and cause tissue damage (Jancar and Sanchez Crespo, 2005), autoimmunity (Adams, 1996, Kronenberg and Rudensky, 2005) and even death (Vincent et al., 2002). It is therefore of great interest to understand host factors that can limit inflammatory response in the setting of autoimmunity, or promote immune functions, such as efficient targeting of malignant cells in cancer therapy. Only by understanding the molecular mechanism by which the immune system is regulated, can we identify targets, strategies and therapies to treat or protect individuals at risk.

One distinct and often overlooked feature of the immune system is its ability to mount immune responses that vary in their intensity according to time-of-day (Halberg et al., 1960). Congruent with this, disruption of the internal timing system - the circadian clock - is associated with increased susceptibility to diseases with an underlying inflammatory component (Voigt et al., 2013, Bass and Lazar, 2016, Turek, 2016). Although circadian studies on immunity date back to the 1960's (Halberg et al., 1960), little is understood about the mechanistic interplay of those two systems.

The present study investigated two aspects of chrono-immunology. First, fluctuations in the ability of macrophages to ingest infectious and non-infectious material were examined to determine a possible role for phagocytosis in rhythmic immunity following infection. Secondly, two known clock regulatory, environmental signals - light and food - and their ability to regulate oscillations in the susceptibility to inflammatory stimulation were investigated. This study was further extended to identify the underlying cues, and is an on-going project that could not be finished in the course of this thesis, but will be brought to completion in the following months.

1.1 Immunology

The environment is covered with microorganisms and other potentially pathogenic material. Without an intact immune system, a host would succumb to infections acquired in the course of a normal day. This tightly regulated system evolved to specifically target foreign material by sophisticated self/non-self distinction (Kumar and McNerney, 2005) and recognizes and clears mutated or otherwise malignant host cells (Hanahan and Weinberg, 2011). Failure to recognize self-antigens is the foundation of autoimmune disease, where healthy host cells are attacked by immune cells (Metzger and Anderson, 2011). While the immune system is generally protective, hyper-inflammation can cause tissue injury that can be fatal (Wallach et al., 2014). Accordingly, there is a critical need for the immune system to balance initiation of a sufficient immune response to clear infections, while keeping tissue damage at a minimum. This chapter outlines the structure of the immune system and some of the many inflammatory cues that are induced upon inflammatory stimulation.

1.1.1 Adaptive and Innate Immunity

Traditionally, we distinguish between innate and adaptive immunity (Hoebe et al., 2004). Innate immunity is often referred to as the "unspecific defence mechanism" and includes in its simplest form barriers, such as the skin. The innate immune system utilizes common, widely conserved features, from size of encountered material to common pathogen or damage associated molecular patterns (PAMPs (Janeway, 1989) or DAMPs (Matzinger, 1994)). In contrast, adaptive immunity utilizes genetic rearrangement of antigen receptors for its specificity (Capra and Kindt, 1974, Hozumi and Tonegawa, 1976). The vast variety of antigen specific immune cells, such as T- and B-cells, evolve independent of inflammatory stimulation, but cells that recognize a certain antigen, such as T-cells, will markedly expand upon engagement and once the threat has cleared, continue to persist in small numbers to allow for a greater response upon re-stimulation; a process called immunological memory (Kurtz, 2004).

The adaptive immune response is significantly slower and generally appears days after the infection, leaving the first response to the innate system. However, adaptive and innate immunity cannot be considered as independent machineries, as the interplay between those two systems is critical. Proper attraction and activation of adaptive immune cells for instance depends on soluble mediators that are widely produced by cells of the innate immune system, such as cytokines and chemokines. Ingested material can be further presented by innate antigen-presenting cells to facilitate antigen directed immune response by the adaptive immune compartment. Although there is a tight communication between the systems, the current study focused on the innate immune response, and macrophages in particular.

1.1.2 Macrophages

Macrophages were first identified 1883 by the Russian Zoologist Metchnikoff, as he found mobile cells in the larvae of starfish that appeared to migrate to sites of inflammation, which, as he believed, could ingest pathogenic material (Metchnikoff, 1905). This gave rise to the concept of professional phagocytes and phagocytosis in general. Phagocytic ingestion of material, as discussed in a later paragraph, is critical for homeostasis (Arandjelovic and Ravichandran, 2015) as well as clearance of pathogens (Underhill and Ozinsky, 2002). From Metchnikoff's basic understanding of phagocytes, immunologist have progressed in identifying additional roles for macrophages beyond ingestion of material. Macrophages, as part of the very first line of defence following an inflammatory insult, release a plethora of chemokines and cytokines (Nau et al., 2002) and through antigen presentation to helper T cells, activate the adaptive immune system (Unanue and Allen, 1987, Pozzi et al., 2005). Besides the recruitment of other immune cells to sites of infection, the production of IL-6, TNF, IL-1β by macrophages modulates metabolic pathways, such as insulin resistance to decrease nutrient storage and increase glucose availability for the brain and immune cells (Chawla et al., 2011, Hotamisligil et al., 1993). Besides the macrophages' role of regulating whole body metabolism, their own metabolic state is indeed central to direct their inflammatory responses.

Classically activated M1 macrophages display widely pro-inflammatory features (Unanue and Allen, 1987) and are characterized by their highly glycolytic metabolism (Newsholme et al., 1986). Alternatively activated M2 macrophages (Stein et al., 1992) on the other hand are known to depend on oxidative phosphorylation (Vats et al., 2006) and seem to be involved in immune resolution and response to parasitic manifestations (Zhu et al., 2014). Dysregulation of macrophages appears central in a range of autoinflammatory and chronic diseases (Vlahos and Bozinovski, 2014, Kinne et al., 2000). Macrophages are generally identifiable by their expression of the surface marker F4/80 (Austyn and Gordon, 1981) , but despite this common feature on their cell surface, they display incredible diversity (Gautier et al., 2012). Although the origin of macrophages is still under debate, it appears that tissue resident macrophages develop in the yolk sack and are seeded early in embryogenesis (Wynn et al., 2013), while patrolling monocytes, which maintain the ability to differentiate into macrophages - which are distinct from tissue resident macrophages in a range of characteristics - and infiltrate inflamed tissues at high numbers, develop in the bone marrow in adults (Kurihara et al., 1997). Tissue resident macrophages are widely diverse between organs, and even within one organ, macrophages can vary depending on their localization within the tissue (Davies and Taylor, 2015, Gordon et al., 2014). This exemplifies how specific these cells of the "unspecific", innate immune system in fact are.

1.1.3 Cytokine Response

Following an inflammatory insult to the body, cytokines and chemokines are produced to activate and recruit cells from the innate and adaptive immune system (Dinarello, 2000). This response is not a rigid cascade that varies solely in intensity, but is a finely tuned response and dependent on the properties of the insult to allow an efficient response to protect the organism, while minimizing tissue damage (Takeuchi and Akira, 2010). A myriad of cytokines have been described over the years and while they all possess important roles

in a functional immune system, only some of the key inflammatory cytokines will be mentioned here.

Upon inflammatory stimulation and engagement of pattern recognition receptors, such as Toll-like or NOD-like receptors (Kawai and Akira, 2010), the pro-inflammatory signalling cascade is initiated and expression of pro-inflammatory cytokines like Interleukin (IL-) 1β (Dinarello, 1996), TNF and IL-6 are produced. All of these cytokines can be produced by activated macrophages amongst other cell types, but while IL-1β and TNF are primarily originating form macrophages, IL-6 is primarily derived from hepatocytes (Bultinck et al., 2006), emphasizing the role of macrophages and the liver in the immune response. IL-1β is produced as a pro-form (Lomedico et al., 1984) and requires a secondary signal to induce the inflammasome and activation of caspase-1 to cleave IL-1β into the active form (Cerretti et al., 1992) and induce its pyrogenic properties along with cell proliferation and differentiation signalling though the IL1-receptor (Boraschi and Tagliabue, 2013). IL-6 is directly produced in its active from and activates the JAK-STAT signalling (Zhong et al., 1994) and induces the release of acute phase proteins in the liver (Bode et al., 2012) as well as maturation of B-cells (Kitani et al., 1992). The production of IL-6 has been associated with outcomes in the setting of sepsis (Hack et al., 1989), however, inhibition of IL-6 was not found to be protective (Barkhausen et al., 2011). Tumor necrosis factor, TNF, is another pro-inflammatory cytokine of critical importance during an immune response which is rapidly induced, with peak serum abundance approximately two hours post infection (Richard et al., 1999). TNF is also believed to induce IL-6 production in the liver (Bultinck et al., 2006) and activates pro-inflammatory signalling in target cells, such as phagocytes, but can also induce caspase-8 dependent apoptosis (Varfolomeev and Ashkenazi, 2004, Hsu et al., 1996). A member of the anti-inflammatory cytokine family worth mentioning is IL-10. Similarly to some pro-inflammatory cytokines, IL-10 is produced by a range of immune cells including macrophages. Being anti-inflammatory, IL-10 inhibits pro-inflammatory response via inhibition of T-cell proliferation and activation (Fiorentino, 1989), as well as macrophage production of chemokines and cytokines and abundance of MHCII molecules (de Waal Malefyt, 1991). Chemokines, another

subfamily of cytokines, are prominent for their role to induce chemotaxis of immune cells to mediate infiltration to sites of inflammation (Moser et al., 2004), and also maintain homeostasis and regulate angiogenesis (Anders et al., 2014).

1.1.4 Sepsis

Infections are usually effectively cleared by the immune system, but excessive triggering of the immune response, due to high bacterial load or tissue injury can induce sepsis (Cohen, 2002). This severe systemic inflammation initially causes immense production of inflammatory cytokines and chemokines, generally referred to as the "cytokine storm" (Ferrara et al., 1993). Following this initial hyper-reactivity of the immune system, a state of immune-paralysis establishes in affected individuals, rendering them highly susceptible to secondary infections (Bone, 1996).

Sepsis is a leading cause of death in intensive care units and patient care is currently solely supportive due to a lack of effective treatments. Previous efforts have aimed to use anti-cytokine treatments to prevent cytokine storm and tissue injury caused by hyper-inflammation. While there were some promising mouse studies, its effectiveness was not to be recapitulated in humans (Dinarello, 2000). Although inflammation is the foundation of sepsis, it is not clear what exactly is causing mortality (Leon et al., 1998). Several pathways have been implemented in the progression of this disease, but when targeted independently did not improve mortality. Serum levels of the inflammatory cytokine IL-6 have been correlated with the outcome of sepsis (Damas et al., 1992), however IL-6 inhibition did not improve mortality (Barkhausen et al., 2011, Vyas et al., 2005). The source of tissue damage in sepsis is also not entirely clear and whether necrosis can contribute to mortality has to be explored. It is nevertheless clear, that tissue damage contributes to the overall phenotype; whether markers of necrosis can be used as predictors of survival and if inhibition of necrotic cues can be targeted for therapy is however not yet known (Hotchkiss et al., 2003).

The liver has been identified as a critical organ in the course of sepsis (Yan et al., 2014) and besides its homeostatic roles in detoxification and metabolic

regulation, the liver appears to be a main regulator of pro-inflammatory response in systemic infection (Crispe, 2009, Tiegs and Lohse, 2010). Inflammatory material, such as bacteria, are cleared from the blood stream effectively by the liver to remove the infectious load predominantly by Kupffer cells, the liver resident macrophages (Deng et al., 2013). Depletion of these cells in mice - via administration of gadolinium chloride - protects against systemic inflammation and organ failure due to the lack of particle ingestion induced inflammatory response; however, without removal of the inflammatory agent, infection persists and the outcome is negatively affected in the long run (Koo et al., 1999). There is certainly a central role for the liver during sepsis, and understanding the molecular mechanism by which the liver responds to infection and how the liver state preceding infection affects disease progression can help to identify new targets for drug development and provide new insights as to the cause of sepsis-induced mortality.

1.1.5 Uptake of Extracellular Material

Single cell organisms, the earliest life forms on earth, already required structures to ingest extracellular material to meet their nutritional demands. Although the purpose is different, the importance of uptake in the context of immunity is not lessened, as the ability of immune cells to ingest material is indeed critical to the organism's survival (Andrews and Sullivan, 2003). Phagocytic ingestion not only ensures efficient clearance of infectious material following an inflammatory insult (Metschnikoff, 1887), it is also central in maintaining homeostasis (Arandjelovic and Ravichandran, 2015).

Cells are constantly dying as they reach the end of their life span and are replaced by new cells, as well as in the course of tissue remodelling, or in the resolution phase of an inflammatory insult when short-lived infiltrating immune cells undergo apoptosis (Elmore, 2007). Phagocytes ingest these apoptotic cells and induce an anti-inflammatory cascade to prevent inflammation under homeostatic conditions or even promote resolution following an inflammatory response (Maderna and Godson, 2003). However, when pathogenic material is

encountered, macrophages can induce a variety of pro-inflammatory cascades and fully activate the immune system (Underhill and Ozinsky, 2002).

Generally, uptake can be categorized into three steps; *Binding* of particles to the cell surface, *Ingestion* of the material, and *Degradation*. The exact pathways are thereby heavily dependent on the type of material to be ingested (Underhill and Goodridge, 2012). Some of the internalization pathways that have been described are outlined below and illustrated in Figure 1.1.5.1. Given the necessity to induce uptake of material that varies dramatically in size, chemical composition and viability, the complexity of material ingestion and the load of receptors involved, is not surprising (Aderem, 2003).

Receptors on the surface of phagocytes are very diverse and recognize a myriad of patterns that are commonly shared between or within bacterial families. Fc- and complement receptors diversify recognition even further by engaging antibody and complement opsonized targets (Stuart and Ezekowitz, 2005). Upon phagocytosis, macrophages are able to tailor processing and downstream signalling of ingested material depending to the "threat" they possibly pose on the organism, finely balancing the response they will initiate (Underhill and Goodridge, 2012).

The complexity of the uptake process, accompanied by a vast redundancy and simultaneous engagement of multiple receptors, make investigations regarding the role of specific receptors within this process challenging.

1.1.5.1 Efferocytosis

The ingestion of apoptotic cells is summarized in the term efferocytosis (Korns et al., 2011). Generally, efferocytosis is anti-inflammatory (Fadok et al., 1998) and appears to be involved in the resolution of an immune response (Sun and Shi, 2001). While the term does not distinguish between ingestion of infected and uninfected cells, the program that is induced upon ingestion appears to be dependent on the entity of the material, and as such, apoptotic cells that were infected with various materials will cause divergent signalling and processing.

1.1.5.2 Endocytosis

Endocytosis is a general form of actin independent uptake of small molecules (Johannes et al., 2015) and includes ingestion via clathrin coated pits (Kirchhausen et al., 2014) and caveolae (Nabi and Le, 2003). Endosomes, which contain the ingested material are further processed and mature to degrade the ingested material.

1.1.5.3 Phagocytosis

Internalization of material that exceeds 0.5 µm in diameter occurs in an actin dependent mechanism called phagocytosis. The emerging structure, the Phagosome, whose contents are initially similar to the extracellular matrix, maturates and fuses with the Lysosome to cause acidification and activation of proteases to initiate killing and degradation of ingested material (Stuart and Ezekowitz, 2005).

1.1.5.4 Macropinocytosis

Macropinocytosis, or cell drinking, is an actin dependent mechanism that involves formation of membrane ruffles which subsequently collapse and fuse with the plasma membrane to engulf the matter within the inclusions that were formed (Swanson and Watts, 1995). These inclusions are generally in the range of 0.5 to 5 µm in diameter.

1.1.5.5 Autophagy

Phagosomes are not only formed to ingest extracellular material, but can also engulf intracellular structures and are then termed Autophagosomes (Mizushima, 2007). A verity of organelles can be enclosed in these structures and according to the target, autophagy is often further specified (Glick et al., 2010). For instance, when mitochondria are being targeted for autophagy, the process is termed mitophagy to immediately indicate the cargo (Ding and Yin, 2012).

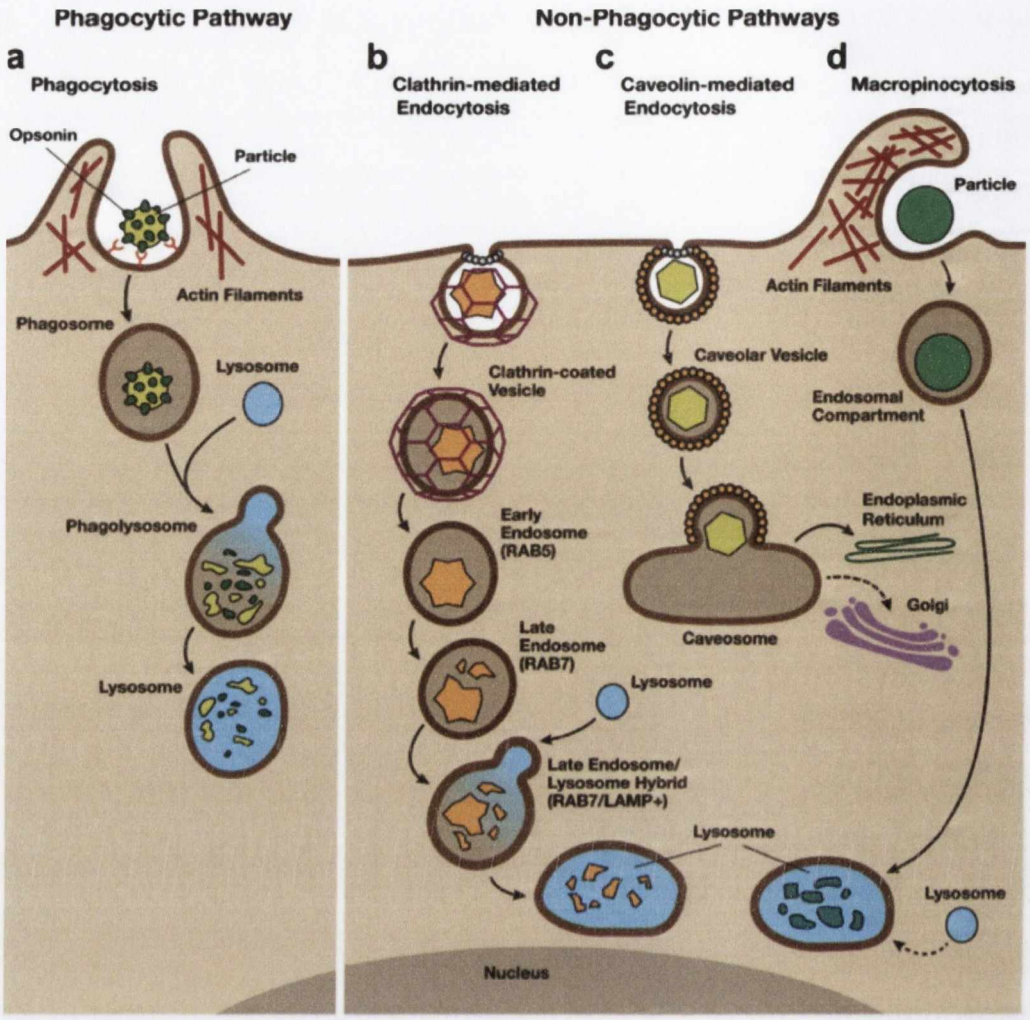


Figure 1.1.5.1: Overview of selected ingestion mechanisms

Graphic summary of ingestion pathways such as phagocytosis **(A)**, clathrin **(B)** or caveolin **(C)** mediated endocytosis, and micropinocytosis **(D)**. Graphic from Stern, 2012 (Stern et al., 2012).

1.1.6 Immuno-Metabolism

In every organism metabolism is central for survival, and historically, the pathway to produce energy, mainly in form of ATP, was believed to depend merely on oxygen levels and glucose abundance. Although there is for sure a great dependency on these factors in the regulation of metabolism, control is often more complex than this.

In the context of the immune system, metabolism is central to the ability of an immune cell to proliferate and induce a pro-inflammatory response (Vander

Heiden et al., 2009, Krawczyk et al., 2010). This has been shown already in early studies where phagocytic ingestion of particles by leukocytes significantly increased their oxygen consumption (Sbarra and Karnovsky, 1959). Now, we have a much more complete understanding on the regulation of metabolism during an inflammatory insult, and the pathways that are being induced (Tannahill et al., 2013, Pearce et al., 2009, van der Windt et al., 2012).

As proliferation and pro-inflammatory response are energy consuming tasks, and cells need to consume large amounts of glucose (Jacobs et al., 2008), it initially appears surprising that a cell would switch from high energy producing oxidative phosphorylation, to glycolysis, a pathway that is not very energy efficient. In recent years it has however become clear that glycolysis is highly induced to produce intermediates to meet the anabolic demand of an activated cell (Vander Heiden et al., 2009). While a switch from oxidative phosphorylation to glycolysis in immune cells following activation is evident (Krawczyk et al., 2010, Michalek et al., 2011, Hard, 1970, Newsholme et al., 1986), the cytokines subsequently produced appear to further propagate this conversion by more systemically modulating metabolic pathways, such as insulin resistance to decrease nutrient storage and promote glucose titers (Chawla et al., 2011).

Following the concept of systemic nutrient availability, specific diets have been shown to affect overall metabolism, and modulating abundance of certain metabolites with diets are now strong tools to modulate immunity (Galland, 2010, Minihane et al., 2015). For example, the starvation induced ketone body β-Hydroxybutyrate decreases immune intensity by inhibiting the NLRP3 inflammasome, and a ketogenic diet is sufficient to increases abundance of this metabolite in the system (Youm et al., 2015).

Dietary modulation of the immune system may have utility beyond animal studies, and a better understanding on how nutritional composition and possibly mealtimes can affect inflammation will help physicians to find better strategies to prevent and support therapy by well contemplated diet plans, and will also provide new targets for drug development.

1.2 The Circadian Clock

1.2.1 The Circuitry of the Mammalian Circadian Clock

Circadian rhythms are daily oscillations in behaviour and physiology that prepare organisms to better react to and anticipate the daily changes in the solar environment. These cellular clocks are conserved from cyanobacteria to mammals and are accordingly found in almost every cell in multicellular organisms that evolved from unicellular progenitors.

Higher life forms, as they faced the task of sustaining synchrony of their central clock in the brain and peripheral clocks throughout the body, started to use exogenous signals - termed *zeitgeber*, the German word for 'time giver' (Aschoff, 1951) - that could be sensed by the organism to entrain and align circadian rhythms across multiple tissues. Under free running conditions - an environment that lacks zeitgeber signals - robust circadian outputs are sustained, whereas diurnal outputs are lost as they are a direct effect of exogenous signals. Environmental conditions can additionally obscure circadian outputs, which is described in a concept called masking (Aschoff, 1960). Outputs can thereby be phase-shifted directly by masking stimuli without clock entrainment; yet in the absence of the masking stimulus, the originally entrained rhythm is restored. Daily oscillations that were examined in this work have been termed diurnal throughout the study as sustained rhythmicity under free-running conditions has not been experimentally verified.

Light is a major contributor to the circadian system, however it is not the only zeitgeber. A variety of signals such as temperature, food and social cues (Brown et al., 2002a, Mistlberger and Marchant, 1995, Edmonds and Adler, 1977, Aschoff et al., 1971) among others have been described as zeitgebers with varying potential. Under normal, physiological circumstances all zeitgebers are tightly correlated. For example, the light cycle, outdoor temperature and food availability tend to fluctuate in a predictable way according to time-of-day.

In Zebrafish, peripheral clocks in the liver and heart are directly light entrained and changes in light patterns result in rapid phase shifts of core clock proteins in these organs (Whitmore et al., 2000). Equally, locomotor activity in blinded

birds remains an immediate function of light, supporting that light sensing cells in these animals are present outside of the retina (Menaker, 1968).

In other organisms, such as mammals, extra-retinal cells have lost the ability to directly interpret photic cues. Studies using mechanical destruction of mammalian brain regions instead identified a light regulated circadian master pacemaker in the suprachiasmatic nucleus (SCN), which regulates subordinate peripheral clocks (Moore and Eichler, 1972, Stephan and Zucker, 1972). This central pacemaker resides in the hypothalamus and is innervated via the retinohypothalamic tract by malanopsin containing retinal ganglion cells in response to light, the primary environmental stimulus which correlates with the earth's rotation and therefore with time-of-day. The SCN subsequently synchronizes peripheral clocks via mediators including hormones and neuronal signals, primarily using the hypothalamic-pituitary-adrenal axis (HPA) and the autonomic nervous system (ANS) Figure 1.2.1.1.

This model of a hierarchical organization of the body clock, with the brain-clock at the top, has recently been refined. Specific ablation of the cellular clock in the SCN in mice on a light/dark regime did not result in loss of circadian behaviour as expected. When these mice were however placed in constant darkness, the amplitude of clock genes in the periphery diminished over time (Husse et al., 2014). Therefore, it appears that besides the conventional master clock, which is dependent on a functional cellular clock, there is a molecular-clock independent, light responsive element. In the absence of both SCN signals (light, and the molecular clock), animals lose SCN mediated synchronization of peripheral tissues, and while rhythmicity in these tissues can be temporarily sustained, gradual weakening of the amplitude eventually results in loss of synchrony, similarly to what is seen in peripheral clocks *in vitro* (Keller et al., 2009). This suggests a dual role for the SCN in processing light signals, which remained undetected in studies that used destruction of the brain region in which the SCN resides, as the molecular-clock dependent as well as the molecular-clock independent elements were both destroyed.

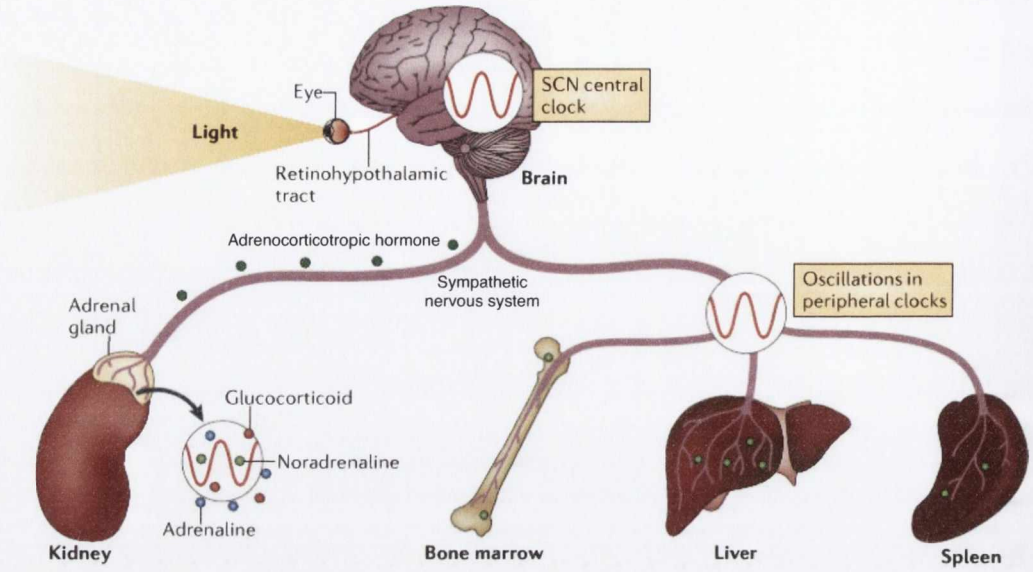


Figure 1.2.1.1: Light entrainment of the SCN and peripheral organs.

Light signals are detected by photosensitive retinal cells and conveyed to the SCN via the retinohypothalamic tract. Neuronal and hormonal signals of the hypothalamic-pituitary-adrenal axis then synchronize peripheral tissues. Rhythmic release of the adrenocorticotropic hormone manifests oscillation in the adrenal gland, which is highlighted as it produces daily oscillations in glucocorticoids, and catecholamines, such as epinephrine and norepinephrine, that exhibit clock and immune regulatory functions. These mediators further enhance entrainment of other peripheral organs such as the liver, spleen and bone marrow. Light directly and indirectly induces daily oscillations of signals such as body temperature and food intake which further enhance robust synchronization of peripheral tissues. Adapted from Scheiermann, 2013 (Scheiermann et al., 2013).

1.2.2 The Clock at the Molecular Level

The core molecular clock, in both the periphery and the SCN, is comprised of two main transcriptional-translational feedback loops, which counter-regulate each other to generate a circadian cycle of gene expression. Brain and Muscle ARNT-like 1 (BMAL1) and Circadian Locomotor Output Cycles Kaput (CLOCK) proteins heterodimerize (Gekakis et al., 1998) and bind to E-boxes (CACGTG) (Hao et al., 1997) to induce transcription of target genes (Ripperger and Schibler, 2006) along with a set of regulatory proteins including PERIOD (PER1, 2 and 3), CRYPTOCHROME (CRY1 and 2), REV-ERB (REV-ERBα and

β) and RAR-Related Orphan Receptor (RORα, β and γ), which feed back to regulate their own transcription. REV-ERBs and RORs bind to ROR responsive elements (RREs) (Harding and Lazar, 1993, Giguere et al., 1994) to regulate *BMAL1* transcription, whereas PER and CRY dimerize to inhibit the BMAL1:CLOCK dimer (Figure 1.2.2.1). CRY recruitment is facilitated via CLOCK mediated acetylation of BMAL1, while PER and CRY phosphorylation and degradation is controlled by the Casein kinases I delta and epsilon (CKIδ and ε) to restrict their negative feedback potential (Keesler et al., 2000, Camacho et al., 2001). These feedback loops are the fundamental building blocks of the cellular clock, however many more genes are directly regulated by the clock machinery, resulting in rhythmic expression of clock controlled genes via E-boxes, D-boxes and RREs, which are also responsible for phase delays of circadian genes (E-boxes at the transition into the active phase, D-boxes during activity and RREs at rest) (Ukai-Tadenuma et al., 2008, Ueda et al., 2005). Primary and secondary clock regulated genes can also regulate the level of transcription and post-transcriptional modification of central clock genes, thereby reinforcing its integrity. 8% of the transcriptome in murine peritoneal macrophages has been shown to be cycling (Keller et al., 2009), which is probably an underestimate of the actual amount of circadian outputs, as posttranslational modifications can also result in circadian activity of genes whose transcription is not cyclic (Hastings et al., 2007).

A total of 55% of all mouse protein-coding genes are estimated to be oscillating in at least one location throughout the organism, many of which present peak levels around dawn and dusk, the transcriptional "rush hour" (Zhang et al., 2014). While oscillations of core circadian clock genes are conserved in most organs, the majority of other rhythmic genes appear to be expressed organ specific. This underpins the necessity to redefine the model of clock regulation. Although there is undoubtedly an important role for the core feedback loops described previously, the clock and its outputs are regulated on a multitude of levels throughout the process of gene expression from chromatin remodelling to RNA polymerase II recruitment and initiation, and genome-wide analyses revealed that epigenetic modifications create a poised state to facilitate rhythmic gene expression (Takahashi, 2016).

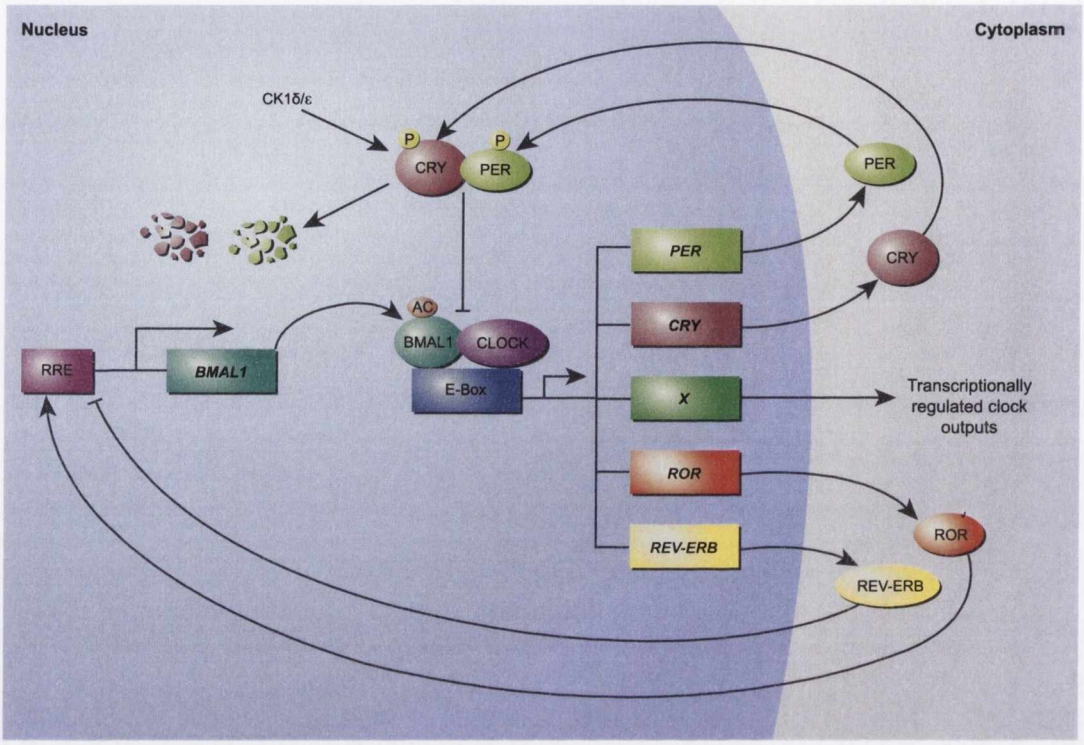


Figure 1.2.2.1 The Molecular Clock

BMAL1 (Brain and Muscle ARNT-like 1) heterodimerizes with CLOCK (Circadian Locomotor Output Cycles Kaput) to initiate transcription of target genes via E-boxes. PER (PERIOD) and CRY (CRYPTOCHROME) proteins dimerize and inhibit their own expression by disrupting the acetylated (AC) BMAL1:CLOCK dimer. REV-ERB (nuclear receptor subfamily 1, group D) and ROR (RAR-Related Orphan Receptor) bind to ROR responsive elements (RRE) to regulate *BMAL1* transcription. PER and CRY phosphorylation (P) and degradation is governed by casein kinases I delta and epsilon (CKIδ/ε).

Recently, interest in circadian rhythms and the effect this might pose on the immune system has grown and much progress has been made unravelling the mechanisms of the clock and its outputs. Nevertheless, many circadian phenotypes remain to be understood. Even though it is challenging to decipher the importance of a distinct zeitgeber on a specific phenotype, roles for zeitgebers other than light that may impact the immune system are starting to be appreciated.

1.3 Chrono-Immunology

1.3.1 "Sleep will Heal": Immunological Memory and Immune Activity during Sleep

The sleep/wake cycle is one of the most prominent manifestations of the circadian rhythm and communicates tightly with the immune system in a bidirectional manner. Although a direct role was only shown for Interleukin (IL)-1β, Tumor Necrosis Factor (TNF)α, Interferon (IFN)γ (Krueger, 1990) and IL-6 (Späth-Schwalbe et al., 1998), pro-inflammatory cytokines are generally classified as somnogenic (reviewed in (Imeri and Opp, 2009)), and basal plasma levels of these cytokines appear higher during the rest phase.

Infection-associated sleepiness (Toth and Krueger, 1988), in conjunction with increased duration and intensity of SWS (slow-wave sleep) and decreased REM (rapid eye movement) sleep (reviewed in (Bryant et al., 2004)), have been attributed to increased pro-inflammatory cytokine plasma levels. In support of this, IL1- and TNF-receptor deficient mice display decreased baseline sleep and lack an increase in SWS and decrease in REM sleep following stimulation with IL-1 or TNF, respectively (Fang et al., 1998, Fang et al., 1997). In contrast, anti-inflammatory cytokines, such as IL-4 and IL-10, are induced after awakening (Krueger et al., 2001) and exhibit inhibitory effects on sleep (Young and Matthews, 1995). Sleep also directly regulates oscillations of an assortment of cytokines and cytokine receptors, such as IL-2 (Born et al., 1997), which can enhance proliferation of activated T-cells, and soluble IL-6 receptor (Dimitrov et al., 2006), that are both abolished in sustained wakefulness.

Equally, a collection of immuo-regulatory hormones such as renin, growth hormone and prolactin are dependent on sleep, and sleep deprivation is sufficient to abrogate daily oscillations (Dimitrov et al., 2006). Other rhythmic hormones, like melatonin and cortisol, however, do not appear to be affected by sleep directly.

Although the reason why we sleep is still largely elusive and highly investigated, its role in immune memory formation (Born et al., 2006) is generally accepted. Findings of blunted response to vaccination in humans (Lange et al., 2003) and mice (Brown et al., 1989) as a result of sleep deprivation, argue for a similar

role of sleep in immunological memory formation, which was later associated with slow-wave sleep. The early rest phase (the time when SWS is dominating) is correlated with high levels of pro-inflammatory cytokines, high growth hormone and prolactin levels and low catecholamine and cortisol levels, paralleled by a high abundance of memory cells (Dimitrov et al., 2009) in the bloodstream, providing excellent conditions for immunological memory formation. In contrast, local cytotoxic activities, in particular NK cell function, appear to be restricted to times of activity (Arjona and Sarkar, 2005), when wounding and acute pathogen exposure is more prominent.

Sleep has tremendous effects on health and wellbeing, and represents a considerable proportion of our lives. The molecular mechanism of sleep regulation is not entirely clear, however, the two-process model of sleep regulation provides a conceptual framework, which has been validated over the last decades in various experimental settings. The model describes the interaction of two processes; a Process S, a homeostatic process dependent on sleep/wake e.g. sleep debt, and a Process C, which is under circadian control. Process S declines during sleep and increases upon awakening throughout the day, with a periodicity that is entrained by the circadian pacemaker and normally correlates to day and night. As Process S reaches nadir levels, awakening is induced, and respectively, peak levels promote sleepiness. Some experimental outcomes also suggest a role for the metabolic rate in the regulation of Process S and the timing of sleep, however, this remains to tested (Borbély et al., 2016).

Immunology research has mainly focused on sleep deprivation assays, which hardly control for effects caused by other zeitgebers. In a recent study however, the effect of simulated night shift on PBMC cytokine response as well as total leukocyte number in the blood stream of human volunteers was investigated. A significant shift in the acrophase of cytokine production following inflammatory stimulation *ex vivo* was present, while abundance of $CD3^+$ and $CD14^+/CD11b^+$ cells was unaffected (Cuesta et al., 2016). This further supports a critical role for sleep in the immune response, however more detailed investigations are needed to provide insights into the mechanism and the effect of other zeitgebers, such as food, and the interaction of the molecular clock in immune

cells in this system. Immunological studies on individuals in an environment that only allows for sleep during the natural active phase or exposure of subjects to light during the inactive, and darkness in the active phase will generally be of great interest.

1.3.2 Rhythmic Cytokine Production and Cytotoxic Activities

In 1960, Halberg laid the foundation for modern chrono-immunology research by illustrating a diurnal susceptibility pattern in mice challenged with the bacterial endotoxin Lipopolysaccharide (LPS), with lethality ranging from 80% towards the end of the rest (light) phase to 20% in the middle of the active (dark) phase (Halberg et al., 1960). Even though much progress has been made and some human pathologies reported to follow similar daily rhythms, we understand little about the mechanistic basis of this significant finding.

Daily variations in the intensity of symptoms in chronic diseases like rheumatoid arthritis (RA) (Kowanko et al., 1982, Scott, 1960) and rhinitis (Trousseau, 1865, Reinberg et al., 1988) are highly prevalent and morning stiffness, as it occurs in RA patients, has been correlated with elevated pro-inflammatory cytokine production (Clarke et al., 2011). Systemic pro-inflammatory activity is basally elevated during the rest phase in healthy individuals and anti-inflammatory mediators are sharply induced upon awakening (Krueger et al., 2001) (Figure 1.3.2.1). In addition to a possible contribution from mechanical stiffness after rest, morning stiffness in RA patients may result from a hyper-inflammatory phase at night that is sustained into the awakening phase. Joint stiffness only slowly improves as activity commences and anti-inflammatory mediators reach higher systemic levels.

Whole blood stimulation with LPS *in vitro,* at night and early in the morning, displayed increased IFNγ, TNFα, IL-6, IL-1 and IL-12 production compared to stimulations during the day-time in samples that were taken hourly from healthy volunteers (Petrovsky et al., 1998). Similar results were obtained during a human *in vivo* study, where *Escherichia coli* LPS injection at mid-night resulted in increased IL-6 and TNF levels compared to infection at noon (Alamili et al., 2014). Increased cytokine production and sensitivity to cytokines (Hrushesky et

al., 1994b) was also seen in nocturnal organisms such as mice when stimulated during the inactive phase or at the transition into the active phase (Marpegan et al., 2009, Nguyen et al., 2013).

Before functional clocks in immune cells were discovered, inflammatory outputs were correlated with hormone levels to mechanistically investigate the interplay between the clock and immunity. Cortisol and melatonin both regulate immunity and their expression follows a strong diurnal pattern. Cortisol reaches peak serum levels at the beginning of the active phase and suppresses inflammation and cytokine production (Petrovsky et al., 1998). The role of melatonin in contrast appears rather diverse, as studies showing immuno-stimulatory effects of melatonin are equally abundant as reports claiming an immuno-inhibitory role. Melatonin may therefore act as an immune buffer, stimulating the immune response under basal conditions, while promoting anti-inflammatory pathways in states of inflammation (reviewed in (Carrillo-Vico and Lardone, 2013)).

The characterization of functional, cell autonomous clocks in almost every cell in the human body sparked interest in the mechanistic role of clocks in immune cells. In macrophages, inflammatory outputs such as phagocytosis, cytokine and chemokine mRNA are regulated by the cell autonomous clock and induced at various times of the day (Hayashi et al., 2007). Cytotoxic NK-cell activity is similarly dependent on the cell intrinsic clock, with TNF being rapidly induced at the beginning of the active phase, and granzyme and perforin protein levels peaking later in the active phase (Arjona and Sarkar, 2005).

Recent investigations also described a functional clock in microglia (Hayashi et al., 2007), the brains' prominent innate immune cells, which may control diurnal sickness behaviour following inflammogenic stimulation (Fonken et al., 2015). The molecular clock in microglia can be entrained by, but persist independent of corticosterone, and cytokine production by microglia basally and following inflammatory insult is similarly not dependent on corticosterone, but appears to correlate with *Per1* and *Per2* oscillation. The amplitude of these clock genes is significantly decreased in aged animals, which may in part cause increased susceptibility to inflammatory material in age subjects (Fonken et al., 2016).

The molecular clock in microglia also basally controls brain function. Cathepsin S, a lysosomal cysteine protease, is exclusively expressed in microglia within the central nervous system; and regulated by the molecular clock, cathepsin S downscales the synaptic strength during the inactive phase, which is critical to allow new information to be acquired upon awakening (Hayashi et al., 2013). Long lasting post septic cognitive and affective impairment may also be a result of microglial activation, as post septic animals display increased abundance of this cell type in the hippocampus and co-treatment with an NF-κB inhibitor attenuates many post sepsis symptoms (Anderson et al., 2015).

Besides macrophages, a molecular clock has also been described in other cells of the myeloid compartment such as dendritic cells (Silver et al., 2012a), neutrophils (Kusanagi et al., 2004, Ella et al., 2016), monocytes (Boivin et al., 2003), eosinophils and mast cells (Baumann et al., 2013), and we are only beginning to understand the consequences this has on immune function throughout the day.

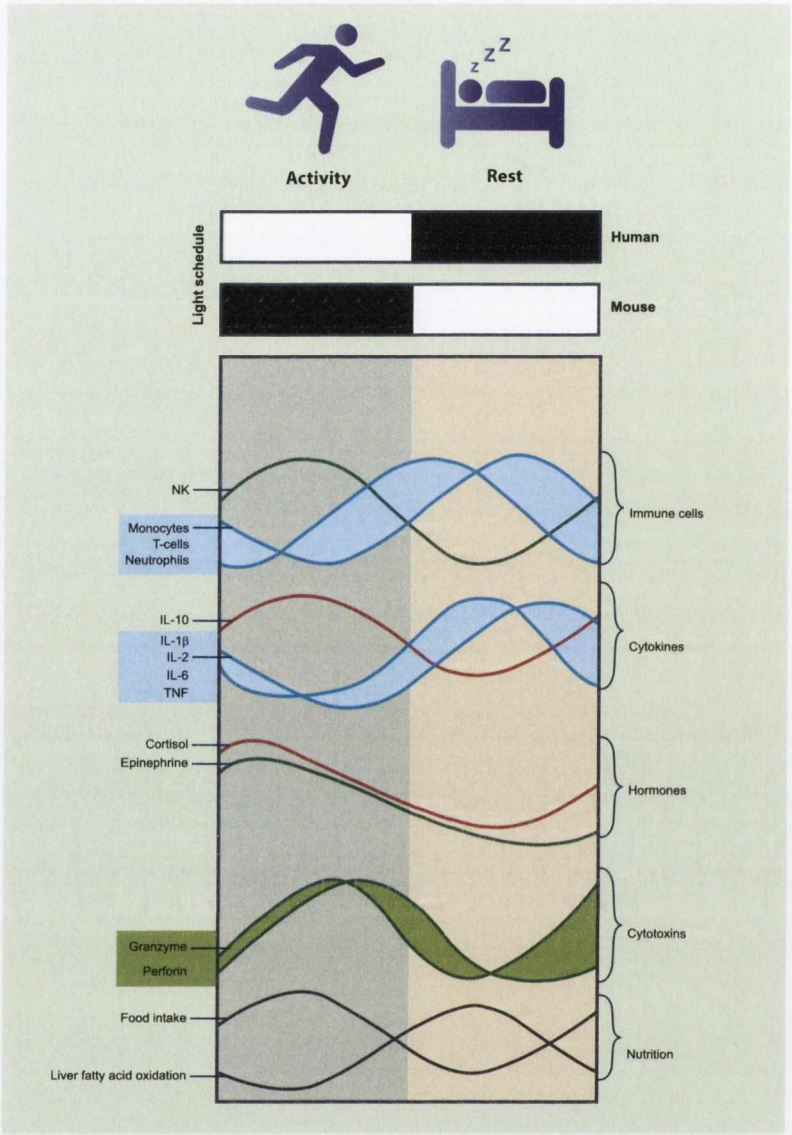


Figure 1.3.2.1 Circadian Oscillations of Immune Factors

Schematic illustration of rhythmic immunological readouts under homeostatic conditions. Activity in nocturnal mice is restricted to the dark phase (filled bar), which coincides with the rest phase of humans. A range of immunological processes oscillate similarly in mice and humans in regard to rest and activity. Memory formation and systemic inflammatory response (area between blue curves) are denoted by high blood count of neutrophils, T-cells and monocytes and increased pro-inflammatory cytokine production. Anti-inflammatory signals (red curves) such as IL-10 and cortisol peak during the active phase when local inflammation (area between green curves) - as indicated by blood abundance of NK-cells as well granzyme and perforin production and epinephrine abundance - is increased. Food intake parallels activity and delivers nutrients to support anabolic metabolism, whereas times of starvation due to inactivity generally promote catabolism as indicated by increased fatty acid oxidation in the liver.

Cytokine signalling pathways and the clock appear to reciprocally regulate each other. For example, pro-inflammatory signalling triggered by TNF is intensified in *Cry* mutants via the regulation of GSK3β (Glycogen Synthase Kinase 3 Beta) dephosphorylation and subsequent NF-κB (Nuclear Factor Of Kappa Light Polypeptide Gene Enhancer In B-Cells) induction (Lee and Sancar, 2011). Upon engagement of TNF with TNF receptor 1, the negative arm of the molecular clock (*Per1/2*, *Cry1*) is induced in a P38-MAPK (Mitogen-Activated Protein Kinase) dependent fashion (Petrzilka et al., 2009) and in the absence of the central clock machinery, NF-κB-mediated transcription is up-regulated, thereby reinforcing the inflammatory response (Spengler et al., 2012). Interestingly, when the CLOCK protein is not occupied in a BMAL1 dimer to induce E-box driven transcription, CLOCK can form a complex with p65 and promote its acetylation, possibly by the recruitment of histone acetyltransferases (HATs). Surprisingly, CLOCK, despite exhibiting intrinsic (HAT) activity, does not appear to convey p65 acetylation itself. The transcriptional transactivation capacity of CLOCK on E-boxes is similarly not critical in the induction of NFκB target genes, exemplifying the functional diversity of this protein (Spengler et al., 2012).

In addition to the direct influence of the circadian clock cycle on immune cell gene expression and function, a role for core clock components exists independently of a functional clock. *Rev-erbα* deficiency for example abrogates rhythmic cytokine response in macrophages, particularly IL-6 production, while a functional clock is sustained (Gibbs et al., 2012). However, silencing of *Cry2* also induces IL-6 expression (Hoffman et al., 2009), arguing for *Rev-erbα* not being exclusively responsible for rhythmic IL-6 regulation. Discrimination and attribution of phenotypes to single clock components is not always possible, and can be confounded by the effects of deletion of core clock elements such as *BMAL1*, which result in a complete collapse of the cellular clock. However, it is clear that the entity of a functional clock and its constituents are critical for immune-balance.

The intensity of cytokine production upon stimulation appears to sustain rhythmicity in constant darkness, illustrating that indeed the rhythms in cytokine production are due to the endogenous clock and can therefore be termed

circadian (Gibbs et al., 2012, Adams et al., 2013). However, rhythmicity in survival in response to LPS could not be observed under these conditions (Marpegan et al., 2009). As only two time points were investigated, this may however be due to a shifted response in constant darkness. Locomotor activity in both, LD and DD mice, following LPS stimulation is initially abrogated, however, phase, amplitude and period of locomotor and temperature rhythms rebound to pre-LPS levels after approximately 3 days. This suggests that a functional clock is sustained following LPS stimulation in constant darkness, and therefore argues against the possibility of LPS leading to internal desynchrony and a dampened response under free running conditions (Marpegan et al., 2009). The correlation of cytokine production and mortality the authors made for LD, however appears not to hold true for DD conditions and raises the question to what extend investigations concerning cytokine production can be used to dissect the molecular mechanism of diurnal LPS induced mortality.

It should be noted that the majority of studies investigating diurnal rhythms in susceptibility to infection are very consistent with regard to an observed trough in survival during the late rest phase across a range of different protocols using TNF (Hrushesky et al., 1994a) and LPS in BALB/c mice (Halberg et al., 1960) to Coxsackie B3 infection in CD-1 mice (Feigin R. D, 1972). Persistence of circadian rhythms without appropriate cues, like light (free running conditions), that are necessary to classify rhythmic oscillations as circadian or diurnal, has not been tested. In contrast, bacterial burden and pro-inflammatory response are heightened following *Salmonella* infection at the beginning of the rest phase as compared to infections during the early active phase (Bellet et al., 2013). Considering other comparable studies mentioned above, it appears that the interplay of bacterial burden and cytokine response is greatly affected by the route, dose and type of the pathogen that is administered; however, what is consistent is that time of day variation always exist.

Besides cytokine regulation, toll-like receptors such as TLR9 and accordingly TLR9-mediated responsiveness to CpG Oligodeoxynucleotide adjuvanted vaccination in miche, display daily variations with peak values during the active phase (Silver et al., 2012b). In humans, morning vaccination displayed

enhanced antibody response over afternoon vaccination in a cluster-randomized study (Long et al., 2016). ZAP70 (Zeta-Chain Associated Protein Kinase 70kDa) is another immune-regulator that is rhythmically expressed under physiological and inflammatory conditions, which mediates increased T-cell proliferation upon T-cell receptor stimulation in the organism's inactive phase (Fortier et al., 2011).

Inflammation is tightly regulated and while we do not fully understand why and how immune function displays such strong diurnal variation, a more systemic, pro-inflammatory response during the inactive phase that allows immunological memory formation, and a generally anti-inflammatory state during the active phase that promotes a local immune response in case of pathogen exposure, for example as a result of wounding, has been described (reviewed in (Lange et al., 2010))(Figure 1.3.2.1).

1.3.3 Shift work

Around 20% of the working population is subject to some sort of shift work, including permanent or alternating shifts, or frequent transmeridian travel, and only 13% of day-time workers do not report social jetlag, a milder but chronic form of shift work (Roenneberg et al., 2012). A multitude of epidemiological studies identified increased risk in the development of metabolic and coronary diseases as well as cancer and inflammatory diseases in cohorts with different types of internal clock desynchronization (Wyse et al., 2017, Esquirol et al., 2011, Pietroiusti et al., 2006, Hedstrom et al., 2011). The underlying mechanism is however less well defined and is focus of multiple in field studies as well as in more artificial laboratory settings. A great challenge investigating the effect of shift work is that the type of work and the exact schedule vastly impact the internal state of a subject (Haus and Smolensky, 2013).

Transmeridian travel results in a phase shift of all zeitgebers, from light to social cues and as the central clock in the brain appears to adapt relatively rapid to new light schedules, peripheral clocks are generally slower, causing a transient state of internal desynchrony (Reppert and Weaver, 2002). In the setting of

night shift work, the environment continues to oscillate in the habitual way, however, the sleep wake pattern is shifted to times that are in disagreement with the natural rhythm.

Interestingly, the majority of shift workers do not phase shift their circadian rhythm (Dumont et al., 2001), and the duration of night-shift thereby appears to correlate with the intensity of phase modulation. Short rotations (3-4 days) widely maintain day-time oriented patterns, while weekly rotations more often induce phase shifts without reaching full phase adaptation to the new night oriented routine (Haus and Smolensky, 2006), and it is now becoming clear that misalignment of peripheral and central clocks is critically involved in conveying the adverse effects in health and wellbeing that are observed in individuals with a non day-centric and irregular work schedule (Reutrakul and Knutson, 2015, Videnovic and Zee, 2015, Martino et al., 2008).

Shift work seems inevitable in industrialized society and is likely to further increase in the future. A more complete understanding of the molecular consequences that accompany these work settings may allow identification of more suitable work schedules and possibly targets to counteract the development of associated diseases (Haus and Smolensky, 2006) and is therefore of great interest to improve public health.

1.4 The Role of Chrono-Nutrition

Recently, interest in the effects of metabolism on immunity has flourished and provided a new level of understanding regarding the role of the Warburg effect in immune cell function. Warburg's initial observation (Warburg, 1956) of a shift from oxidative phosphorylation towards increased levels of glycolysis in tumor cells has been linked to a pro-inflammatory state of immune cells in multiple systems (Krawczyk et al., 2010). Whether immune cell metabolism can be influenced via nutritional signals is not yet clear, however specific diets, such as high fat, or ketogenic diets, have been reported to modulate the immune response (Youm et al., 2015, Calder, 1998).

Obesity is highly prevalent and promotes inflammatory diseases including type-2 diabetes and certain forms of cancer, and control of weight is central in disease prevention. Recently, a critical role for timed food intake in terms of duration and solar time in the development of obesity has been identified. Restriction of food availability to 8 hours during the active phase prevents weight gain compared to *ad libitum* feeding, although caloric intake is sustained (Hatori et al., 2012), and even food restriction to the inactive phase limits weight gain compared to *ad libitum* feeding on a high fat diet (HFD) (Paschos et al., 2012). Locomotor and feeding activity on HFD are additionally blunted, promoting increased food intake during the inactive phase and subsequent progression of metabolic disease (Kohsaka et al., 2007).

Food restriction to the inactive phase in mice and rats rapidly shifts the clock in liver and a collection of other peripheral tissues by 12 h, while SCN clocks remain unaffected (Damiola et al., 2000, Stokkan et al., 2001). Even gradual changes in the light schedule are ineffective to re-synchronize food entrained clocks in peripheral organs to the light rather than the feeding schedule (Hara et al., 2001). However, liver entrainment to food signals is accelerated in mice with surgically lesioned SCNs, pointing at a role of the master pacemaker in the brain under homeostatic conditions that is subordinate to nutritional signals in a collection of organs, possibly via glucocorticoid signalling (Balsalobre et al., 2000, Le Minh et al., 2001).

Similar to the light entrained master regulator (LEMR) in the SCN, a food entrained master regulator (FEMR) has been proposed to regulate food entrained oscillators (FEO), such as food anticipatory activity (FAA) (Figure 1.3.3.1). FAA is characterized by elevated hormone levels (e.g. the glucocorticoid corticosterone and ghrelin (Patton et al., 2014)) and increased core body temperature, and is sustained under temporal food restriction even in BMAL1-deficient and SCN-lesioned mice (Pendergast et al., 2009). The location and the mechanism by which FEMR is entrained by food stimuli and how it subsequently regulates subordinate, peripheral tissues is however unknown.

Like most cells in the body, intestinal cells possess functional clocks (REF Froy and Chapnik) and paralleling the movement of digested food, the phases of clock gene expression varies along the cranio-caudal axes of the gut (Polidarova et al., 2009). The intestinal microbiome has also recently been shown to oscillate in the course of a day (Thaiss et al., 2014), however it appears that not the cellular clocks of the host cells, but rather food intake *per se* controls the host's microbiome composition. The impact of the microbiome on general health and wellbeing is well documented, and it may be reasonable to speculate that food intake could control immune function via multiple cues, one of them targeting the microbiome and the metabolites they produce.

Consideration should also be given to sleep, which indirectly navigates metabolism via the release of mediators like growth hormone, which induces the liberation of glucose and free fatty acids. Further, the expression of glucose transporters oscillates over the course of a day (Tavakkolizadeh et al., 2005, Houghton et al., 2008) in a food dependent manner (Pan et al., 2004), providing an additional layer in the regulation of glucose homeostasis and pathways that are glucose dependent. Metabolic cues also regulate the abundance of NAD^+ and $NADP^+$, both of which strongly inhibit the interaction of CLOCK and NPAS2 with E-box elements (Rutter et al., 2001), and metabolites and nutrient sensors similarly present clock regulatory functions. As such, AMPK, which is activated at times of low nutrient abundance, phosphorylates and destabilizes CRY1 (Lamia et al., 2008), and glucose activates the circadian oscillator in fibroblasts via inhibition of *Per2* expression (Hirota et al., 2002). In the liver, rapidly

digested starch induces high *Per2* expression via rapidly elevated blood glucose levels and subsequent insulin production.
Surprisingly, circadian rhythms - in contrast to former beliefs - not necessarily require the classical transcriptional-translational feedback loops as redox systems also display 24 h rhythmicity even in the absence of transcriptional activity (O'Neill and Reddy, 2011). These redox cycles are sensitive to metabolic cues and may consolidate some food regulated phenotypes independently of the molecular clock. As the composition of food by itself differentially affects the ability to entrain the clock (Hirao et al., 2009, Oike et al., 2010, Oishi et al., 2009, Oike, 2017), dissecting how certain nutrients can modulate the clock may further provide new mechanistic insights of food entrainment. For an in depth review about chrono-nutrition please refer to Tahara and Shibata (Tahara and Shibata, 2013).

Based on current knowledge, it appears that food is a strong zeitgeber, with the ability to shift clock gene expression in a variety of peripheral tissues (Damiola et al., 2000, Stokkan et al., 2001, Hara et al., 2001). Temporal food restriction allows robust entrainment of cellular clocks, and even though misalignment between the master and food entrained clocks has disadvantageous effects on metabolic homeostasis, it appears that complete loss of rhythmicity in FEOs, via unrestricted, *ad libitum* feeding, intensifies metabolic pathology (Paschos et al., 2012). HFD additionally consolidates food intake during the inactive phase, eventually causing loss of FEO rhythmicity. This has significant implications in the prevention and therapy of metabolic diseases and cancer caused by shift work and diet-induced obesity, and it will be of particular interest to investigate whether timed food intake may affect weight loss on non-HFD in obese individuals. Shift work, in particular night shift work or rotating shifts, induce chronic clock disruption and internal desynchrony, and is associated with increased risk of infectious disease (Mohren et al., 2002), metabolic syndrome (Karlsson et al., 2001), which subsequently promotes diabetes (Pan et al., 2011) and cardiovascular disease. It is not known whether this is due to misaligned clocks or is mainly a result of inappropriate mealtimes and requires further investigation. Strikingly, restriction of mealtimes to 4 h during the inactive

phase significantly reduced cancer growth by 40% in mice under normal and hight fat diet, suggesting that modulation of feeding time dependent pathways could be a supportive strategy in cancer therapy and a possibly for prevention in individuals at risk (Li 2010).

It is of great interest to locate and characterize the proposed food entrained master regulator to provide the tools needed to perform detailed studies of the entrainment and sustained rhythmicity of food entrained oscillators using conditional mutations. However, this is a challenging undertaking considering sustained food entrainable rhythmicity in *Bmal1*-deficient mice and the fact that food can only be deprived for a relatively short period of time.

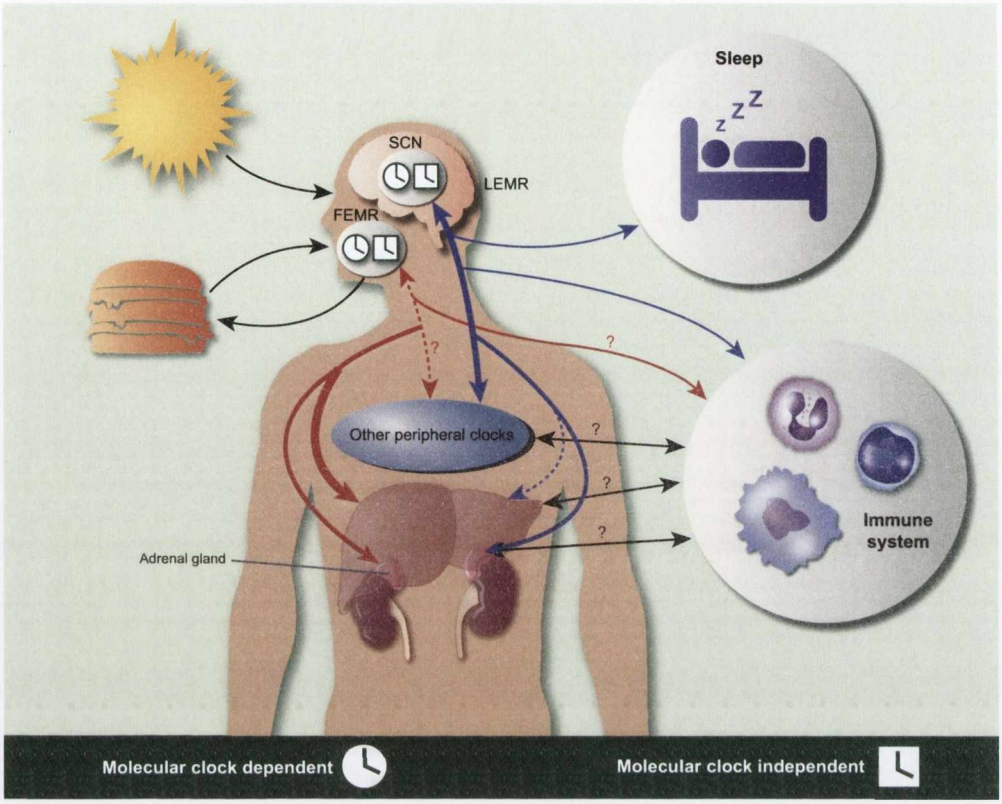


Figure 1.3.3.1 The Body Clock

Zeitgeber, such as food and light, entrain master regulators, which communicate with peripheral clocks in a bidirectional fashion to sustain clock alignment. Light stimuli are processed in the light entrained master regulator (LEMR) in the suprachiasmatic nucleus (SCN), whereas food signals are conveyed to the food entrained master regulator (FEMR), whose location is not yet known. LEMR regulates sleep and immune response, as well as other peripheral clocks (blue arrows). FEMR strongly controls the liver clock among others (red arrows). The question marks indicate a proposed, but not yet proven interplay and the black arrows represent general crosstalk. Round clocks indicate cellular clock involvement, whereas rectangular clock symbols reference a system that is independent of the molecular clock.

1.5 Research Models used Throughout our Studies

1.5.1 Serum Shock

On their quest to discover the signal that possibly resets the phase in peripheral tissues, Balsalobre and colleagues (Balsalobre et al., 1998) found that serum could synchronize the cell autonomous clock *in vitro*. Using high concentrations of horse serum for two hours, followed by serum deprivation, they were able to demonstrate that cells cultured for years still possessed a functional clock that could induce oscillations in gene expression upon serum shock. This introduced the possibility to use tissue culture cells to investigate the circadian clock and became one of the most widely used tools in *in vitro* circadian research. Investigations to determine the molecular mechanism by which the serum shock model induced synchrony in cells, identified a possible role for glucocorticoids (Balsalobre et al., 2000). These hormones are highly abundant in serum and were known to fluctuate over the course of a day (Tronche et al., 1998). As a consequence, a second synchronization method emerged which involved stimulation of cells with the artificial glucocorticoid dexamethasone (Nagoshi et al., 2004).

1.5.2 Entrainment

Modification of an animals' environment allows to investigate certain aspects of the circadian system without the immediate need for genetic models. As such, light and food entrained cues can be rather easily discriminated by maintaining a regular 12:12 Light:Dark regiment, but restricting access to food to either the light or the dark phase (Damiola et al., 2000). As mice are naturally nocturnal and therefore predominantly eat at night, the night-time fed group in a time restricted feeding model serves as the control group. In circadian biology, the time of the day is generally indicated as Zeitgeber Time (ZT) 0-24. ZT0 thereby refers to the time the light phase is initiated, and ZT12 indicates the beginning of the dark phase (lights off). While light dependent phenotypes are expected to follow the light cycle independent of the feeding schedule, day-time feeding will

reverse (phase shift by 12 h) oscillations of food regulated phenotypes. As daytime feeding may evoke a discrepancy between food and light entrained oscillators, reversed feeding may not simply cause a phenotype to be antiphasic, but may affect the phenotype beyond that, and has to be accounted for.

In this work a model of constant light was implemented to overcome this concern. According to early studies by Aschoff (Pittendrigh, 1960), constant light in diurnal subjects causes a phase delay in locomotor activity, and respectively a phase advance in nocturnal creatures. Many labs have recapitulated this observation, generally known as 'Aschoff's rule'. Besides this, a 'split' phenotype in which the animals' behavioural rhythm is split into two bouts of activity as well as complete loss of locomotor rhythmicity has been seen. In a study from 2005, the McMahon lab discovered that oscillations in single SCN neurons were sustained under constant light conditions, however the orchestration of all the neurons within the nuclei was different between mice that showed locomotor rhythmicity with a prolonged period, mice that were arrhythmic, or mice that displayed a split phenotype. While neurons within both nuclei from arrhythmic animals were almost entirely out of synchrony, their phase was widely aligned in mice with sustained rhythmicity. Remarkably, neurons within each nucleus were synchronized in 'split' animals, however, the two nuclei were phase shifted by 12 h (Ohta et al., 2005).

The prolonged phase seen in some of the animals is potentially due to disrupted degradation of PER2 protein, and enhancement of the phase-delaying limp of the molecular clock (Munoz et al., 2005). Surprisingly, *Per2/Cry1* double knockout mice, which are arrhythmic in constant darkness (DD), become rhythmic regarding locomotor activity, as well as *Per1* and *Bmal1* expression in SCN and periphery under constant light (LL) conditions. These animals further display - in contrast to what Aschoff's rule would suggest - shortened period lengths (Abraham et al., 2006), possibly underpinning the previously argued role for continuously elevated PER2 protein levels in conveying phase elongation.

It is yet unclear why animals present these three different phenotypes with a seemingly random pattern. It does appear however that stronger light intensity in the range of 300 to 500 lux results in greater proportions of arrhythmic

locomotor activity (Chen et al., 2008). Strikingly, using an in vivo PER2:LUC visualization system, it appears that constant illumination causes a dampened amplitude and phase distribution in peripheral tissues independently of the animals' locomotor activity (Hamaguchi et al., 2015). qPCR studies have generated similar results in which - dependent on the specific gene - the amplitude of clock gene oscillations in peripheral tissues such as the liver, was significantly decreased, often resulting in completely ablated rhythmicity (Polidarova et al., 2011).

While the model of constant light is debatable and can result in many different phenotypes, some of the here presented work implemented constant illumination of high intensity (~300 lux) to generate mice with significantly impaired oscillations in most peripheral tissues. These studies should however be regarded as preliminary as only two time points were studied, which does not allow discrimination between phase delays and lack of oscillation. Recording the locomotor activity of animals could further be used to identify animals that displayed arrhythmic locomotor activity to facilitate interpretation. In the herein presented preliminary studies, recording of locomotor activity could however not be realized. In concordance with comparable studies, while being aware of the limitations, constant light in this work was used to render animals arrhythmic behaviourally as well as molecular, causing clock disruption without perturbing functionality of the clock *per se* (Ohta et al., 2005). This allowed subsequent introduction of time restricted feeding (Hamaguchi et al., 2015), thereby restoring rhythmicity only in tissues that are entirely dependent on the feeding regiment (Polidarova et al., 2011).

Of note is the 12:12 feeding schedule that was used throughout the study. While this is in concordance with the first study that identified a reversed clock oscillation in the liver upon time restricted feeding (Damiola et al., 2000), a 4 h feeding interval starting 2-6 h post onset of illumination has been the widely used in the majority of following studies (Stokkan et al., 2001). As food availability had to be manually regulated in most experiments, a 12:12 was preferred over the 4 h regime for practical reasons. Further, this setup better simulates conditions in shift workers, a population that is generally know to be at high risk of developing inflammatory diseases possibly due to clock

desynchronization. As this study was intended to lay the groundwork for investigations on how to help improve and treat inflammatory diseases in individuals at risk, the 12 h food deprivation regime to widely mimic daily habits of night shift workers appeared to be the most appropriate.

1.5.3 Selection of Time Points

Phenotypes throughout the here presented study were often tested solely at ZT0 and ZT12, as the times of peak and trough expression of the core clock gene *Bmal1*. These time points have previously been shown to result in contrasting inflammatory responses in multiple studies (Halberg et al., 1960, Gibbs et al., 2012, Curtis et al., 2015, Hrushesky et al., 1994a), and are known to be the transcriptional "rush hours" (Zhang et al., 2014) which frequently correspond to distinct diurnal phenotypes. A full time course would however be advantageous to experimentally define peak and nadir times.

Further, a lack of difference between two time points may not necessarily be interpreted as evidence for the absence of rhythmicity, as a 6 h shift in the oscillation could similarly result in comparable values at ZT0 and ZT12 (Figure 1.5.3.1). In some of the herein presented studies more time-points were included to overcome this concern. Due to limitations in the accessibility of mice during the dark phase, time-points between ZT12 and ZT0 were less frequently included, and such experiments had to be performed in facilities that were fitted with red lights in corridors as well as mouse holding and procedure rooms to ensure preservation against any light stimulation These setting were not readily available in the majority of animal facilities, and dark phase samples could therefore not always be included.

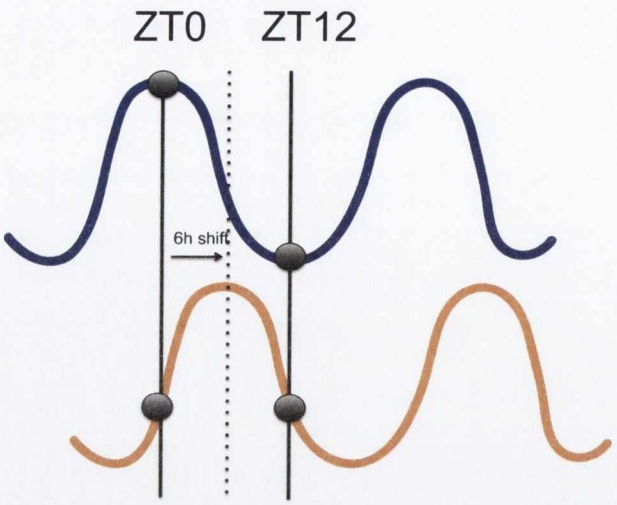


Figure 1.5.3.1: A phase shift can falsely be interpreted as absence of oscillation when only two time-points are being used.

An observed oscillation with peak and nadir times at ZT0 and ZT12 (blue curve) may shift due to experimental alteration of the system and can thereby result in delayed peak and trough times (orange curve). Sampling at ZT0 and ZT12 would therefore result in similar values and may be misinterpreted as constitutive. More frequent sampling would overcome this concern.

1.5.4 Models of Lethality

Chrono-Immunology centres around the observation of rhythmic mortality following LPS stimulation, which was initially made in 1960 (Halberg et al., 1960). Death as an endpoint in a mouse study is generally not acceptable from an ethics standpoint, but as lethality studies to investigate the signal responsible for this phenotype were absolutely necessary, a scoring system was constructed to predict mortality before death occurred (the materials and methods section includes the full list and scoring system). While this was appropriate, a marker to objectively predict mortality was desirable to further reduce the use of animals. Currently, there is no serum factor described that indicates mortality that is generally accepted and is standardly used (Marshall et al., 2009). However, some studies suggest IL-6, and liver enzymes liberated to the serum, to exert these functions in models of sepsis (Damas et al., 1992).

1.6 Aims

It is clear that immunity oscillates over the course of a day, and much progress has been made identifying mechanisms by which the circadian system regulates certain pathways that are being activated in the course of an immune response. However, the interplay of the circadian and the immune system is still widely unknown. In this study we aimed to investigate two aspects to improve our understanding of this crosstalk.

- Macrophages are the first responders following an immunological insult and are critical for mounting an appropriate immune response. Much research has therefore centred on the circadian control of these cells, reporting daily oscillations in trafficking as well as cytokine response. As particle uptake generally involves receptors that can trigger pro-inflammatory signalling as well as internalization, we aimed to examine a role for rhythmic particle uptake in the regulation of downstream inflammatory signalling. In this study, we intended to test diurnal particle ingestion by peritoneal macrophages in an *ex vivo* model, and continue mechanistic investigations regarding the exact role of the molecular clock and the receptors involved before examining these findings in an *in vivo* environment.

- In a second study we addressed a more fundamental aspect of the immune and the circadian crosstalk. The role of metabolism in immunity has garnered much attention over the past decade, however, the implication of rhythmic metabolism in regulating daily oscillations in the immune response have not been investigated. This study aimed to test the effects of rhythmic food ingestion on daily oscillations in immunity and to phenotypically describe consequences of artificial feeding cycles in homeostasis and disease. We intended to extend these preliminary investigations to further characterize the underlying mechanism using a selection of genetic and entrainment models.

This is the first report examining the role of melatonin-independent diurnal particle ingestion and the influence of the feeding cycle in daily oscillations in the immune response. The findings made in the process of these investigations have the potential to have far reaching consequences in the field of chrono-immunology, as well as therapeutic implications, but will certainly complement the current body of knowledge and provide the basis for future studies.

2 Materials and Methods

2.1 Mice

2.1.1 Bmal1 LyzM-Cre colony

Bmal1 floxed animals (B6.129S4(Cg)Arntl^{tm1Weit}/J stock number 007668) and LyzM-Cre mice (B6.129P2-Lyz2$^{tm1(cre)Ifo}$/J stock number 004781) have been purchased from the Jackson laboratory on C57Black6J background and have been intercrossed to generate BMAL1$^{fl/fl}$LyzM-Cre$^{+/+}$, which lack the *Bmal1* gene in the myeloid lineage, and BMAL1$^{fl/fl}$LyzM-Cre$^{-/-}$ that served as control mice with an intact *Bmal1* gene in all cell types.

2.1.2 Cd36 knockout colony

A breeder pair of Cd36 knockout mice (B6.129S1-Cd36^{tm1Mfe}/J stock number 019006) was obtained from the Jackson laboratory and experimental mice were generated in house. Wild type control mice (C57BL/6J stock number 000664) were purchased from the Jackson laboratory.

2.1.3 WT C57bl6/J mice

Wild type (WT) C57 black 6/J (C57BL/6J stock number 000664) mice were purchased from the Jackson laboratory.

2.2 Animal entrainment schedules and *in vivo* protocols

2.2.1 General animal holding

Animals at 9-13 weeks of age were housed in 12h:12h light:dark conditions (~70 Lux at times of illumination if not indicated otherwise) at least one week prior to use, in rooms accessible under red lights during the dark period. Studies presented in the first results chapter were conducted using male and female mice. No difference was apparent between sexes. In the second part of

this study (TRF study) only female mice were used to facilitate blinding. Whether sex differences are present in these experimental models awaits further investigation.

To control for technical variation, some experiments in which time-points that were 12 h apart were compared, a reverse-light-room was used. The light schedule in this room was anti-phasic to the regular mouse holding room, allowing ZT0 vs. ZT12 experiments to be performed simultaneously (e.g. lights off in the regular room = lights on in the reverse room). Mice were acclimatized for at least 3 weeks in the reverse-light-room before they participated in any study to allow full recovery of the circadian clock.

2.2.2 Time restricted feeding (TRF)

Mice were housed in a 12:12 light:dark environment on ad libitum feeding for at least one week, before food was restricted to either the light or the dark phase (Damiola et al., 2000) for 5 days if not specified otherwise. On day 5, mice were either stimulated or euthanized for tissue collection at ZT0 or ZT12.

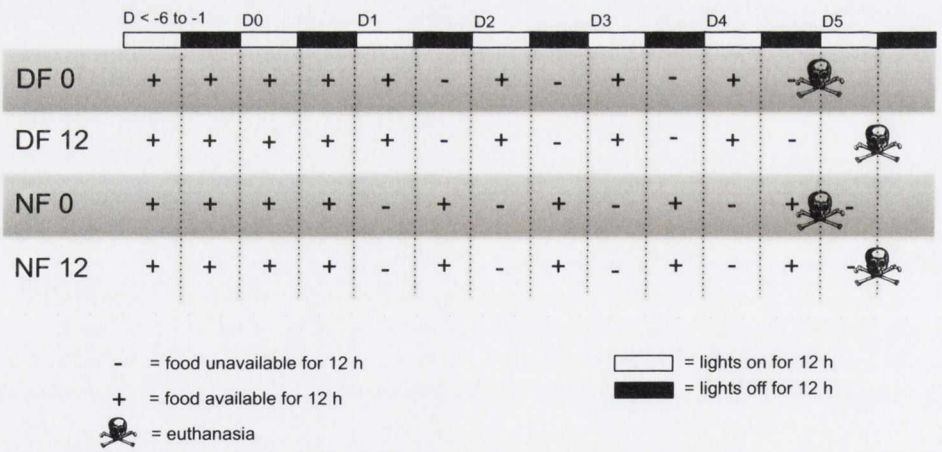


Figure 2.2.2.1: Time restricted feeding schedule.

Food availability of day-time fed (DF) and night-time fed (NF) mice on regular TRF before euthanasia at ZT0 or ZT12 on day 5.

2.2.3 Time restricted feeding in Constant light

To disrupt the light entrained clock, mice were fed ad libitum and housed in constant light (~300 Lux) for 7 days after being housed in 12:12 LD conditions with illumination times from 7AM to 7PM. Following 7 days of constant light, mice received food solely from 7AM to 7PM (DF group), or from 7PM to 7AM (NF group) while they remained in constant light for an additional 5 days. Mice were then sacrificed at the transition of feeding or fasting periods (7AM or 7PM) and tissues were collected for analysis.

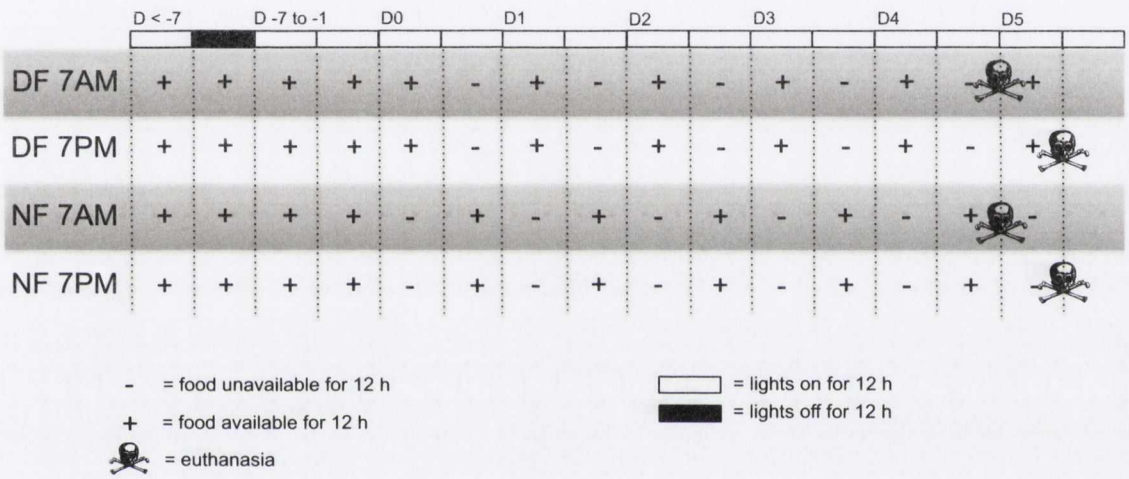


Figure 2.2.3.1: Feeding schedule of TRF in constant light.

Mice were housed in constant light for a total of 12 days. On day 8 of constant light TRF was introduced for 5 days. Mice were euthanized at 7AM or 7PM on day 5 of the TRF.

2.2.4 LPS mortality

Mice were acclimatized to the time restricted feeding schedule as outlined above. 24 h before the subjects received an intra peritoneal injection of 20 mg/kg LPS (Sigma, Cat# L2630 Lot# 014M4018V), serum was collected via the submandibular route for baseline level determination. Following stimulation, mice either continued the restricted feeding schedule, or received ad libitum feeding which allowed randomized allocation to holding cages and blinded scoring. 6 h post injection a second submandibular bleed was performed for serum collection. Mice were euthanized upon a cumulative score of 8 or a score

of 3 in any category and the time-point of death was recorded. The scoring sheet is outlined below. LPS was sonicated for 5 min prior to preparation in sterile PBS to guarantee a homogenous solution.

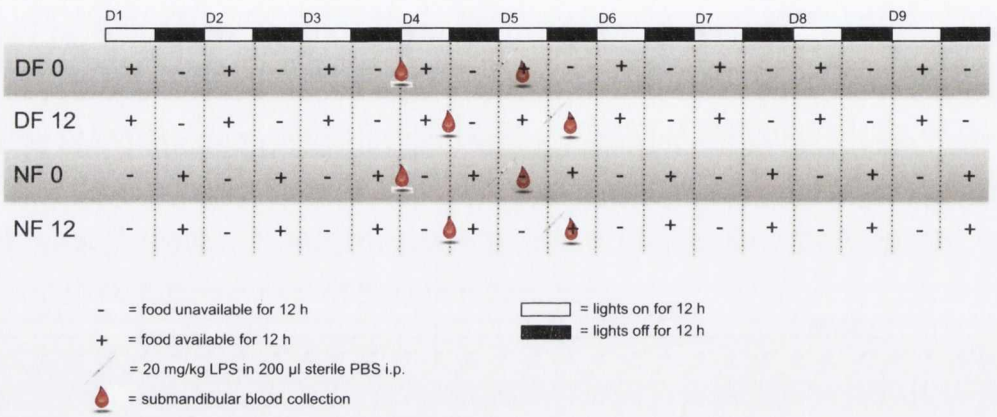


Figure 2.2.4.1: LPS mortality schedule with continued TRF post stimulation.

Food availability was restricted under regular light schedules for 5 days before stimulation with 20 mg/kg LPS i.p. at ZT0 or ZT12. 24 h prior to stimulation one submandibular bleed was performed. TRF was continued post stimulation until euthanasia.

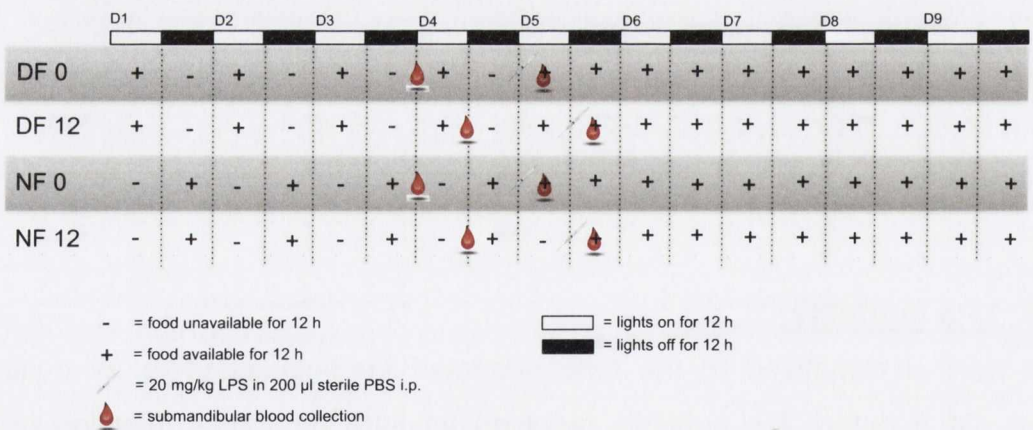


Figure 2.2.4.2: LPS mortality schedule with ad libitum feeding post stimulation.

Food availability was restricted for 5 days under regular light schedules before stimulation with 20 mg/kg LPS i.p. at ZT0 or ZT12. 24 h prior to stimulation one submandibular bleed was performed. Post stimulation access to food was not restricted.

Body Weight Changes	
0	Normal
1	7-15 percent weight loss
2	15-20 percent weight loss
3	> 20 percent weight loss
Physical Appearance	
0	Normal
1	Lack of grooming
2	Rough coat
3	Eyes closed or milky with a rough coat
Measurable Clinical Signs	
0	Normal
1	Vertigo (cannot balance on edge of cage)
2	No grip (falls into cage when hung on edge of cage)
3	Unable to right itself when placed on back (or needs >10 sec)
Unprovoked Behavior	
0	Normal amount of activity. Mouse is any of: eating, drinking, climbing, running, fighting
1	Slightly suppressed activity. Mouse is moving around bottom of cage
2	Suppressed activity. Mouse is mainly stationary
3	Unsolicited vocalizations, self-mutilation, either very restless or immobile
Behavioral Responses to External Stimuli	
0	Mouse responds immediately to touch
1	Strong to moderate response to touch (moves to escape
2	Mild response to touch (no locomotion)
3	Stationary when stimulated (no response)

Figure 2.2.4.3: Mortality study scoring sheet.

Mice were continuously scored and euthanized upon a cumulative score of 8, or a score of 3 in any category.

2.2.5 CLAMS, Comprehensive Lab Animal Monitoring System

The CLAMS (Columbus Instruments) is an enclosed animal holding system that allows measurement of various metabolic parameters such as oxygen consumption, carbon dioxide production, locomotor activity as measured by beam breaks in all three dimensions, and food consumption. Food access as well as timing and duration of the light phase can also be regulated and adapted to experimental requirements. Up to 12 mice are single housed and data is acquired from each individual separately. The ratio of oxygen consumption to carbon dioxide production is referred to as the respiratory exchange ratio (RER) and is an indication of the energy source that is used by the animal. An RER of 1 is indicative of a glucose centric metabolism, while a value of 0.7 points towards fatty acid oxidation.

EchoMRI was performed by facility staff as part of selected CLAMS studies prior and post housing in metabolic cages to record possible changes in lean and fat mass.

2.3 Primary cell isolation and cell culture

2.3.1 Peritoneal lavage

Mice were euthanized and decapitated at the indicated time points. After skinning of the abdomen to expose the peritoneum, 5 ml of ice-cold PBS, together with 1 ml of air were rapidly injected into the peritoneum with a G21 needle. Then, the liquid was retrieved back to the needle and the cell suspension was kept on ice until it was spun down 5 min at 2000 rpm at 4˚C. The cell pellet, which contained mainly B-cells and macrophages was then used for further applications.

2.3.2 Magnetic Purification of Peritoneal Macrophages

Macrophages were isolated from the peritoneal lavage by negative magnetic isolation, using the EasySep system. To ensure the shortest possible purification times, Mouse Streptavidin Rapidspheres were used in conjunction

with a custom selection cocktail. The peritoneal cells were pelleted at 2000 rpm for 5 min at 4˚C and subsequently resuspended in 100 µl PBS in a polystyrene FACS tube. Unspecific binding was prevented using 2.5 µl Fc-block (1.2 mg/ml) for 5 min prior to incubation with biotinylated antibodies directed against B-cell (CD19 & B220, 0.5 µg), T-cell (Thy1.2, 1 µg) and erythrocyte (TER119, 1 µg) surface marker for 10 min. The magnetic Rapidspheres were vortexed 1 min before 1.5 µl were added to the isolation mix for 2.5 min. The reaction was resuspended in 2.5 ml PBS and inserted into a purple EasySep magnet for an additional 2.5 min before the purified macrophage suspension was carefully decanted into a new tube. To ensure homogenous distribution, the reaction was vigorously mixed after every addition of reagents.

2.3.3 Bone marrow derived macrophages

Mice were sacrificed using CO_2 and the rear leg bones were dispensed from surrounding tissue. The bone marrow was flushed into a 50 ml Falcon using a G25 needle until the bone appeared white. The cell suspension was centrifuged for 5 min at 1500 rpm and the cell pellet was dislocated by pulling the tube over a grid. Red blood cells were lysed during a 3 min incubation in 3 ml ACK Lysis buffer. 17 ml DMEM were added to stop the reaction and the suspension was strained through a 100 µm cell strainer and subsequently pelleted by centrifugation for 5 min at 1500 rpm. The cell pellet was dislocated and resuspended in 30 ml DMEM supplemented with 1% Pen/Strep, 10% FCS and 20% L929 conditioned medium and distributed to three 10 cm Petri-Dishes to be differentiated for 7 days at 37˚C, 5% CO2 in a tissue culture incubator. On day 4, 1 ml L929 conditioned medium was added to each plate. On day 7, the cells were washed with 5 ml PBS before they were scraped in 5 ml ice-cold PBS from the culture plate using a cell scraper and transferred into a Falcon tube. After centrifugation for 5 min at 1500 rpm, the cell pellet was dislocated and resuspended to 1 million cells per ml in 1% Pen/Strep, 10% FCS and 10% L929 conditioned medium and plated into experimental plates for usage on day 8.

2.3.4 L929 conditioned medium

L929 cells were cultured in filtered, PenStrep (1%) and FCS (10%) supplemented RPMI until confluency, before they were replated at 0.5 x 10^6 cells/ml to grow for 7 days in tissue culture flasks. The supernatant was then filtered and stored at -20˚C until use.

2.3.5 Immortalized BMDMs

Immortalized BMDMs were cultured in DMEM supplemented with 10% FCS and 1% PenStrep in tissue culture flasks. Confluent flasks were gently washed with warm PBS to remove floating dead cells before trypsin was added for cell detachment. iBMDMs were then spun at 1500 rpm for 5 min and resuspended in fresh culture medium and replated at the desired concentration.

2.3.6 Serum Shock

Cells were plated at the desired concentration in the appropriate medium. The following day, they were gently washed with PBS before DMEM with 50% horse serum (Gibco, Cat# 26050-088) and 1% PenStrep was added for 2 h. The cells were once again gently washed with PBS and remained in DMEM with 1% PenStrep until they were collected at the indicated time points.

2.4 Uptake protocols

2.4.1 *In vivo* uptake

Heat-inactivated, fluorescent *S. aureus*, or fluorescently labelled oxLDL (DiI-oxLDL) were injected intra-peritoneal at the indicated time points in 200 µl sterile PBS. After one hour, the peritoneal cells were harvested and vigorously washed three times before they were stained for subsequent flow cytometry or microscopy analysis.

2.4.2 *Ex vivo* uptake

0.5 x 10^6 peritoneal leukocytes were treated with applicable particles at concentrations specified below for 1 hour if not indicated otherwise. For the uptake inhibition studies, indicated concentrations of Latrunculin A (Invitrogen, Cat# L12370 Lot# 796178) were added to the cells 10 minutes prior to addition of the particles, and remained in the cell medium until the end of the study (1 h for uptake measurements and 4 h for cytokine measurements). Deviating particle concentrations as indicated in the figure legends. Cells were vigorously washed three times for subsequent quantification of fluorescence by flow cytometry, microplate reader or microscopy.

Particles used:	Amount used if not specified otherwise
S. aureus particles	2.5 x 10^6
E. coli particles	5 x 10^6
Vybrant (heat-inactivated *E. coli*)	100 µl
living GFP expressing *E. coli*	2.5 x 10^8
latex beads	2.5 x 10^8
pHrodo Green *S. aureus* particles	2.5 x 10^6
pHrodo Green *E. coli* particles	5 x 10^6
oxLDL	25 µg/ml

2.4.3 Colony Formation Assay

To investigate killing of bacterial pathogens by macrophages, the number of viable pathogens were quantified as the ability to form colonies on an Ampicillin-resistance selective LB Agar plate. Peritoneal macrophages were adhered to tissue culture plates for 30 min before non-adherent cells were removed in the course of three washes with warm DMEM. The cells were then incubated with Ampicillin resistant living *E. coli* (MOI20) for 30 min at 37˚C. Following a wash with warm medium, cells were incubated with 100 µg/ml Gentamycin containing medium supplemented with 10% FCS for 30 min to destroy extracellular bacteria while ingested material remained unaffected. The cells were further cultured in 10 µg/ml Gentamycin containing medium

supplemented with 10% FCS to maintain gentle bactericidal activity to account for bacterial release due to host cell lysis. At the indicated time points, cells were washed twice with warm PBS before they were lysed in 200 µl of freshly prepared, ice cold 0.1%TritonX PBS. Cell lysis was reinforced by harsh up and down pipetting. Serial dilutions were prepared from the lysate and 100 µl were plated on Ampicillin containing LB Agar. Colonies were quantified following approximately 16 h of incubation at 37˚C and the number of living bacteria per cell were calculated while accounting for the lysate dilution that was used.

2.4.4 *E. coli* culture for uptake studies with living bacteria

A stock of Log-phase GFP expressing, Ampicillin resistant *E. coli* was prepared and stored at 4˚C to be used as the inoculant for the experimental *E. coli* cultures. 24 h prior to initiation of an uptake experiment by addition of bacteria to the cells, 100 µl of the stock culture was used to inoculate 4.9 ml of Ampicillin supplemented LB medium for growth at 37˚C on a shaker. After the OD was measured to calculate the number of bacteria, they were pelleted at 3000 rpm for 10 minutes and resuspended in the appropriate amount of DMEM.

The bacterial growth curve in Figure 2.4.4.1 indicates that expansion of bacteria for 24 h resulted in a stationary phase culture, while log phase was present around 5 h following inoculation. For practical reasons, cultures could not be inoculated 5 h before use in each study. In order to keep consistency between experiments and circumvent inoculation times during the night time, 24 h cultures were used in the here presented studies.

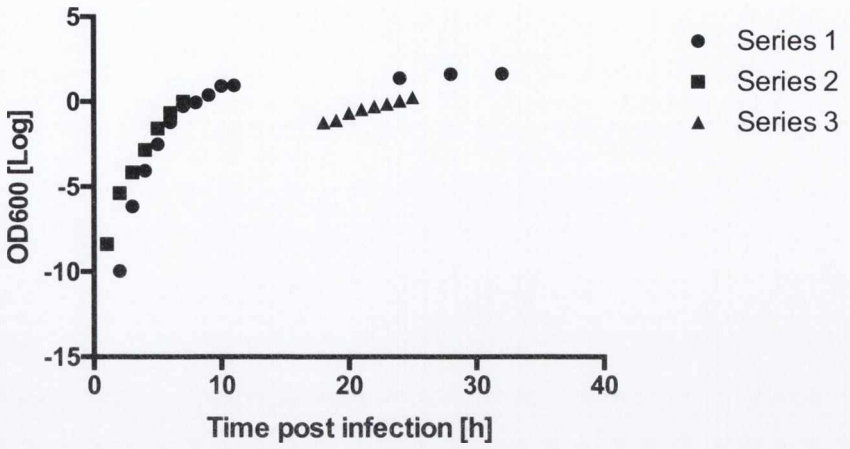


Figure 2.4.4.1: *E. coli* growth curve.

100 µl of inoculant was diluted with 4.9 ml fresh medium and OD_{600} was measured at indicated time points. Data was collected in three independent experiments (series 1-3).

2.4.5 Phagocytic Index

The phagocytic index, which was originally introduced in microscopy experiments, combines the average fluorescence intensity per cell and the number of uptake positive cells within a population. The formula by which the phagocytic index was calculated is the following.

$$\frac{MFI_{uptake^+\,cells}}{\#cells\ screened} * \frac{\#cells\ screened}{(\#uptake^+cells)^2} * 100$$

2.5 Fluorescence measurement

2.5.1 Flow cytometry

Cells were vigorously washed three times with PBS to remove bacterial particles from the cell surface, before they were treated with Fc-block (Bioxcell Cat# CUS-HB-197-A02) for 10 min at 4˚C and stained for F4/80 PE-Cy7 (Biolegend, Cat# 123114) and Live/Dead blue fixable stain (Life Technologies,

Cat# L23105) (or with indicated antibodies) for 30 min at 4˚C. Following two additional washes, the cells were fixed with 3% PFA for 10 min at room temperature, washed one more time and subsequently analysed on an LSR Fortessa.

For intracellular staining, the Foxp3/Transcription Factor Staining Buffer Set (eBioscience, Cat# 00-5523-00) was used. In short, cells were stained as indicated above for F4/80 and Live/Dead blue fixable stain for 30 min at 4˚C. After two washes, 200 µl of the Foxp3 Fixation/Permeabilization working solution was added and pipetted up and down several times, before the sample was incubated for 60 min in the dark at RT. Then, the permeabilized samples were centrifuged at 350 x g for 5 min at RT and washed twice with 200 µl 1x Permeabilization Buffer. In a final volume of 50 µl the cells where subsequently stained with an anti-CD36 antibody for 30 min at RT in the dark. After addition of 200 µl 1x Permeabilization Buffer, cells were centrifuged at 350 x g for 5 min at RT and washed again with 200 µl 1x Permeabilization Buffer, before they were fixed with 3% PFA for 10 min at room temperature, washed one more time and subsequently analysed on an LSR Fortessa.

The gating strategy or *ex vivo* and *in vivo* uptake studies is shown below.

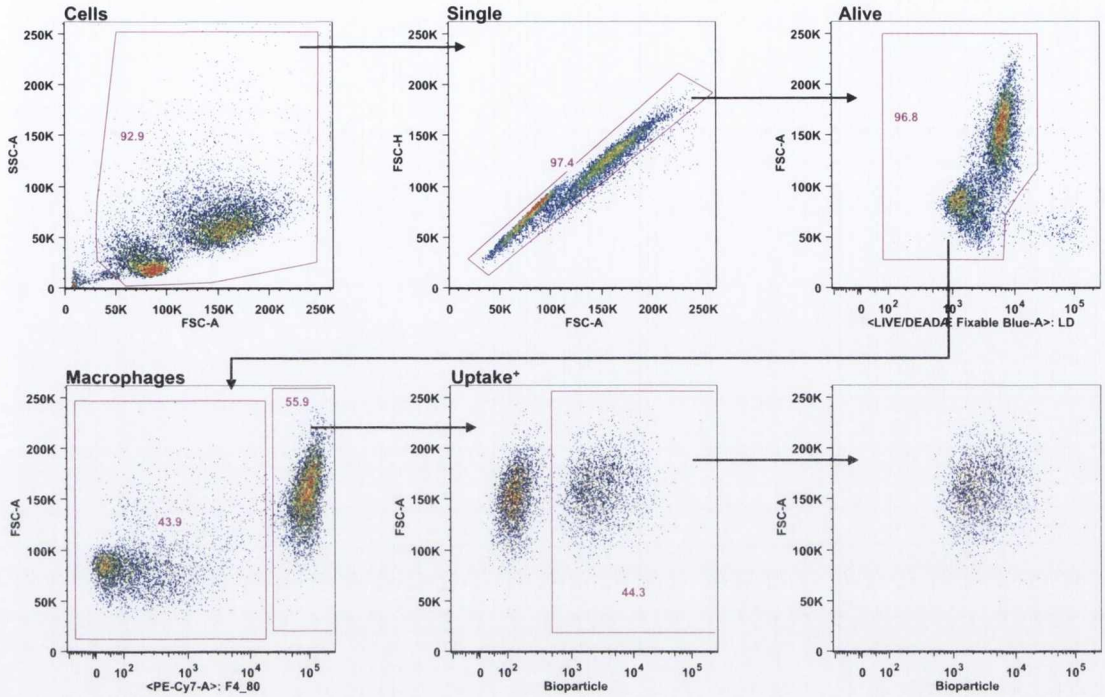


Figure 2.5.1.1: Gating strategy of uptake positive peritoneal macrophages following particle uptake.

Debris was gated out via FSC and SSC and cells were further gated on FSC-H and FSC-A to select for single cells. Live/Dead negative, living cells were then separated into F4/80 negative or F4/80 positive macrophages, which were further analysed for particle derived fluorescence. MFI of particle fluorescence was analysed in uptake positive cells only.

2.5.2 Fluorescence plate reader

Following adherence of 0.1 x 10^6 cells to a flat bottom 96-well plate over night (BMDMs) or for 30 min (peritoneal cells), they were stimulated with 50 x 10^6 living GFP-labelled *E. coli*, or with Vybrant (heat-inactivated *E. coli*) particles according to the manufacturers instructions. Extracellular signal was quenched with Trypan blue for 1 min at room temperature immediately before fluorescence was determined by a FLUOstar OPTIMA fluorescent plate reader (BMG Labtech).

2.5.3 Confocal microscopy

Cells were vigorously washed three times with PBS to remove bacteria from the cell surface and allowed to adhere to Poly-L-Lysin coated cover glasses for 30 min at room temperature. After 10 min Fc-blockage at 4˚C, the cells were stained with a FITC conjugated anti-*S. aureus* antibody (Abcam, Cat# ab68950) for 30 min at 4˚C, followed by a 5 min incubation with CellMask (Invitrogen, Cat# C10046) and Hoechst 33342 (Sigma, Cat# 14533). The cells were then washed three times and fixed with 3% PFA for 10 min at room temperature. Mounted cells (Mounting medium Vectashield (Vector Laboratories, Cat # H-1000)) were sealed with nail polish and stored at 4˚C until visualized using a Leica SP5 NLO confocal system.

2.5.4 FACS purification

Peritoneal macrophages were isolated and stained for F4/80 and Propidium iodide (PI) to discriminate dead cells and were then sorted on a MoFlow cell sorter according to F4/80 positivity or negativity in two separate, RLT containing tubes. Only PI negative, single cells were considered and sorted cells were kept on ice until further processing.

2.6 RNA protocols

2.6.1 RNAlater

Tissue samples were temporarily stored in RNAlater stabilization solution (Ambion, Cat# AM7021) to preserve tissue RNA without the need to immediately process the sample. Tissues were submerged in RNA later following extraction and stored at -20˚C until further use.

2.6.2 TRIzol isolation

RNA isolation using TRIzol Reagent (Life Technologies, Cat# 15596-018) was performed according to the manufacture's instructions. Homogenized samples

containing 1 ml TRIzol were incubated for 5 minutes at RT to allow denaturation of proteins before 0.2 ml chloroform was added. During centrifugation at 12 000 x g for 15 min at 4˚C, the RNA containing aqueous phase (top phase) was separated from the DNA at the interphase and protein in the (bottom) organic phase. During KC and PM isolation 15 µg of GlygoBlue (Thermo Fisher Scientific, Cat# AM9516) was added to the aqueous phase to improve visibility of the RNA pellet. RNA was precipitated from the aqueous phase during incubation with 0.5 ml isopropanol. Following centrifugation at 12 000 x g for 10 min at 4˚C, the supernatant was discarded and the pellet washed with 1 ml 75% ethanol, before the pellet (at 7 500 x g for 5 min at 4˚C) was air-dried for ~10 min at RT. The purified RNA was then resuspended in an appropriate amount of ultra pure water (10-100 µl) and incubated for 12 min at 57 ˚C to facilitate complete solubilisation of the RNA. In order to remove DNA contaminations, the samples were digested with DNase using Turbo DNA-free Kit (Life Technologies, Cat# AM1907) according to the manufacturer's instructions. 0.1 volume of DNase Buffer was added to the sample together with 1 µl of DNase and incubated for 30 min at 37˚C, before 0.1 volume of inactivation reagent was added. Following a 5 min incubation at RT, the sample was centrifuged at 10 000 x g for 1.5 min to pellet the DNase inactivation reagent. The DNase digested RNA was then transferred into a fresh vial and stored at -80˚C until further use.

In the case of RNA isolation from tissues, the organ was transferred in a Micro-Bead tube 2.38 mm (MoBio, Cat# 13117-50) containing 1 ml Trizol Reagent. In a Precellys 24, the sample was homogenized and subsequently centrifuged at 12 000 x g for 10 min at 4˚C. The clear supernatant (without the fatty layer if present) was transferred to a new vial. The procedure then commenced as described above.

2.6.3 RNeasy Mini Kit

RNA from cell cultures was mainly isolated using the commercially available RNeasy Mini Kit (Qiagen, Cat# 74106).

Cells were washed with PBS before 350 µl RLT buffer was added to the cells. To improve cell lysis, the cell suspension was then placed at -80˚C for at least

one day and vigorously pipetted up and down several times after being defrosted. The RNA was precipitated by addition of 525 µl (1.5 vols) of 100% pure ethanol and loaded to an RNeasy spin column. During a 15 sec spin at 8000 x g, the RNA was enriched within the column and washed twice with 500 µl RPE buffer. The column was centrifuged at 8000 x g for 15 sec during the first, and 2 min during the second wash, and the flow through was discarded after each spin. Remaining ethanol was removed by an additional centrifugation at full speed for 1 min, while using a fresh collection tube. Lastly, the column was placed into an RNase free Eppendorf tube and the RNA was eluted in 25 µl RNase free H_2O during a 1 min centrifugation at 8000 x g. The eluted RNA was re-loaded onto the column for a second elution step to maximize the yield of recovered RNA.

2.6.4 Reverse Transcription PCR (RT-PCR)

cDNA was prepared from RNA using the commercially available kit iScript (BioRad, Cat# 170-8841) according to the manufacturers instructions. 500 ng RNA was diluted in ultra pure water and added to 2 µl of the iScript Supermix, which contained all necessary ReverseTranscription-PCR components (including RNase H+ MMLV reverse transcriptase, RNase inhibitors, dNTPs, oligo(dT), random primers as well as $MgCl_2$) in a final volume of 10 µl. The reaction was initiated in a thermal cycler using the program outlined below. Following reverse transcription, the cDNA was stored at -20˚C. Prior to use in a qPCR, the cDNA was diluted in the range of 1:2 to 1:10 in ultra pure water. During the procedure the RNA and resulting cDNA were kept on ice.

Priming	5 min 25˚C
Reverse transcription	20 min 46˚C
Reverse Transcriptase inactivation	1 min 95˚C

2.6.5 qPCR

Real time PCR was performed using TaqMan Primer/Probe sets purchased from ThermoFisher. 5 µl of Sso Advanced Universal Probes Supermix (BioRad, Cat# 172-5284) was mixed with 2-5 µl cDNA in a total volume of 10 µl in a chilled 384 well qPCR plate (BioRad, Cat# HSP3805). Sealed with optical tape, the plate was transferred to a CFX384 Touch Real-Time PCR Detection System (BioRad, Cat# 1855485), which was set to the program shown below. During analysis, the cycle number which resulted in a fluorescent signal above threshold (C_T) was recorded. Data was normalized to the average C_T of three housekeeping genes that have previously been validated in a circadian setting (RPS18, Actin, GAPDH). To generate more useful axis ranges, mRNA abundance was shown as values normalized to the first data-point, or the average of all data-points of the gene of interest in a given experiment.

$$realative\ mRNA\ abundance = 2^{-\left(C_{T\,Gene\ of\ interest} - C_{T\,Average\ Housekeeping\ Genes}\right)}$$

Polymerase activation and DNA denaturation	30 sec 95˚C	
Amplification	Denaturation	10 sec 95˚C
	Annealing/Extension +Plate Read	30 sec 95˚C
	Cycles	49

2.6.6 NanoString

To allow simultaneous quantification of mRNAs from multiple genes, while using little RNA input (down to 50 ng), NanoString technology was used according to the manufacturer's instructions. Genes involved in the circadian machinery, metabolism and immune response were incorporated amongst 5 housekeeping genes in two CodeSets (Clock 1 and Clock 2). NanoString

utilizes probe sets specific to RNAs of interest and combines these probes with tags that allow purification and immobilization of RNAs to a cartridge, as well as barcoding of RNAs for final assignments as illustrated below (Figure 2.6.6.1). Barcoding uses defined sequences of a range of fluorescent probes.

50-800 ng RNA was mixed with 8 µl Reporter CodeSet in a total volume of 13 µl, before 2 µl Capture ProbeSet was added and the reaction immediately incubated for ~18 h at 65˚C in a thermal cycler. The hybridized samples were then loaded to the NanoString PrepStation for further processing. Inside the PrepStation samples were transferred onto a cartridge, which lastly had to be placed into the NanoString Digital Analyzer for data collection.

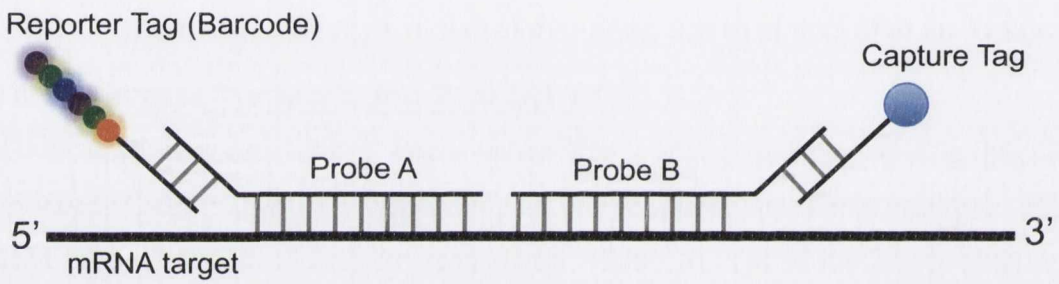


Figure 2.6.6.1: Schematic illustration of RNA quantification via NanoString technology.

A probe set is comprised of two probes specific for each target RNA. Probe A contains a unique target sequence that will hybridize with a reporter sequence, which carries a fluorescent reporter tag that was allocated to the target RNA. Probe B possesses a common sequence, which will bind a capture sequence that carries a purification tag to allow biotin/streptavidin mediated immobilization of the hybrid.

2.6.7 RT^2 Profiler Plates

RT^2 Profiler Plates were used to cost-effectively screen for differences in Mouse Phagocytosis (Qiagen, Cat# PAMM-173ZC) and Mouse Oxidative Stress (Qiagen, Cat# PAMM-065ZC) pathways in samples of interest, based on SYBR Green qPCR array.

cDNA - that was generated from RNA samples using RT^2 First Strand Kit (Qiagen, Cat# 330401) - was mixed with SYBR Green qPCR Mastermix

(Qiagen, Cat# 330520) and distributed to RT^2 Profiler plates which were preloaded with primer sets for pathway relevant genes. Amplification was then initiated in a real time cycler 7900HT Fast (Applied Biosystems, Cat# 4351405) and data was analysed on the $\Delta\Delta C_T$ method.

2.6.8 Quantification via Nanodrop

Absorbance at 260 nm was used to define the concentration of RNA in a sample as $1OD_{260}$= 40 µg/ml. Ratios of the absorbance at 260 nm, 230 nm and 280 nm were further calculated as indicators of solvent and protein contaminations.

2.7 Other protocols

2.7.1 Genotyping

KAPA Mouse Genotyping Kits (KAPA Biosystems, Cat# KK7352) were used to extract DNA from mouse tails using the KAPA Express Extract to produce PCR compatible DNA, and perform a genotyping PCR with the KAPA2G Fast HS Genotyping Mix. Mouse tails were incubated with 100 µl Genotyping Mix as specified below for 5 min at 75˚C, followed by 10 min at 95˚C. 4 µl of the DNA isolate were subsequently used in a 20 µl PCR reaction using BMAL1 or CRE primer sets (100 µM stock) and programs as indicated below.

18µl of the PCR product was then loaded on a 3% Agarose Gel (in TAE, with GreenGlo DNA Dye (Denville, Cat# CA3600)) next to 3 µl of DNA Ladder (Thermo Scientific, Cat# SM1333) for gel electrophoresis. The size of the PCR products were estimated according to the ladder to allow allocation to specific genotypes.

Genotyping Mix

2 µl	KAPA Express Extract Enzyme
10 µl	10x KAPA extract Express Buffer
88 µl	H_2O

BMAL1 PCR

10 µl	2x KAPA2G Fast HS Genotyping Mix
0.1 µl	WT primer
0.1 µl	common primer
0.1 µl	Mutant primer
5.7 µl	H_2O

Temperature [°C]	Time [s]*
94	300
95	30
61	30
65	60
72	300
4	∞

Estimated Band Size:

WT	327 bp
Floxed	431 bp
KO	570 bp

LyzM-CRE PCR

10 µl	2x KAPA2G Fast HS Genotyping Mix
0.1 µl	WT primer
0.1 µl	common primer
0.05 µl	Mutant primer
5.75 µl	H_2O

Temperature [°C]	Time [s]*
94	300
94	30
61	30
72	60
72	300
4	∞

Estimated Band Size:

WT (Cre^-)	350 bp
Cre^+	700 bp

Alb-CRE PCR

10 µl	2x KAPA2G Fast HS Genotyping Mix
0.1 µl	WT primer
0.1 µl	common primer
0.1 µl	Mutant primer
5.7 µl	H_2O

Temperature [°C]	Time [s]*
95	300
95	15
63	15
72	15
72	300
4	∞

Estimated Band Size:

WT (Cre^-)	351 bp
Cre^+	390 bp

Name	Sequence 5' → 3'	Gene	Specificity
oIMR7525	ACT GGA AGT AAC TTT ATC AAA CTG	Bmal1 flox	WT forward
oIMR7526	CTG ACC AAC TTF CTA ACA ATT A	Bmal1 flox	Common reverse
R4	TCC TAA CTT GGT TTT TGT CTG T	Bmal1 flox	KO forward
oIMR3066	CCC AGA AAT GCC AGA TTA CG	LyzM	Mutant forward
oIMR3068	TTA CAG TCG GCC AGG CTG AC	LyzM	WT forward
oIMR3067	CTT GGG CTG CCA GAA TTT CTC	LyzM	Common reverse
20239	TGC AAA CAT CAC ATG CAC AC	Alb Cre	WT forward
oIMR5374	GAA GCA GAA GCT TAG GAA GAT GG	Alb Cre	Mutant forward
20240	TTG GCC CCT TAC CAT AAC TG	Alb Cre	Common reverse

Figure 2.7.1.1: Genotyping Primer Sequences.

Jackson Primer Name and sequence of genotyping primers for Bmal1 floxed, LyzM-Cre and Albumin Cre mice.

* repeat step 2-4 for 35 cycles

2.7.2 Cytokine measurement

In vivo cytokines were measured at the indicated time points by terminal blood collection following decapitation or via the submandibular route for survival bleeds. Serum was separated in Z-gel micro tubes (Sarstedt Cat# 41.1500.005) after a 30 min incubation and centrifugation at 10.000g for 5 min. Serum was stored at -20°C until use. Supernatants from *ex vivo* stimulations were separated from the cells by centrifugation for 5 min at 2000 rpm at 4°C and stored at -20°C until further use. Cytokines were measured using the Bio-Plex system (BioRad) in a multiplex assay according to the manufacturers instructions. In short, appropriate magnetic capture beads were washed twice with wash buffer in a magnetic plate washer, before the samples and standards were added to the plate and incubated for 30 min while shaking. Following three washes, the respective biotinylated detection antibodies were added for 30 min while shaking, before the plate was washed three times. Lastly, PE conjugated Streptavidin was added for 10 minutes before the magnetic beads were washed three times and resuspended in 125 µl assay buffer. The conjugates were then analysed using a Bio-Plex MagPix Multiplex Reader (BioRad).

2.7.3 Corticosterone measurement

Corticosterone levels were quantified using a commercially available ELISA kit (Enzo Cat# ADI-900-097). In short, serum samples were incubated with steroid displacement reagent to free bound Corticosterone from steroid binding proteins. 1:40 diluted samples and freshly prepared Corticosterone standards were then loaded to a Donkey anti-Sheep IgG Microtiter Plate and incubated on a plate shaker for 2 h at 500 rpm RT. Following three washes, pNpp Stop solution was added and absorption was read at 405 nm, while absorption at 580 nm was used for correction. Corticosterone concentrations were extrapolated from a Percent Bound versus Corticosterone Standard plot.

2.7.4 Beta-Hydroxybutyrate measurement

β-Hydroxybutyrate was measured using a commercially available colorimetric assay (Cayman, Cat# 700190). Oxidation of β-Hydroxybutyrate to Acetoacetate results in simultaneous reduction of NAD^+ to $NADH+H^+$. The colorimetric detector WST-1 then reacts with NADH to form a formazan dye, whose absorbance at 450 nm is proportional to the β-Hydroxybutyrate concentration. To initiate the reaction, serum samples and β-Hydroxybutyrate standards were incubated for 30 min at RT in the dark with Developer solution. Absorbance of β-Hydroxybutyrate standards was plotted against the concentrations followed by linear regression, from which sample concentrations were extrapolated.

2.7.5 Liver enzymes

Serum samples were diluted 1:10 in PBS and sent to the Department of Laboratory Medicine for liver enzyme testing.

2.7.6 CD36 blocking studies

To block CD36 functionality, cells were incubated with the indicated concentrations of CD36 blocking peptide (Cayman, Cat# 300011) or anti-CD36 antibodies for 60 minutes before uptake was initiated by addition of fluorescent

particles. IgG or IgA mock stimulations were included as controls at similar concentrations whenever anti-CD36 antibodies were used.

2.7.7 Transfection

Cells were plated at 1 x 10^6 cells per ml in a 12 well plate the day before the transfection. Two solutions were prepared separately and let rest for 10 minutes at RT, before solution B was added to solution A and incubated at RT for further 45 min. Cells were washed and medium was replaced with 1 ml of fresh media, before 250 µl of the transfection mix was added for 4 or 6 h as indicated.

Solution A) 4 µl Lipofectamin in 125 µl OptiMem

Solution B) 0.75-1 µg per Vector in 125 µl OptiMem

2.8 Statistics

Error bars represent the standard error of the mean. Statistical analysis was performed using appropriate tests in Prism6. To identify rhythmic data sets, JKT Cycle (Freeware provided by the Hughes Lab) (Hughes et al., 2010) was used.

2.9 Materials

2.9.1 Taq man probes

Nr1d1	Mm00520708_m1
Bmal1	Mm00500226_m1
Cry1	Mm00514392_m1
Per2	Mm00478099_m1
Tnfa	Mm00443258_m1
Il1b	Mm00434228_m1
CD36	Mm01135198_m1
Clock	Mm00455950_m1
Per1	Mm00501813_m1
Cry2	Mm01331539_m1
Atg7	Mm00512209_m1
Cd14	Mm00438094_g1
Dynactin6	Mm00495994_m1
Marco	Mm00440265_m1
Pparg	Mm00440940_m1
Msr1	Mm00446214_m1
Actinb	Mm00607939_s1
Gapdh	Mm99999915_g1
Rps18	Mm02601777_g1

2.9.2 General

DMEM (Gibco, Cat# 61965-026)

RPMI (Gibco, Cat # 11875-093)

OptiMem (Gibco, Cat# 51985091)

Pen/Strep (Sigma, Cat# P4333)

FCS (Sigma, Cat# F7524)

Recombinant Murine M-CSF (PeproTech, Cat# 315-02)

PBS (Gibco, Cat# 10010-023)

HBSS (Gibco, Cat# 14175-095)

ACK (Quality Biological, Cat# 118-156-721)

15 ml Polypropylene Conical Tube (Falcon, Cat# 352097)

50 ml Polypropylene Conical Tube (Falcon, Cat# 352070)

FACS tube, 5 ml Polystyrene Round-Bottom Tube (Falcon, Cat# 352052)

FACS tube inserts, 1.2 ml natural polypropylene tube (USA scientific, Cat# 1412-1000)

Eppendorf tubes (Denville, Cat# C2170)

5 ml Polystyrene Round-Bottom Tube with Cell-Strainer Cap (Falcon, Cat# 352235)

Ultra pure water (Quality Biological, Cat# 351-029-721)

Chloroform (Fisher Scientific, Cat# C298-500)

Isopropanol (J.T. Baker, Cat# 9084-01)

Ethanol (The Warner-Graham Company, Cat# 264511)

LPS (Sigma, Cat# L2630 Lot# 014M4018V)

Recombinant Murine TNF-α (PeproTech, Cat# 315-01A)

Horse serum (Gibco, Cat# 26050-088)

Corticosterone ELISA kit (Enzo Cat# ADI-900-097)

-Hydroxyutyrate colorimetric assay (Cayman, Cat# 700190)

Z-Gel Serum tubes (Sarstedt, Cat# 41.1500.005)

KAPA Mouse Genotyping Kits (KAPA Biosystems, Cat# KK7352

GreenGlo DNA Dye (Denville, Cat# CA3600))

GeneRuler 1 kb Plus DNA Ladder (Thermo Scientific, Cat# SM1333)

Foxp3 / Transcription Factor Staining Buffer Set (eBioscience, Cat# 00-5523-00)

Fc-block anti-mouse CD16/32 clone 2.4G2 (Bioxcell Cat# CUS-HB-197-A02)

Poly-L-Lysin (Sigma, P8920)

Mounting medium Vectashield (Vector Laboratories, Cat # H-1000)

Lipofectamin (Invitrogen, Cat# 52887)

Bmal1 plasmid pBMPC3 (Addgene, Cat# 31367)

Clock plasmid pCKPC4 (Addgene, Cat# 31366)

2.9.3 Particles

Beads FluoSpheres polystyrene, 1.0 µm, yellow green (Life Technologies, Cat# F13081, Lot# 1421042)

pHrodo® Green E. coli BioParticles® Conjugate for Phagocytosis (Life Technologies, Cat# P35366)

pHrodo® Green S. aureus Bioparticles® Conjugate for Phagocytosis (Life Technologies, Cat# P35367)

Staphylococcus aureus BioParticles Alexa Fluor 488 or 594 conjugate (Life Technologies, Cat# S23371 or S23372)

Escherichia coli BioParticles Alexa Fluor 488 or 594 conjugate (Life Technologies, Cat# E13231)

Vybrant Phagocytosis Assay Kit (Life Technologies, Cat# V6694)

living GFP expressing *E. coli* (kind gift from Jay Hinton)

oxLDL, Dil-Lipoprotein, low density, oxidized, human plasma, BT-920 (Alfa Aeaser, Cat# J64164)

2.9.4 RNA

GlygoBlue Coprecipitant (Thermo Fisher Scientific, Cat# AM9516)

Micro-Bead tube 2.38 mm (MoBio, Cat# 13117-50

iScript™ Reverse Transcription Supermix for RT-qPCR (BioRad, Cat# 170-8841)

SsoAdvanced™ Universal Probes Supermix (BioRad, Cat# 172-5284)

Hard-Shell PCR plate, 384-well, thin-wall (BioRad, Cat# HSP3805)

RT^2 SYBR Green ROX qPCR Mastermix (Qiagen, Cat# 330520)

Mouse Phagocytosis (Qiagen, Cat# PAMM-173ZC

Mouse Oxidative Stress (Qiagen, Cat# PAMM-065ZC)

RT^2 First Strand Kit (Qiagen, Cat# 330401)

RNAlater stabilization solution (Ambion, Cat# AM7021)

RNeasy Mini Kit (Qiagen, Cat# 74106)

TRIzol Reagent (Life Technologies, Cat# 15596-018)

Turbo DNA-free Kit (Life Technologies, Cat# AM1907)

2.9.5 Blocking Antibodies and inhibitors

Anti-CD36 Antibody (Novus, Cat# NB110-59724 lot C-1)

Anti-CD36 (H-300) Antibody (Santa Cruz, Cat# sc-9154)

Anti-CD36 (sr-b3) Antibody (R&D, Cat# ag2519)

Anti-CD36 Antibody JC63.1 (Cayman, Cat# CAY188150)

AffiniPure Goat Anti-Mouse IgG (H+L) (Jackson ImmunoResearch, Cat# 115-005-003)

Goat anti mouse IgA H&L (Abcam, Cat# ab9161)

CD36 blocking peptide (Cayman, Cat# 300011)

Latrunculin A (Invitrogen, Cat# L12370 Lot# 796178)

2.9.6 Magnetic bead separation Antibodies

Biotin anti-mouse CD19 Antibody (BioLegend, Cat# 115504)

Biotin anti-mouse TER-119 Antibody (BioLegend, Cat# 116204)

Biotin anti-mouse CD90.2 Antibody (Thy1.2) (BioLegend, Cat# 105304)

Biotin anti-mouse/human CD45R/B220 Antibody (BioLegend, Cat# 103204)

PE anti-mouse F4/80 Antibody (BioLegend, Cat# 123110)

2.9.7 Staining Antibodies and Dyes

Anti-CD36 Antibody for staining clone HM36 (BioLegend, Cat# 102612)

FITC labelled anti-S.aureus antibody (Abcam Cat# Ab 68950)

CellMask Deep Red (Invitrogen, Cat# C10046)

F4/80 PE-Cy7 (Biolegend, Cat# 123114)

Live/Dead blue fixable stain (Life Technologies, Cat# L23105)

Hoechst 33342 (Sigma, Cat# 14533)

2.9.8 Equipment

T100 Thermo Cycler (BioRad, Cat# 1861096)

NanoString nCounter Max Analysis System Gen1 (NanoString Technologies)

Flow cytometer (BD, LSRFortessa, Special Order Product)

NanoDrop ND-1000 Spectrophotometer (NanoDrop Technologies, Cat# 455)

Precellys 24 (Bertin, MoBio, Cat# 13112)

CFX384 Touch Real-Time PCR Detection System (BioRad, Cat# 1855485)

7900HT Fast Real-Time PCR System (Applied Biosystems, Cat# 4351405)

Ultrasonic Cleaner (Misonix, Cat# 151OR-DTH)

FLUOstar OPTIMA fluorescent plate reader (BMG Labtech)

Leica SP5 NLO confocal system (Leica)

MoFlo XDP Cell Sorter ML99030 Beckman Coulter

3 Diurnal particle uptake by immune cells is limited to *ex vivo* settings and is independent of the scavenger receptor CD36

3.1 Introduction

Circadian rhythmicity in the innate immune response was first reported in 1960 (Halberg et al., 1960), and recent years have seen advances in understanding the molecular and cellular basis of this phenomenon, particularly building on the discovery of the cell-intrinsic circadian clock (Curtis et al., 2015, Nguyen et al., 2013, Gibbs et al., 2012, Scheiermann et al., 2012). There is however much to learn about how circadian control of immunity takes place.

Immune responses vary from acute responses mediated by inflammatory and immunogenic stimuli, to chronic inflammation and autoimmunity, all of which differ in cause and progression. While there is some work published that addresses clock function in chronic inflammatory disease models (Hand et al., 2016), most research in this area has focused on circadian regulation of the acute inflammatory response. In the course of this, implications of distinct clock components have been demonstrated. As such, Rev-erbα inhibition increased IL-6 production in macrophages in an *in vitro*, as well as an *in vivo* model, without affecting functionality of the clock (Gibbs et al., 2012). However, *Cry2* ablation similarly induced IL-6 production, arguing for a pathway that cannot be fully ascribed to a single clock component (Hoffman et al., 2009).

Nevertheless, it is clear that the molecular clock in macrophages regulates inflammatory responses, and mice with deficiencies in the molecular clock in the myeloid lineage become hyper-responsive to inflammatory challenge (Curtis et al., 2015). Congruent with increased mortality, *in vitro* stimulation of peritoneal macrophages that bear a deficiency in the core clock component *Bmal1* - which results in complete break-down of the molecular clock (Bunger et al., 2000) - with the bacterial component LPS results in the production of

increased amounts of pro-inflammatory cytokines such as IL-6 (Gibbs et al., 2012, Curtis et al., 2015).

It is clear that engagement of inflammogenic material with surface receptors of immune cells is necessary to mount immune responses and induce cytokine production. However, this interaction also results in internalization of these materials by some immune cells. For example macrophages, which are often studied in the context of LPS induced immunity, are professional phagocytes with a significant capacity of particle ingestion. Considering that a multitude of surface receptors induce internalization as well as cytokine production, it stands to reason that these pathways may be principally connected. This is underpinned by a strong complexity and correlation of the type of material encountered and the inflammatory response induced as well as the mechanism by which it is internalized (Underhill and Goodridge, 2012).

As some literature already suggests that cytokine response correlates with the ability of phagocytes to ingest material in the setting of bacterial infection (Azevedo et al., 2012), the question arose whether particle ingestion may be circadian and could potentially explain daily oscillations in cytokine response and mortality in infected animals, and possibly constitute a previously unknown interface of the immune and the circadian system. Because rhythmic ingestion of particles had been investigated in numerous model systems to define a role for melatonin as a rhythmic stimulant of particle uptake (Rodríguez et al., 1999, Hriscu, 2005, Pires - Lapa et al., 2013), rhythmicity in phagocytosis in the setting of immune response appeared plausible. In contrast to previous studies, and to make findings more applicable to the majority of chrono-immunological reports, we deliberately utilized the widely used mouse strain C57BL/6J to investigate daily rhythmicity in bacterial uptake. This strain has a naturally occurring deletion in the serotonin N-acetyltransferase (arylalkylamine N-acetyltransferase, AANAT) gene, causing a defect in the production of melatonin (Roseboom et al., 1998), thereby eliminating any effect this hormone may have on particle uptake. Internalization of Zymosan by peritoneal cells in this system has been previously shown to oscillate over the course of a day; and while the authors argued a possible role for phagocytosis triggered NFκB activation, a causal link and mechanistic insights have not been provided.

Investigating the molecular mechanism by which the circadian system may affect phagocytic ingestion of infectious material, has the potential to reveal new strategies to modify the immune response following an inflammatory insult. It was therefore of interest to evaluate circadian control of particle internalization and the underlying mechanism.

In the present study we tested daily oscillations in the ability of tissue resident peritoneal macrophages to ingest heat-inactivated gram-positive and -negative bacteria, and the possible contribution of the class b scavenger receptor CD36. CD36 was initially found to mediate ingestion of thrombospondin and modified low density lipoprotein (oxLDL) (Endemann et al., 1993), but has recently been implicated in uptake of bacteria (Stuart et al., 2005) and regulation of inflammatory pathways (Sheedy et al., 2013). CD36 was also described as being circadian controlled (Ramakrishnan et al., 2005), and is highly expressed on macrophages, and has pro-inflammatory and pro-ingestion features, making it a viable candidate to mediate circadian particle uptake.

As the specificity of receptors mediating uptake of particles can be remarkably broad or very distinct, it was desirable to use a range of stimuli, which could uncover uniformity or variation in diurnal uptake. Inert latex beads were used to induce rather unspecific uptake with no pathogen associated patterns, while living *E. coli* was used to mimic genuine gram-negative infection.

Pathogenicity of living bacteria heavily depends on the state of the culture, and is highest during the exponential growth phase (McIver et al., 1995, Unnikrishnan et al., 1999), which could be attained around 5 h post inoculation. For practical reasons this could not be realized in the herein presented studies, and cultures were inoculated 24 hours before the assay which produced stationary phase bacteria for following uptake studies. To facilitate and reduce variability in the stimulant, heat-inactivated bacteria were also used and became focus of the studies later in the project. These bacteria were commercially available with different fluorescent tags that were pH sensitive or pH stable. This allowed examination of uptake as well as acidification of the phagosomes following uptake, using the same strain.

To account for differences between two large groups of bacteria (categorized according to their cell wall constituents) representatives of gram-positive (*S. aureus*), and a gram-negative (*E. coli*) bacteria were selected for further use. A second, heat-inactivated *E. coli* strain was used as the stimulant in some of the studies, which was part of a commercially available phagocytosis kit (Vybrant). Here, stimulation was performed according to the manufacturers instructions disregarding the total amount of particles.

Although indication of total particle number can be meaningful, in most settings the ratio of cell to particle is of greater importance. This multiplicity is usually referred to as MOI (multiplicity of infection), however, infection generally implies the use of viable microorganism. Therefore MOS (multiplicity of stimulation) was used instead whenever heat-inactivated bacteria were used.

All uptake assays in this study utilized fluorescence of particles to determine uptake capacity, and although not always indicated, all stimuli (from beads to bacteria and oxLDL) were fluorescently labelled. Fluorescence was thus the readout, which was measured on a fluorescence microplate reader that recorded an average fluorescence signal per well, or flow cytometry, where fluorescence could be determined on a single cell basis. Flow cytometry not only allowed to identify fluorescence per cell, but also limit analysis to specific cell populations, such as macrophages as indicated by F4/80 positivity. Considering macrophages not being the prominent cell type in the peritoneal washout, this presented as a great advantage. Besides mean fluorescence intensity (MFI), the percentage of uptake positive cells (fluorescence positive cells) could be determined. This in turn provided the possibility to display the data according to the phagocytic index, which was originally introduced in microscopy experiments and combines the average fluorescence intensity per cell and the number of uptake positive cells within a population. Although the phagocytic index (PI) is helpful to grasp the data, illustrations of MFI and the percentage of uptake positive cells side by side is often more informative and was therefore emphasized through the study.

Considering the body of literature, circadian control of particle ingestion by macrophages to control circadian proinflammatory signalling appeared reasonable, and the work presented in this chapter aimed to thoroughly test this possibility. Initially, daily oscillations in uptake were tested using *ex vivo* and *in vitro* models to allow and facilitate further investigations regarding the mechanism and the exact role of the molecular clock as well as the receptors involved. This was then translated to *in vivo* models to examine relevance in physiology.

3.2 Results

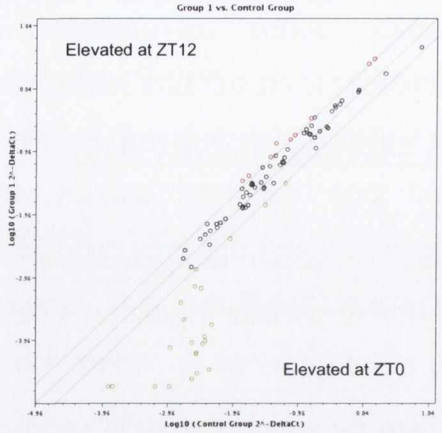
3.2.1 Phagocytosis and oxidative stress pathways display daily rhythmicity in macrophages

In the past decade, several studies reported circadian phagocytosis in a selection of cell types and the possibility of rhythmic particle ingestion to affect circadian oscillations in the immune response (Rodríguez et al., 1999, Hriscu, 2005, Pires - Lapa et al., 2013). The mechanism by which the cells regulated circadian phagocytosis was however not investigated far beyond addition of melatonin or inhibition of its receptor, as melatonin was thought to be the driver of circadian particle ingestion. Considering that C57BL/6J mice present circadian oscillations in immunity, but are deficient in melatonin, it was of interest to investigate daily oscillations in phagocytosis in a melatonin independent manner.

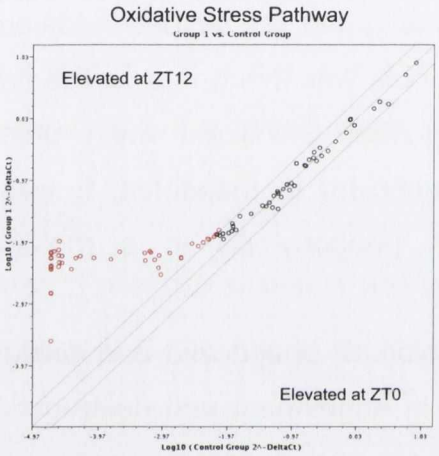
To test possible oscillations in gene expression of phagocytic and oxidative stress pathways, both of which are involved in engulfment and destruction of pathogens, commercially available 96-well format gene-expression arrays were used. Peritoneal macrophages were isolated at ZT0 and ZT12 from the peritoneal fluid of wild type mice by FACS sorting of F4/80 positive, living cells. In order to minimize the mouse-to-mouse variation error in our mini-array, we combined isolated RNA from five mice for both, the ZT0 and the ZT12 input sample. A full list of genes that were included in the mini-array can be found in the appendix (Appendix 2).

In both pathway arrays, a cluster of genes was found to be differentially expressed at ZT0 vs. ZT12 (Figure 3.2.1.1). Unexpectedly, genes related to oxidative stress, which is important in inflammatory signalling as well as destruction of internalized bacteria, and phagocytosis - the process of particle ingestion - did not appear to be up-regulated at similar times. Whereas oxidative stress genes were strongly induced at ZT12, expression of genes associated with phagocytosis was increased at ZT0.

A



B



C

Phagocytosis Pathway	
Differentially expressed genes	
ZT12 vs. ZT0	
Gene Symbol	Fold Regulation
Stab2	-126.8768
Tnfsf11	-96.0689
Ceacam3	-94.2822
Adipoq	-57.2031
Csf2	-44.1957
Mcoln3	-43.2145
Sftpd	-39.5348
Wnt5a	-38.609
Mbl2	-34.9154
Crp	-31.7413
Ifng	-26.661
Pla2g5	-25.7866
Rapgef3	-14.1983
Tlr9	-8.2873
MGDC	-7.7612
Gulp1	-6.6172
Cyp2s1	-4.7672
Pecam1	-4.0084
Pip5k1a	-3.5511
Tgm2	-2.2049
Siglec1	-2.1662
Was	-2.0432
Tnf	-2.0177
Itgam	2.0391
Itgb2	2.099
Cd47	2.1015
C3	2.1067
Fcgr2b	2.172
Crk	2.2276
Fyn	2.4207
Colec12	2.5296
Clec7a	2.9659

D

Oxidative Stress Pathway	
Differentially expressed genes	
ZT12 vs. ZT0	
Gene Symbol	Fold Regulation
Ift172	2.0107
Ercc2	2.0608
Xpa	2.1625
Als2	2.2117
Gss	2.3298
Gpx7	2.352
Prdx1	2.4811
Ehd2	2.9403
Fancc	3.0077
Atr	3.1649
Ercc6	3.3945
Scd1	4.5509
Txnrd3	5.2589
Ptgs2	6.8794
Cdl5	7.0898
Prnp	9.6194
Txn1	10.464
Recql4	11.5123
Noxo1	12.8266
Gpx5	13.0894
Ngo1	33.4823
Ngb	34.8165
Mpo	65.9746
Noxa1	77.6323
MGDC	80.0114
Nox1	95.9687
Epx	113.1701
Nox4	126.5274
Gpx6	162.66
Lpo	168.4693
Alb	186.454
Rag2	192.7267
Nos2	195.9149
Aox1	213.3585
Krt1	214.1475
Gpx2	216.8581
Cygb	222.5303
Fmo2	247.6166
Mb	293.83
Tpo	300.6669
Duox1	305.0214
Ucp3	345.0673
Sod3	347.3672
Il19	367.737
Il22	419.819

Figure 3.2.1.1: Peritoneal macrophages differentially express phagocytic and oxidative stress genes dependent on the time of the day.

Peritoneal macrophages were isolated and FACS purified according to the surface marker F4/80. RNA from 5 mice was pooled and used for the RT Profiler plates. Genes up-regulated in ZT12 samples (Group1) compared to ZT0 samples (Control group) are displayed in **red**, whereas **green** data points mark a down-regulation. **A, C)** Phagocytosis RT Profiler data. **B, D)** Oxidative stress RT Profiler data.

3.2.2 *Ex vivo* uptake capacity in macrophages is diurnal

The gene-array indicated that bacterial uptake and breakdown may oscillate over the course of a day. Hence, we extended our investigation to functional studies, and decided to use fluorescent, inert latex particles (~ 2 µm Ø), as well as Gram-positive (*S. aureus*) and Gram-negative (*E. coli*) bacteria. Most studies were conducted using heat inactivated, fluorescent bacterial particles that were commercially available (bioparticles), but in certain experiments living, fluorescent bacteria were used as indicated. Fluorescence intensity was used as a measure of uptake capacity in peritoneal and bone marrow derived cells, and whenever possible, fluorescence was only measured in macrophages. However, as shown in Figure 3.2.2.2 A-C, F4/80 negative cells hardly contributed to the overall signal seen in the entity of the peritoneal fluid. Therefore, total fluorescent intensity was a valid measurement, even without exclusion of F4/80 negative cell populations.

To investigate rhythmic ingestion of bacterial particles by primary macrophages, we harvested resident peritoneal cells from mice that were housed under strict 12 h light, 12 h darkness schedules, in the morning (the onset of light and rest-phase of nocturnal animals; ZT0) and the evening (beginning of the dark- and active-phase of mice; ZT12) and incubated these cells for 1 h with bioparticles followed by acquisition of the fluorescence signal on a flow cytometer.

In an initial experiment, in order to control for technical variability between time points, mice were housed for three consecutive weeks in two separate holding rooms that were on reversed light cycles. This provided the opportunity to simultaneously test phagocytosis in cells that were extracted from ZT0 and ZT12 mice. In subsequent studies, ZT0 and ZT12 samples were however not prepared simultaneously, as all mice were housed in the same holding room.
In the original study that implemented a reverse light cycle room to allow simultaneous challenge of morning and evening cells, both, *E. coli* and *S. aureus* bio-particle uptake was significantly increased at ZT12 (Figure 3.2.2.1).

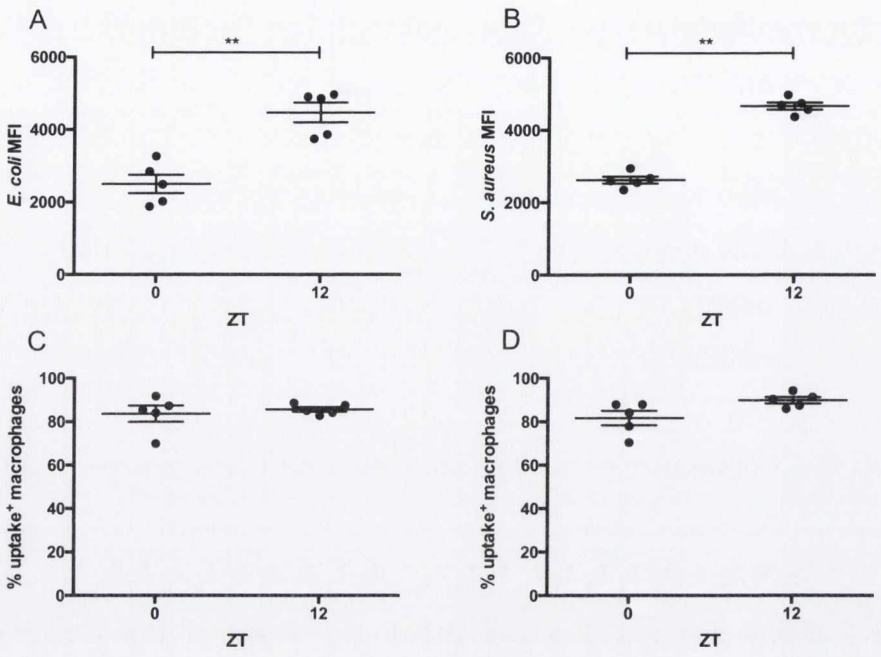


Figure 3.2.2.1: Efficiency of *E. coli* and *S. aureus* bioparticle uptake in peritoneal macrophages is increased at ZT12.

Mice that were housed in reversed light cycle rooms were euthanized at the indicated times and PECs were isolated. Following 1 h stimulation with *E. coli* **(A, C)** or *S. aureus* **(B, D)** bioparticles, mean fluorescence intensity in uptake positive macrophages **(A, B)** and percentage of uptake positive cells **(C, D)** was analysed using flow cytometry. All error bars represent the standard error of the mean from biological replicates. Statistical analysis using Mann-Whitney. n=5.

To achieve bright signals without saturation of the system (e.g. % uptake positive cells < 100%) (Figure 3.2.2.2) particle concentrations were initially titrated, and if not stated otherwise, a multiplicity of stimulation (MOS, particle to cell ratio) of 5 was used for *S. aureus*, and MOS10 for *E. coli* stimulations in following experiments.

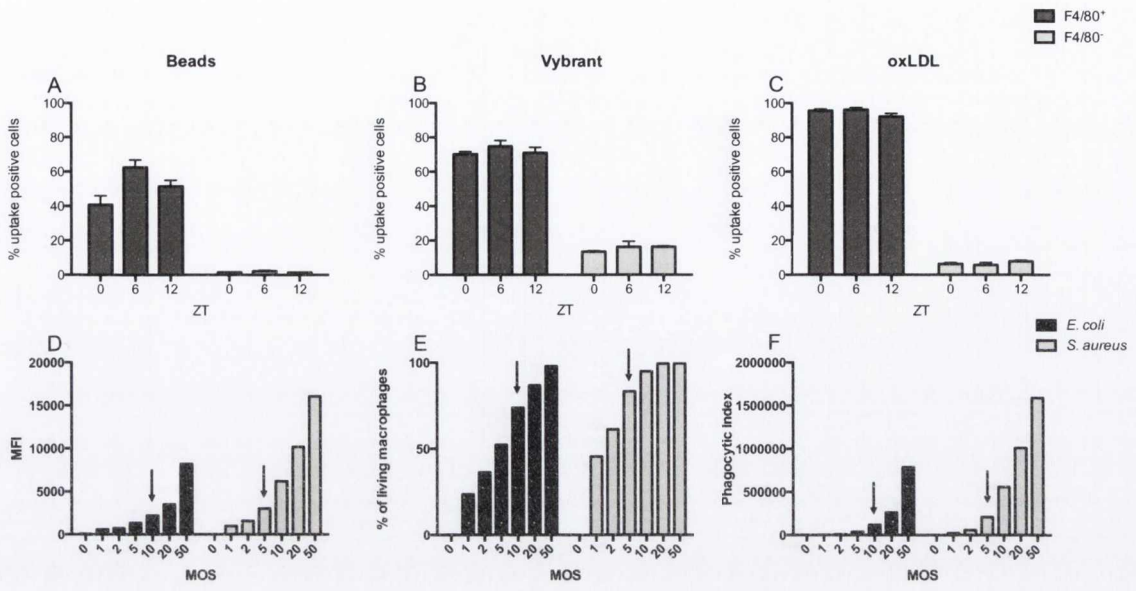


Figure 3.2.2.2: F4/80$^-$ cells do not impact on uptake measurements.

A-C) Peritoneal washouts were extracted at indicated times and subsequently stimulated with fluorescent beads (MOS10) (**A**), Vybrant (**B**) or 25µg/ml oxLDL (**C**) for 1 h *ex vivo*. Upon flow cytometry analysis, the percentage of uptake positive cells in the F4/80$^+$ and F4/80$^-$ population was quantified. All error bars represent the standard error of the mean from biological replicates. Statistical analysis using two way ANOVA: **A)** Interaction: DF=2, F=5.543, p=0.0105. ZT: DF=2, F=6.374, p=0.006. F4/80: DF=1, F=378.3, p<0.0001. **B)** Interaction: DF=2, F=0.3417, p=0.714. ZT: DF=2, F=1.159, p=0.3307. F4/80: DF=1, F=831.8, p<0.0001. **C)** Interaction: DF=2, F=3.935, p=0.0333. ZT: DF=2, F=0.4206, p=0.6614. F4/80: DF=1, F=8369, p<0.0001. n=5. **D-F)** Peritoneal exudate cells were stimulated for 1 h with heat inactivated fluorescent bacterial particles and a dose dependent increase in fluorescence was measured in peritoneal macrophages as defined by F4/80 positivity. **D)** Mean fluorescent intensity. **E)** Percent of uptake positive cells. **F)** Phagocytic index. Arrows indicate the concentration used in following experiments. Graph originates form a single experiment with N=1.

Daily oscillations that were found when cells were stimulated with *E. coli* or *S. aureus* bioparticles, were also present using a broad range of other fluorescent particles, such as inert latex beads, Vybrant (heat inactivated *E. coli* particles) (Figure 3.2.2.3) and living *E. coli* bacteria (Figure 3.2.2.4), all of which showed a trend towards increased particle ingestion at ZT12. Rhythmic uptake was additionally verified using alternative methods such as fluorescence plate reader and colony formation assay (CFA) besides flow cytometry, which was the main method that was used throughout the study.

While increased uptake at ZT12 compared to ZT0 was generally consistent when bacterial particles were used, latex bead ingestion displayed much greater variability. Reduced consistency between experiments may be a result of day-to-day variation, as time-points within each experiment were not necessarily performed at the same day. Technical divergence, such as variations in stimulus concentration, and flow cytometry analysis may also be a source of uncontrolled variation. Considering that latex beads - the only particles that would not trigger pattern recognition receptors such as TLRs - displayed highest variability could further indicate a specific role for PAMP recognizing receptors in diurnal particle uptake. Further, the latex beads were advertised to have a diameter of 1-2 µm - a size comparable to single bacteria - however, microscopy analysis revealed a particle size significantly exceeding this specification (data not shown). This, together with the high variability that was seen using inert latex beads in comparison to heat inactivated bacteria, made these particles less suitable, although initial studies resulted in the most significant differences in uptake compared to other material. *E. coli* and *S. aureus* bioparticles therefore became focus of the majority of future studies.

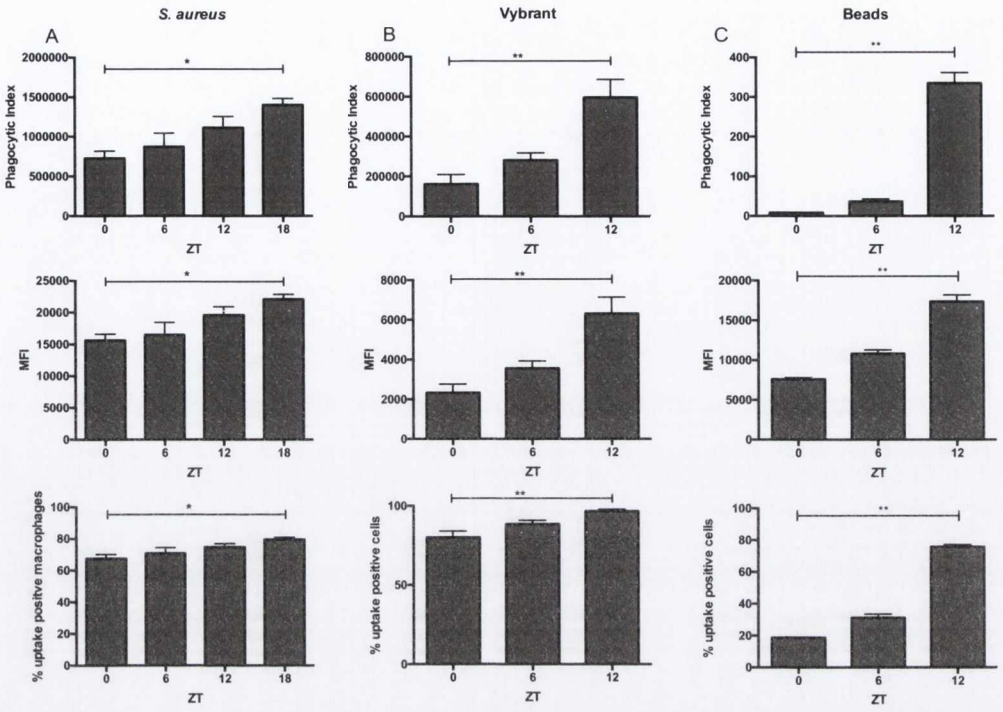


Figure 3.2.2.3: Peritoneal macrophages show diurnal uptake of various particles.

Peritoneal cells were stimulated for 1 h with fluorescent *S. aureus* (**A**) or Vybrant (**B**) particles, and fluorescence was measured in F4/80^{+} cells by flow cytometry. **C**) Latex beads (MOS50) were used to stimulate peritoneal macrophages for 1 h and fluorescence intensity was recorded using a flow cytometer. Phagocytic index (top), MFI (middle) and percentage of uptake positive cells (bottom) are displayed. All error bars represent the standard error of the mean from biological replicates. Statistical analysis using Kruskal Wallis ANOVA and Dunn's post-hoc multiple comparison (indicated in the graph with *p<0.05, **p<0.01). Kruskal Wallis ANOVA from top to bottom: **A**) p=0.0182, p=0.0171, p=0.0261. **B**) p= 0.0001, p=0.003, 0.0037. **C**) p<0.0001, p<0.0001, p<0.0001. n=4-6.

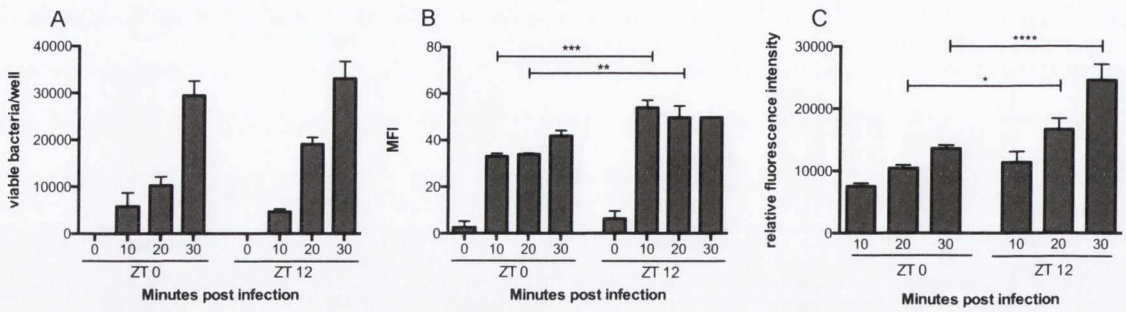


Figure 3.2.2.4: Ingestion of living and heat-inactivated *E. coli* bacteria is increased at ZT12 as measured by various methods.

Living *E. coli* bacteria (MOI20) (**A**, **B**) or Vybrant (**C**) was used to stimulate peritoneal cells for up to 30 minutes. Bacterial uptake was quantified using CFA (**A**), or fluorescence intensity as measured by flow cytometry (**B**) or a plate reader (**C**). All error bars represent the standard error of the mean from biological replicates. Statistical analysis using two way ANOVA RM and Sidak's multiple comparison test. *p<0.05, **p<0.01, ***p<0.001, ****p<0.0001. **A)** Interaction: DF=3, F=2.208, p=0.1399. ZT: DF=1, F=3.126, p=0.1518. Minutes post infection: DF=3, F=82.46, p<0.0001. **B)** Interaction: DF=3, F=3.458, p=0.0512. ZT: DF=1, F=60.38 p=0.0015, Minutes post infection: DF=3, F=90.61, p<0.0001. **C)** Interaction: DF=2, F=13.1, p=0.0004. ZT: DF=1, F=12.91, p=0.0071. Minutes post infection: DF=2, F=92.98, p<0.0001. n=3-5.

Following ingestion of material, phagosomes become rapidly acidified to initiate breakdown of the contents. Acidification-rate can therefore be used as an indicator of bacterial removal following uptake. Secondly, acidification has the potential to impinge on the fluorescent signal emitted by fluorochromes. To test manipulation of the uptake signal that is recorded in uptake experiments due to oscillations in the acidification rate and to simultaneously investigate the possibility of diurnal breakdown of bacteria, pH sensitive fluorochromes (pHrodo) - which emit only in an acidic environment, such as the phagosome - were used. Emission of pHrodo labelled *E. coli* as well as *S. aureus* bacteria did however not vary over the course of the day (Figure 3.2.2.5), indicating time independent acidification rates.

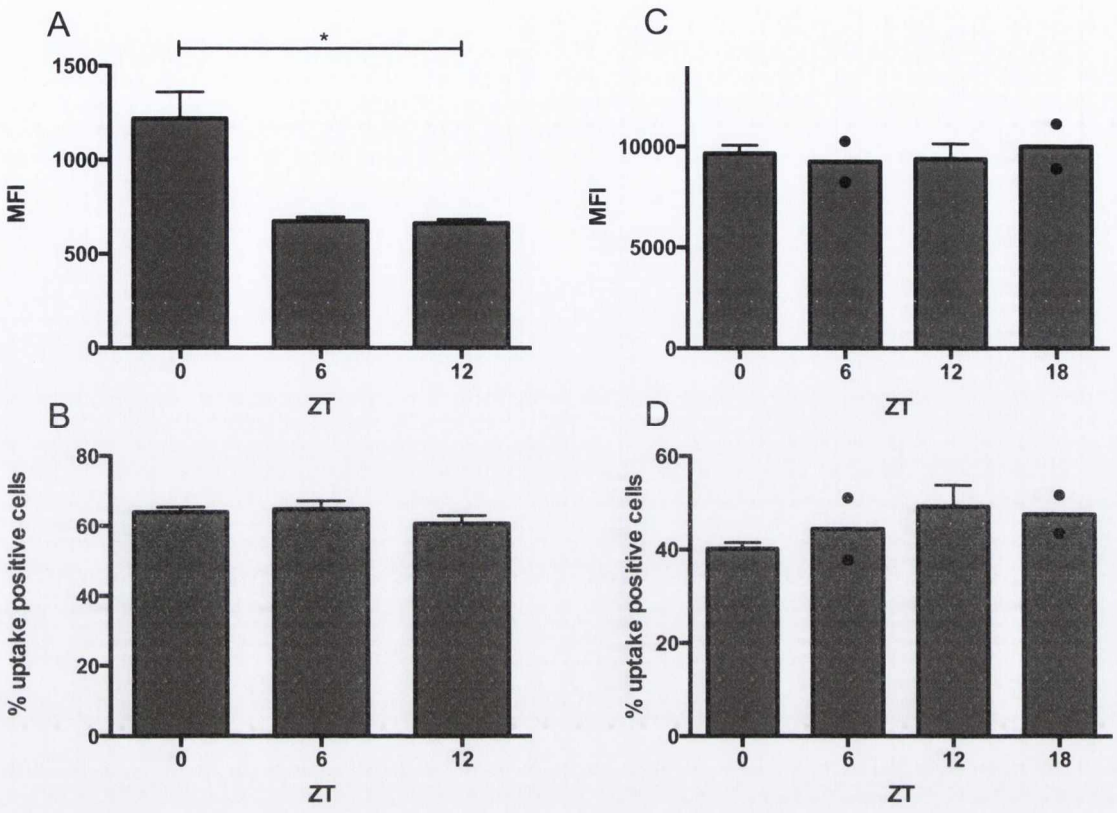


Figure 3.2.2.5: Acidification of phagosomes is not diurnal.

Isolates of peritoneal cells from different times of the day were stimulated for 1 h with pHrodo labelled *E. coli* **(A, B)** or *S. aureus* **(C, D)** *ex vivo*. Fluorescence intensity of F4/80^{+} cells as measured by flow cytometry did not indicate changes in acidification of phagosomes following ingestion according to MFI **(A, C)** or percentage of uptake positive cells **(B, D)**. Statistical analysis using Kruskal Wallis ANOVA and Dunn's post-hoc multiple comparison (indicated in the graph with *p<0.05). Kruskal Wallis ANOVA: **A**) p=0.005. **B**) p= 0.4163. **C**) p=0.8849. **D**) p=0.3290. n=5 (or n=2 if indicated).

3.2.3 The fluorescence signal detected in uptake studies originates from ingested, not surface bound particles

Flow cytometry analysis of fluorescence signals has many advantages, such as the ability to measure multiple signals in thousands of cells, while maintaining single cell resolution. This provides the opportunity to perform correlation studies that focus for example on functionality and a particular marker of interest, as was done in the course of this study (Figure 3.2.6.3). However, spatial resolution gets lost with this technology. It was therefore of importance to verify that the signal that was seen indeed originated from ingested and not surface bound particles. Confocal microscopy on cells that were processed similar to samples that were used for flow cytometry, and subsequent staining of the plasma membrane (with CellMask) to facilitate identification of the cell boundaries, was used to address this concern (Figure 3.2.3.1). Additional incorporation of a fluorescent antibody directed against the *S. aureus* particles that were used in this study, provided an extra layer of evidence that particles were truly on the inside of the cell, as the antibody was incapable of penetrating thought the plasma membrane and could only stain surface bound material (Figure 3.2.3.1).

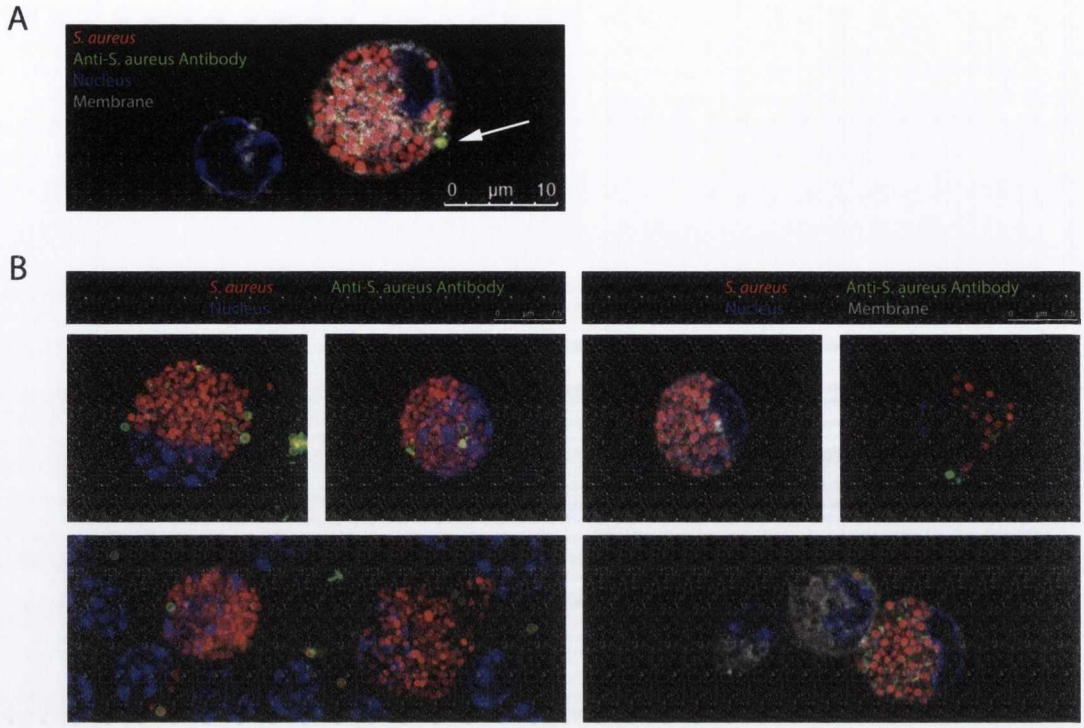


Figure 3.2.3.1: Confocal microscopy verifies ingestion, rather than surface binding of particles.

Mouse peritoneal macrophages were isolated and stimulated with fluorescent *S. aureus* bioparticles for 1 h. Following vigorous washing, cells were adhered to Poly-L-Lysin coated cover slips and stained for CellMask, Hoechst 33342, and anti-S. aureus before mounting onto a microscopy slide for confocal microscopy. The majority of *S. aureus* particles were clearly located within the cell boundaries, which was confirmed by absence of the anti-S. aureus antibody staining. **A)** One particle (indicated with arrow) appeared to be within a not entirely closed phagocytic cup, allowing staining of the particle with the anti-S. aureus antibody. **B)** Screening of increased cell numbers recapitulated observation of intracellular localization of particles. *S. aureus* particles which were not associated with any cells present with a halo, verifying detection by the anti-S. aureus antibody.

To further support that the detected signal was originating from phagocytosed material, actin polymerization in peritoneal cells was inhibited and particle ingestion was prevented. Increasing concentrations of the actin polymerization inhibitor, Latrunculin A, resulted in a dose dependent decrease in the fluorescent signal (Figure 3.2.3.2 A). This not only provided proof of principle,

but also an opportunity to investigate pathways while abolishing possible variations due to differences in uptake.

The previously reported dependency of cytokine response on uptake (Azevedo et al., 2012) could also be recapitulated as cytokine levels decreased equally to particle uptake, in a dose dependent manner with increasing Latrunculin A concentrations (Figure 3.2.3.2 B). To verify that cytokine production, rather than export was affected following Latrunculin A treatment, cytokine mRNA needed to be measured. These experiments were underway, but not completed before submission of this work.

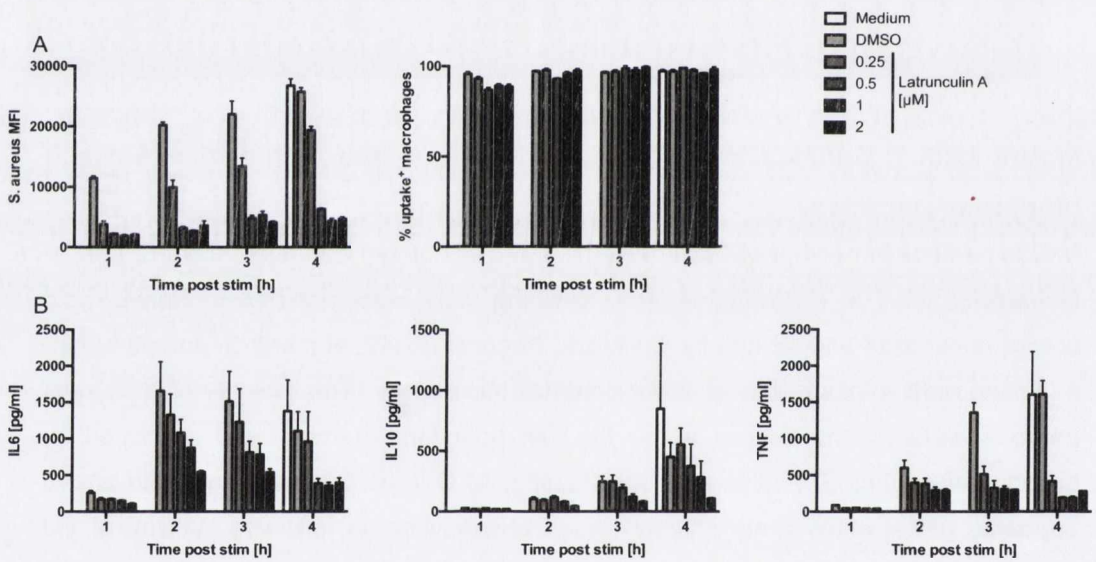


Figure 3.2.3.2: Latrunculin A inhibition dose dependently decreases bacterial uptake and cytokine secretion.

Peritoneal cells were pre-incubated with increasing amounts of Latrunculin A for 10 min before *S. aureus* bioparticles were added to initiate uptake. At the indicated time points cells were prepared for flow cytometry analysis of the fluorescent signal in F4/80$^+$ cells **(A)** and supernatants were collected for subsequent measurement of IL-6, IL-10 and TNF **(B)**. No effect of DMSO alone was found in controls with or without equal amounts of DMSO that were used to prepare the Latrunculin A solutions. N=3.

3.2.4 Serum shock is not a reliable method to investigate rhythmic uptake

Balsalobre and colleagues described a method, referred to as serum shock, to investigate the molecular clock in tissue culture cells by inducing synchronized rhythmicity (Balsalobre et al., 1998). As mice have to be euthanized to extract primary cells for uptake studies in peritoneal macrophages, an opportunity to investigate the underlying molecular mechanism in cultured macrophages was desirable to reduce the number of animals. Further, timed synchronization in tissue culture cells introduced the opportunity to challenge cells from different clock states simultaneously, thereby reducing technical variability. Stimulation of primary bone-marrow-derived macrophages (BMDMs) or peritoneal exudate cells with 50% horse serum for two hours, followed by serum deprivation was used in the following studies to examine the possibility to interrogate clock oscillations and particle uptake in this system.

While uptake of latex beads, Vybrant or living *E. coli* in serum shocked BMDMs appeared to vary between time points and was oscillating in a circadian manner according to JKT cycle analysis (Hughes et al., 2010), this fluctuation was also apparent in non-serum shock control cells (Figure 3.2.4.1). This unexpected finding suggested that re-plating, or washing of the control cells to mock treat similarly to the serum shocked cells, could potentially induce some synchronization in these cells and that oscillations seen in the serum shocked samples were most likely independent of the serum shock treatment. Considering the importance of temperature as an entraining signal (Brown et al., 2002b), this may also have been caused by a temperature pulse, as heat shock at 43˚C for 30 minutes has been reported to be sufficient for clock synchronization in fibroblasts (Tamaru et al., 2011). Cooling of the cells as they were handled in the biosafety cabinet to serum or mock treat, and subsequent warming of the cells as they were placed back into a 37˚C incubator, may have therefore already been sufficient to induce mild synchronization. Regardless of the source of this oscillation in the mock treated cells, the use of these cells as control cells seemed inappropriate and likely disadvantageous.

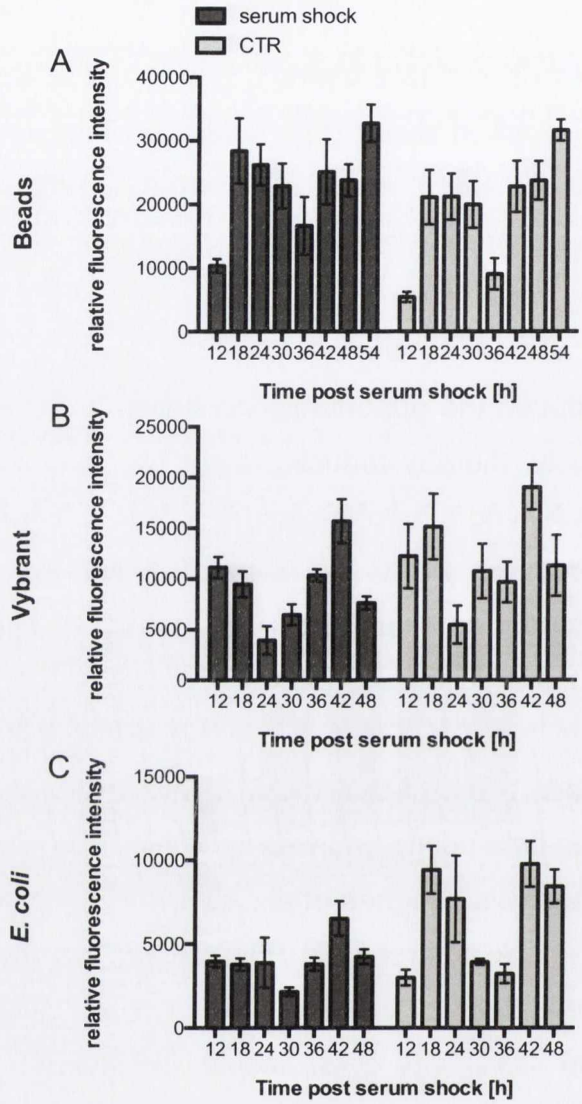


Figure 3.2.4.1: Uptake in serum shocked and control BMDMs.

BMDMS were serum shocked and stimulated for 60 min with fluorescent particles at the indicated time points with latex beads (MOS500) **(A)**, Vybrant **(B)**, or living *E. coli* (MOI500) **(C)**, and fluorescence was measured using a fluorescence plate reader. Ingestion of particles appeared to vary over time in serum shocked and control cells. Compiled data from two independent experiments. N=5. Adjusted p value according to JKT Cycle analysis: **A)** SS: p=0.0448, CTR: p=0.0485, **B)** SS: p=0.00000916, CTR: p=0.0834 **C)** SS: p=0.01785, CTR: p=0.00345. Interaction of time and serum shock treatment using two way ANOVA: **A)** p=0.9728, **B)** p=0.7731, **C)** p=0.0275.

To further investigate the possibility of using the serum shock model, a genetic approach was implemented. *Bmal1* is the only single clock gene that when knocked out results in a complete breakdown of the clock (Bunger et al., 2000), allowing simple genetic modification to conditionally deplete the clock in specific lineages. While *Bmal1* expression normally cycles in peritoneal cells over the course of a day (Figure 3.2.4.2 A), ablation of *Bmal1* in the BMAL1$^{fl/fl}$LyzMCre$^{+/+}$ animals resulted in steady low levels of Nr1d1 mRNA, indicating successful breakdown of the clock (Figure 3.2.4.2 B, C). Because the serum shock model is dependent on the presence of a functional clock within each cell, stimulation of *Bmal1* deficient cells with 50% serum in a preliminary study, as expected, did not appear to induce rhythmic clock gene expression, as clock gene mRNA levels in WT but not *Bmal1* knockout BMDMs seemed to oscillate when serum shocked in parallel (Figure 3.2.4.3). It should be noted that sample size was limited and statistical analysis could not be performed to support this quantitatively.

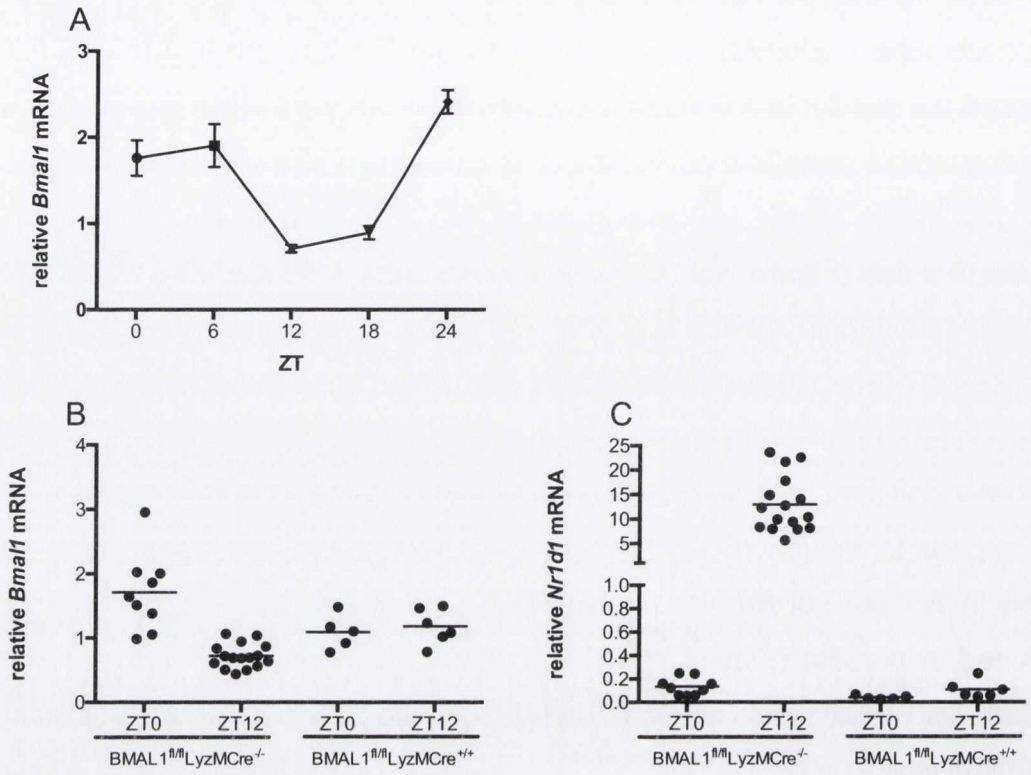


Figure 3.2.4.2: The clock in peritoneal cells is functional and can be ablated in BMAL1$^{fl/fl}$LyzMCre$^{+/+}$ animals.

A) Rhythmic expression of *Bmal1* in peritoneal cells over the course of a day as measured by qPCR. **B, C)** BMAL1$^{fl/fl}$LyzMCre$^{-/-}$ control animals possessed a functional clock as indicated by *Bmal1* **(B)** and *Nr1d1* **(C)** fluctuations. *Bmal1* deficiency in BMAL1$^{fl/fl}$LyzMCre$^{+/+}$ animals **(B)** abolished *Nr1d1* oscillations **(C)**, indicating complete break down of the clock. Compiled data from two independent experiments. **A)** Adjusted p value according to JKT Cycle analysis: $p<0.000001$. **B, C)** Statistical analysis using two way ANOVA: **B)** Interaction: DF=1, F=17.09, p=0.0002. ZT: DF=1, F=11.91, p=0.0016. Genotype: DF=1, F=0.3731, p=0.5456. **C)** Interaction: DF=1, F=19.73, $p<0.0001$. ZT: DF=1, F=20.16, p= $p<0.0001$. Genotype: DF=1, F=20.32, $p<0.0001$. N=5-37.

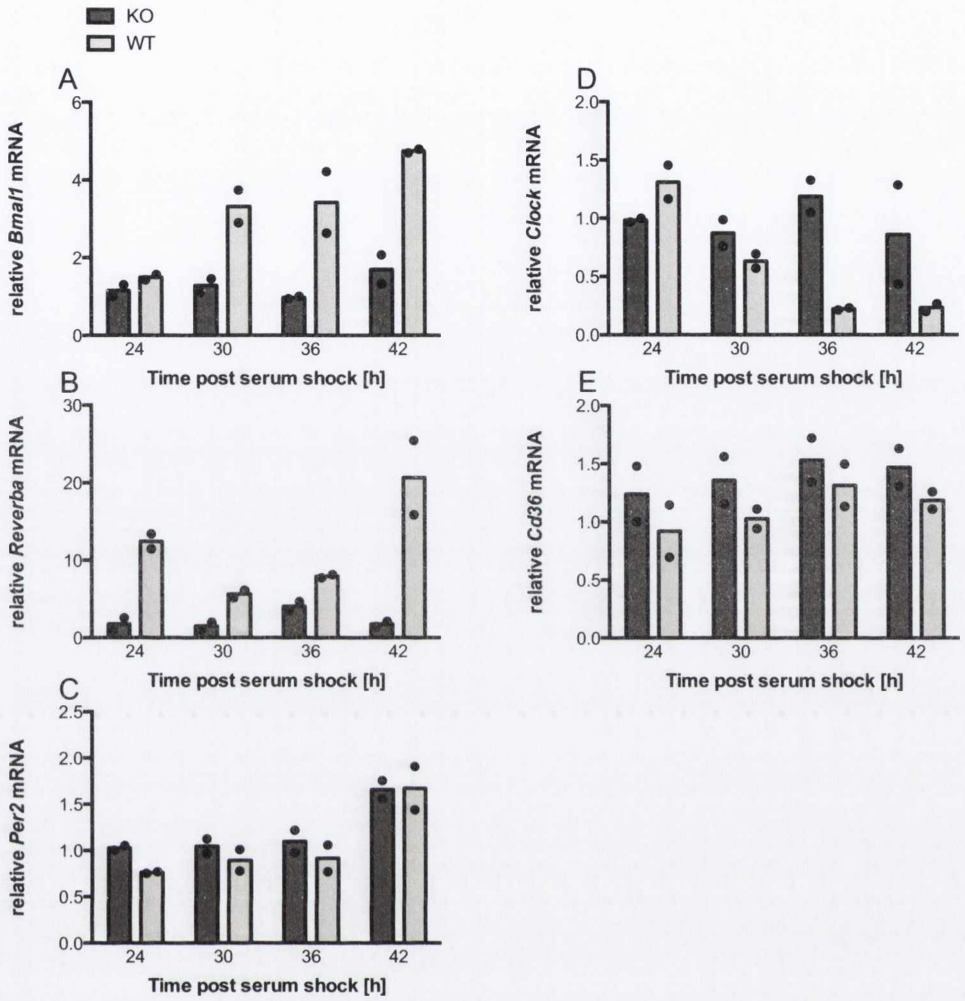


Figure 3.2.4.3: Serum shock appears to induce clock gene oscillation in WT, but not in *Bmal1* knockout macrophages.

RNA from WT and *Bmal1* knockout BMDMs was isolated at the indicated times following serum shock and expression of clock genes and *Cd36* was measured via qPCR. *Bmal1* knockout cells did not display changes of clock gene or *Cd36* expression over time, while WT cells appeared to induce clock gene fluctuation. N=2.

As the final control to verify the unsuitability of the serum shock model for functional phagocytosis studies, particle uptake in serum shocked wild type and *Bmal1* knockout cells was examined. In this study, peritoneal macrophages were used, as primary tissue resident cells often differ in many aspects from *in vitro* differentiated bone marrow derived macrophages, and the initial observation of diurnal uptake had been made in this cell type immediately post isolation. It was found that ingestion of latex beads, heat-inactivated and living *E. coli* by peritoneal exudate cells was not rhythmic, (Figure 3.2.4.4), and particle ingestion further displayed similar levels in wild type and *Bmal1* knockout cells, arguing for a molecular clock independent pathway of uptake regulation. This confirmed the serum shock model being inappropriate for functional phagocytosis studies.

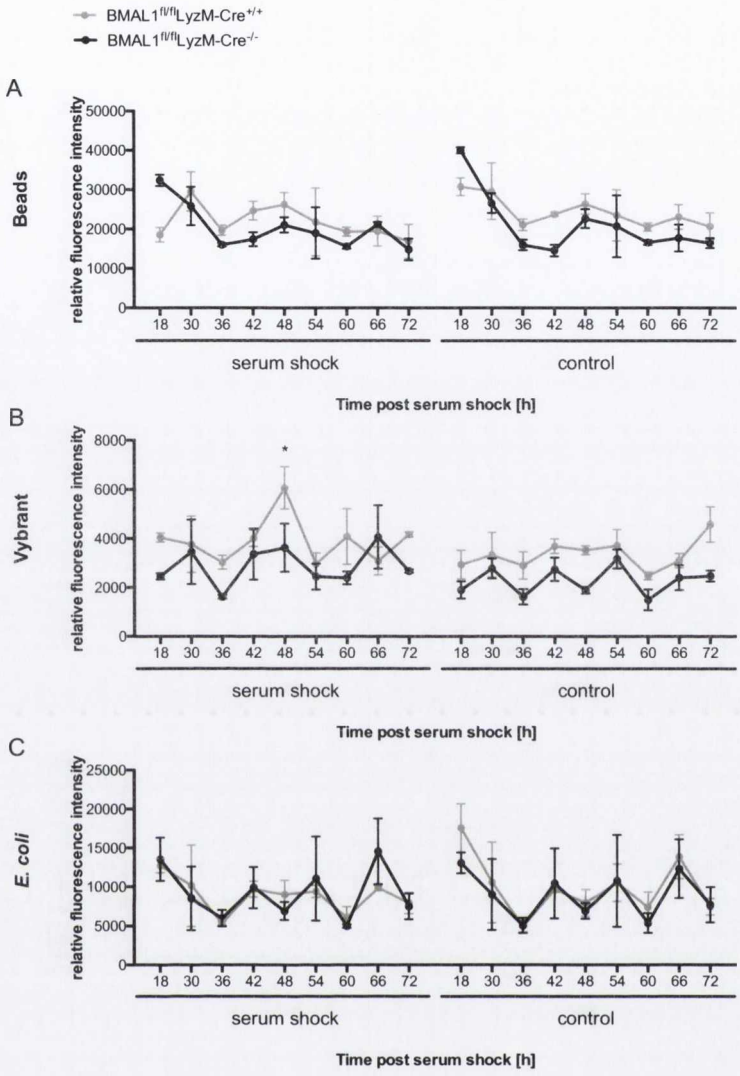


Figure 3.2.4.4: Cells lacking *Bmal1* have similar uptake properties to wild type cells.

Peritoneal cells were extracted from myeloid specific *Bmal1* knockout and WT mice and subsequently serum shocked or control treated. At the indicated times post serum shock, cells were treated with fluorescent latex beads (MOS500) **(A)**, Vybrant **(B)**, or living *E. coli* (MOI500) **(C)** for 1 h before fluorescence was measured using a fluorescence plate reader. Particle ingestion appeared arrhythmic in both, the KO and the WT mice, and similar between the genotypes. Error bars represent the standard error of the mean. Statistical analysis using two way ANOVA and Sidak's multiple comparison test. *$p<0.05$. **A)** Interaction: DF=24, F=0.9238, p=0.5711. Time post shock: DF=8, F=5.976, $p<0.0001$. Group: DF=3, F=2.02, p=0.119. **B)** Interaction: DF=24, F=1.107, p=0.3602. Time post shock: DF=8, F=2.187, p=0.0387. Group: DF=3, F=10.71, $p<0.0001$. **C)** Interaction: DF=24, F=0.164, $p>0.9999$. Time post shock: DF=8, F=4.14, p=0.0004. Group: DF=3, F=0.2787, p=0.8406. N=3.

3.2.5 The cell intrinsic clock is dispensable for diurnal oscillations in particle uptake

To investigate the necessity of the molecular clock to mediate rhythmic particle ingestion, genetic deletion of *Bmal1*, which causes a complete loss of clock functionality in cells of interest, was used in *ex vivo* studies besides overexpression of clock components in a more artificial *in vitro* setting.

Initial studies showed that neither uptake after 1 hour, nor the kinetics of Vybrant uptake was affected in *Bmal1* knockout peritoneal or bone marrow derived macrophages compared to WT (Figure 3.2.5.1 A, D). Similar results were found in BMDMs using living *E. coli* (Figure 3.2.5.1 B, E), and in line with previous findings, equal uptake rates between the genotypes were also found following serum shock treatment (Figure 3.2.5.1 E).

Congruent with this, phagocytosis of inert latex beads by peritoneal macrophages isolated at different times throughout the day resulted in similar uptake rates between *Bmal1* KO and WT mice, with increased ingestion at ZT12 compared to ZT0 (Figure 3.2.5.1 C).

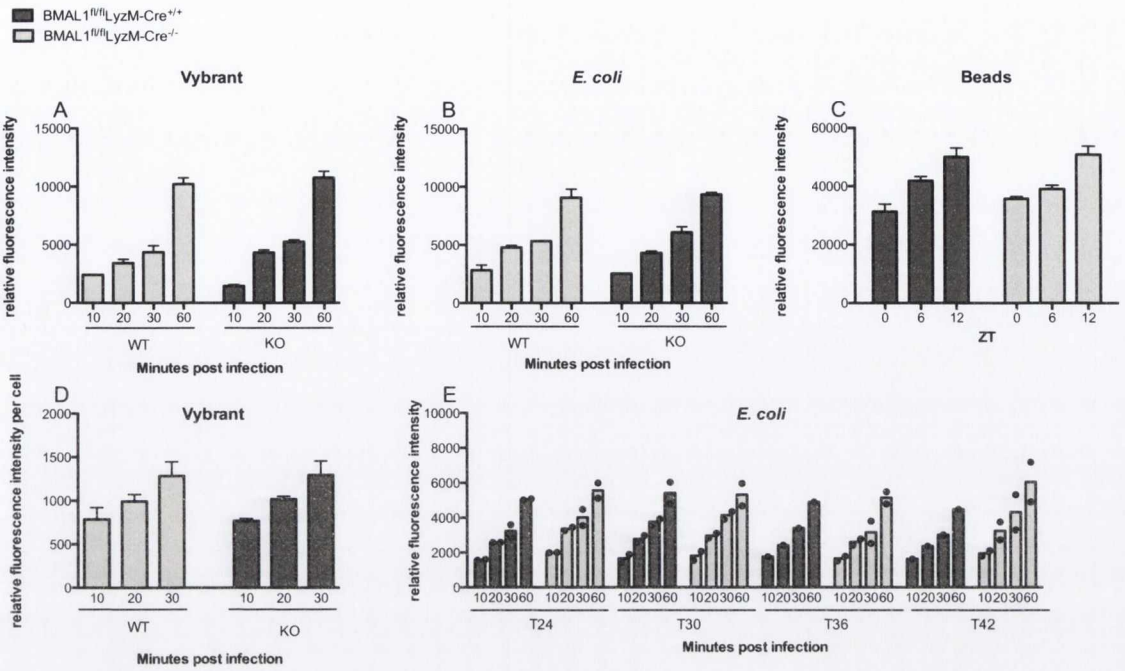


Figure 3.2.5.1: *Bmal1* deletion does not alter bacterial particle uptake in macrophages.

Cells from *Bmal1* KO and *Bmal1* WT mice were incubated for the indicated times with living fluorescent particles before fluorescence was measured using a fluorescent plate reader. **A)** BMDMs incubated with Vybrant. **B)** BMDMs incubated with *E. coli* (MOI500). **C)** Peritoneal macrophages were isolated at the indicated times and stimulated for 1 h with fluorescent latex beads (MOS500). **D)** Peritoneal macrophages incubated with Vybrant. **E)** Serum shocked BMDMs incubated with *E. coli* (MOI500). *Bmal1* KO and *Bmal1* WT cells displayed similar fluorescence intensity, with increased values at ZT12. Statistical analysis using two way ANOVA and Sidak's multiple comparison test. **A)** ANOVA RM Interaction: DF=3, F=1.008, p=0.4231. Time: DF=3, F=95.8, p<0.0001. Genotype: DF=1, F=0.126, p=0.7403. **B)** ANOVA RM Interaction: DF=3, F=1.008, p=0.4231. Time: DF=3, F=95.8, p<0.0001. Genotype: DF=1, F=0.126, p=0.7403. **C)** Interaction: DF=2, F=1.378, p=0.2714. Time: DF=2, F=30.06, p=0.2714. Genotype: DF=1, F=0.1960, p=0.662. **D)** ANOVA RM Interaction: DF=2, F=0.05288, p=0.9488. Time: DF=2, F=28.13, p=0.0002. Genotype: DF=1, F=0.001342, p=0.9725.. n=2-5.

In agreement with these results and further supporting that the cellular clock was dispensable for rhythmic uptake, overexpression of core clock components in iBMDMs did not appear to alter uptake capacity and kinetics. Accordingly, in preliminary studies, *Bmal1* overexpression did not affect uptake of living *E. coli* four and six hours after transfection (Figure 3.2.5.2 A, B) and single or duplex

overexpression of *Bmal1* and/or *Clock* similarly did not alter uptake of latex beads, Vybrant and living *E. coli* (Figure 3.2.5.2 C-E). mRNA analysis confirmed significant induction of the overexpressed genes, while selected candidate genes (*Cd36*, *Atg7*, *Cd14*, *Dynactin6*, *Macro*, *Ppara*, *Msr1*) that had the potential to induce particle uptake, as well as other clock genes (*Per2*, *Nr1d1*) remained unchanged (data not shown). It should however be noted that these studies would need repetition and increased sample numbers for verification.

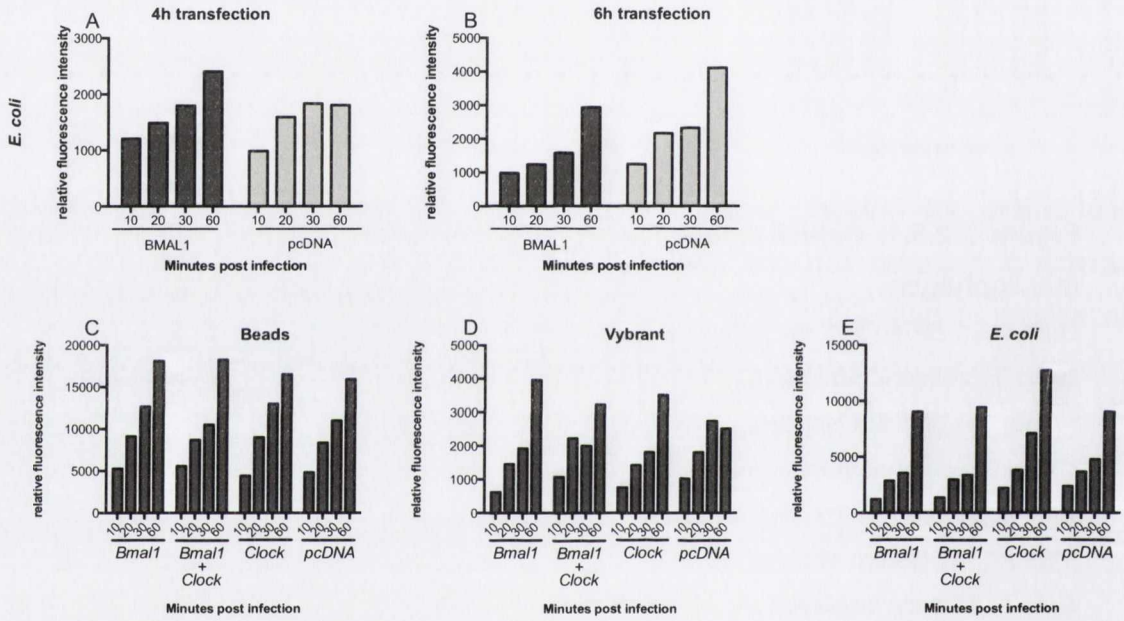


Figure 3.2.5.2: *Bmal1* and *Clock* overexpression does not affect particle uptake.

iBMDMs were transfected with *Bmal1* or *Clock* alone, or a combination of both, or the empty pcDNA vector control, at 1 µg **(A, B)** or 0.75 µg per plasmid **(C-E)** for 4 h **(A, C-E)** or 6 h **(B)**. Cells were then stimulated with fluorescent latex beads (MOS500) **(C)**, Vybrant **(D)** or living *E. coli* (MOI500) **(A, B, E)** for the indicated times, before fluorescence was measured on a fluorescence plate reader. N=1.

3.2.6 Rhythmicity of CD36 and its role in bacterial uptake

CD36 has been shown to mediate phagocytic uptake of a range of different materials, from oxidized LDL to bacteria (Stuart et al., 2005, Endemann et al., 1993), and influence the intensity of downstream inflammatory responses (Sheedy et al., 2013). It therefore appeared to be a plausible candidate to regulate diurnal particle ingestions that was seen in *ex vivo* studies. To validate a role for CD36 in this system, oscillations in surface expression had to be present. While total CD36 protein levels did not appear diurnal in peritoneal macrophages as measured by intra-cellular flow cytometry (Figure 3.2.6.1 D), surface abundance was generally increased at ZT12, correlating with increased particle ingestion in previous experiments (Figure 3.2.6.1).

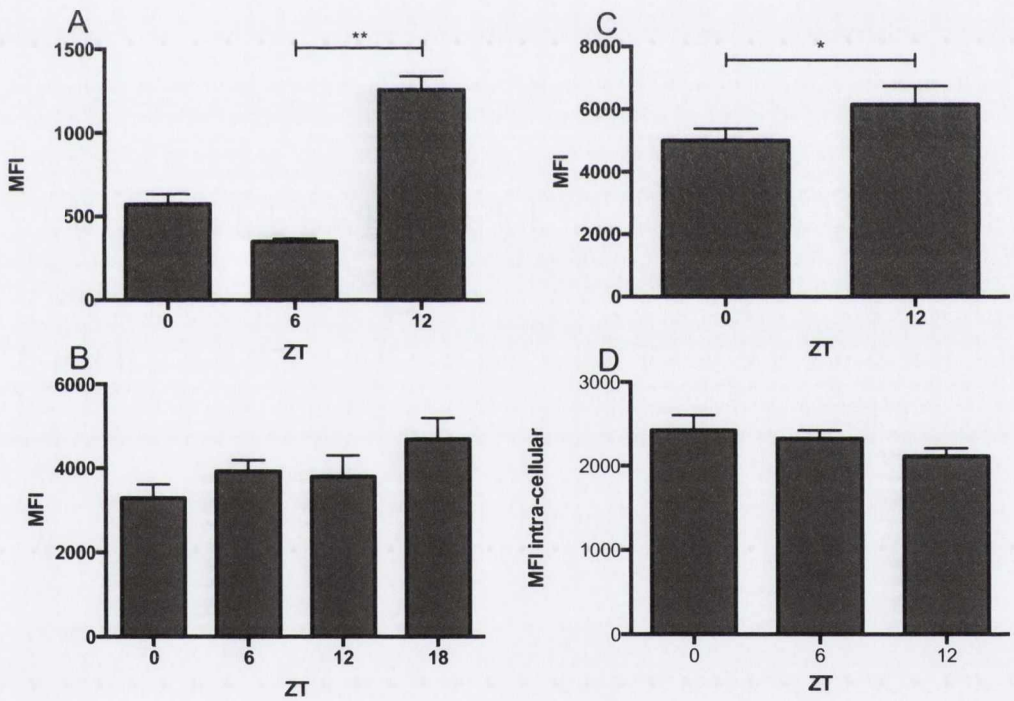


Figure 3.2.6.1: CD36 surface, but not total level is time-of-day dependent.
Peritoneal cells were isolated at the indicated time points and stained for CD36. **A, B)** Surface staining in F4/80$^+$ naïve macrophages in two independent experiments. **C)** Surface staining in F4/80$^+$ macrophages stimulated for 1 h with bioparticles *ex vivo*. **D)** Intracellular staining in F4/80$^+$ naïve macrophages. Statistical analysis according to Mann-Whitney (**C**) or Kruskal Wallis ANOVA and Dunn's post-hoc multiple comparison (indicated in graph). *p<0.05, **p<0.01). Kruskal Wallis ANOVA: **A**) p<0.0001. **B**) p=0.2322. **D**) p=0.2391. N=5-6.

Congruent with constitutive total CD36 protein abundance, *Cd36* mRNA levels in FACS purified F480$^+$ macrophages were not found to fluctuate over the course of a day, while clock gene expression remained cyclic, verifying that these cells had an intact molecular clock. Analysis of F4/80$^-$ peritoneal exudate cells illustrated that clock genes as well as *Cd36* were mainly expressed in F4/80$^+$ cells, suggesting that F4/80$^-$ contaminations in assays that could not discriminate these two populations may be tolerable (Figure 3.2.6.2).

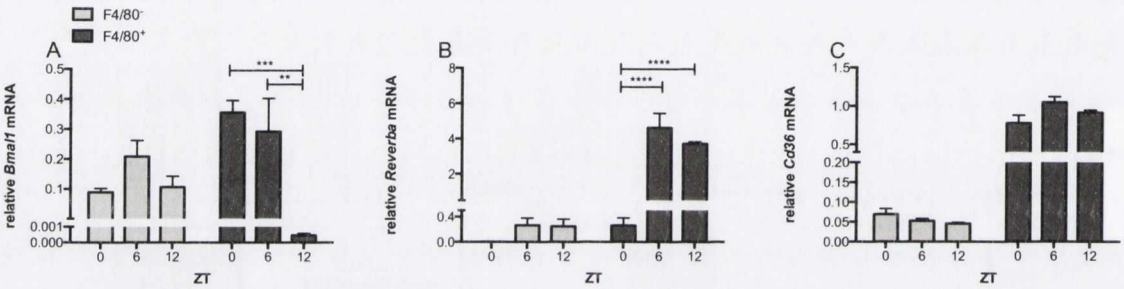


Figure 3.2.6.2: *Cd36* mRNA is not rhythmic in F4/80$^+$ or F4/80$^-$ peritoneal macrophages.

Peritoneal cells were isolated at the indicated time points and FACS sorted using an Aria Cell sorter for F4/80$^+$ and F4/80$^-$ living cells into RLT buffer for subsequent RNA isolation. A functional clock was present in F4/80$^+$ cells as indicated by rhythmic *Bmal1* **(A)** and *Reverba* **(B)** expression, but not in F4/80$^-$ cells. *Cd36* mRNA level did not vary over the course of the day in F4/80$^+$ and F4/80$^-$ cells and was hardly detectable in F4/80$^-$ cells **(C)**. Statistical analysis using two way ANOVA RM and Sidak's multiple comparison test (indicated in graph with *p<0.05, **p<0.01, ***p<0.001, ****p<0.0001). **A)** Interaction: DF=2, F=5.766, p=0.009. ZT: DF=2, F=7.501, p=0.0029. F4/80: DF=1, F=3.265, p=0.0833. **B)** Interaction: DF=2, F=0.05127, p=0.0443. ZT: DF=2, F=2.745, p=0.0844. F4/80: DF=1, F=381.8, p<0.0001. n=5. **C)** Interaction: DF=2, F=12.72, p=0.0003. ZT: DF=2, F=16.35, p<0.0001. F4/80: DF=1, F=62.73, p<0.0001.

To further examine the role of CD36 in rhythmic particle uptake, CD36 surface abundance was plotted against particle fluorescence within the cells, which was used to determine uptake capacity. While in some studies increased uptake capacity appeared to correspond to increased CD36 surface abundance, there

was overall no strong association (Figure 3.2.6.3). Of note, ingestion of oxLDL, a known CD36 ligand (Endemann et al., 1993), similarly did not appear to be dependent on CD36 surface abundance (Figure 3.2.6.3 J, K).

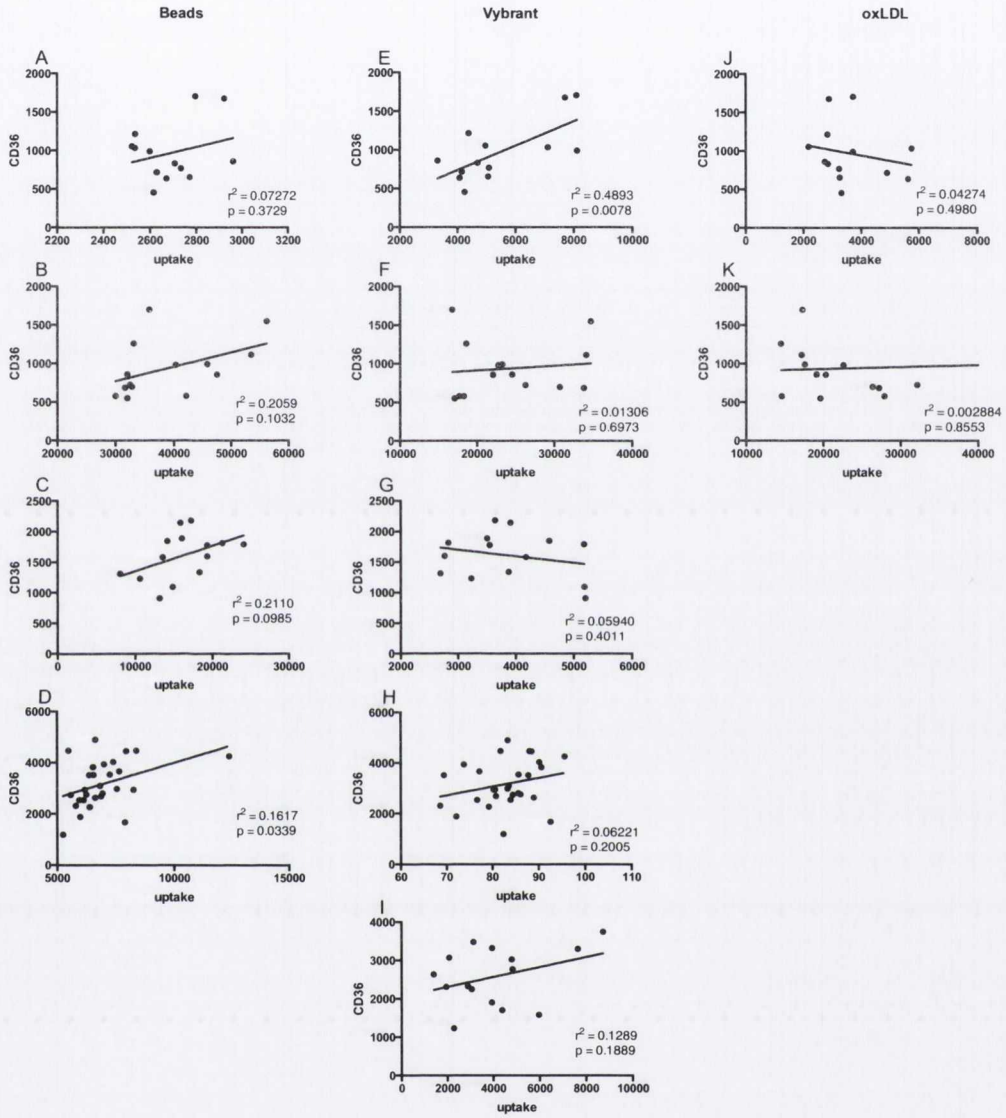


Figure 3.2.6.3: CD36 surface expression levels do not correlate with uptake capacity across experiments.

Peritoneal macrophages were isolated at different times of the day and stained for surface CD36 or stimulated with fluorescent latex beads (MOS500) **(A-D)**, Vybrant **(E-I)** or fluorescent oxLDL (25 µg/ml) **(J, K)** for 1 h. Samples were analysed by flow cytometry and the MFI of the appropriate particle in uptake positive macrophages was plotted against the MFI of the CD36 signal in F4/80$^+$ cells. Predictability (r^2) and significance (p) values did not indicate a correlation between the variables after linear regression.

A lack of association between oxLDL uptake and CD36 surface abundance was unexpected as uptake of oxLDL had been reported in multiple studies to be dependent on CD36 (Nozaki et al., 1995, Jay et al., 2015). The amount of oxLDL that was used in the presented study was based on previous publications and was verified as being appropriate in a dose response study where 25 µg/ml oxLDL resulted in a strong signal, that was not yet reaching plateau levels in MFI or the percentage of uptake positive macrophages within the population (Figure 3.2.6.4). Therefore, the concentration was unlikely to cause discrepancies between this and previous studies. However, this should be verified using increased numbers of replicates.

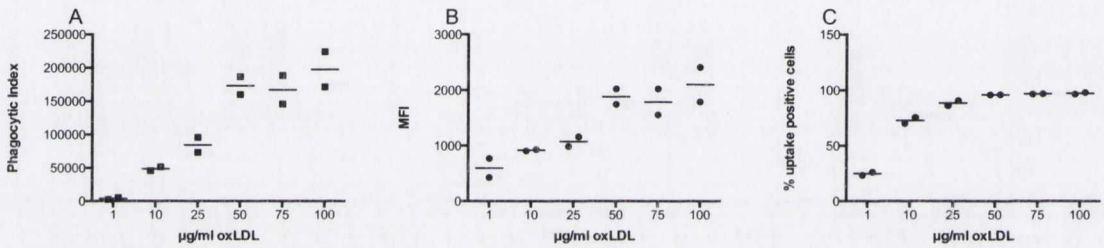


Figure 3.2.6.4: OxLDL is taken up by macrophages in a dose dependent manner.

Peritoneal cells were isolated and treated for 1 h with DiI-labeled oxLDL at the indicated concentrations and fluorescence was analysed by flow cytometry. Phagocytic index **(A)**, MFI in the uptake positive macrophages **(B)**, and percentage of uptake positive macrophages **(C)** displayed a dose dependent induction. N=2.

CD36 expression has been shown to be induced following a high fat diet (Cameron-Smith et al., 2003, Greenwalt et al., 1995), which suggested a regulation by dietary signals. Natural oscillations in food intake had therefore the potential to be causal for the rhythmicity in CD36 surface abundance that was seen. To examine a possible regulation of CD36 by the feeding cycle, food availability was restricted to either the dark - the natural feeding time - or the light phase. A reversed phase of CD36 fluctuation in the day-time fed animals would then support a food dependent regulation of the scavenger receptor. As

ad libitum fed mice generally eat during the night phase, these animals were used as controls of time restricted feeding (TRF) and displayed comparable levels to the night-time fed animals (data not shown). Entrainment of mice to the altered feeding schedules for 5 days did not result in significant changes of CD36 surface levels, and uptake of *S. aureus* and *E. coli* bioparticles was similarly not affected (Figure 3.2.6.5). Seemingly increased *E. coli* uptake at ZT1, has to be interpreted with caution as low sample numbers were used, and was most likely due to technical variability, as this could not be recapitulated in comparable experiments with longer entrainment times (Figure 3.2.6.6). Unexpectedly, ZT12 ingestion of *S. aureus* particles did not appear increased compared to ZT0 in the night-time fed control animals. Each time point had to be a separate experiment due to the limited capacity of the CLAMS facility and the need to single house animals. Variation between time points could therefore be due to technical variations as discussed earlier, or other environmental or social effects. Also due to the limited capacity of the CLAMS facility, only *S. aureus* uptake was tested at four different time points, while *E. coli* uptake and CD36 surface abundance was only investigated at ZT0, ZT1 and ZT6. As this preliminary data argued against a role for feeding time in oscillations in particle uptake, it was not invested in further repeats to complete the time course in this experimental setting, however, statistical analysis of this limited time course already pointed towards a time-dependency in CD36 as well as uptake capacity similarly to what has been observed in earlier studies.

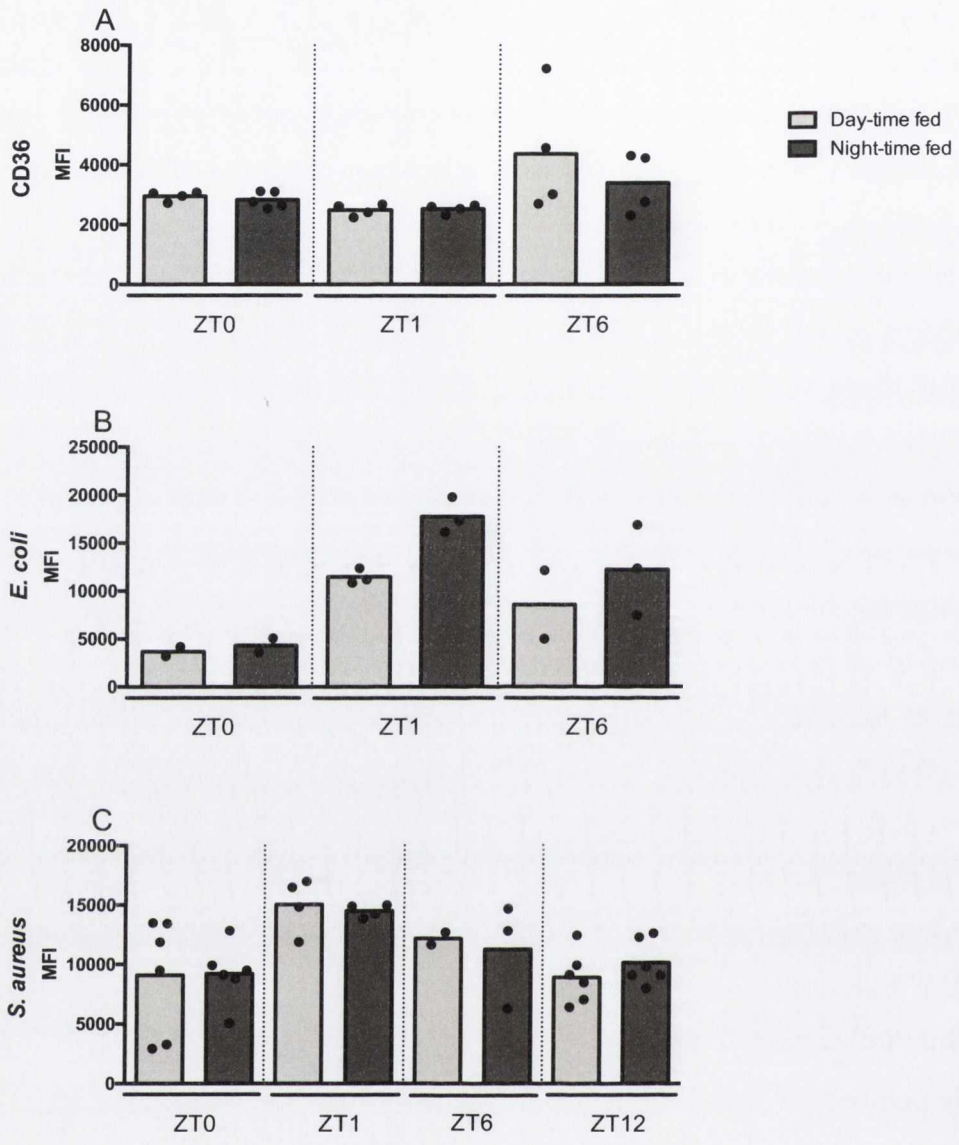


Figure 3.2.6.5: Restricted feeding schedules for 5 days do not alter uptake capacity of peritoneal macrophages *ex vivo*.

Mice were housed in the CLAMS for 5 days and peritoneal cells were isolated at the indicated time points and stained for surface CD36 **(A)** or stimulated for 1 h with heat inactivated, fluorescent *E. coli* (MOS10) **(B)** or *S. aureus* (MOS5) **(C)** particles. Fluorescence intensity was analyzed in F4/80$^+$ cells by flow cytometry. CD36 surface abundance and uptake was not affected by the feeding schedule, but appeared time-of day dependent. Statistical analysis using two way ANOVA and Sidak's multiple comparison test. **A)** Interaction: DF=2, F=0.6918, p=0.5129. ZT: DF=2, F=4.682, p=0.0222. Feeding: DF=1, F=0.8989, p=0.355. **B)** Interaction: DF=2, F=1.086, p=0.3781. ZT: DF=2, F=15.26, p=0.0013. Feeding: DF=1, F=5.075, p=0.0508. **C)** Interaction: DF=3, F=0.2299, p=0.8748. ZT: DF=3, F=7.156, p=0.001. Feeding: DF=1, F=0.0005991, p=0.9806.

To verify that an entrainment period of 5 days was sufficient and that CD36 and bacterial uptake regulation by restricted feeding did not require longer entrainment times, the experiment was repeated with TRF periods of 12 days. Similarly to what was observed after 5 days, CD36 surface abundance, as well as *ex vivo E. coli* and *S. aureus* bioparticle uptake remained similar between TRF groups (Figure 3.2.6.6 A, B, Figure 3.2.6.7 A, B). Acidification rate of phagosomes was similarly unaffected by TRF as signal intensity of pHrodo *S. aureus* bioparticles was comparable between the distinct groups (Figure 3.2.6.7 C, D). To unravel a possible role for TRF *in vivo*, *S. aureus* bioparticles were also given i.p. in a similar experimental setting, however, CD36 surface expression in stimulated cells, as well as *in vivo* uptake still appeared independent of the feeding schedule (Figure 3.2.6.6 C, D).

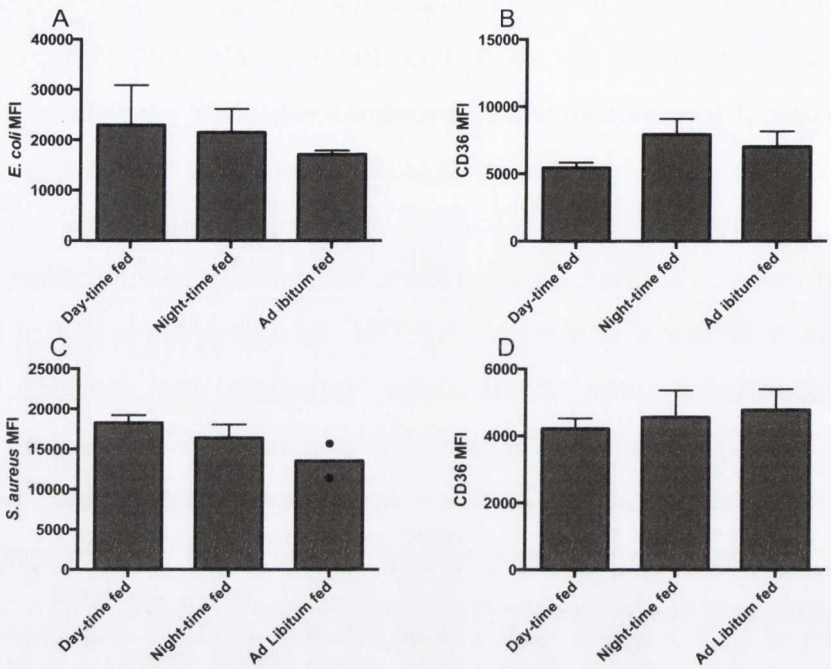


Figure 3.2.6.6: Prolonged restricted feeding schedules do not affect uptake capacity and CD36 surface expression in peritoneal macrophages at ZT6.

Mice were housed in the CLAMS for 12 days receiving food for 12 h either at night, during the day or ad libitum. **A, B)** Peritoneal cells were isolated at ZT6 and stimulated for 1 h with heat inactivated, fluorescent *E. coli* (MOS5) before they were stained for F4/80 and surface CD36. **C, D)** At ZT6 mice were stimulated for 1 h with 20 x 10^6 *S. aureus* particles injected i.p. before they were euthanized and the peritoneal cells harvested to be stained for F4/80 and surface CD36. Fluorescence intensity was analysed in F4/80$^+$ cells by flow cytometry. CD36 surface abundance **(B, D)** and particle uptake **(A, C)** was not affected by the feeding schedule *ex vivo* and *in vivo* at ZT6. Statistical analysis according to Kruskal Wallis ANOVA and Dunn's post-hoc multiple comparison. Kruskal Wallis ANOVA: **A)** p=0.8698. **B)** p=0.2338. **C)** p=0.1397. **D)** p=0.7463. n=2-4.

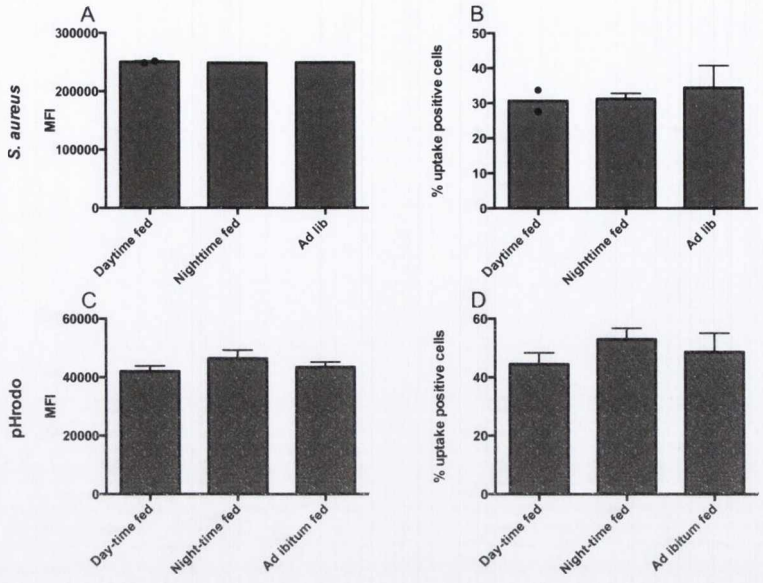


Figure 3.2.6.7: 12 days of time restricted feeding does not affect *ex vivo* particle uptake in peritoneal macrophages at ZT0.

Mice were housed in the CLAMS for 12 days receiving food for 12 h either at night, during the day or ad libitum. Peritoneal cells were isolated at ZT0 and stimulated for 1 h with heat inactivated, constitutively fluorescent *S. aureus* particles (MOS5) **(A, B)** or pH sensitive pHrodo *S. aureus* particles (MOS30) **(C, D)** before they were stained for F4/80. Fluorescence intensity was analysed in F4/80$^+$ cells by flow cytometry and the MFI in uptake positive macrophages **(A, C)** and the percentage of uptake positive macrophages were plotted, both of which were not altered by the feeding schedule. Statistical analysis using Kruskal Wallis ANOVA and Dunn's post-hoc multiple comparison. Kruskal Wallis ANOVA: **A)** p=0.3214. **B)** p>0.9999. **C)** p=0.6197. **D)** p=0.4208. n=2-4.

In the early phase of this project, genetic models to investigate the role of CD36 in rhythmic particle uptake were not available and other models to induce or repress CD36 had to be examined. As published data reported CD36 induction in mice following 5 days of high fat diet (HFD) (Cameron-Smith et al., 2003), CD36 abundance was measured over the course of 10 days in mice that were introduced to HFD. No increase in CD36 surface or total levels in peritoneal macrophages of these animals could be found, and *E. coli* bioparticle uptake similarly remained unaffected (Figure 3.2.6.8).

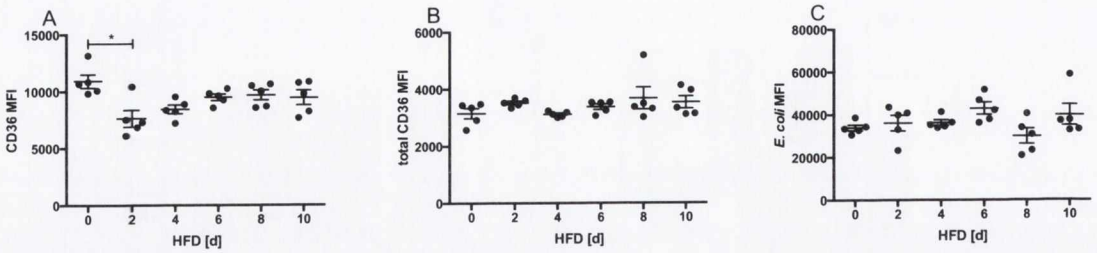


Figure 3.2.6.8: High fat diet does not induce CD36 expression.

Mice were housed in 12:12 light:dark conditions on a high fat diet and were euthanized every 2 days (~ZT4). Peritoneal cells were harvested or stained for surface **(A)** or total **(B)** CD36, or were stimulated with fluorescent *E. coli* bioparticles (MOS10) for 1 h **(C)**. Uptake capacity and total CD36 levels were not affected by HFD over 10 days. CD36 surface levels appeared to be moderately down regulated in the first 2 days of HFD, but relapsed close to initial levels during continued HFD. Statistical analysis according to Kruskal Wallis ANOVA and Dunn's post-hoc multiple comparison. Kruskal Wallis ANOVA: **A)** p=0.0196. **B)** p=0.1239. **C)** p=0.1161. n=5.

Next, manipulation of CD36 levels by repression was tested in a preliminary study. Antibodies and blocking peptides have been successfully used by others to inhibit uptake of oxLDL, a known CD36 ligand (Endemann et al., 1993). However, uptake of latex beads, Vybrant and living *E. coli* in iBMDMs that were treated with anti-CD36 antibodies did not seem to decrease compared to IgG controls. In contrast, addition of antibodies, independent of specificity, appeared to induce particle uptake in general (Figure 3.2.6.9). These results have however not been repeated and are therefore only indicative.

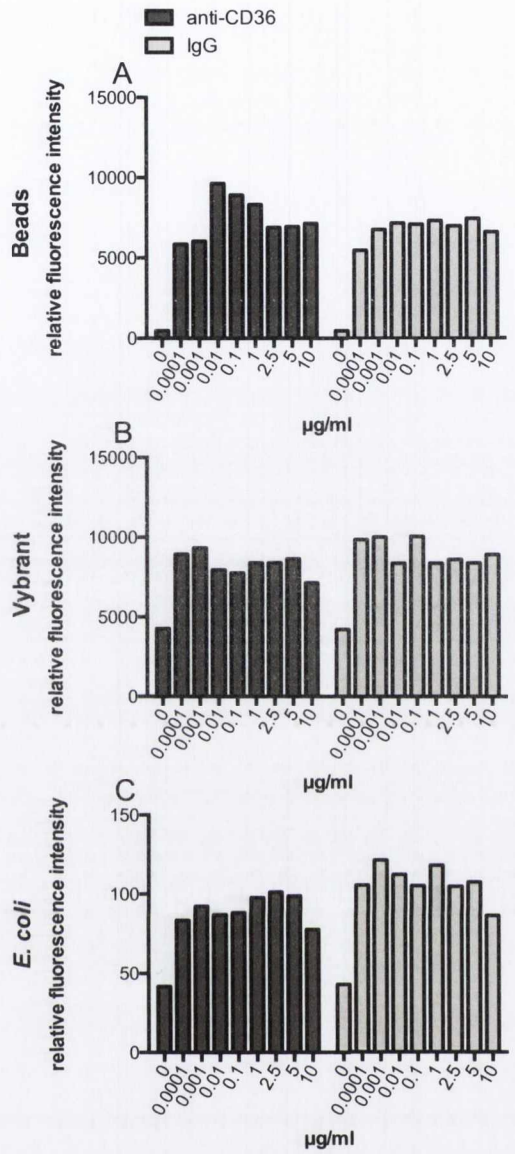


Figure 3.2.6.9: Particle uptake by iBMDMs seemingly cannot be inhibited with an antibody directed against CD36.

iBMDMs were incubated with anti-CD36 (R&D) or IgG control antibodies for 24 h at varying concentrations, before they were stimulated with fluorescent latex beads (MOS500) **(A)**, Vybrant **(B)**, or living *E. coli* (MOI500) **(C)** for 1 h. Fluorescence intensity was acquired using a fluorescence plate reader. Pre-incubation with an antibody increased the level of particle uptake, but antibody concentration and specificity did not appear to affect the level of uptake in IgG control and anti-CD36 treated cells. N=1.

Multiple anti-CD36 antibodies were commercially available and a range of them was tested in preliminary studies for their ability to block uptake of latex beads by BMDMs. As serum can act as a synchronizer and further cannot be used in conjunction with the serum shock model, these experiments were generally performed in serum free conditions. To examine the effect of serum, some experiments included serum supplemented samples as indicated. Unexpectedly, addition of serum resulted in slightly decreased uptake rates. High antibody concentrations further appeared to promote toxicity, potentially explaining the drop in fluorescence in those wells (Figure 3.2.6.10 B). In a first study, exclusively the Cayman antibody (JC63.1) was capable of reducing latex bead uptake (Figure 3.2.6.10 A), which could however not be recapitulated in follow up experiments (Figure 3.2.6.10 B, C).

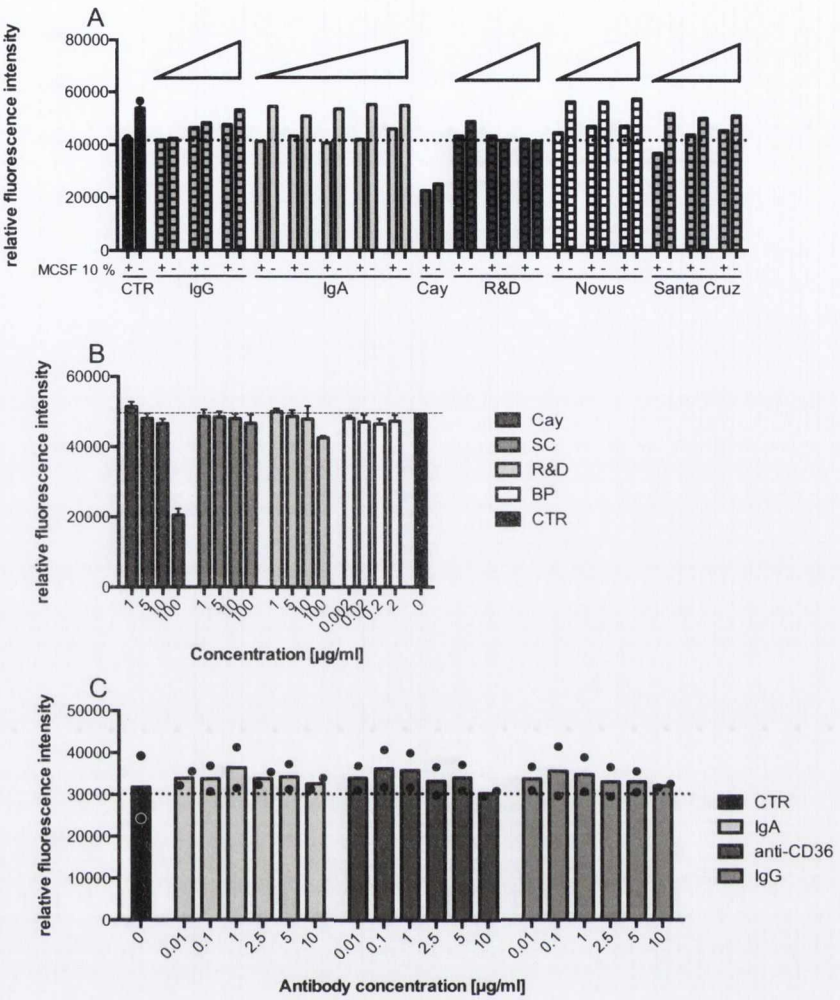


Figure 3.2.6.10: CD36 surface blockage does not appear to inhibit uptake of fluorescent latex particles.

BMDMs were incubated with various concentrations of assorted anti-CD36 antibodies and CD36 blocking peptide purchased from various vendors or IgG or IgA controls for 1 h or left untreated, before being stimulated with fluorescent latex beads (MOS500) for 1 h. **A)** Cells that were cultured in the presence of MCSF (10%) for 1 day displayed marginally decreased uptake. Only CD36 blockage with the Cayman antibody (JC63.1) resulted in decreased uptake capacity compared to control. **B)** Pre-incubation with various concentrations of selected antibodies did not affect particle uptake, except for 100 µg/ml of the Cayman antibody (JC63.1), which did also appear to affect cell viability. **C)** Pre-incubation with various concentrations of the anti-CD36 antibody Cayman (JC63.1) or IgG or IgA control antibodies did not affect uptake capacity in BMDMs. Fluorescence intensity was analysed using a fluorescence plate reader. Three independent experiments. N=1-3.

Analogously to BMDMs, treatment of peritoneal macrophages with various antibodies directed against CD36 and block peptides (BP) was not indicative of decreased uptake of fluorescent latex beads (Figure 3.2.6.11).

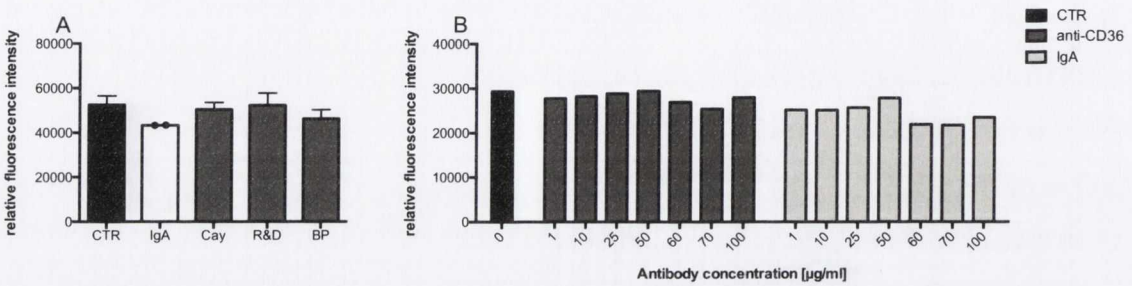


Figure 3.2.6.11: Uptake of latex particles by peritoneal cells does not seem to be inhibited by CD36 blockage.

Peritoneal cells were incubated with or without a CD36 blocker or IgA control before they were stimulated with fluorescent latex beads (MOS500) for 1 h and fluorescence was determined using a fluorescence plate reader. **A)** Pretreatment with either 10 µg/ml of IgA or anti-CD36 antibodies from Cayman or R&D, or incubation with 2 µg/ml blocking peptide did not inhibit particle uptake. **B)** Increasing concentrations of the Cayman (JC63.1) anti-CD36 antibody or IgA control, did not reduce particle uptake by peritoneal cells. Two independent experiments. **A)** Statistical analysis using Kruskal Wallis ANOVA and Dunn's post-hoc multiple comparison. Kruskal Wallis ANOVA: p=0.3587. N=1-3.

Modulation of CD36 levels and/or functionality seemed exceptionally challenging. Therefore, it was invested in a genetic model to further examine the role of CD36. No changes in *ex vivo* uptake of *E. coli* and *S. aureus* bioparticles or acidification rate of the phagosomes with pHrodo labelled *S. aureus* bioparticles in *Cd36* knockout and WT peritoneal macrophages was found in an initial study, arguing against CD36 involvement in uptake of these particles and downstream breakdown (Figure 3.2.6.12).

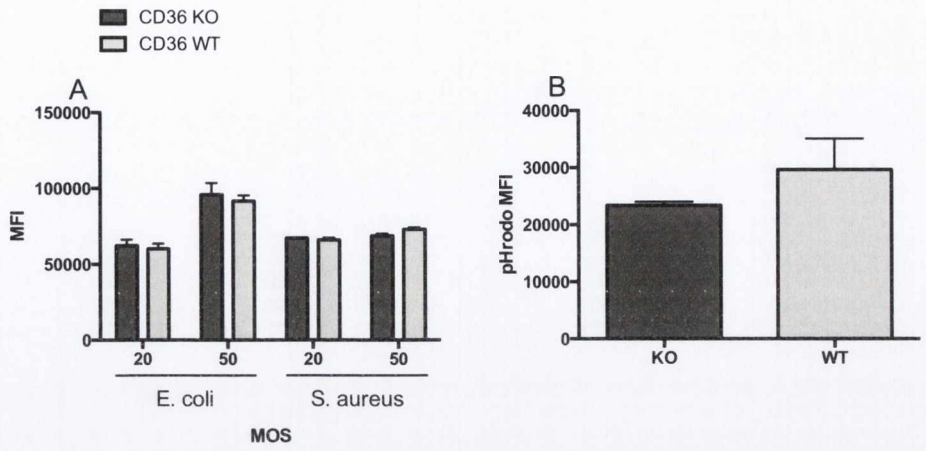


Figure 3.2.6.12: *Ex vivo* bacterial particle uptake is not CD36 dependent.
A) Peritoneal cells were stimulated with stably fluorescent *E. coli* or *S. aureus* particles at the indicated concentrations. **B)** BMDMs were stimulated with pH sensitive pHrodo *S. aureus* particles (MOS150). Following 1 h of stimulation, similar fluorescence was recorded in F4/80^{+} uptake positive *Cd36* WT and KO cells by flow cytometry. **A)** Statistical analysis two way ANOVA and Sidak's post-hoc test comparing genotypes. *E. coli*: Interaction: DF=1, F=0.04287, p=0.8411. Dose: DF=1, F=43.63, p=0.0002. Genotype: DF=1, F=0.4028, p=0.5434. *S. aureus*: Interaction: DF=1, F=5.564, p=0.046. Dose: DF=1, F=13.21, p=0.0066. Genotype: DF=1, F=1.639, p=0.2363. **B)** No significance according to Mann-Whitney. N=3.

To substantiate functionality of CD36 in WT and absence of the scavenger receptor in the knockout animals, CD36 surface abundance - as measured by flow cytometry - and uptake of the known CD36 ligand - oxLDL - was examined. CD36 surface abundance was at background levels in the CD36 knockout, while highly abundant in the WT cells. Uptake of oxLDL appeared dose dependent in WT cells, indicating oxLDL specific uptake; however, similar results were obtained in *Cd36* knockout cells (Figure 3.2.6.13).

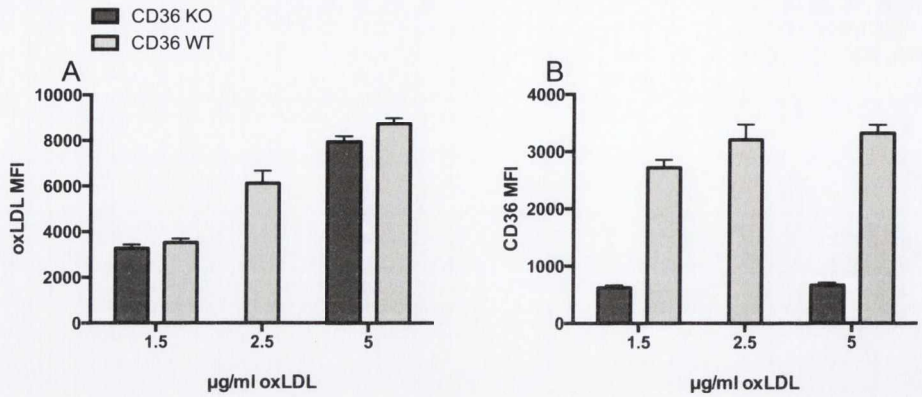


Figure 3.2.6.13: Uptake of oxLDL, a known CD36 ligand, is not impaired in *Cd36* knockout macrophages *ex vivo*.

Following incubation with the indicated concentrations of DiI labelled oxLDL for 1 h, oxLDL fluorescence and CD36 surface abundance in *Cd36* WT and KO peritoneal cells was measured by flow cytometry in uptake positive cells. **A)** Dose dependent oxLDL uptake in *Cd36* KO and WT cells. **B)** Verification of *Cd36* knockout by impaired CD36 surface abundance. N=2-4.

oxLDL uptake in CD36 deficient cells was unexpected and inconsistent with the body of literature. Considering differences between the studies performed as part of this project and work by others, a critical role for serum appeared plausible. This was substantiated by a recent publication that demonstrated the need for free fatty acids, oleic acid in particular, to associate within the CD36 receptor cavity to allow subsequent binding of oxLDL (Jay et al., 2015). Therefore, oxLDL and *S. aureus* bioparticle uptake in CD36 WT and deficient BMDMs and peritoneal macrophages in the presence or absence of serum or oleic acid was examined. Surprisingly, oxLDL uptake was independent of serum or oleic acid supplementation as well as the presence or absence of CD36. *S. aureus* bioparticle uptake was equally not affected by the addition of serum, however uptake increased in a dose dependent manner in serum supplemented as well as serum deprived samples (Figure 3.2.6.14).

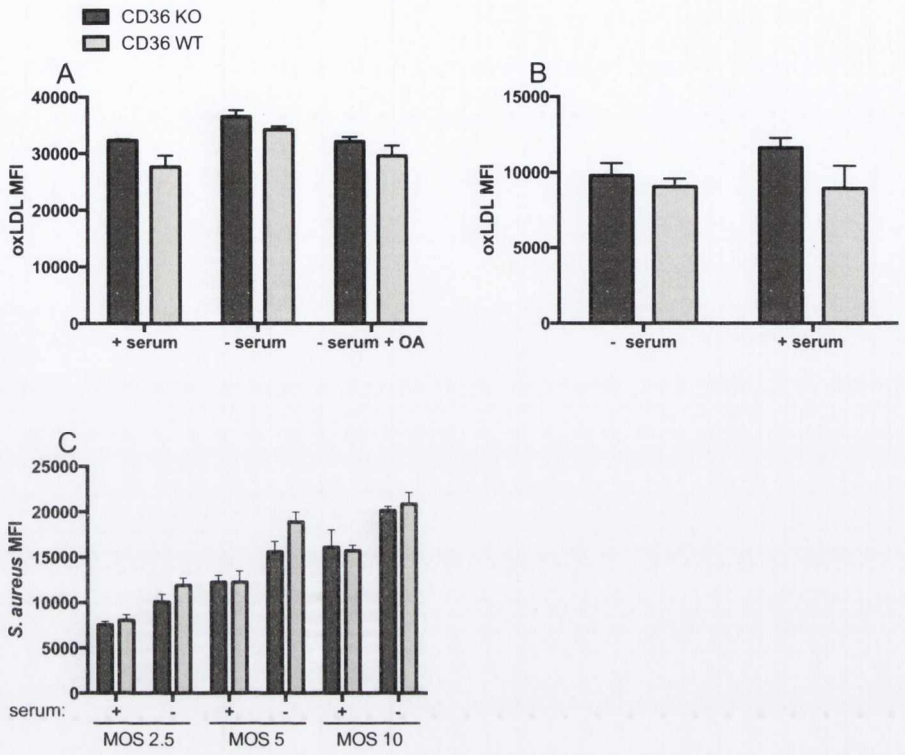


Figure 3.2.6.14: Serum and Oleic acid do not affect oxLDL and *S. aureus* uptake.

Cd36 WT and knockout cells were stimulated for 1 h with 25 µg/ml fluorescent oxLDL or fluorescent *S. aureus* particles at the indicated concentrations in the absence or presence of 10 % serum or 250 µgM oleic acid. **(A)** BMDMs stimulated with oxLDL. **(B)** Peritoneal cells stimulated with oxLDL. **(C)** BMDMs stimulated with *S. aureus*. Supplementation of the medium did not affect uptake, while the dose dependent uptake of *S. aureus* particles was sustained, as measured by flow cytometry in uptake positive cells. Statistical analysis using two way ANOVA and Sidak's multiple comparison test. **A)** Interaction: DF=2, F=0.5326, p=0.6003. Serum: DF=2, F=10.72, p=0.0021. Genotype: DF=1, F=9.791, p=0.0087. **B)** Interaction: DF=1, F=1.051, p=0.3353. Serum: DF=1, F=0.8399, p=0.3862. Genotype: DF=1, F=3.307, p=0.1065. **C)** Interaction: DF=5, F=0.8878, p<0.0001. Stimulation: DF=5, F=41.41, p=0.1048. Genotype: DF=1, F=3.307, p=0.1065. N=3.

Despite unexpected results regarding CD36, it appeared interesting whether oxLDL uptake could possibly oscillate throughout the day, which could in turn indicate diurnal development of atherosclerotic plaques. Analysis of oxLDL uptake by peritoneal macrophages at different times of the day in an *ex vivo* model did however not support diurnal oxLDL uptake in these cells (Figure 3.2.6.15).

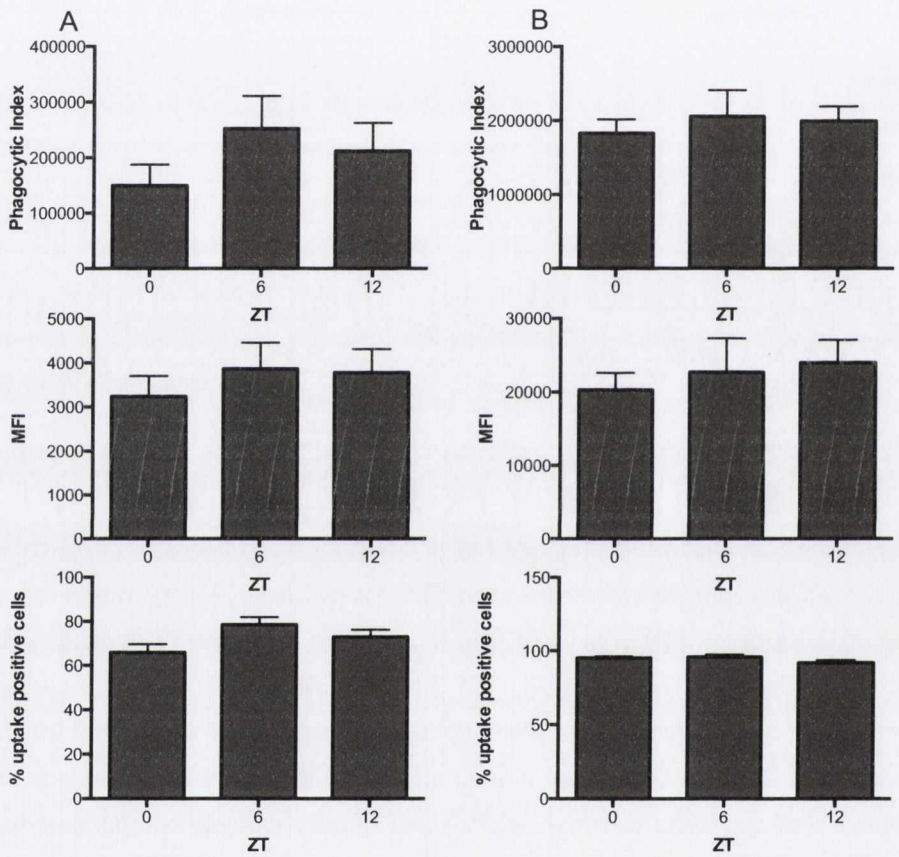


Figure 3.2.6.15: *Ex vivo* oxLDL uptake does not follow a diurnal rhythm.
Peritoneal cells were isolated at the indicated times and stimulated *ex vivo* with 25 µg/ml DiI labelled oxLDL for 1 h, before fluorescence (middle) in F4/80$^+$ uptake positive cells and the percentage of uptake positive cells (bottom) was acquired by flow cytometry to calculate the phagocytic index (top). **(A)** and **(B)** represent two independent experiments. Statistical analysis using Kruskal Wallis ANOVA and Dunn's post-hoc multiple comparison (indicated in graph). *p<0.05, **p<0.01. Kruskal Wallis ANOVA from top to bottom: **A**) p=0.2648, p=0.62, p=0.1012. **B**) p=0.65, p=0.7027, p=0.2311. n=5.

Even though *ex vivo* particle uptake was CD36 independent, it remained possible that CD36 may control phagocytosis of particles *in vivo*. To test this, *S. aureus* bioparticles particles were injected intraperitoneally into *Cd36* KO and WT mice. Macrophage marker F4/80 positive peritoneal exudate cells that were harvested one hour following stimulation displayed only background CD36 levels in the KO cells, whereas the WT cells had significant levels of CD36. Congruent with previously presented *ex vivo* data, there was yet no change in the amount of *S. aureus* uptake in these cells (Figure 3.2.6.16), finally confirming that S. aureus uptake was entirely independent of CD36.

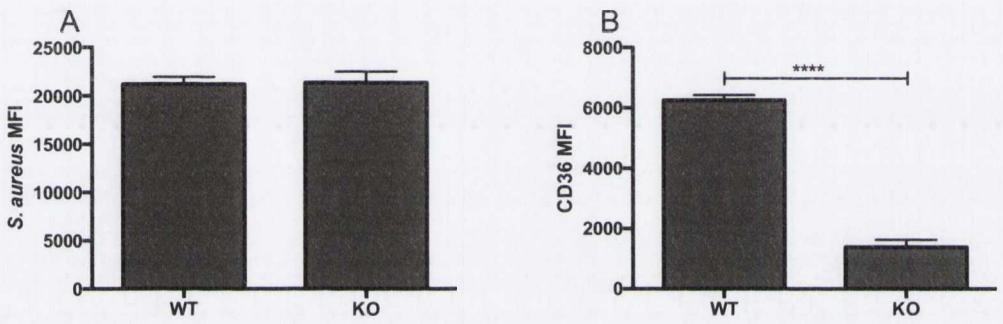


Figure 3.2.6.16: *S. aureus* uptake is not impaired in *Cd36* knockout mice *in vivo*.

1 h after i.p. injection of 2 x 10^6 fluorescent *S. aureus* particles into *Cd36* WT and KO mice, peritoneal cells were harvested and fluorescence in uptake positive cells **(A)** and CD36 surface abundance **(B)** was determined in F4/80$^+$ cells by flow cytometry. **A)** *S. aureus* ingestion was similar between genotypes. **B)** *Cd36* knockout was confirmed by impaired CD36 surface abundance. Compiled data from two independent experiments. Statistical according to Mann-Whitney. **A)** p=0.6730. **B)** p****<0.0001. n=8-9.

Sustained oxLDL uptake in CD36 deficient cells could not be explained throughout the project. To account for suboptimal oxLDL doses that may induce CD36 independent uptake pathways at excess concentrations, a final oxLDL study was performed. In order to use the most physiological conditions, this was done in an *in vivo* model. To this end, different oxLDL doses were injected intra peritoneal and F4/80 positive cells were harvested an hour later from the peritoneum. Congruent with data within this project, but still contrasting work by others, no significant difference between genotypes was observed for concentrations below10 µg, and more data points at concentrations exceeding 10 µg would be necessary to verify the decreased uptake that became apparent at this concentration within the presented dataset (Figure 3.2.6.17).

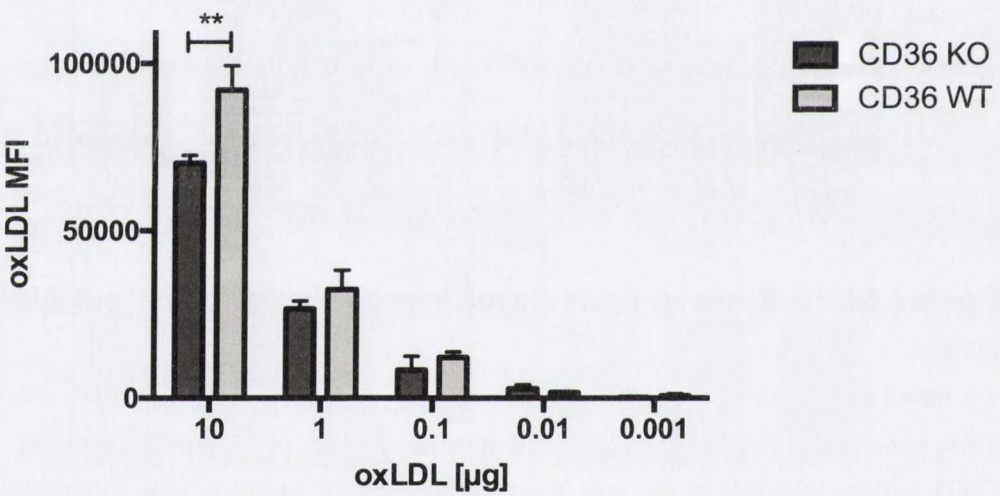


Figure 3.2.6.17: *In vivo* oxLDL uptake is dose dependent, but CD36 independent.

Cd36 WT and KO mice were injected i.p. with increasing doses of DiI labelled oxLDL. After 1 h, peritoneal cells were extracted and fluorescence was measured in F4/80$^+$ cells by flow cytometry. Uptake of oxLDL was increasing with dose, but no change between the genotypes was observed. Statistical analysis using two way ANOVA and Sidak's multiple comparisons test (indicated in graph with *p<0.05, **p<0.01). Interaction: DF=4, F=3.211, p=0.0373. Dose: DF=4, F=175.2, p<0.0001. Genotype: DF=1, F=6.879, p=0.0172. n=3-5.

3.2.7 Particle uptake by macrophages is not diurnal *in vivo*

In the course of *ex vivo* studies presented earlier in this work, the contribution of the molecular clock in circadian particle ingestion was tested. While a functional clock appeared redundant in this artificial environment, it was possible that cells could be manipulated in a circadian manner within the organism, independent of their own clock, to create a poised state that could be maintained even after extraction from the organism. To better understand the molecular mechanism and potential factors that could regulate this poised state in clock deficient cells, uptake studies were performed in an *in vivo* setting.

Intraperitoneal injection of *S. aureus* bioparticles at concentrations comparable to preceding *ex vivo* studies (20 x 10^6 particles, MOS5 assuming 4 million macrophages per peritoneum based on previous peritoneal lavage counts) unexpectedly did not display differences in particle uptake despite a thorough time course with data-points every three hours over the course of a day (Figure 3.2.7.1 C, D). Comparison of the percent of uptake positive macrophages in this and previous *ex vivo* studies revealed that almost all macrophages in the *in vivo* setting (Figure 3.2.7.1 D), but only 50-80% of F4/80 positive cells in *ex vivo* studies were uptake positive. A dose response in the *in vivo* model illustrated that a decrease to 0.4 x 10^6 particles was required to achieve uptake rates comparable to the *ex vivo* studies (Figure 3.2.7.1 A, B). Rhythmicity in particle uptake could however still not be recapitulated in an *in vivo* model that was adjusted to compare to the *ex vivo* setting by using the low concentration of 0.4 x 10^6 particles per injection (Figure 3.2.7.1 E, F).

It should be noted that experiments shown in Figure 3.2.7.1 C-F were performed using reverse light cycle rooms, allowing simultaneous testing of mice that differed by 12 h in regard to their solar time. Although all time points within the experiments were done in the course of one day, variations between time points were sill present; however, mice that were injected simultaneously (e.g. ZT3 and ZT15 in Figure 3.2.7.1 C) displayed very consistent values (with no statistical significance according to Dunn's post-hoc testing). This supports the notion that timely separated stimulations may be a major source of variability within some of the here presented studies.

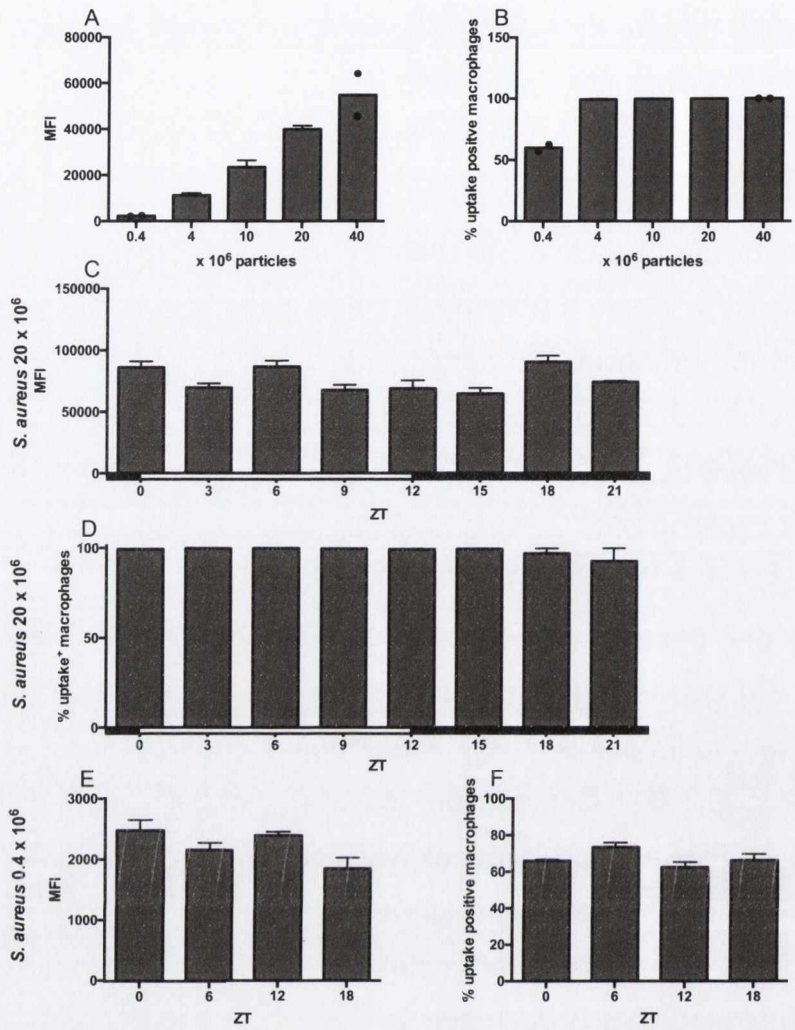


Figure 3.2.7.1: *S. aureus* ingestion by peritoneal macrophages is not rhythmic *in vivo*.

Mice were stimulated with the indicated amounts of fluorescent *S. aureus* particles at the indicated time points for 1 h before the peritoneal cells were harvested and fluorescence was analysed in F4/80$^+$ cells by flow cytometry. **A, B)** *S. aureus* uptake increased in a dose dependent manner in MFI **(A)**, while the percentage of uptake positive macrophages reached a plateau already at low concentrations **(B)**. **C, D)** Uptake capacity as measured by MFI **(C)** and percentage of uptake positive macrophages **(D)** remains unchanged over the course of a day at a concentration of 20 x 10^6 particles per stimulation. **E, F)** Decreased amounts of *S. aureus* particles per stimulation of 0.4 x 10^6 recapitulated the phenotype seen at higher doses in MFI **(E)**, while the percentage of uptake positive macrophages was comparable to previous *ex vivo* studies, and remained steady below the maximum over time **(F)**. Statistical analysis using Kruskal Wallis ANOVA and Dunn's post-hoc multiple comparison. Kruskal Wallis ANOVA: **A**) $p<0.0001$. **B)** $p=0.0363$. **C)** $p=0.0121$. **D)** $p=0.0474$. **E)** $p=0.038$. **F)** $p=0.1129$. n=2-5.

In line with this data, *in vivo* uptake of *S. aureus* bioparticles was not different between myeloid specific *Bmal1* knockout and WT animals and did not display a divergence in uptake capacity comparing ZT0 and ZT12 (Figure 3.2.7.2). The percentage of uptake positive *Bmal1* knockout macrophages was marginally increase from ZT0 to ZT12 and was most likely a result of minimal variation within the data.

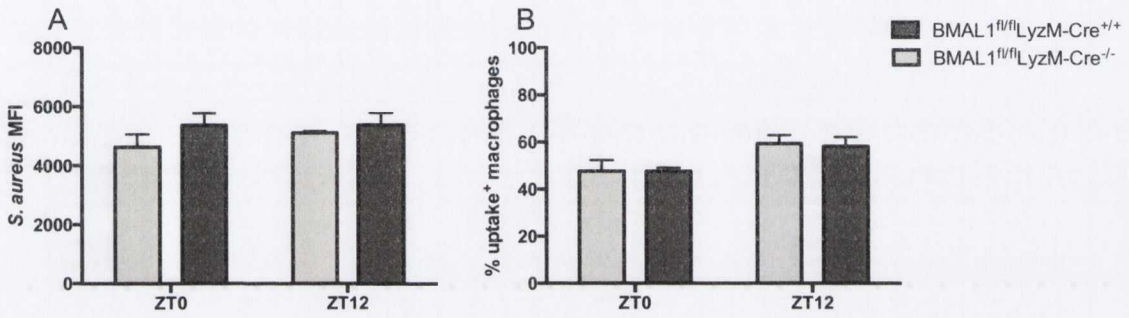


Figure 3.2.7.2: The macrophage intrinsic biological clock does not affect *S. aureus* ingestion *in vivo*.

BMAL1$^{fl/fl}$LyzM-Cre$^{+/+}$ and BMAL1$^{fl/fl}$LyzM-Cre$^{-/-}$ mice were stimulated i.p. with 0.4 x 10^6 *S. aureus* particles for 1 h before the peritoneal lavage was extracted and fluorescence was measured in F4/80$^+$ cells by flow cytometry. **A)** MFI between genotypes was invariable and stable over time. **B)** Percentage of uptake positive macrophages was similar between genotypes, and moderately increased at ZT12 compared to ZT0. Statistical analysis using two way ANOVA and Sidak's multiple comparisons test. **A)** Interaction: DF=1, F=0.4288, p=0.5232. ZT: DF=1, F=0.3542, p=0.5612. Genotype: DF=1, F=1.688, p=0.2148. **B)** Interaction: DF=1, F=0.02332, p=0.8808. ZT: DF=1, F=10.06, p=0.0068. Genotype: DF=1, F=0.03337, p=0.8577. n=5.

While *in vivo* uptake of particles was not found to be rhythmic, breakdown of ingested material still had the potential to be circadian. Before diurnal differences in the acidification rate could be tested, an *in vivo* dose response had to be performed to determine the concentration that should be used. Particle numbers of 3 x 10^6 per peritoneum resulted in 100% uptake positive macrophages, causing saturation of the system. 0.3 x 10^6 particles in contrast resulted in a percentage of uptake positive cells below the anticipated 70-80% (Figure 3.2.7.3). Therefore a slightly higher particle number of 0.5 x 10^6 should be used in subsequent studies, to assure strong signal intensity without saturation of the system.

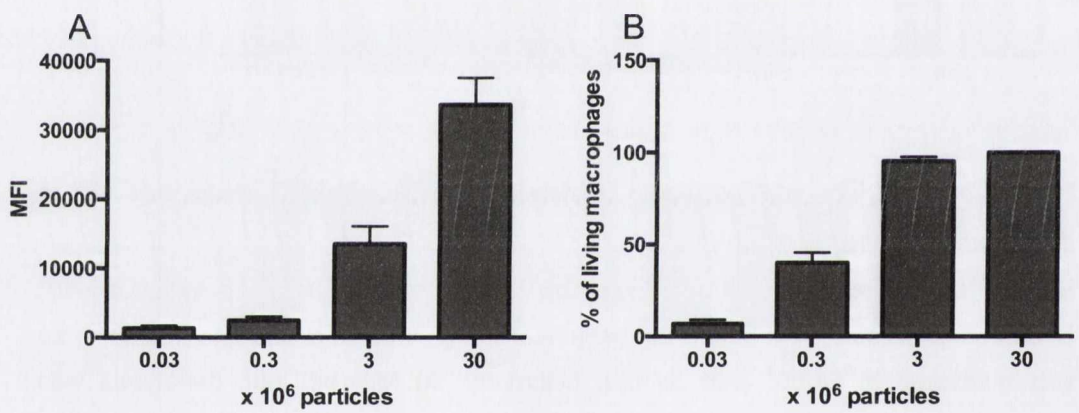


Figure 3.2.7.3: pHrodo uptake *in vivo* is dose dependent.

Mice were stimulated with the indicated amounts of pHrodo labeled *S. aureus* particles i.p. for 1 h before peritoneal cells were extracted and fluorescence was analysed by flow cytometry. **A)** Particle ingestion increased in a dose dependent manner. **B)** Percentage of uptake positive macrophages similarly increased dose dependent, and reached a plateau at 3-30 x 10^6 *S. aureus* particles. Statistical analysis using Kruskal Wallis ANOVA. **A**) $p=0.0006$. **B)** $p<0.0001$. N=3.

3.3 Discussion

The aim of this project was to define a role for circadian particle uptake in the regulation of innate immune responses and mortality following exposure to LPS, which have been reported to cycle over the course of a day (Halberg et al., 1960, Feigin R. D, 1972, Feigin et al., 1996). The present study provides evidence that uptake of bacterial particles *ex vivo* is diurnal with increased ingestion by peritoneal macrophages at ZT12, the transition into the dark- and active phase of nocturnal mice, and time of enhanced susceptibility to LPS (Figure 3.2.2.1). However, ingestion of bacterial particles in the more physiologically relevant *in vivo* environment is not diurnal (Figure 3.2.7.1) and therefore presumably does not contribute to diurnal variation in innate immune responses.

While this outcome was not anticipated - considering the body of literature that argues for a significant contribution of particle uptake in cytokine response following infection (Azevedo et al., 2012), as well as publications from the circadian field reporting rhythmicity in the ability to ingest material in a range of cell types (Rodríguez et al., 1999, Hriscu, 2005, Pires - Lapa et al., 2013) - it is a meaningful discovery. Association of uptake and pro-inflammatory immune response, such as cytokine production, would obstruct a possibility to target clock components to inhibit cytokine response, while maintaining or even promoting clearance of pathogens by phagocytosis.

This is particularly interesting in the setting of sepsis, where an infection causes hyper-inflammation and consequently tissue damage in patients, while the host appears unable to effectively clear the pathogen. Targeting the clock to manipulate hyper-responsiveness via pro-inflammatory cytokine production, without diminishing clearance by phagocytes may therefore be an effective strategy.

Early in the project RT-Profiler plates were used which indicated differential regulation of phagocytic and oxidative stress pathways in peritoneal macrophages that were isolated at ZT0 or ZT12 (Figure 3.2.1.1). While oxidative stress genes were expected to be induced at ZT12 (the time of hyper-

inflammatory states), increased abundance of genes involved in phagocytosis at ZT0 were surprising given that phagocytic uptake appeared elevated at the transition to the dark phase (ZT12) in functional studies. The reason for this observation is not entirely clear, and as multiple genes appeared to be induced at ZT0 but not at ZT12, it seems unlikely that this was caused by an error within the assay. However, repeat experiments would be necessary to evaluate the accuracy of this result and provide experimental reasoning.

Fluorescence as a readout for the amount of particles that were taken up was measured in a 96-well format on a fluorescence microplate reader, especially in the early studies. Although more technical replicates could be done, as fewer cells were required per measurement, the resolution was limited.
The plate reader measures the total fluorescence emitted from the entire well, not allowing discrimination of specific cell populations or even free particles that remained in the well despite several washing steps. Washing by itself harboured the risk of data manipulation by accidental removal of cells. Similarly, differences in the cell number plated or differences in cell survival following stimulation could affect comparability of the detected fluorescent signal and possibly variation in the MOS.
On the other hand, the plate reader could generate data that was certainly indicative of a possible effect, and considering that these results could be recapitulated in other models, this technique appeared an adequate and valid tool for preliminary studies. Flow cytometry analysis and mRNA levels in FACS purified peritoneal F4/80$^+$ and F4/80$^-$ cells further supported validity of the plate reader, as F4/80$^-$ cells did neither display significant uptake capacity (Figure 3.2.2.2), nor detectable levels of clock mRNAs (Figure 3.2.6.2). This is however only a valid argumentation assuming equal ratios of F4/80$^+$ and F4/80$^-$ cells between time points.

Flow cytometry is a more sophisticated method that allowed to selectively study F4/80$^+$ cells within a mixed population. Although measurements were less prone to variability in the process of sample preparation, there were still technical challenges that could not always be overcome. As such, MFI of

surface markers appeared to vary between stainings when cells were not processed in parallel. Similarly, the fluorescent signal from the ingested particles seemed to vary between experiments, which dramatically decreased consistency in the data obtained.

These challenges can exclusively be avoided by the use of conventional and light reversed rooms to generate ZT0 and ZT12 mice contemporaneous. Extraction and processing of ZT0 and ZT12 cells can only then be performed simultaneously, and day-to-day variations are prevented. But even this potentially harbours another matter of controversy, as studies have been published that challenge the notion that mice can be fully entrained to reverse light cycles in their adult life (Azzi et al., 2014). Further, differences in housing may be present between rooms and could also potentially cause variation among groups. Despite these concerns, some experiments were performed using this type of setting to test the possibility that differences that were seen in *ex vivo* uptake studies could solely be accounted to technical variation (Figure 3.2.2.1). Although all experimental settings that were used contained their own flaws, and generated significant variability, the entirety of the presented data makes a strong case for a genuine increase in uptake capacity in *ex vivo* models at ZT12 compared to ZT0.

Validity of the model in terms of actual uptake compared to binding of the particles to the cells was confirmed by confocal microscopy analysis of cells following uptake (Figure 3.2.3.1). Fluorescent particles were localized within the boundaries of the plasma membrane or presented within a phagocytic cup that was not yet closed, but no significant number of particles was found to be simply attached to the cell surface. Inhibition of uptake, using the actin polymerization inhibitor Latrunculin A, also resulted in a dose dependent decrease in the fluorescent signal, further supporting that the measured signals originated from ingested material (Figure 3.2.3.2).

Rather than investigating which clock component may be causing oscillations in *ex vivo* uptake, it was primarily focused on the receptor that was responsible. Both ways seem sensible, but identifying the target of the clock first, appeared to provide a better readout for subsequent pathway investigations. Literature

and experts in the field of phagocytosis suggested a potential role of CD36 in this context (Stuart et al., 2005). As surface abundance, at first, appeared to fluctuate correspondingly to uptake capacity, this confirmed CD36 as a suitable candidate (Figure 3.2.6.1).

Subsequent investigations were troublesome as *in vitro* models, such as the serum shock did not prove to be appropriate for functional studies, and techniques to modulate CD36 levels were ineffective. Despite tenacious effort, this hurdle could not be overcome until it was invested in a genetic model of *Cd36* deficiency. Following a few *in vivo* and *ex vivo* experiments, it however quickly became apparent that CD36 was not involved in the uptake phenotype that was seen (Figure 3.2.6.12, Figure 3.2.6.16).

Despite this, it was very surprising that uptake of oxLDL, a known ligand of CD36 (Endemann et al., 1993), did not vary between *Cd36* knockout and wild type cells *in vivo* and *ex vivo*. This may have been a feature of the oxLDL particle itself, which was labelled with a lipophilic stain (DiI). Potentially, this stain had the ability to desolate from the oxLDL and integrate into the plasma membrane of cells, a process that would be entirely unspecific and CD36 independent. As this would be an exclusive feature of the oxLDL stimulus, which could not occur in the other particles used, this was not further investigated. Non-fluorescent Oil-Red-O staining could have however been used as the common method to quantify oxLDL inclusions under the microscope, verifying CD36 dependency and supporting the notion that the DiI staining may be causative for discrepancies that were found.

From a more technical point of view this study raised multiple concerns. How valid are *ex vivo* and *in vitro* findings in the context of a physiological environment? Daily oscillations in cytokine response have been investigated in *ex vivo* models, but how much of this may be attributed to extraction of cells from the animal rather than true rhythmicity?

The data presented within this work clearly reveals substantial divergence of rhythmic uptake capacity between *in vivo* and *ex vivo* models. However, it has to be pointed out that this may be a result of multiple effects; two of which appear most likely. Either, the process of cell extraction affects the cell state

differently at different times of the day (altering poising of the cell), or, mechanisms that are only in place in an *in vivo* environment, such as temperature fluctuations, autocrine or humoral and neuronal signals, mask the differences that are seen *ex vivo*. Considering the entirety of the presented data, none of these possibilities can be ruled out, yet we do not have evidence supporting one or the other.

Because a wide range of time points and particle concentrations were used in the *in vivo* models (Figure 3.2.7.1), it is unlikely that the absence of diurnal phagocytosis *in vivo* was caused by differences in experimental properties. One mechanism that was deliberately prevented in *ex vivo* studies, that could potentially explain differences between *in vivo* and *ex vivo* results, was Fc-receptor and complement mediated ingestion. Natural antibodies and opsonins (proteins that bind to distinct target molecules present on matter such as microbes) are permanently present in the serum and can bind material to enhance clearance by phagocytes. In a serum free condition, such as the one used in *ex vivo* assays throughout this study, these factors are not present and Fc- receptor and complement mediated uptake is consequently prevented.

The complement system which is present as pro-forms in the blood stream, can be rapidly activated by immune complexes (classical complement), hydroxyl- or amino- groups (alternative pathway), as well as mannose- groups (Lectin pathway) on the surface of cells or pathogens, and subsequently attract phagocytes and induce ingestion of tagged material. Because uptake of particles comprises such a vast range of pathways, it appeared beneficial to employ a setting that reduced the number of affected signalling cascades. Antibody, and opsonin mediated uptake studies in general, further require opsonization of particles for 30 minutes in serum before addition to the cells to initiate uptake; but as serum has the potential to induce synchronization of cells, we refrained from including serum in the *in vitro* uptake conditions. To determine a role for these pathways, genetic deletion of Fc-receptors on phagocytes or destruction of core complement factors *in vivo* could be used.

Taken together, this study provides evidence that bacterial particle uptake ex *vivo*, but not *in vivo* is rhythmic over the course of a day, and that this is entirely independent of a functional clock within the cell. It also defines a redundancy of CD36 in ingestion of heat-inactivated *E. coli* and *S. aureus* particles. However, it emphasizes the importance to verify *ex vivo* results in an *in vivo* model, and questions chrono-immunological findings that were made with peritoneal macrophages using exclusively *ex vivo* techniques.

4 Food entrainment determines oscillations in the susceptibility to LPS

4.1 Introduction

Chrono-immunological research has unravelled a range of mechanistic insights how the molecular clock and its constituents can affect the immune response following an inflammatory stimulation. Which signals are causal for daily variations in morbidity and mortality, and how disruption of the circadian system in individuals increases the risk of developing diseases with an underlying inflammatory component, has however not yet entirely been deciphered.

As light is the most widely studied zeitgeber in the context of circadian biology, it does not come as a surprise that chrono-immunological research equivalently focused on the role of light as the entraining signal of circadian immunity. In recent years, the importance of metabolism and metabolic shifts following infection has become apparent and we are only starting to fully grasp all aspects of this (Gleeson and Sheedy, 2016). The inflammatory response in a range of immune cells, from macrophages to T-cells, can already be vastly remodelled experimentally by targeted manipulation of metabolic pathways with validated inhibitors.

Even specific diets, such as high fat, or ketogenic diets, have been demonstrated to affect immune responses (Youm et al., 2015, Calder, 1998). This not only illustrates the technical advancements, but also suggests that dietary signals possibly have the ability to modify the nutrient microenvironment of immune cells, thereby priming them for a more intense or less intense immune response. While dietary studies generally adjust intake prior to inflammatory stimulation to closer model eating habits of population-groups at risk, it is worth noticing a recent publication that reported significant increase in the mortality of mice that were force-fed immediately post bacterial stimulation (Wang et al., 2016).

Besides these intriguing concepts, circadian biologists have also described a pivotal role for nutritional signals in the regulation of the molecular clock. While the light receptive master clock in the SCN remains unaffected by deviating feeding regimens, the liver rapidly and completely adapts to align its clock phase to new feeding schedules (Damiola et al., 2000). This provides a platform to investigate and differentiate the significance of nutritional and food entrained signals in an intact animal without the immediate need for genetic models. As mice are naturally nocturnal animals, they generally restrict activity and feeding to the dark phase, but by artificial restriction of food availability to the light phase, the animals can be forced to invert their feeding pattern.

The present study, for the first time, investigated the role of the feeding and the solar cycle in regulating diurnal morbidity upon bacterial LPS stimulation. To characterize the effect of time restricted feeding, metabolic properties, such as temporal resolution of dietary intake, whole respiratory exchange ratio, the average amount of ingested food, and activity were tested. Additionally, phase and amplitude of clock genes as well selected hormones and cytokines were examined in naïve and LPS challenged mice.

The data presented in this chapter argues that the feeding cycle may be the major signal to regulate diurnal mortality following an inflammogenic insult, as day-time fed animals displayed significantly decreased mortality rates at times when night-time fed control animals were highly susceptible to LPS stimulation. This was accompanied by strict food dependency of the liver clock and the main energy source utilized by the animal, while caloric intake, body composition and activity were similar in day- and night-time fed animals. Detailed investigations to further explain the molecular mechanisms responsible, and the tissues contributing to the novel findings we made are underway.

4.2 Results

4.2.1 LPS induced mortality is a function of feeding time

In an initial study the effect of time restricted feeding (TRF) on mortality following a lethal dose of lipopolysaccharide (LPS), a cell wall constituent of gram-negative bacteria, was examined (Figure 4.2.1.1, compiled data from three independent experiments). Congruent with the existing body of literature (Halberg et al., 1960, Curtis et al., 2015), night-time fed control animals were more susceptible when stimulated at the transition to the dark and active phase (ZT12), compared to ZT0 (Figure 4.2.1.1 B). Interestingly, feed restriction to the day-time reversed this phenotype, causing significant protection at ZT12 compared to ZT0 (Figure 4.2.1.1 C). The phenotypes of the two feeding groups did however not result in a mirror image, but in comparable mortalities at ZT0. While the first two studies continued TRF following stimulation (Figure 4.2.1.2 A, B), ad libitum feeding post injection was introduced in a subsequent study (Figure 4.2.1.2 C) to determine a role for the entrainment prior to stimulation rather than food intake post stimulation, as this has been shown to influence mortality in a recently published study (Wang et al., 2016). No difference was apparent between ad libitum and TRF feeding post LPS stimulation and samples that were taken in the course of these studies were further analysed in parallel in a range of assays presented in this chapter and are shown as purple (ad lib post LPS) or black (TRF post LPS) data points as indicated. Throughout the assays, no divergence was found between the datasets.

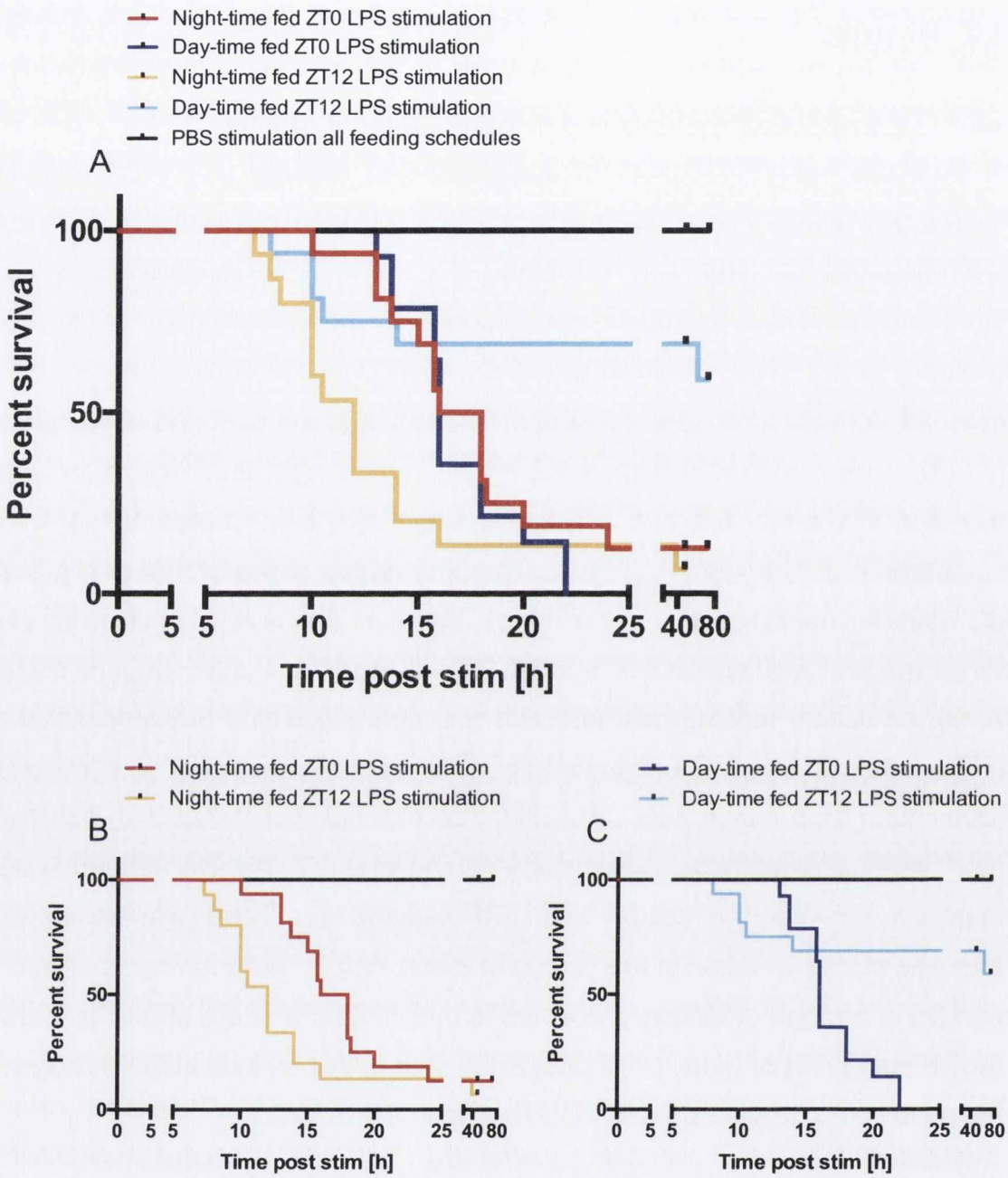


Figure 4.2.1.1: LPS induced, rhythmic mortality is a function of food availability.

Survival time of mice that were entrained to TRF schedules for 5 days before receiving 20 mg/kg LPS i.p. at either ZT0 or ZT12. **A-C)** Cumulative data from three independent experiments. **A)** Compiled data from night- (**N**) and day-time (**D**) fed animals stimulated at ZT0 (**0**) or ZT12 (**12**). Mantel-Cox test N0LPS vs. D0LPS P=0.48, N12LPS vs. D12LPS P=0.0009, N0LPS vs. N12LPS P=0.0387, D0LPS vs. D12LPS P=0.0027. **B)** Night-time fed mice stimulated at ZT0 or ZT12. **C)** Day-time fed animals stimulated at ZT0 or ZT12. LPS stimulated groups n=14-16, PBS control groups n=3.

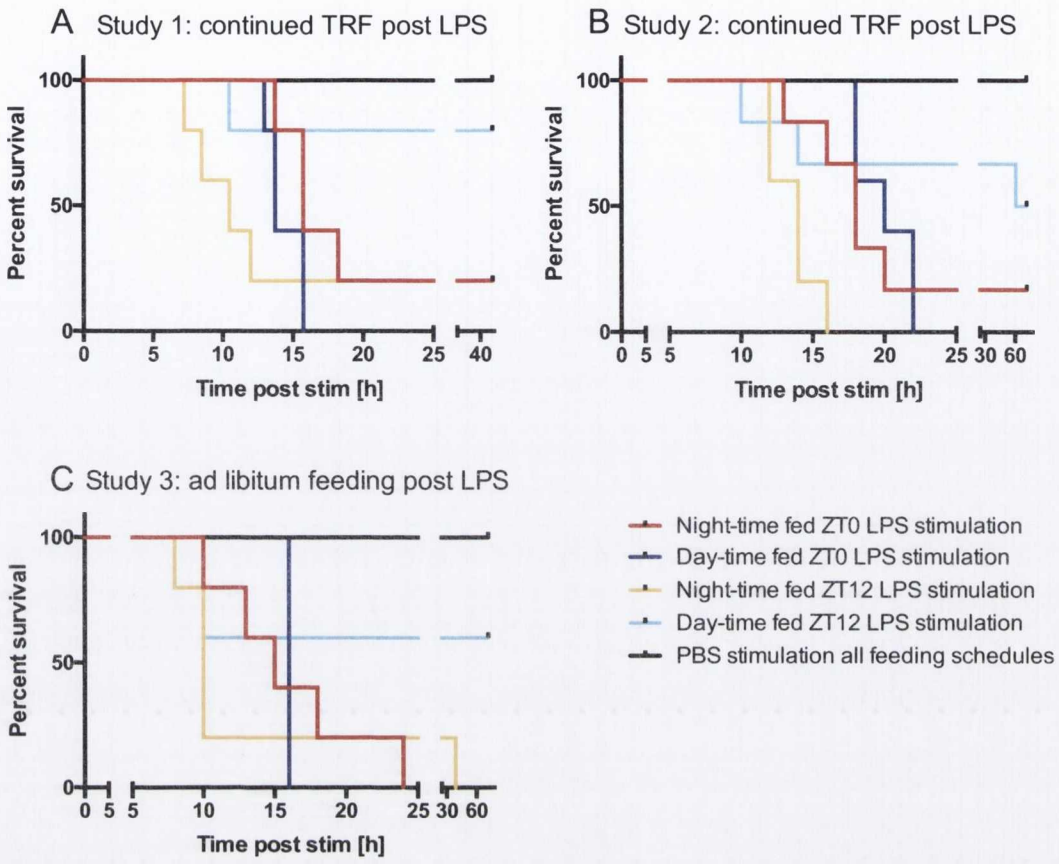


Figure 4.2.1.2: The effect of food availability following LPS stimulation.
Survival times of mice challenged with LPS (20mg/kg) i.p. at ZT0 or ZT12 on day 5 of TRF. Three independent studies. **A, B)** Continued TRF following LPS stimulation. **C)** Ad libitum feeding post LPS. LPS stimulated groups n=4-6, PBS control groups n=3.

4.2.2 Feeding time determines the clock phase in the liver, but not in other peripheral organs or the brain

Morbidity in the LPS model of sepsis was clearly a function of rhythmic food intake, but the mechanism by which this was regulated was uncertain. As dietary signals were expected to differentially influence various compartments, food entrainment of an assortment of immunologically vital tissues was examined. Besides being a thorough characterization of TRF animals, this had the potential to localize the tissue expressing food entrained immune-regulatory genes.

First, changes in gene expression in response to shifted feeding schedules were measured in a subset of tissues. Besides the liver, which was anticipated to fully entrain to the new regime (Damiola et al., 2000), and peritoneal macrophages – which appeared central in prior studies of diurnal control of immunity (Curtis et al., 2015) - also the spleen and adipose tissue, as two other important immunologically active compartments, were examined. To efficiently screen expression of an assortment of genes that were of interest in mice subject to 5 days of day- or night-time food availability, NanoString technology was used. In contrast to qPCR, this method does not rely on amplification, but direct binding to mRNA molecules and making them visible for subsequent counting. A full list of genes that were tested can be found in the appendix (Appendix 1). Here, only genes with counts above threshold are shown.
Representation of the results in form of heat-maps of unsupervised gene clustering (Figure 4.2.2.1) facilitates a first impression of diurnal oscillations within the organs. The liver, as expected, showed strong rhythmicity, which followed the feeding schedule. However, spleen, adipose tissue and peritoneal macrophages all presented as slaves of the light cycle, rather than food, although to different extents. Spleen and peritoneal macrophages maintained the same phase in day-time compared to night-time fed animals, but with a reduced amplitude. Adipose tissue on the other hand, appeared to lose diurnal expression entirely when the feeding mismatched the light schedule.

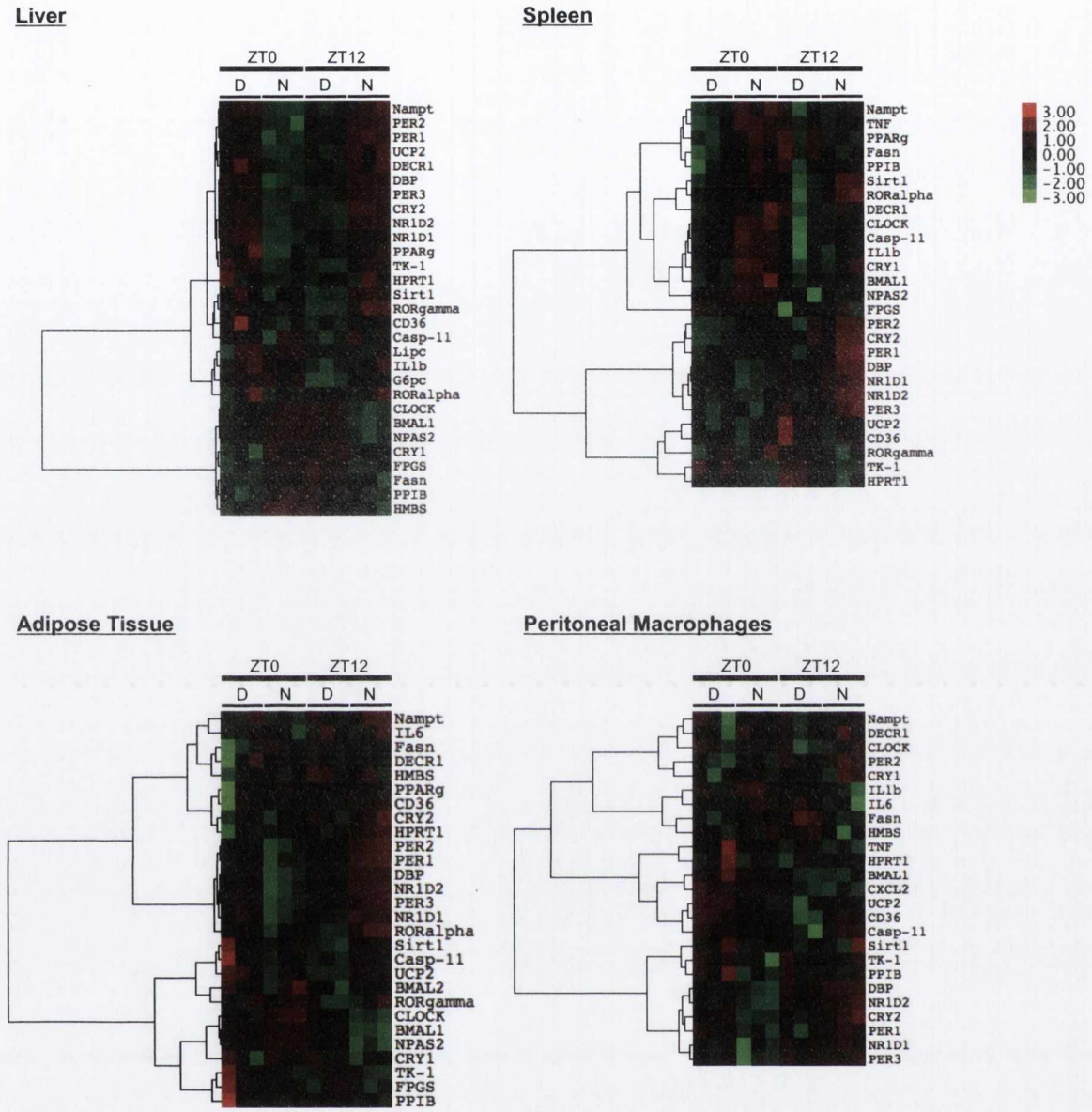


Figure 4.2.2.1: Day-time restricted feeding induces a 12 h period shift in the liver, but not in the spleen, adipose tissue and peritoneal macrophages.

Unsupervised gene clustering of < threshold data from NanoString Codeset Clock1 in selected tissues extracted at ZT0 or ZT12 from time restricted fed mice on day 5.

Although heat-maps are helpful to visualize larger data sets, the amplitudes of oscillations can't be appreciated. The results from each tissue were therefore graphed individually to allow more precise analysis (Figure 4.2.2.4, Figure 4.2.2.5, Figure 4.2.2.7, Figure 4.2.2.6).

Besides NanoString, gene expression of a smaller set of clock genes was also analysed in liver and spleen samples by conventional qPCR to test consistency between techniques (Figure 4.2.2.2, Figure 4.2.2.3). Similar results in both, the liver and the spleen, were achieved with NanoString and amplification based qPCR.

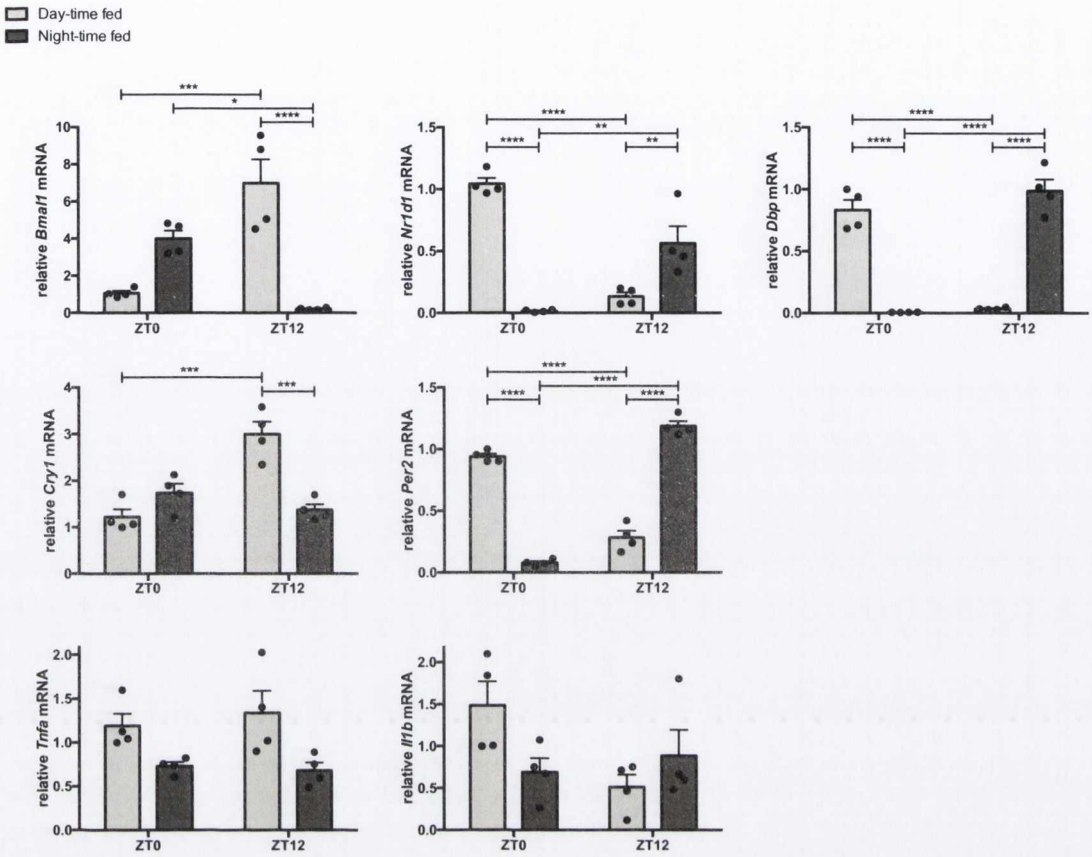


Figure 4.2.2.2: The liver clock, but not *Tnfa* and *Il1b* expression, is reversed in day-time fed animals.

qPCR from liver samples extracted at ZT0 or ZT12 from animals fed only during the night or the day for 5 days. Statistical analysis using two way ANOVA and Sidak's multiple comparisons test (indicated in graph with *p<0.05, **p<0.01, ***p<0.001, ****p<0.0001). *Bmal1*: Interaction: DF=1, F=51.06, p=0.0001. ZT: DF=1, F=2.456, p=0.1431. Feeding: DF=1, F=2.456, p=0.1431. *Nr1d1*: Interaction: DF=1, F=95.11, p<0.0001. ZT: DF=1, F=5.867, p=0.322. Feeding: DF=1, F=15.9, p=0.0018. *Dbp*: Interaction: DF=1, F=212.3, p<0.0001. ZT: DF=1, F=2.241, p=0.1602. Feeding: DF=1, F=1.033, p=0.3295. *Cry1*: Interaction: DF=1, F=30.92, p=0.0001. ZT: DF=1, F=13.51, p=0.0032. Feeding: DF=1, F=8.382, p=0.0134. *Per2*: Interaction: DF=1, F=592.3, p<0.0001. ZT: DF=1, F=38.91, p<0.0001. Feeding: DF=1, F=0.3488, p=0.5658. *Tnf*: Interaction: DF=1, F=0.4075, p=0.5352. ZT: DF=1, F=0.0999, p=0.7574. Feeding: DF=1, F=13.44, p=0.0032. *Il1*: Interaction: DF=1, F=6.1, p=0.0295. ZT: DF=1, F=2.7, p=0.1263. Feeding: DF=1, F=0.7885, p=0.392.

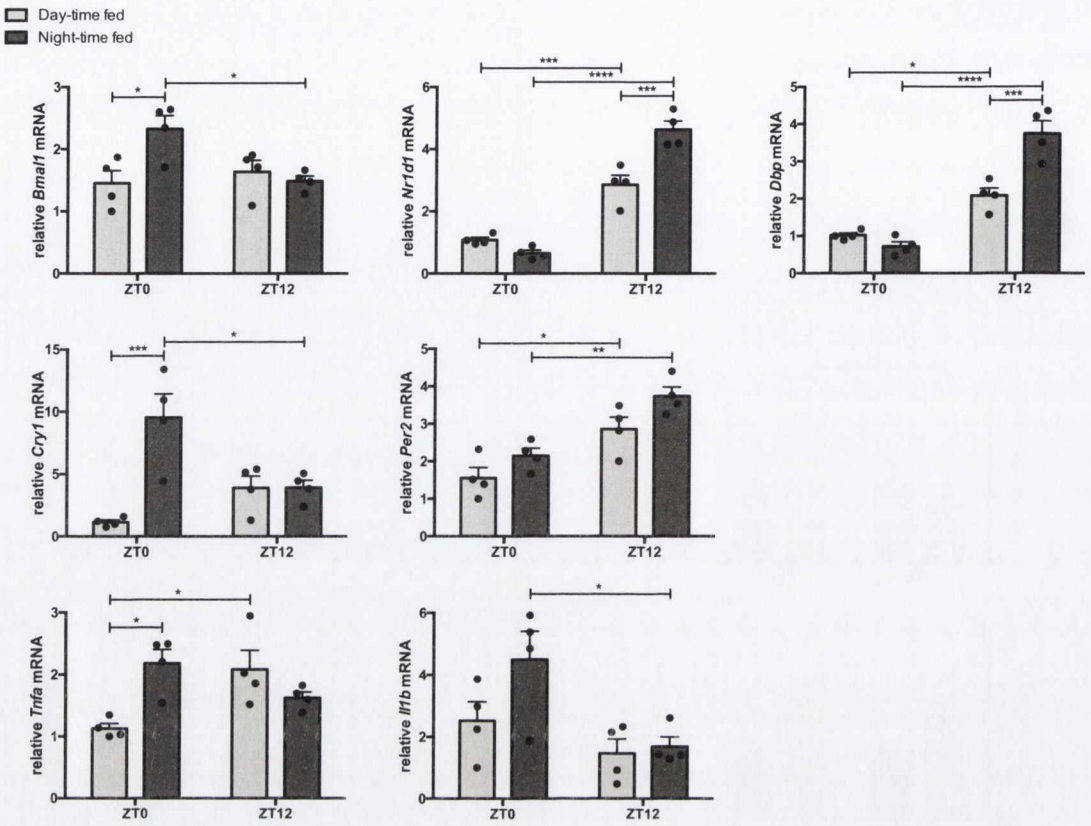


Figure 4.2.2.3: TRF does not reverse the spleen clock, but causes a mild attenuation of diurnal cycling, while *Tnfa* expression appears to follow the feeding cycle.

qPCR analysis of spleen samples extracted at ZT0 or ZT12 from day 5 TRF animals. Statistical analysis using two way ANOVA and Sidak's multiple comparisons test (indicated in graph with *p<0.05, **p<0.01, ***p<0.001, ****p<0.0001). *Bmal1*: Interaction: DF=1, F=8.174, p=0.0144. ZT: DF=1, F=3.369, p=0.0913. Feeding: DF=1, F=4.163, p=0.0639. *Nr1d1*: Interaction: DF=1, F=25.95, p=0.0003. ZT: DF=1, F=176.9, p<0.0001. Feeding: DF=1, F=9.679, p=0.009. *Dbp*: Interaction: DF=1, F=23.1, p=0.0004. ZT: DF=1, F=100.2, p<0.0001. Feeding: DF=1, F=11.23, p=0.0058. *Cry1*: Interaction: DF=1, F=14.5, p=0.0025. ZT: DF=1, F=1.68, p=0.2194. Feeding: DF=1, F=14.63, p=0.0024. *Per2*: Interaction: DF=1, F=0.2893, p=0.6005. ZT: DF=1, F=30.48, p=0.0001. Feeding: DF=1, F=7.915, p=0.0157. *Tnf*: Interaction: DF=1, F=14.56, p=0.0025. ZT: DF=1, F=1.008, p=0.3352. Feeding: DF=1, F=2.218, p=0.1622. *Il1*: Interaction: DF=1, F=2.079, p=0.1749. ZT: DF=1, F=10.04, p=0.0081. Feeding: DF=1, F=3.244, p=0.0969.

qPCR and NanoString analysis of liver samples from mice that had access to food either during the light or during the dark phase for 5 consecutive days resulted in a clear food dependency of clock genes (Figure 4.2.2.2, Figure 4.2.2.4 A). While the phase of oscillation was inversed, the amplitude was not significantly affected, suggesting no or little light control.

Genes involved in metabolism similarly displayed extensive food dependency as the phases of these genes were inversed (Figure 4.2.2.4 B), which was anticipated given the central role of the liver in metabolism. In contrast, the abundance of inflammatory genes was low and widely lacked rhythmicity in day- as well as night-time fed animals (Figure 4.2.2.4 C, Figure 4.2.2.2). However, as inflammatory genes are generally expressed at low levels under homeostatic conditions, a lack of diurnal expression of these genes should not be mistaken as a predictor that gene induction following inflammatory insult would be clock independent.

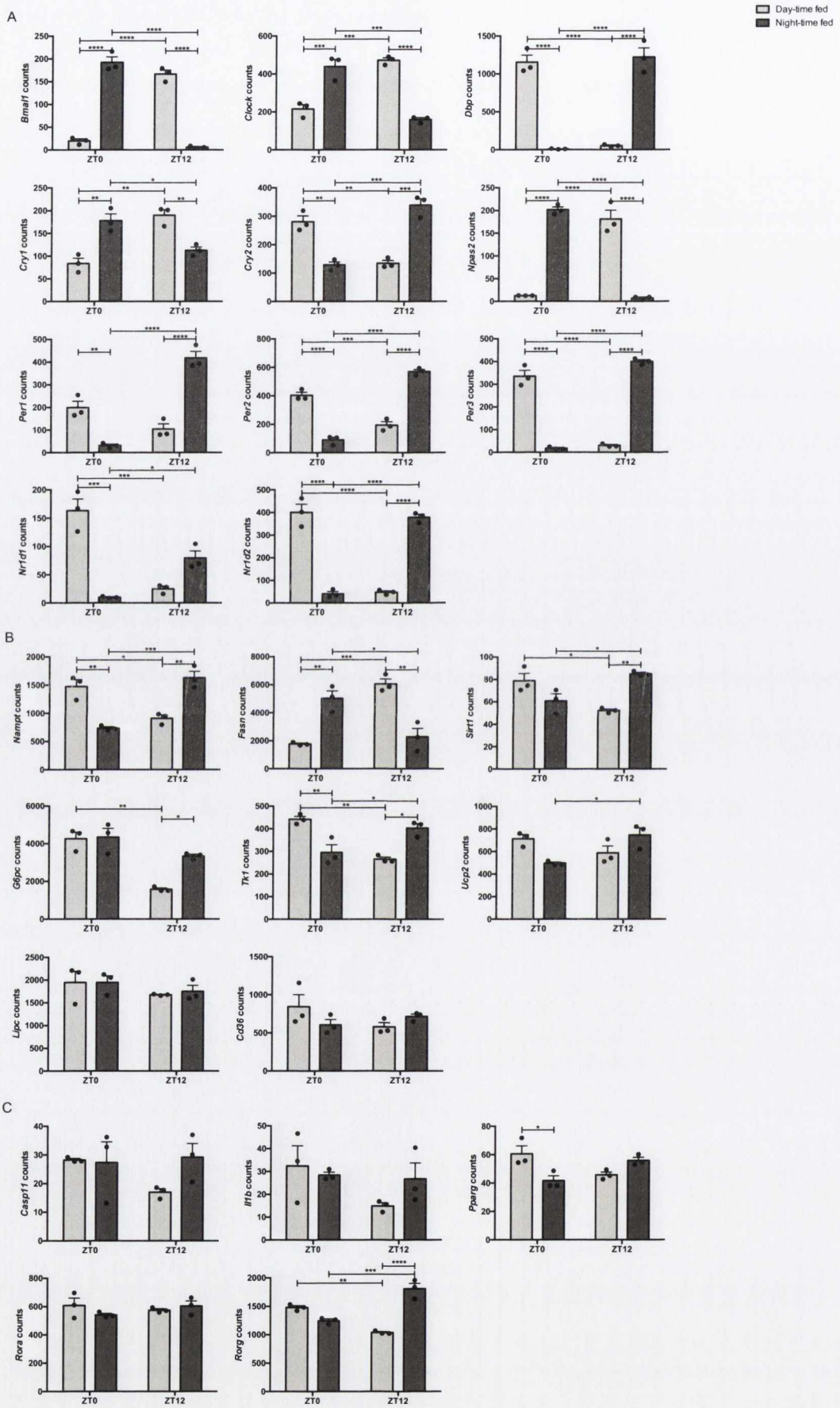

Day-time fed
Night-time fed
A
Bmal1 counts
Clock counts
Dbp counts
Cry1 counts
Cry2 counts
Npas2 counts
Per1 counts
Per2 counts
Per3 counts
Nr1d1 counts
Nr1d2 counts
B
Nampt counts
Fasn counts
Sirt1 counts
G6pc counts
Tk1 counts
Ucp2 counts
Lipc counts
Cd36 counts
C
Casp11 counts
Il1b counts
Pparg counts
Rora counts
Rorg counts
ZT0
ZT12

Figure 4.2.2.4: Metabolic and clock gene expression, but not basal inflammatory gene expression in the liver is a function of food availability. NanoString data of liver RNA samples extracted at ZT0 and ZT12 from TRF mice on day 5. Compiled data from all < threshold results from NanoString Codeset Clock 1, which comprised a selection of circadian **(A)**, metabolic **(B)**, and inflammatory **(C)** genes. Statistical analysis using two way ANOVA and Sidak's multiple comparisons test (indicated in graph with *p<0.05, **p<0.01, ***p<0.001, ****p<0.0001). **A)** *Bmal1*: Interaction: DF=1, F=453.3, p<0.0001. ZT: DF=1, F=6.48, p=0.0344. Feeding: DF=1, F=0.6035, p=0.4596. *Clock*: Interaction: DF=1, F=129.1, p<0.0001. ZT: DF=1, F=0.2442, p=0.6345. Feeding: DF=1, F=3.478, p=0.0992. *Dbp*: Interaction: DF=1, F=233.5, p<0.0001. ZT: DF=1, F=0.5383, p=0.4841. Feeding: DF=1, F=0.02017, p=0.8906. *Cry1*: Interaction: DF=1, F=54.2, p<0.0001. ZT: DF=1, F=3.072, p=0.1178. Feeding: DF=1, F=0.5357, p=0.4851. *Cry2*: Interaction: DF=1, F=113.7, p<0.0001. ZT: DF=1, F=3.613, p=0.0939. Feeding: DF=1, F=2.495, p=0.1528. *Npas2*: Interaction: DF=1, F=315.6, p<0.0001. ZT: DF=1, F=1.63, p=0.2375. Feeding: DF=1, F=0.5134, p=0.4941. *Per1*: Interaction: DF=1, F=106.2, p<0.0001. ZT: DF=1, F=38.92, p=0.0002. Feeding: DF=1, F=9.743, p=0.0142. *Per2*: Interaction: DF=1, F=297.3, p<0.0001. ZT: DF=1, F=45.52, p=0.0001. Feeding: DF=1, F=2.462, p=0.1552. *Per3*: Interaction: DF=1, F=628.7, p<0.0001. ZT: DF=1, F=7.899, p=0.0228. Feeding: DF=1, F=3.547, p=0.0964. *Nr1d1*: Interaction: DF=1, F=73.05, p<0.0001. ZT: DF=1, F=8.062, p=0.0218. Feeding: DF=1, F=16.56, p=0.0036. *Nr1d2*: Interaction: DF=1, F=300.5, p<0.0001. ZT: DF=1, F=0.1462, p=0.7121. Feeding: DF=1, F=0.5272, p=0.4885. **B)** *Nampt*: Interaction: DF=1, F=67.75, p<0.0001. ZT: DF=1, F=3.45, p=0.1003. Feeding: DF=1, F=0.01667, p=0.9004. *Fasn*: Interaction: DF=1, F=65.19, p<0.0001. ZT: DF=1, F=3.147, p=0.114. Feeding: DF=1, F=0.3528, p=0.5689. *Sirt1*: Interaction: DF=1, F=30.7, p=0.0005. ZT: DF=1, F=0.05767, p=0.8163. Feeding: DF=1, F=2.506, p=0.152. *G6pc*: Interaction: DF=1, F=8.111, p=0.0215. ZT: DF=1, F=39.58, p=0.0002. Feeding: DF=1, F=9.736, p=0.0142. *Tk1*: Interaction: DF=1, F=44.64, p=0.0002. ZT: DF=1, F=2.603, p=0.1453. Feeding: DF=1, F=0.05265, p=0.8243. *Ucp2*: Interaction: DF=1, F=15.37, p=0.0044. ZT: DF=1, F=1.682, p=0.2308. Feeding: DF=1, F=0.3806, p=0.5544. *Lipc*: Interaction: DF=1, F=0.06536, p=0.8047. ZT: DF=1, F=2.312, p=0.1669. Feeding: DF=1, F=0.05365, p=0.8226. *Cd36*: Interaction: DF=1, F=4.193, p=0.0748. ZT: DF=1, F=0.7178, p=0.4215. Feeding: DF=1, F=0.3057, p=0.5954. **C)** *Casp11*: Interaction: DF=1, F=2.266, p=0.1706. ZT: DF=1, F=1.176, p=0.3097. Feeding: DF=1, F=1.677, p=0.2314. *Il1b*: Interaction: DF=1, F=1.96, p=0.1991. ZT: DF=1, F=2.841, p=0.1304. Feeding: DF=1, F=0.4717, p=0.5116. *Pparg*: Interaction: DF=1, F=16.4, p=0.0037. ZT: DF=1, F=0.006425, p=0.9381. Feeding: DF=1, F=1.525, p=0.2519. *Rora*: Interaction: DF=1, F=2.272, p=0.1702. ZT: DF=1, F=0.1996, p=0.6669. Feeding: DF=1, F=0.3497, p=0.5706. *Rorg*: Interaction: DF=1, F=88.02, p<0.0001. ZT:

DF=1, F=1.251, p=0.2958. Feeding: DF=1, F=25.19, p=0.001.

In the spleen, the amplitude of clock gene oscillation was generally lower than what was seen in the liver, and was further reduced upon day restricted feeding (Figure 4.2.2.3, Figure 4.2.2.5 A). Analysis by NanoString and qPCR revealed comparable results, but it appeared that clock gene oscillation was more pronounced when measured by qPCR than NanoString, where hardly any significant oscillation remained in day-time fed animals. This may have been a matter of slightly bigger errors within the groups in the NanoString data, as the trends were similar between the techniques. While metabolic and inflammatory genes widely appeared constitutive in both experimental groups, diurnal expression of *Tnfa* and *Il1b* stood out (Figure 4.2.2.3, Figure 4.2.2.5 C). Similarly to clock genes in the spleen, *Il1b* oscillation was decreased, but maintained the phase, while *Tnfa* displayed reversed phase in day-time fed animals. Analogously to what was seen before, differences were more pronounced in qPCR measurements compared to NanoString data.

Considering the data gathered in the LPS lethality studies (Figure 4.2.1.1), the gene expression patterns that were found in the spleen argued against a significant role for this organ in controlling increased protection at ZT12 following LPS stimulation of day-time fed animals. Nevertheless, the spleen could potentially be vital in explaining why day- and night-time fed animals did not display mirror image survival curves.

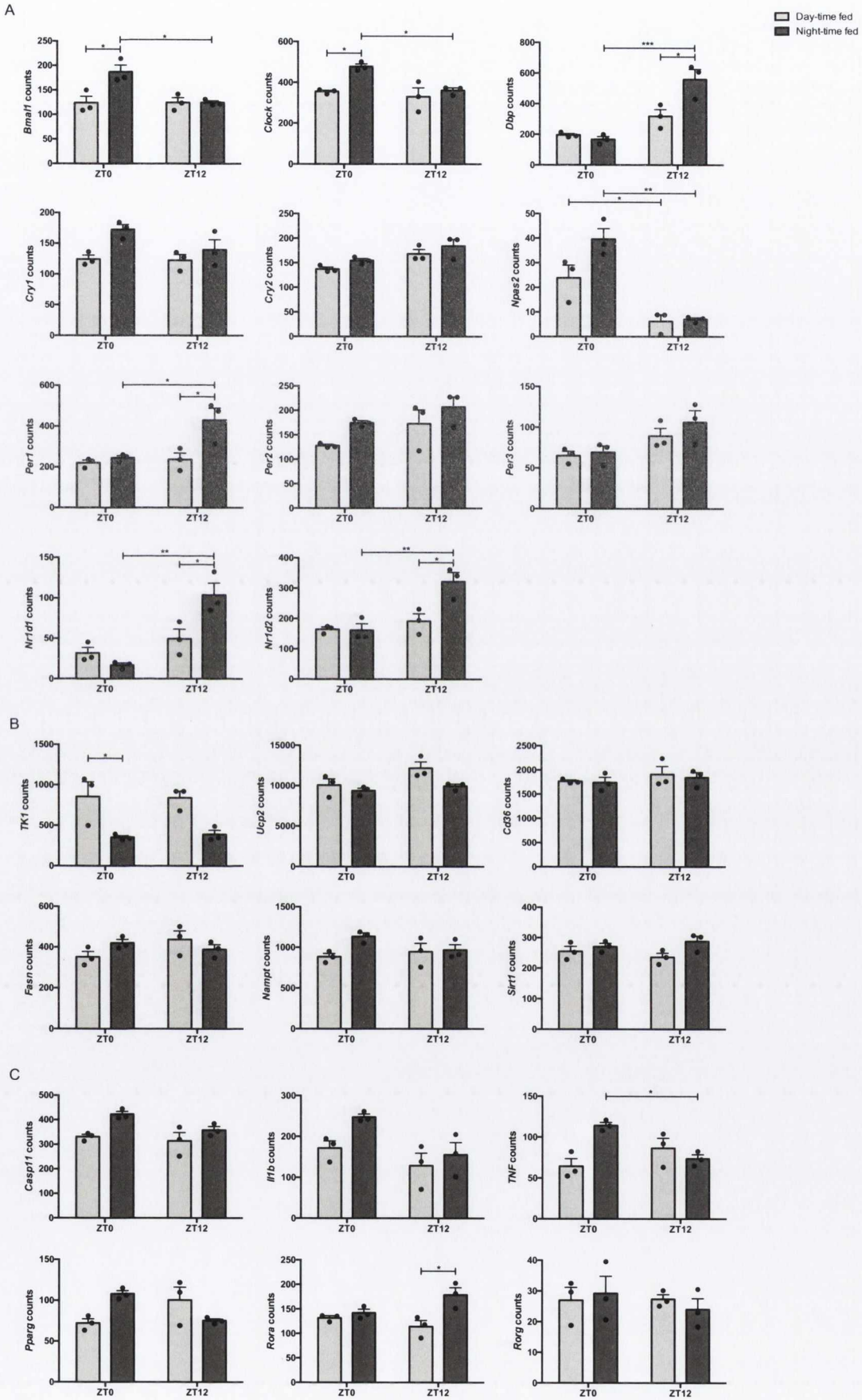

A
Day-time fed
Night-time fed
Bmal1 counts
Clock counts
Dbp counts
Cry1 counts
Cry2 counts
Npas2 counts
Per1 counts
Per2 counts
Per3 counts
Nr1d1 counts
Nr1d2 counts
B
TK1 counts
Ucp2 counts
Cd36 counts
Fasn counts
Nampt counts
Sirt1 counts
C
Casp11 counts
Il1b counts
TNF counts
Pparg counts
Rora counts
Rorg counts
ZT0
ZT12

Figure 4.2.2.5: Gene expression oscillations in the spleen are less pronounced, and amplitudes are further reduced upon day-time feeding.

Spleen samples extracted at ZT0 and ZT12 from TRF mice on day 5 were analysed by NanoString. Compiled data from all < threshold results from NanoString Codeset Clock 1, which comprised a selection of circadian **(A)**, metabolic **(B)**, and inflammatory **(C)** genes. Statistical analysis using two way ANOVA and Sidak's multiple comparisons test (indicated in graph with *p<0.05, **p<0.01, ***p<0.001, ****p<0.0001). **A)** *Bmal1*: Interaction: DF=1, F=8.582, p=0.019. ZT: DF=1, F=8.25, p=0.0208. Feeding: DF=1, F=8.519, p=0.0193. *Clock*: Interaction: DF=1, F=3.845, p=0.0855. ZT: DF=1, F=9.269, p=0.016. Feeding: DF=1, F=11.03, p=0.0105. *Dbp*: Interaction: DF=1, F=10.93, p=0.0108. ZT: DF=1, F=39.82, p=0.0002. Feeding: DF=1, F=6.847, p=0.0308. *Cry1*: Interaction: DF=1, F=2.115, p=0.1839. ZT: DF=1, F=2.633, p=0.1433. Feeding: DF=1, F=9.379, p=0.0155. *Cry2*: Interaction: DF=1, F=0.002528, p=0.9611. ZT: DF=1, F=12.36, p=0.0079. Feeding: DF=1, F=3.775, p=0.0879. *Npas2*: Interaction: DF=1, F=4.368, p=0.07. ZT: DF=1, F=49.2, p=0.0001. Feeding: DF=1, F=5.313, p=0.0501. *Per1*: Interaction: DF=1, F=5.999, p=0.04. ZT: DF=1, F=8.475, p=0.0196. Feeding: DF=1, F=9.904, p=0.0137. *Per2*: Interaction: DF=1, F=0.1292, p=0.7286. ZT: DF=1, F=4.957, p=0.0566. Feeding: DF=1, F=5.369, p=0.0491. *Per3*: Interaction: DF=1, F=0.4278, p=0.5314. ZT: DF=1, F=9.483, p=0.0151. Feeding: DF=1, F=1.11, p=0.323. *Nr1d1*: Interaction: DF=1, F=11.77, p=0.009. ZT: DF=1, F=26.8, p=0.0008. Feeding: DF=1, F=3.798, p=0.0871. *Nr1d2*: Interaction: DF=1, F=8.991, p=0.0171. ZT: DF=1, F=17.85, p=0.0029. Feeding: DF=1, F=8.327, p=0.0203. **B)** *Tk1*: Interaction: DF=1, F=0.06792, p=0.801. ZT: DF=1, F=0.01216, p=0.9149. Feeding: DF=1, F=21.77, p=0.0016. *Ucp2*: Interaction: DF=1, F=1.755, p=0.2219. ZT: DF=1, F=5.094, p=0.054. Feeding: DF=1, F=6.195, p=0.0376. *Cd36*: Interaction: DF=1, F=0.02868, p=0.8697. ZT: DF=1, F=1.178, p=0.3093. Feeding: DF=1, F=0.1595, p=0.7001. *Fasn*: Interaction: DF=1, F=4.104, p=0.0774. ZT: DF=1, F=0.9195, p=0.3657. Feeding: DF=1, F=0.1193, p=0.7387. *Nampt*: Interaction: DF=1, F=2.783, p=0.1338. ZT: DF=1, F=0.5667, p=0.4731. Feeding: DF=1, F=3.981, p=0.0811. *Sirt1*: Interaction: DF=1, F=1.544, p=0.2493. ZT: DF=1, F=0.004356, p=0.949. Feeding: DF=1, F=5.358, p=0.0493. **C)** *Casp11*: Interaction: DF=1, F=1.365, p=0.2762. ZT: DF=1, F=4.118, p=0.0769. Feeding: DF=1, F=11.56, p=0.0094. *Il1b*: Interaction: DF=1, F=1.11, p=0.3229. ZT: DF=1, F=8.386, p=0.02. Feeding: DF=1, F=4.856, p=0.0587. *TNF*: Interaction: DF=1, F=14.56, p=0.0051. ZT: DF=1, F=1.253, p=0.2955. Feeding: DF=1, F=4.984, p=0.0561. *Pparg*: Interaction: DF=1, F=12.28, p=0.008. ZT: DF=1, F=0.07524, p=0.7908. Feeding: DF=1, F=0.3752, p=0.5572. *Rora*: Interaction: DF=1, F=6.684, p=0.0323. ZT: DF=1, F=0.8138, p=90.3933. Feeding: DF=1, F=12.6, p=0.0075. *Rorg*: Interaction: DF=1, F=0.49, p=0.5038. ZT: DF=1, F=0.3683, p=0.5608. Feeding: DF=1, F=0.01895, p=0.8939.

While the spleen sustained some rhythmicity in day-time fed animals, oscillations in adipose tissue of these mice were widely ablated in clock, metabolism (with the exception of *Ucp2*) and inflammatory genes alike (Figure 4.2.2.6). Constitutive expression of these genes in the day-time fed animals indicated that the adipose tissue, similarly to the spleen was not central to reversed susceptibility patterns that were seen upon LPS stimulation in these mice. However, it was arguable that adipose tissue may require longer entrainment times, as it could be under dual control of light and food. The lack of entrainment of adipose tissue in the setting of TRF under constant light conditions, as presented later in this work, argues against this notion (Figure 4.2.2.11, C).

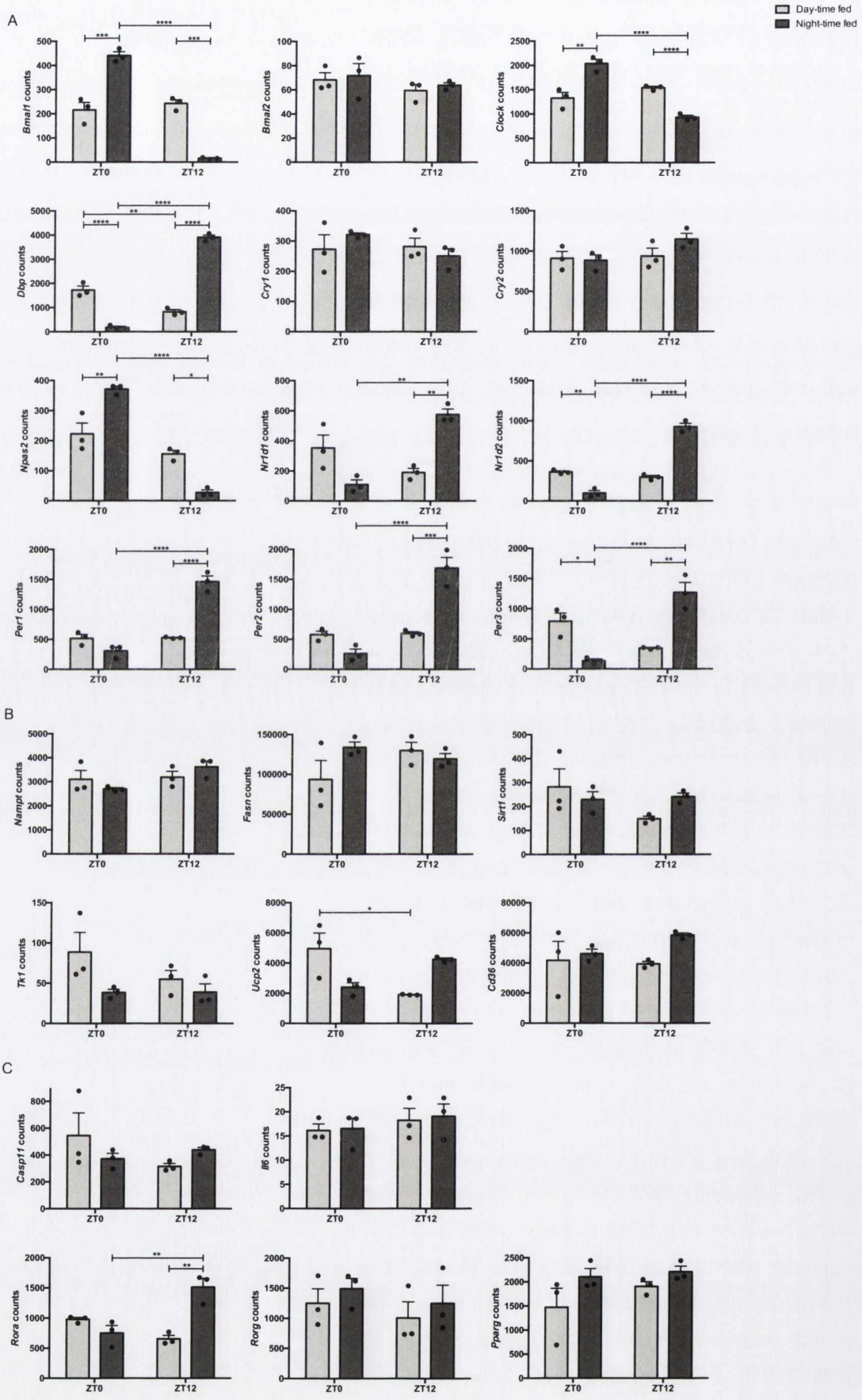

Day-time fed
Night-time fed
A
Bmal1 counts
Bmal2 counts
Clock counts
Dbp counts
Cry1 counts
Cry2 counts
Npas2 counts
Nr1d1 counts
Nr1d2 counts
Per1 counts
Per2 counts
Per3 counts
B
Nampt counts
Fasn counts
Sirt1 counts
Tk1 counts
Ucp2 counts
Cd36 counts
C
Casp11 counts
Il6 counts
Rora counts
Rorg counts
Pparg counts
ZT0
ZT12

Figure 4.2.2.6: Rhythmicity of clock gene expression in adipose samples is diminished in day-time fed animals.

RNA samples from adipose tissue extracted at ZT0 and ZT12 from TRF mice on day 5 and analysed by NanoString. Compiled data from all < threshold results from NanoString Codeset Clock 1, which comprised a selection of circadian **(A)**, metabolic **(B)**, and inflammatory **(C)** genes. Statistical analysis using two way ANOVA and Sidak's multiple comparisons test (indicated in graph with *p<0.05, **p<0.01, ***p<0.001, ****p<0.0001). **A)** *Bmal1*: Interaction: DF=1, F=144, p<0.0001. ZT: DF=1, F=112.2, p<0.0001. Feeding: DF=1, F=0.003906, p=0.9517. *Bmal2*: Interaction: DF=1, F=0.004751, p=0.9467. ZT: DF=1, F=1.727, p=0.2252. Feeding: DF=1, F=0.3682, p=0.5608. *Clock*: Interaction: DF=1, F=71.62, p<0.0001. ZT: DF=1, F=32.8, p=0.0004. Feeding: DF=1, F=0.4353, p=0.5279. *Dbp*: Interaction: DF=1, F=479.5, p<0.0001. ZT: DF=1, F=180, p<0.0001. Feeding: DF=1, F=51.68, p<0.0001. *Cry1*: Interaction: DF=1, F=1.708, p=0.2275. ZT: DF=1, F=1.03, p=0.3398. Feeding: DF=1, F=0.08196, p=0.7819. *Cry2*: Interaction: DF=1, F=2.148, p=0.181. ZT: DF=1, F=3.242, p=0.1095. Feeding: DF=1, F=1.297, p=0.2878. *Npas2*: Interaction: DF=1, F=48.23, p=0.0001. ZT: DF=1, F=106.4, p<0.0001. Feeding: DF=1, F=0.272, p=0.6161. *Nr1d1*: Interaction: DF=1, F=38.68, p=0.0003. ZT: DF=1, F=8.964, p=0.0172. Feeding: DF=1, F=1.988, p=0.1962. *Nr1d2*: Interaction: DF=1, F=245.8, p<0.0001. ZT: DF=1, F=180.6, p<0.0001. Feeding: DF=1, F=40.89, p=0.0002. *Per1*: Interaction: DF=1, F=76.85, p<0.0001. ZT: DF=1, F=79.56, p<0.0001. Feeding: DF=1, F=30.58, p=0.0006. *Per2*: Interaction: DF=1, F=48.26, p=0.0001. ZT: DF=1, F=51.21, p<0.0001. Feeding: DF=1, F=14.63, p=0.0051. *Per3*: Interaction: DF=1, F=54.08, p<0.0001. ZT: DF=1, F=10.22, p=0.0127. Feeding: DF=1, F=1.541, p=0.2496. **B)** *Nampt*: Interaction: DF=1, F=2.682, p=0.1401. ZT: DF=1, F=3.94, p=0.0824. Feeding: DF=1, F=0.003141, p=0.9567. *Fasn*: Interaction: DF=1, F=3.37, p=0.1037. ZT: DF=1, F=0.6265, p=0.4515. Feeding: DF=1, F=1.166, p=0.3118. *Sirt1*: Interaction: DF=1, F=3.027, p=0.1201. ZT: DF=1, F=2.116, p=0.1838. Feeding: DF=1, F=0.226, p=0.6472. *Tk1*: Interaction: DF=1, F=1.42, p=0.2676. ZT: DF=1, F=1.327, p=0.2826. Feeding: DF=1, F=5.333, p=0.0497. *Ucp2*: Interaction: DF=1, F=20.56, p=0.0019. ZT: DF=1, F=1.23, p=0.2996. Feeding: DF=1, F=0.04246, p=0.8419. *Cd36*: Interaction: DF=1, F=1.265, p=0.2933. ZT: DF=1, F=0.5926, p=0.4635. Feeding: DF=1, F=3.197, p=0.1116. **C)** *Casp11*: Interaction: DF=1, F=2.903, p=0.1268. ZT: DF=1, F=0.874, p=0.3772. Feeding: DF=1, F=0.0843, p=0.7789. *Il6*: Interaction: DF=1, F=0.01071, p=0.9201. ZT: DF=1, F=1.141, p=0.3167. Feeding: DF=1, F=0.08179, p=0.7822. *Rora*: Interaction: DF=1, F=29.52, p=0.0006. ZT: DF=1, F=4.812, p=0.0596. Feeding: DF=1, F=9.985, p=0.0134. *Rorg*: Interaction: DF=1, $F=5.414e^{-9}$, p>0.9999. ZT: DF=1, F=0.968, p=0.354. Feeding: DF=1, F=0.9432, p=0.3599. *Pparg*: Interaction: DF=1, F=0.5317, p=0.4867. ZT: DF=1, F=1.408, p=0.2694. Feeding: DF=1, F=4.276, p=0.0725.

As a role for peritoneal macrophages in the regulation of susceptibility to infection has been reported (Curtis et al., 2015), the expression of clock, metabolic and inflammatory genes in this cell type was also examined. Tissue resident macrophages from TRF animals were extracted from the peritoneal fluid, by magnetic bead separation and purity was examined by flow cytometry (Figure 4.2.2.8). The isolates displayed 50% purity, and appeared free of B-cells, the main contaminant, as identified by F4/80 negativity and FSC. Comparable to what was seen in the spleen, peritoneal macrophages from day-time fed animals maintained the phase of clock gene oscillation, but with a dampened amplitude (Figure 4.2.2.7). However, metabolic genes with a diurnal expression in macrophages - *Ucp2* in particular - displayed a trend towards food entrainment, possibly independent of the cellular clock (Figure 4.2.2.7 B). The consequences this may have for susceptibility to LPS is not yet clear, but maintained phases in clock genes argue against a critical role for these cells in mediating anti-phasic susceptibility in day-time fed animals following LPS stimulation. Given the importance of these cells in the response to TLR4 ligands, they may nevertheless be significantly contributing to the overall pattern of mortality, in particular in regard to survival curves that do not present as mirror images.

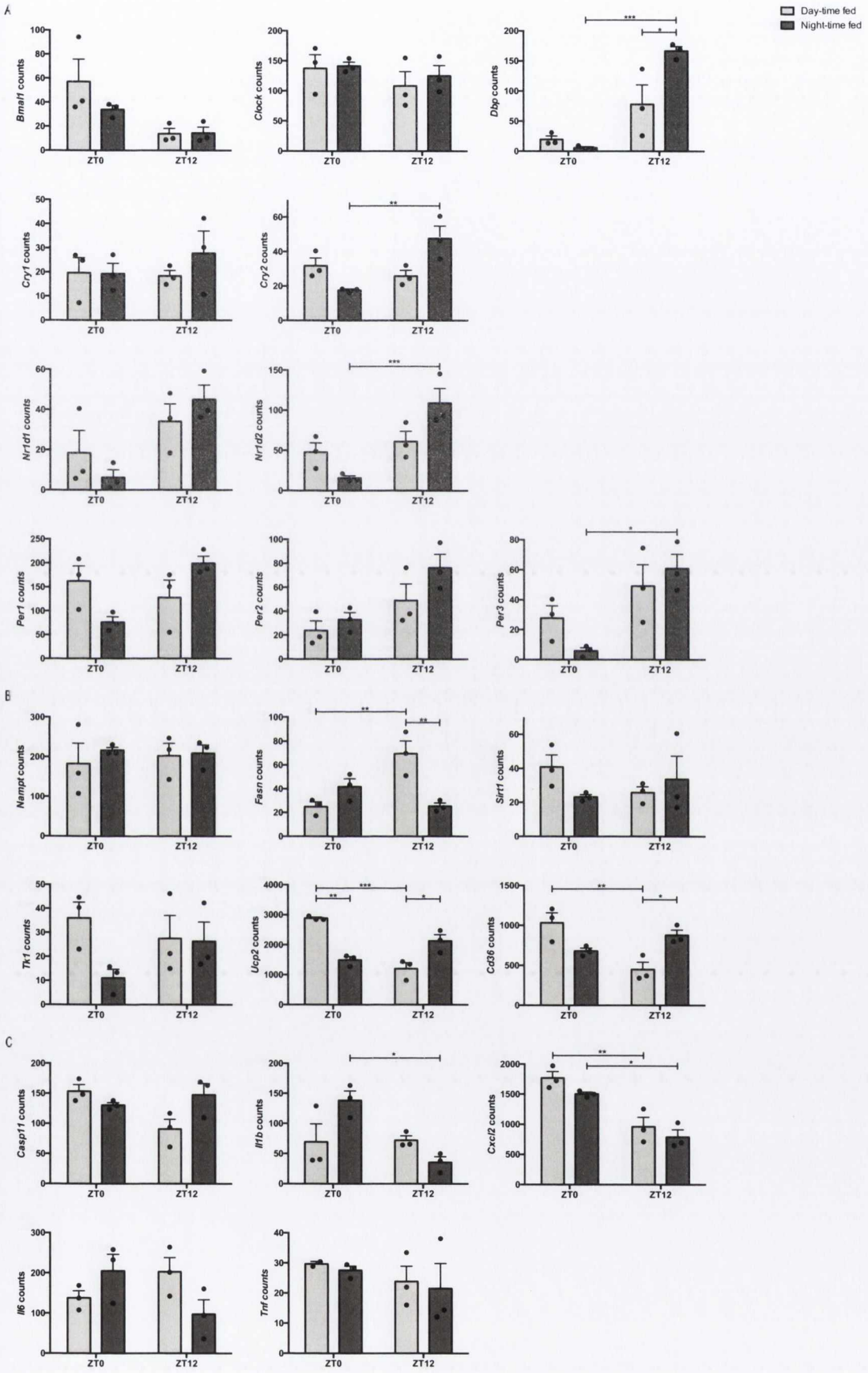

A
B
C
Day-time fed
Night-time fed
Bmal1 counts
Clock counts
Dbp counts
Cry1 counts
Cry2 counts
Nr1d1 counts
Nr1d2 counts
Per1 counts
Per2 counts
Per3 counts
Nampt counts
Fasn counts
Sirt1 counts
Tk1 counts
Ucp2 counts
Cd36 counts
Casp11 counts
Il1b counts
Cxcl2 counts
Il6 counts
Tnf counts
ZT0
ZT12

Figure 4.2.2.7: Expression of circadian genes appears diurnal, but food independent in peritoneal macrophages, while inflammatory genes do not oscillate strongly and metabolic genes exhibit food dependent rhythmicity.

NanoString data of RNA samples from peritoneal macrophages extracted at ZT0 and ZT12 from TRF mice on day 5. Compiled data from all < threshold results from NanoString Codeset Clock 1, which comprised a selection of circadian **(A)**, metabolic **(B)**, and inflammatory **(C)** genes. Statistical analysis using two way ANOVA and Sidak's multiple comparisons test (indicated in graph with *p<0.05, **p<0.01, ***p<0.001, ****p<0.0001). **A)** *Bmal1*: Interaction: DF=1, F=1.41, p=0.2691. ZT: DF=1, F=9.804, p=0.014. Feeding: DF=1, F=1.262, p=0.2938. *Clock*: Interaction: DF=1, F=0.1178, p=0.7403. ZT: DF=1, F=1.464, p=0.2609. Feeding: DF=1, F=0.2971, p=0.6005. *Dbp*: Interaction: DF=1, F=9.308, p=0.0158. ZT: DF=1, F=42.52, p=0.0002. Feeding: DF=1, F=4.948, p=0.0568. *Cry1*: Interaction: DF=1, F=0.6511, p=0.4431. ZT: DF=1, F=0.3532, p=0.5687. Feeding: DF=1, F=0.5597, p=0.4758. *Cry2*: Interaction: DF=1, F=15.94, p=0.004. ZT: DF=1, F=7.096, p=0.0286. Feeding: DF=1, F=0.7119, p=0.4233. *Nr1d1*: Interaction: DF=1, F=2.045, p=0.1905. ZT: DF=1, F=11.31, p=0.0099. Feeding: DF=1, F=0.006286, p=0.9388. *Nr1d2*: Interaction: DF=1, F=10.01, p=0.0133. ZT: DF=1, F=17.76, p=0.0029. Feeding: DF=1, F=0.3767, p=0.5564. *Per1*: Interaction: DF=1, F=9.324, p=0.0157. ZT: DF=1, F=2.913, p=0.1263. Feeding: DF=1, F=0.07113, p=0.7964. *Per2*: Interaction: DF=1, F=0.8131, p=0.3935. ZT: DF=1, F=11.28, p=0.0099. Feeding: DF=1, F=3.209, p=0.111. *Per3*: Interaction: DF=1, F=3.078, p=0.1175. ZT: DF=1, F=15.96, p=0.004. Feeding: DF=1, F=0.2775, p=0.6126. **B)** *Nampt*: Interaction: DF=1, F=0.1892, p=0.675. ZT: DF=1, F=0.03907, p=0.8482. Feeding: DF=1, F=0.394, p=0.5477. *Fasn*: Interaction: DF=1, F=20.81, p=0.0018. ZT: DF=1, F=4.433, p=0.0684. Feeding: DF=1, F=4.193, p=0.0748. *Sirt1*: Interaction: DF=1, F=2.599, p=0.1456. ZT: DF=1, F=0.08604, p=0.7767. Feeding: DF=1, F=0.383, p=0.5532. *Tk1*: Interaction: DF=1, F=2.66, p=0.1416. ZT: DF=1, F=0.2105, p=0.6586. Feeding: DF=1, F=3.206, p=0.1112. *Ucp2*: Interaction: DF=1, F=54.5, p<0.0001. ZT: DF=1, F=11.24, p=0.01. Feeding: DF=1, F=2.249, p=0.1721. *Cd36*: Interaction: DF=1, F=21.06, p=0.0018. ZT: DF=1, F=5.203, p=0.052. Feeding: DF=1, F=0.2099, p=0.659. **C)** *Casp11*: Interaction: DF=1, F=8.381, p=0.02. ZT: DF=1, F=2.744, p=0.1362. Feeding: DF=1, F=1.488, p=0.2572. *Il1b*: Interaction: DF=1, F=8.776, p=0.0181. ZT: DF=1, F=7.869, p=0.023. Feeding: DF=1, F=0.8127, p=0.3937. *Cxcl2*: Interaction: DF=1, F=0.1902, p=0.6743. ZT: DF=1, F=44.71, p=0.0002. Feeding: DF=1, F=3.639, p=0.0929. *Il6*: Interaction: DF=1, F=6.589, p=0.0333. ZT: DF=1, F=0.4036, p=0.543. Feeding: DF=1, F=0.3196, p=0.5873. *Tnf*: Interaction: DF=1, F=0.0003246, p=0.9861. ZT: DF=1, F=1.132, p=0.3226. Feeding: DF=1, F=0.1544, p=0.7061.

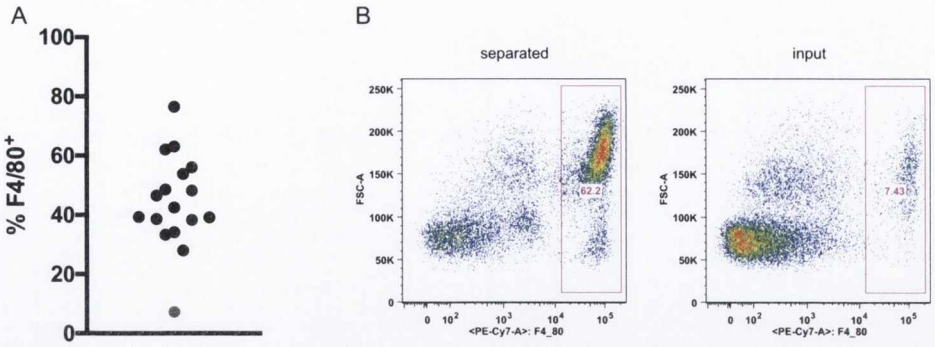


Figure 4.2.2.8: Magnetic, negative selection of peritoneal macrophages results in purity of approximately 50%.

A) Percentage of F4/80$^+$ cells following magnetic separation from the peritoneal fluid as measured by flow cytometry. Average F4/80 abundance in unseparated samples shown in grey. **B)** Representative FSC vs. F4/80 flow cytometry plot of living, single cells, indicating increased F4/80$^+$ populations and significant decrease of F4/80$^-$ contaminants in separated vs. input samples.

These results were further substantiated using an experimental setting that combined time restricted feeding with constant light conditions. This was done aware of the limitations as discussed in the introduction and the discussion. Mice that are continuously housed in constant light have been reported by some laboratories to lose circadian rhythmicity despite a functional clock. Subsequent entrainment of arrhythmic mice with food was anticipated to synchronize the liver clock, while other peripheral tissues as well as the light receptive master clock in the SCN would remain largely arrhythmic. This provided a useful tool to examine the role of food entrainment independent of circadian light signals. Clock genes of peritoneal macrophage isolates (purity ~ 50% (Figure 4.2.2.10)) did not oscillate in a circadian manner under constant light TRF (Figure 4.2.2.9), compared to what was observed under alternating light conditions (Figure 4.2.2.7); showing that light in fact entrains the cellular clock in macrophages. However, metabolic genes displayed oscillations similar to what was found in peritoneal macrophages from TRF mice under regular light conditions (Figure 4.2.2.7). This supports the notion that a range of metabolic genes in peritoneal macrophages can be regulated independently of the molecular clock, in a food dependent manner.

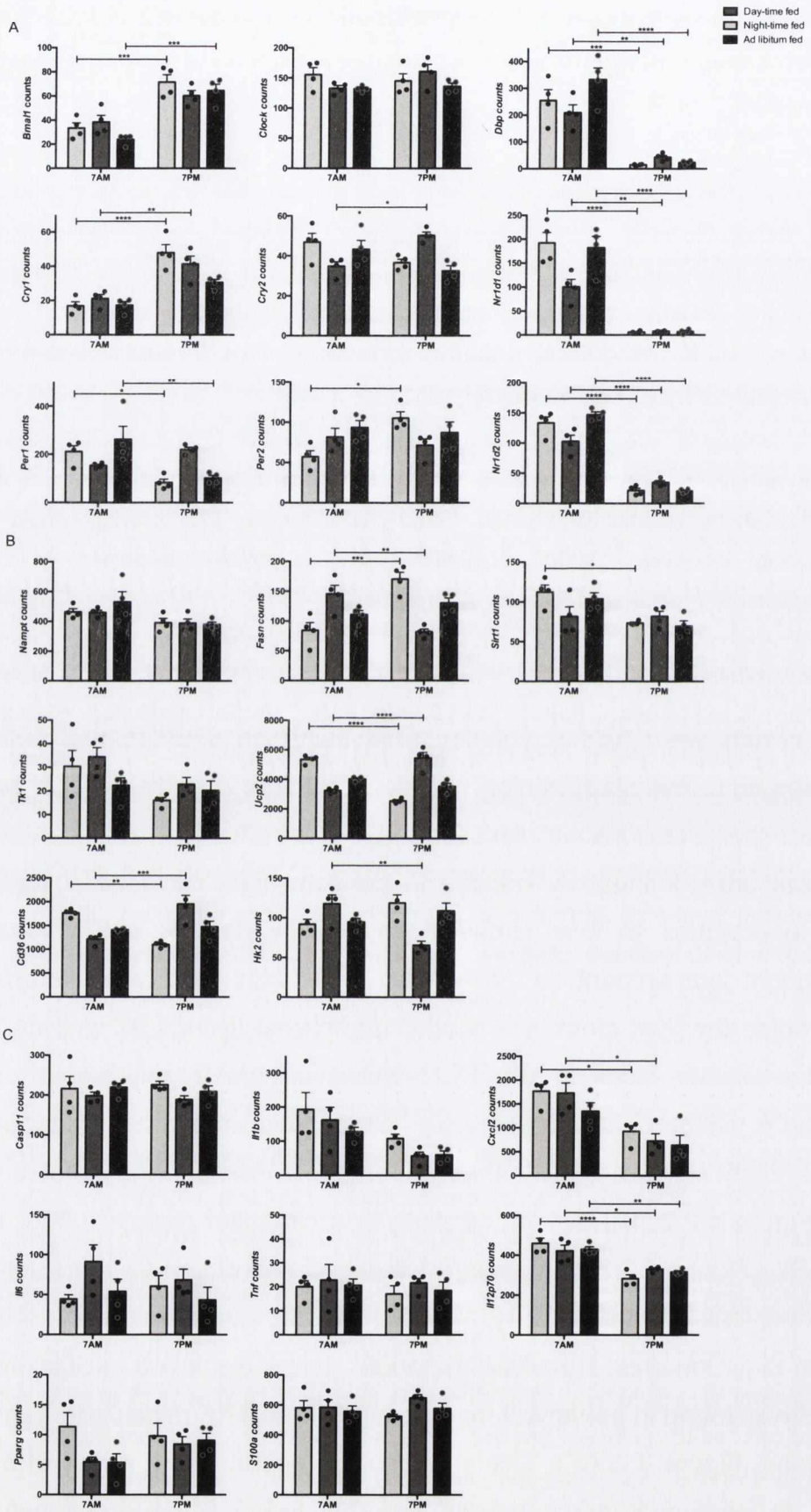

Day-time fed
Night-time fed
Ad libitum fed
A
Bmal1 counts
Clock counts
Dbp counts
Cry1 counts
Cry2 counts
Nr1d1 counts
Per1 counts
Per2 counts
Nr1d2 counts
B
Nampt counts
Fasn counts
Sirt1 counts
Tk1 counts
Ucp2 counts
Cd36 counts
Hk2 counts
C
Casp11 counts
Il1b counts
Cxcl2 counts
Il6 counts
Tnf counts
Il12p70 counts
Pparg counts
S100a counts
7AM
7PM

Figure 4.2.2.9: Ad libitum fed and TRF mice display widely congruent gene expression profiles under constant light conditions in peritoneal macrophages.

Mice were housed in constant light for 7 days before food availability was restricted according to the time of light or dark phases predating the introduction of constant light. On day 5 of TRF under constant light conditions, peritoneal macrophages were extracted at 7AM or 7PM, the times when food availability was changed during TRF. An ad libitum fed group, which received unrestricted access to food was included as a control. Compiled data from all < threshold results from NanoString Codeset Clock 2, which comprised a selection of circadian **(A)**, metabolic **(B)**, and inflammatory **(C)** genes. Statistical analysis using two way ANOVA and Sidak's multiple comparisons test (indicated in graph with *p<0.05, **p<0.01, ***p<0.001, ****p<0.0001). **A)** *Bmal1*: Interaction: DF=2, F=2.221, p=0.1373. Time: DF=1, F=73.76, p<0.0001. Feeding: DF=2, F=1.494, p=0.2509. *Clock*: Interaction: DF=2, F=2.364, p=0.1226. Time: DF=1, F=1.016, p=0.3269. Feeding: DF=2, F=1.902, p=0.1781. *Dbp*: Interaction: DF=2, F=3.467, p=0.0533. Time: DF=1, F=114.6, p<0.0001. Feeding: DF=2, F=2.089, p=0.1528. *Cry1*: Interaction: DF=2, F=3.92, p=0.0386. Time: DF=1, F=68.58, p<0.0001. Feeding: DF=2, F=4.149, p=0.033. *Cry2*: Interaction: DF=2, F=12.11, p=0.0005. Time: DF=1, F=0.5669, p=0.4612. Feeding: DF=2, F=1.314, p=0.2934. *Nr1d1*: Interaction: DF=2, F=6.122, p=0.0094. Time: DF=1, F=160.3, p<0.0001. Feeding: DF=2, F=5.798, p=0.0114. *Per1*: Interaction: DF=2, F=11.58, p=0.0006. Time: DF=1, F=12.73, p=0.0022. Feeding: DF=2, F=1.462, p=0.2581. *Per2*: Interaction: DF=2, F=6.041, p=0.0098. Time: DF=1, F=1.866, p=0.1888. Feeding: DF=2, F=1.11, p=0.3511. *Nr1d2*: Interaction: DF=2, F=11.34, p=0.0006. Time: DF=1, F=381.7, p<0.0001. Feeding: DF=2, F=2.776, p=0.089. **B)** *Nampt*: Interaction: DF=2, F=0.8646, p=0.438. Time: DF=1, F=11.77, p=0.003. Feeding: DF=2, F=0.4897, p=0.6208. *Fasn*: Interaction: DF=2, F=26.55, p<.0001. Time: DF=1, F=2.728, p=0.116. Feeding: DF=2, F=0.8933, p=0.4267. *Sirt1*: Interaction: DF=2, F=3.713, p=0.0447. Time: DF=1, F=14.24, p=0.0014. Feeding: DF=2, F=1.038, p=0.3743. *Tk1*: Interaction: DF=2, F=1.29, p=0.2995. Time: DF=1, F=8.258, p=0.0101. Feeding: DF=2, F=1.782, p=0.1967. *Ucp2*: Interaction: DF=2, F=85.17, p<0.0001. Time: DF=1, F=5.356, p=0.0327. Feeding: DF=2, F=4.594, p=0.0244. *Cd36*: Interaction: DF=2, F=28.27, p<0.0001. Time: DF=1, F=0.3755, p=0.5477. Feeding: DF=2, F=1.678, p=0.2146. *Hk2*: Interaction: DF=2, F=13.34, p=0.0003. Time: DF=1, F=0.311, p=0.5839. Feeding: DF=2, F=1.504, p=0.2489. **C)** *Casp11*: Interaction: DF=2, F=0.2591, p=0.7746. Time: DF=1, F=0.06218, p=0.8059. Feeding: DF=2, F=1.646, p=0.2205. *Il1b*: Interaction: DF=2, F=0.2403, p=0.7889. Time: DF=1, F=15.1, p=0.0011. Feeding: DF=2, F=2.305, p=0.1285. *Cxcl2*: Interaction: DF=2, F=0.3565, p=0.7049. Time: DF=1, F=36.11, p<0.0001. Feeding: DF=2, F=2.212, p=0.1384. *Il6*: Interaction: DF=2, F=0.9052, p=0.4221. Time: DF=1,

F=0.2288, p=0.6382. Feeding: DF=2, F=2.637, p=0.099. *Tnf*: Interaction: DF=2, F=0.02855, p=0.9719. Time: DF=1, F=0.4981, p=0.4894. Feeding: DF=2, F=0.5177, p=0.6045. *Il12p70*: Interaction: DF=2, F=2.694, p=0.0948. Time: DF=1, F=66.54, p<0.0001. Feeding: DF=2, F=0.02783, p=0.9726. *Pparg*: Interaction: DF=2, F=1.564, p=0.2365. Time: DF=1, F=1.666, p=0.2131. Feeding: DF=2, F=3.099, p=0.0697. *S100a*: Interaction: DF=2, F=1.366, p=0.2804. Time: DF=1, F=0.07961, p=0.781. Feeding: DF=2, F=1.629, p=0.2237.

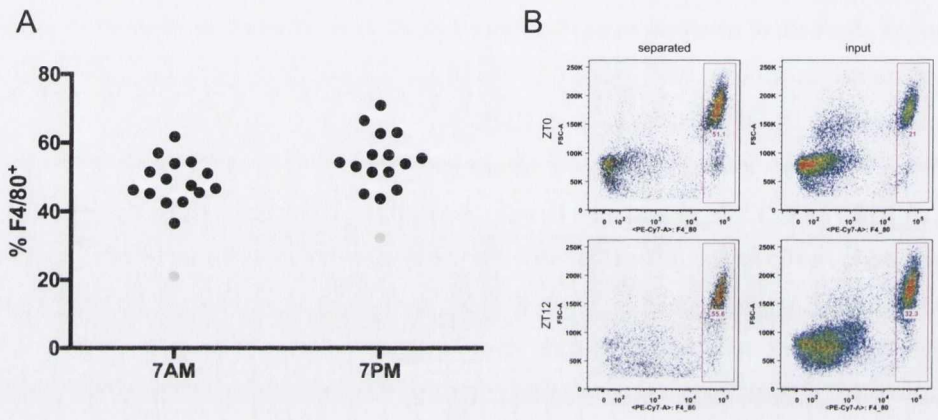


Figure 4.2.2.10: Magnetic, negative selection of peritoneal macrophages from TRF mice in constant light results in purity levels of approximately 50%.

A) Percentage of F4/80$^+$ cells following magnetic separation from the peritoneal fluid of TRF mice housed in constant light as measured by Flow cytometry. Average F4/80 abundance in unseparated samples shown in grey. **B)** Representative FSC vs. F4/80 flow cytometry plot of living, single cells, indicating increased F4/80$^+$ populations and significant decrease of F4/80$^-$ contaminants at 7AM and 7PM in separated vs. input samples.

Besides peritoneal macrophages, the expression of selected clock genes in several tissues harvested from TRF mice that were housed in constant light were analysed. Congruent with the data from TRF animals under regular light regimes, the liver was exceptional in its response to food, as it was the only organ that appeared to entrain to the feeding time and showed inversed gene

expression phase in the day-time (7AM-7PM) compared to the night-time (7PM-7AM) fed animals.

At first it appeared surprising that the ad libitum fed control group, which was included in this experimental setup, revealed clock gene oscillations in the liver comparable to the day-time fed animals. Considering that similar oscillations in the ad libitum fed group were also present in compartments other than the liver (e.g. spleen, adipose and SCN), and that clock gene expression patterns were found to be similar in all three feeding groups (day-, night- and ad libitum) in these tissues, it could be reasoned that oscillations in the ad libitum fed group may have been a remnant of clocks that were not fully desynchronized.

The literature regarding constant light is further not entirely consistent, and many laboratories reported animals with longer periods and decreased activity time under constant light conditions; an observation that is often referred to as Aschoff's rule, which describes circadian behaviour in nocturnal and diurnal animals under constant light or darkness (Pittendrigh, 1960). According to this, 12 days of constant light may have shifted the period in activity patterns and the molecular clock rather than causing complete loss of oscillations. This could be tested using activity recordings prior to sampling - preferably for each individual mouse to account for variation between subjects - and would certainly facilitate the interpretation of results.

It should further be noted that continuous illumination has the potential to act as a stressor (Abilio et al., 1999), which may affect study relevant pathways in a clock independent manner. A more extensive time-course with multiple sampling times over the course of a day could provide a better understanding of the source of variation in the ad libitum as well as the time restricted fed animals, and could help identify whether oscillations were lost or merely phase shifted in the context of constant light.

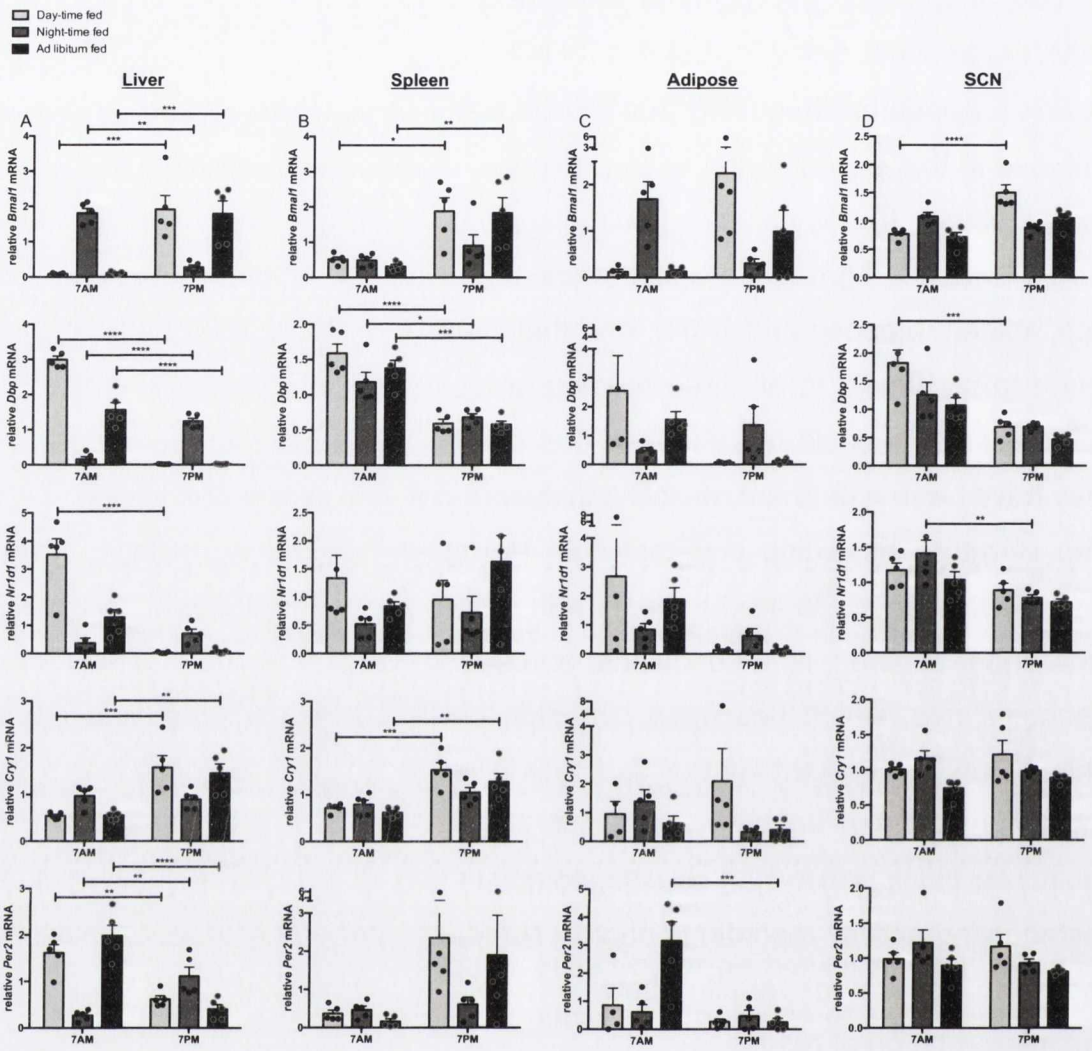


Figure 4.2.2.11: Clock gene expression in the liver, but not in SCN and other peripheral tissues is rhythmic in TRF animals under constant light conditions.

Mice were housed in constant light for 7 days before food availability was restricted according to the time of light or dark phases predating the introduction of constant light. On day 5 of TRF under constant light conditions, liver **(A)**, spleen **(B)**, adipose **(C)** and SCN **(D)** samples were collected at 7AM or 7PM, the time when the food accessibility what inverted, and mRNA levels of selected clock genes were analysed by qPCR. An ad libitum fed group, which received unrestricted access to food was included as a control. Statistical analysis using two way ANOVA and Sidak's multiple comparisons test (indicated in graph with *p<0.05, **p<0.01, ***p<0.001, ****p<0.0001). **A)** *Bmal1*: Interaction: DF=2, F=35.39, p<0.0001. Time: DF=1, F=12.74, p=0.0016. Feeding: DF=2, F=0.08336, p=0.9203. *Dbp*: Interaction: DF=2, F=187.6, p<0.0001. Time: DF=1, F=174.8, p<0.0001. Feeding: DF=2, F=34.35, p<0.0001. *Nr1d1*: Interaction: DF=2, F=24.69, p<0.0001. Time: DF=1, F=42.16, p<0.0001. Feeding: DF=2, F=12.16,

p=0.0002. *Cry1*: Interaction: DF=2, F=8.972, p=0.0012. Time: DF=1, F=27.81, p<0.0001. Feeding: DF=2, F=0.3913, p=0.6804. *Per2*: Interaction: DF=2, F=35.22, p<0.0001. Time: DF=1, F=22.17, p<0.0001. Feeding: DF=2, F=6.451, p=0.0057. **B)** *Bmal1*: Interaction: DF=2, F=2.418, p=0.1105. Time: DF=1, F=24.54, p<0.0001. Feeding: DF=2, F=1.849, p=0.1791. *Dbp*: Interaction: DF=2, F=3.184, p=0.0594. Time: DF=1, F=90.12, p<0.001. Feeding: DF=2, F=1.399, p=0.2663. *Nr1d1*: Interaction: DF=2, F=1.682, p=0.2072. Time: DF=1, F=0.6243, p=0.4372. Feeding: DF=2, F=2.161, p=0.1371. *Cry1*: Interaction: DF=2, F=3.198, p=0.0587. Time: DF=1, F=39.14, p<0.0001. Feeding: DF=2, F=1.929, p=0.1672. *Per2*: Interaction: DF=2, F=1.576, p=0.2274. Time: DF=1, F=7.906, p=0.0097. Feeding: DF=2, F=1.086, p=0.3537. **C)** *Bmal1*: Interaction: DF=2, F=7.65, p=0.0028. Time: DF=1, F=2.073, p=0.1634. Feeding: DF=2, F=0.9945, p=0.3852. *Dbp*: Interaction: DF=2, F=5.53, p=0.0113. Time: DF=1, F=5.542, p=0.0279. Feeding: DF=2, F=0.4362, p=0.6519. *Nr1d1*: Interaction: DF=2, F=1.657, p=0.2126. Time: DF=1, F=8.079, p=0.0092. Feeding: DF=2, F=0.5338, p=0.5935. *Cry1*: Interaction: DF=2, F=1.999, p=0.1584. Time: DF=1, F=0.01462, p=0.9048. Feeding: DF=2, F=1.681, p=0.2082. *Per2*: Interaction: DF=2, F=7.395, p=0.0033. Time: DF=1, F=14.6, p=0.0009. Feeding: DF=2, F=6.02, p=0.0079. **D)** *Bmal1*: Interaction: DF=2, F=16.79, p<0.0001. Time: DF=1, F=18.83, p=0.0002. Feeding: DF=2, F=4.926, p=0.0161. *Dbp*: Interaction: DF=2, F=2.31, p=0.1209. Time: DF=1, F=40.65, p<0.0001. Feeding: DF=2, F=5.505, p=0.0108. *Nr1d1*: Interaction: DF=2, F=1.553, p=0.2321. Time: DF=1, F=20.94, p=0.0001. Feeding: DF=2, F=2.065, p=0.1487. *Cry1*: Interaction: DF=2, F=2.352, p=0.1168. Time: DF=1, F=0.6276, p=0.436. Feeding: DF=2, F=5.65, p=0.0098. *Per2*: Interaction: DF=2, F=2.067, p=0.1485. Time: DF=1, F=0.4522, p=0.1059. Feeding: DF=2, F=2.469, p=0.1059.

4.2.3 Cytokines and liver enzymes, measured basally or 6h post stimulation, are not predictive of LPS induced morbidity

Thus far, susceptibility to LPS stimulation and circadian clock gene expression in the liver have been presented to be dependent on the feeding cycle. To further investigate the mechanism by which diurnal morbidity to inflammogenic material may be regulated, cytokine production and liberation of liver enzymes (as a measurement of liver damage) was examined.

Basal cytokine levels in the serum of TRF mice appeared similar between day- and night-time fed animals and did not to vary according to the time of the day, arguing against a possible poised state of these animals in regard to cytokines (Figure 4.2.3.1).

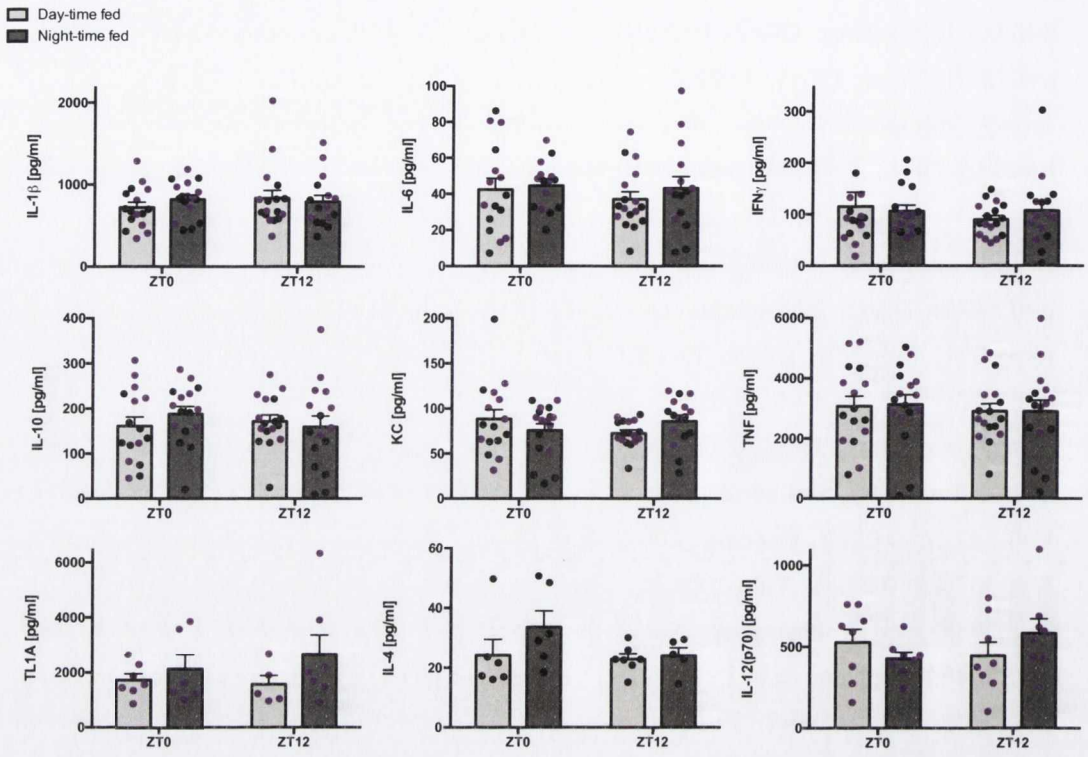


Figure 4.2.3.1: Basal serum cytokines are neither diurnal, nor affected by time restricted access to food.

Serum cytokines in unstimulated animals measured at ZT0 or ZT12 on day 4 on TRF. Black and purple circles indicate affiliation to data shown in Figure 4.2.3.3, as these represent pre-bleeds from the same animals. Data from 3 independent experiments. No significance using two way ANOVA and Sidak's multiple comparisons test. *IL-1β*: Interaction: DF=1, F=0.898, p=0.347. ZT: DF=1, F=0.3179, p=0.5749. Feeding: DF=1, F=0.1375, p=0.712. *IL-6*: Interaction: DF=1, F=0.1483, p=0.7016. ZT: DF=1, F=0.4272, p=0.5159. Feeding: DF=1, F=0.6437, p=0.4256. *IFNγ*: Interaction: DF=1, F=0.5504, p=0.461. ZT: DF=1, F=0.484, p=0.4893. Feeding: DF=1, F=0.05565, p=0.8143. *IL-10*: Interaction: DF=1, F=1.098, p=0.2989. ZT: DF=1, F=0.23, p=0.6332. Feeding: DF=1, F=0.147, p=0.7027. *KC*: Interaction: DF=1, F=3.228, p=0.0772. ZT: DF=1, F=0.1494, p=0.7004. Feeding: DF=1, F=0.0009187, p=0.9759. *TNF*: Interaction: DF=1, F=0.01111, p=0.9164. ZT: DF=1, F=0.3934, p=0.5328. Feeding: DF=1, F=0.006525, p=0.9359. *TL1A*: Interaction: DF=1, F=0.4651, p=0.5027. ZT: DF=1, F=0.1685, p=0.6856. Feeding: DF=1, F=2.121, p=0.1601. *IL-4*: Interaction: DF=1, F=1.049, p=0.318. ZT: DF=1, F=1.815, p=0.193. Feeding: DF=1, F=1.667, p=0.2114. *IL-12(p70)*: Interaction: DF=1, F=2.494, p=0.1255. ZT: DF=1, F=0.2401, p=0.6279. Feeding: DF=1, F=0.06118, p=0.8064.

This result was further substantiated in constant light conditions combined with TRF, which was previously shown to induce circadian clock gene expression in the liver, but not other screened tissues (Figure 4.2.2.11). Basal serum cytokines in this setting remained unaffected by feeding schedules and time of the day, as levels persisted at 7AM and 7PM as well as between day- and night-time fed animals; presenting another layer of evidence that food entrainment was not empowering basal cytokine levels.

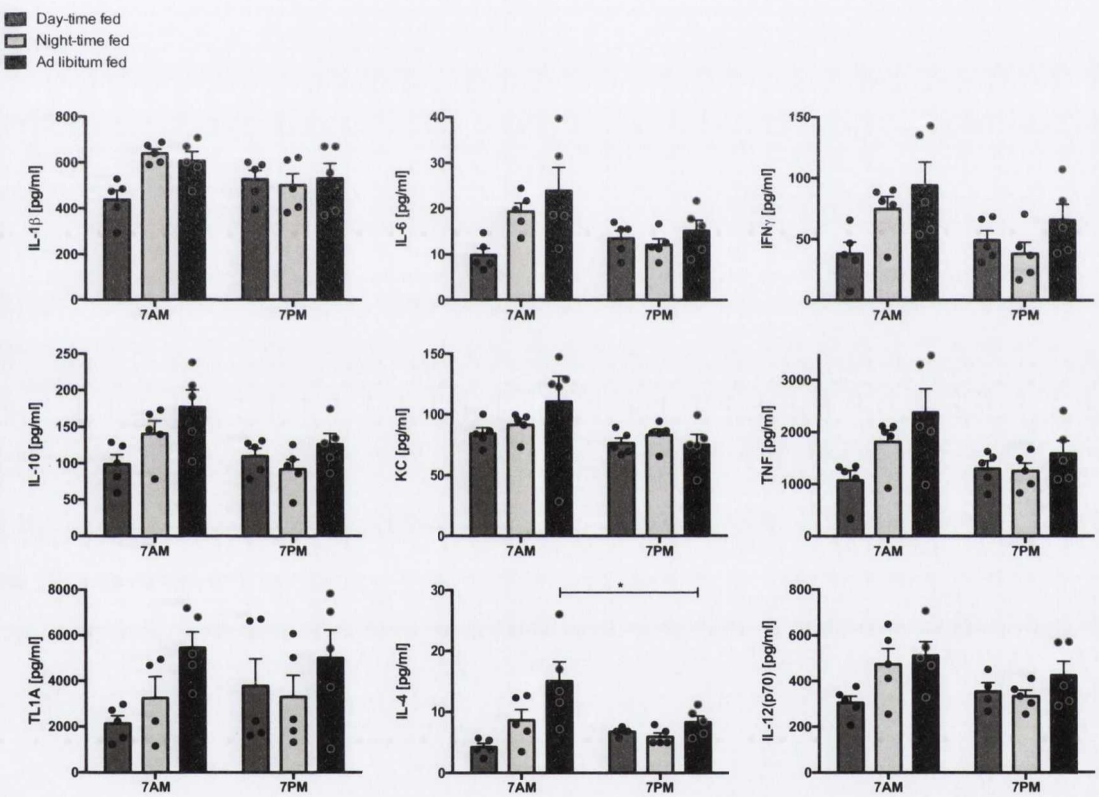


Figure 4.2.3.2: Time restricted feeding under constant light conditions does not affect basal cytokine level or absence of rhythmicity.

Mice were housed in constant light for 7 days before food availability was restricted according to the time of light or dark phases predating the introduction of constant light. On day 5 of TRF under constant light conditions, serum samples were collected at 7AM or 7PM, the times when food availability was inverted during the TRF schedule. An ad libitum fed group, which received unrestricted access to food was included as a control. Significance using two way ANOVA and Sidak's multiple comparisons test (indicated in graph with *p<0.05). *IL-1β*: Interaction: DF=2, F=3.42, p=0.0493. Time: DF=1, F=1.309,

p=0.2639. Feeding: DF=2, F=2.543, p=0.0996. *IL-6*: Interaction: DF=2, F=3.295, p=0.0544. Time: DF=1, F=3.638, p=0.0685. Feeding: DF=2, F=4.436, p=0.0229. *IFNγ*: Interaction: DF=2, F=2.253, p=0.1269. Time: DF=1, F=3.311, p=0.0813. Feeding: DF=2, F=4.606, p=0.0203. *IL-10*: Interaction: DF=2, F=2.399, p=0.1123. Time: DF=1, F=5.071, p=0.0337. Feeding: DF=2, F=4.593, p=0.0205. *KC*: Interaction: DF=2, F=1.242, p=0.3068. Time: DF=1, F=4.393, p=0.0468. Feeding: DF=2, F=0.7751, p=0.4718. *TNF*: Interaction: DF=2, F=2.104, p=0.1439. Time: DF=1, F=3.156, p=0.0883. Feeding: DF=2, F=4.701, p=0.0189. *TL1A*: Interaction: DF=2, F=0.6996, p=0.507. Time: DF=1, F=0.2923, p=0.594. Feeding: DF=2, F=3.511, p=0.0467. *IL-4*: Interaction: DF=2, F=4.319, p=0.025. Time: DF=1, F=3.185, p=0.087. Feeding: DF=2, F=8.173, p=0.002. *IL-12(p70)*: Interaction: DF=2, F=1.733, p=0.199. Time: DF=1, F=1.958, p=0.1751. Feeding: DF=2, F=3.55, p=0.0453.

While basal cytokine levels did not predict susceptibility to a subsequent stimulation, serum cytokines - IL-6 in particular (Damas et al., 1992) - post LPS injection were expected to be indicative of mortality at later time points. Despite significant induction of cytokines following LPS stimulation compared to PBS control injected subjects, the cytokines screened 6 h post challenge were however not predictive of mortality as no significant differences were detectable between the distinct groups (Figure 4.2.3.3). Although IL-1β and IL-12 (p70) displayed some elevation following ZT0 compared to ZT12 stimulation, this increase was not statistically significant and did not recapitulate the changes in mortality that were seen between day- and night-time fed animals challenged at ZT12, arguing against the possibility to use these cytokines as predictors of susceptibility to LPS.

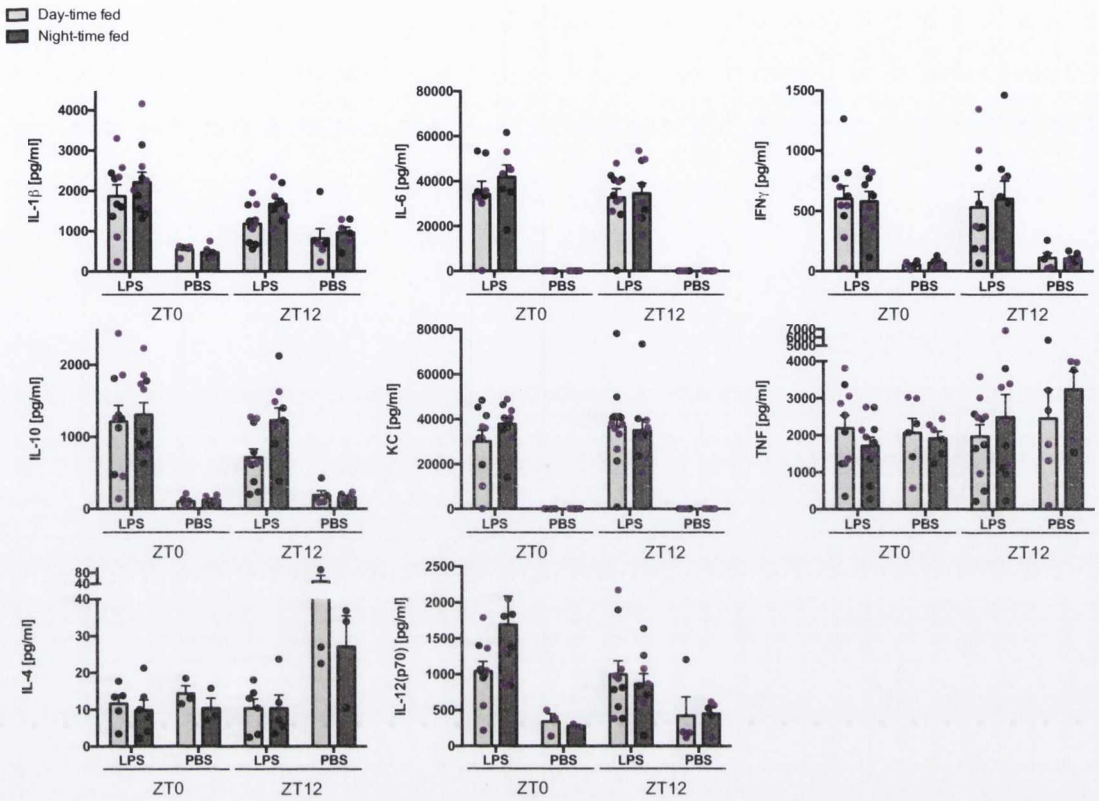


Figure 4.2.3.3: Serum cytokines are uniformly induced in day- and night-time fed animals, and are unaffected by the feeding regimen following LPS stimulation.

Selected serum cytokines 6h post i.p. stimulation with 20 mg/kg LPS or PBS at ZT0 or ZT12. Food availability was restricted to the day- or the night-phase, as indicated, for 5 days prior to LPS stimulation. Black circles indicate continuation of TRF, while purple circles symbolize ad libitum feeding post stimulation. Significance using two way ANOVA and Sidak's multiple comparisons test. *IL-1β*: Interaction: DF=3, F=0.6293, p=0.5991. ZT&Stimulation: DF=3, F=19.68, p<0.0001. Feeding: DF=1, F=2.141, p=0.1489. *IL-6*: Interaction: DF=3, F=0.3842, p=0.7648. ZT&Stimulation: DF=3, F=49.45, p<0.0001. Feeding: DF=1, F=0.6676, p=0.4177. *IFNγ*: Interaction: DF=3, F=0.08269, p=0.9692. ZT&Stimulation: DF=3, F=13.47, p<0.0001. Feeding: DF=1, F=0.03149, p=0.8598. *IL-10*: Interaction: DF=3, F=1.295, p=0.2852. ZT&Stimulation: DF=3, F=24.7, p.<0.0001 Feeding: DF=1, F=1.651, p=0.2041. *KC*: Interaction: DF=3, F=0.5871, p=0.6259. ZT&Stimulation: DF=3, F=40.61, p<0.0001. Feeding: DF=1, F=0.2351, p=0.6296. *TNF*: Interaction: DF=3, F=0.882, p=0.4558. ZT&Stimulation: DF=3, F=1.421, p=0.2457. Feeding: DF=1, F=0.2726, p=0.6036. *IL-4*: Interaction: DF=3, F=0.8616, p=0.4734. ZT&Stimulation: DF=3, F=6.883, p=0.0015. Feeding: DF=1, F=1.926, p=0.177. *IL-12(p70)*: Interaction: DF=3, F=1.101, p=0.3583. ZT&Stimulation: DF=3, F=5.318, p=0.0031. Feeding: DF=1, F=0.2869, p=0.5947.

Tissue, and liver damage in particular, is another feature commonly seen in models of sepsis. Therefore, mouse serum samples that were collected 6 h post LPS stimulation were examined for liver enzymes that get liberated upon liver damage (Figure 4.2.3.4). At this time point, liver enzymes were not elevated in LPS, compared to PBS control injected animals and levels appeared independent of solar time and feeding schedule as they were similar between ZT0 and ZT12 stimulated as well as day- and night-time fed animals, indicating that, at least 6 h post LPS injection, liver enzymes could not be used as predictors of mortality.

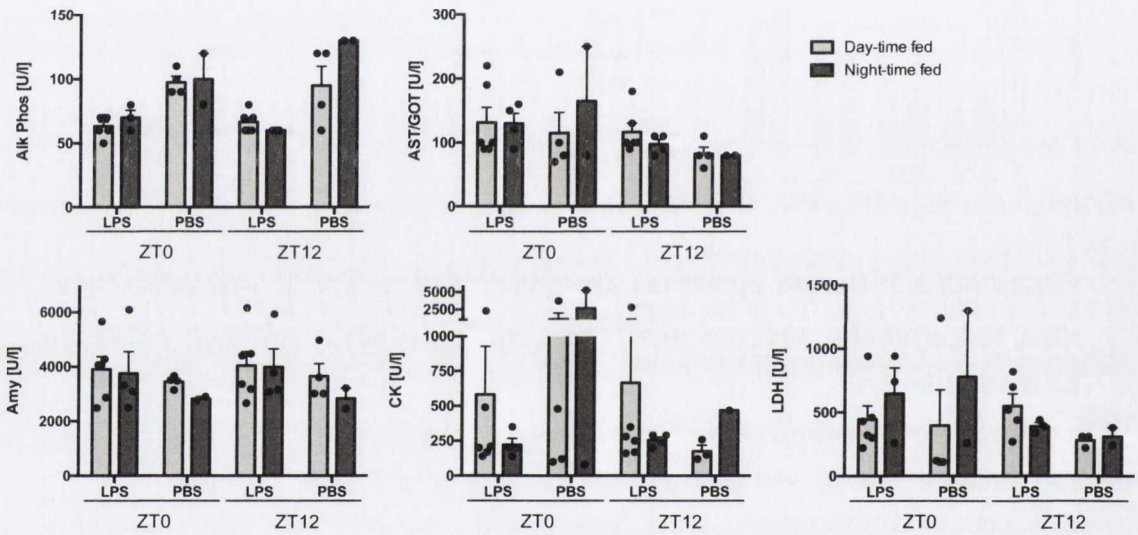


Figure 4.2.3.4: Liver damage as measured by liberation of liver enzymes into the circulation is absent early after LPS stimulation.

Liver enzyme measurement in the serum of TRF mice 6h post i.p. stimulation at ZT0 or ZT12 with 20 mg/kg LPS or PBS control on day 5. Alk Phos: Alkaline Phosphatase; AST: Aspartate Transaminase; Amy: Amylase; CK: Creatine Kinase; LDH: Lactate Dehydrogenase. Statistical analysis using two way ANOVA and Sidak's multiple comparisons test. *Alk Phos*: Interaction: DF=3, F=2.282, p=0.1073. ZT&Stimulation: DF=3, F=17.55, p<0.0001. Feeding: DF=1, F=2.666, p=0.1167. *AST/GOT*: Interaction: DF=3, F=0.6195, p=0.6092. ZT&Stimulation: DF=3, F=1.825, p=0.1696. Feeding: DF=1, F=0.1347, p=0.7169. *Amy*: Interaction: DF=3, F=0.1815, p=0.9079. ZT&Stimulation: DF=3, F=1.019, p=0.4016. Feeding: DF=1, F=0.9158, p=0.3481. *CK*: Interaction: DF=3, F=0.926, p=0.4447. ZT&Stimulation: DF=3, F=2.167, p=0.1207. Feeding: DF=1, F=0.2794, p=0.6024. *LDH*: Interaction: DF=3, F=0.7659, p=0.5265. ZT&Stimulation: DF=3, F=0.763, p=0.528. Feeding: DF=1, F=0.7001, p=0.4127.

4.2.4 The immune modulators β-Hydroxybutyrate and corticosterone are diurnal and food regulated, however do not appear indicative of mortality

Corticosteroids are widely known to be immune regulatory and to oscillate throughout the day. It was possible that altering the feeding schedule might influence morbidity in response to LPS by altering circadian fluctuations in corticosterone, the major corticosteroid found in mouse serum.

Corticosterone levels in the serum of TRF animals housed under normal (Figure 4.2.4.1 A) and constant light conditions (Figure 4.2.4.1 B), displayed a food dependency under both conditions (Figure 4.2.4.1). In line with the literature describing ad libitum fed animals, corticosterone levels in night-time fed animals under regular light cycles were high at the transition to the active- and feeding- phase at ZT12, and low at the beginning of the inactive phase at ZT0. These patterns were inversed in day-time fed animals, arguing for food dependent abundance of this hormone in the circulation (Figure 4.2.4.1 A). This was further substantiated under constant light conditions, where ad libitum access to food ablated diurnal oscillations in corticosterone levels, while food restriction recapitulated findings under regular light schedules with inversed patterns in day-time compared to nigh-time fed animals (Figure 4.2.4.1 B).

However, peak levels of the hormone - which is generally viewed to exert anti-inflammatory functions - coincided with increased susceptibility to LPS, making a contribution of Corticosterones to the observed shifts in susceptibility to LPS unlikely. Following an LPS insult, Corticosterones were further equally induced irrespective of feeding and stimulation time, resulting in similar levels following a ZT0 and ZT12 LPS stimulation within a feeding group as well as between night- and day-time fed animals, substantiating that this hormone had no involvement in the regulation of rhythmic susceptibility to high dose LPS stimulations (Figure 4.2.4.1 C).

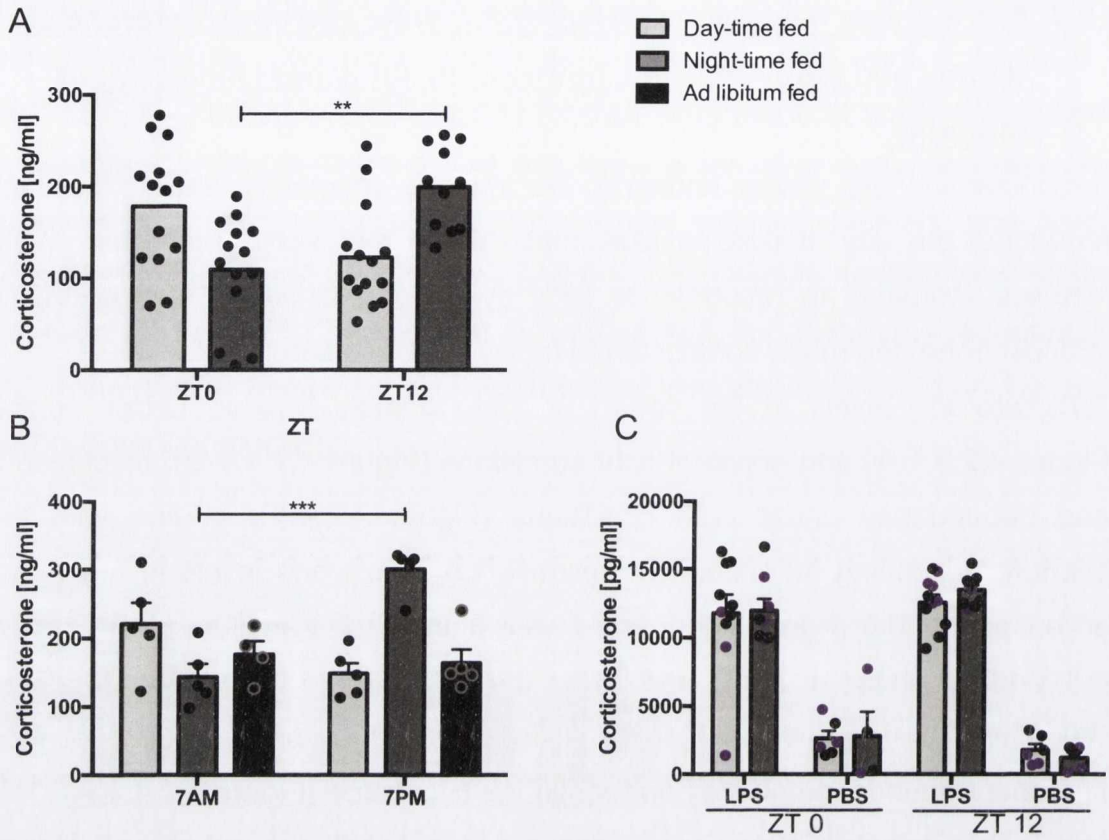


Figure 4.2.4.1: Basal Corticosterone levels are a function of food and are highly induced following LPS stimulation irrespective of feeding time.

Corticosterone abundance in mouse serum. **A)** Basal levels at ZT0 and ZT12 in TRF mice on day 5. **B)** Basal levels in mice that were housed in constant light for 7 days before food availability was restricted according to the time of light or dark phases predating the introduction of constant light. On day 5 of TRF under constant light conditions, serum samples were collected at 7AM or 7 PM, the transition times of food availability. **C)** Corticosterone levels in day 5 TRF mice 6 h post i.p. stimulation with 20 mg/kg LPS at ZT0 or ZT12. Black circles indicate continuation of TRF, while purple circles symbolize ad libitum feeding post stimulation. Statistical analysis using two way ANOVA and Sidak's multiple comparisons test (indicated in graph with *p<0.05, **p<0.01, ***p<0.001, ****p<0.0001). **A)** Interaction: DF=1, F=20.36, p<0.0001. ZT: DF=1, F=1.159, p=0.2869. Feeding: DF=1, F=0.05739, p=0.8117. **B)** Interaction: DF=2, F=17.01, p<0.0001. Time: DF=1, F=2.003, p=0.1704. Feeding: DF=2, F=3.332, p=0.0536. **C)** Interaction: DF=3, F=0.2413, p=0.8671. ZT&Stimulation: DF=3, F=83.86, p<0.0001. Feeding: DF=1, F=0.07212, p=0.7893.

Although corticosterone did not present to be useful as a predictor of mortality, other components in the circulation had the potential to be more appropriate. Studies to unravel more details about the metabolic regulation of the immune response have found an inhibitory effect of the starvation induced metabolite β-Hydroxybutyrate on the NLRP3 inflammasome (Youm et al., 2015), and as diurnal susceptibility to LPS was regulated by feeding cycles, involvement of β-Hydroxybutyrate in this phenotype was possible.

Similarly to corticosterones, basal levels of this metabolite were found to be food-regulated in animals that received time restricted access to food for 5 days, while being housed under normal light conditions. β-Hydroxybutyrate levels peaked at the transition into the feeding phase (ZT12 in night-time, and ZT0 in day-time fed animals) and displayed nadirs at the beginning of food deprivation (ZT0 in night-time and ZT12 in day-time fed animals) (Figure 4.2.4.2 A). Similar patterns were found under constant light conditions in TRF animals while ad libitum fed mice presented constitutive levels at 7AM and 7PM, suggesting a food rather than light dependency in the abundance of this metabolite in the circulation (Figure 4.2.4.2 B). Following LPS stimulation β-Hydroxybutyrate levels were strongly induced and the patterns that were seen at basal levels were maintained. 6 h following LPS administration at the transition into the feeding phase thereby resulted in peak levels, while challenge at the end of the feeding phase presented nadirs levels of β-Hydroxybutyrate (Figure 4.2.4.2 C). However, as peak levels of this inflammation-inhibitory metabolite pre and post LPS stimulation coincided with increased mortality, it is unlikely to play a role in regulating the changes in mortality we observed.

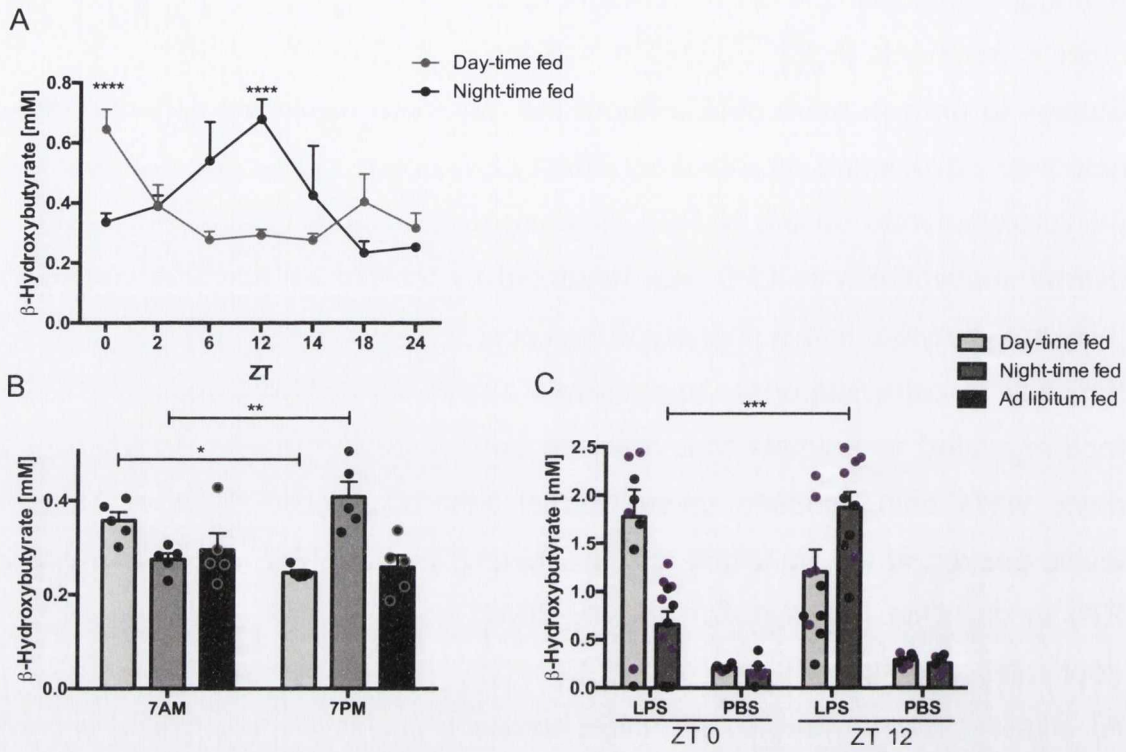


Figure 4.2.4.2: β-Hydroxybutyrate patterns are sustained upon LPS stimulation with increased overall levels.

β-Hydroxybutyrate levels in mouse serum. **A)** Oscillations of basal levels throughout the day in TRF mice on day 5. **B)** Basal levels in mice that were housed in constant light for 7 days before food availability was restricted according to the time of light or dark phases predating the introduction of constant light. On day 5 of TRF under constant light conditions, serum samples were collected at 7AM or 7PM, the times when food availability was inverted. **C)** β-Hydroxybutyrate levels in day 5 TRF mice 6 h post i.p. stimulation with 20 mg/kg LPS at ZT0 or ZT12. Black circles indicate continuation of TRF, while purple circles symbolize ad libitum feeding post stimulation. Statistical analysis using two way ANOVA and Sidak's multiple comparisons test (indicated in graph with *p<0.05, **p<0.01, ***p<0.001, ****p<0.0001). **A)** Interaction: DF=6, F=10.31, p<0.0001. ZT: DF=6, F=2.704, p=0.0215. Feeding: DF=1, F=0.7170, p=0.4004. **B)** Interaction: DF=2, F=13.79, p=0.0001. ZT: DF=1, F=0.04864, p=0.8273. Feeding: DF=2, F=3.698, p=0.0398. **C)** Interaction: DF=3, F=9.296, p<0.0001. ZT&Stimulation: DF=3, F=22.1, p<0.0001. Feeding: DF=1, F=0.8258, p=0.3671.

4.2.5 Time restricted feeding alters oscillations in metabolism

NanoString data from TRF mice revealed that the expression of metabolic genes was regulated by the feeding schedule to varying degrees in different organs. Food entrainment of the liver, a critical metabolic organ, suggested that the animal's overall metabolism may also be a function of feeding time.

Using metabolic cages, metabolic parameters such as oxygen consumption and carbon dioxide production, as well as activity and food intake could be measured. To better understand the metabolic state of animals that were subject to day- or night-time feeding schedules, at the time of stimulation, the respiratory exchange ration was additionally recorded. Very robustly, the RER decreased to levels indicative of fatty acid oxidation at times of food deprivation (RER=0.7), and upon reintroduction of the diet, metabolism immediately switched to glycolysis and RER levels increased (RER=1) (Figure 4.2.5.1, Figure 4.2.5.2). Already 24 h post introduction of the feeding regimen the RER strictly followed food availability and these oscillations were fully sustained for 12 days (Figure 4.2.5.2).



Figure 4.2.5.1: RER is a function of food availability, independent of the time of the day.

RER as a function of time over a 5 day period in night-time (blue), day-time (red), and ad libitum (green) fed animals. Light schedule as indicated by black (dark phase) or white (light phase) bars in 5 independent experiments.

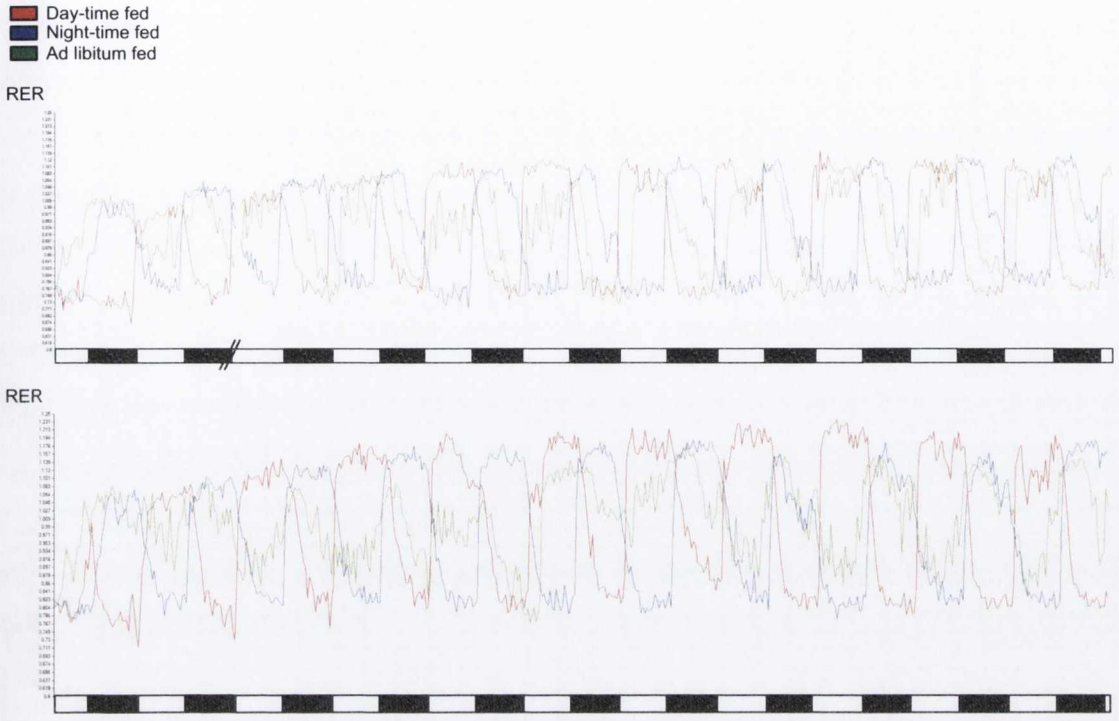


Figure 4.2.5.2: Food dependent oscillations in RER are sustained over the course of two weeks.

RER as a function of time over two weeks in night-time (blue), day-time (red), and ad libitum (green) fed animals. Light schedule as indicated by black (dark phase) or white (light phase) bars in two independent experiments.

As the animals' metabolisms appeared to oscillate in parallel to food availability, we next tested their behaviour in regard to activity as measured by movement along the cage axis.

Restriction of food to specific times of the day has previously been shown to induce food anticipatory behaviour, an increase in activity starting approximately an hour before food should become available according to the preceding days (Mistlberger, 1994). This spike in activity was neither found in day- nor night-time fed animals as measured by x-beam breaks, and activity patterns appeared similar between the feeding groups and were maintained for 12 days on TRF. It is possible that this unexpected result may be a consequence of the properties of a metabolic cage, and experiments are underway to measure activity in form of wheel running in regular cages, which appears to be the standard method in food anticipatory behaviour studies. It should further be pointed out that the original study by Damiola, where food restriction to either the day or the night was first shown to shift the liver clock by 12 h, also did not find food anticipatory behaviour (Damiola et al., 2000). This may indicate that food restriction to 12 h may cause a state of desynchrony rather than actual entrainment of FEO. This bout of activity described as food anticipatory behaviour will however most likely not affect the outcome following an inflammatory insult. Therefore this aspect will not be a major focus of following studies and the question regarding the causality of an absent food anticipatory behaviour would remain.

Nevertheless, similar activity patters in day- and night-time fed animals that were recorded as part of this study, suggested that activity patterns in general will most likely not contribute to phenotypical differences that are seen between day-and night-time fed animals.

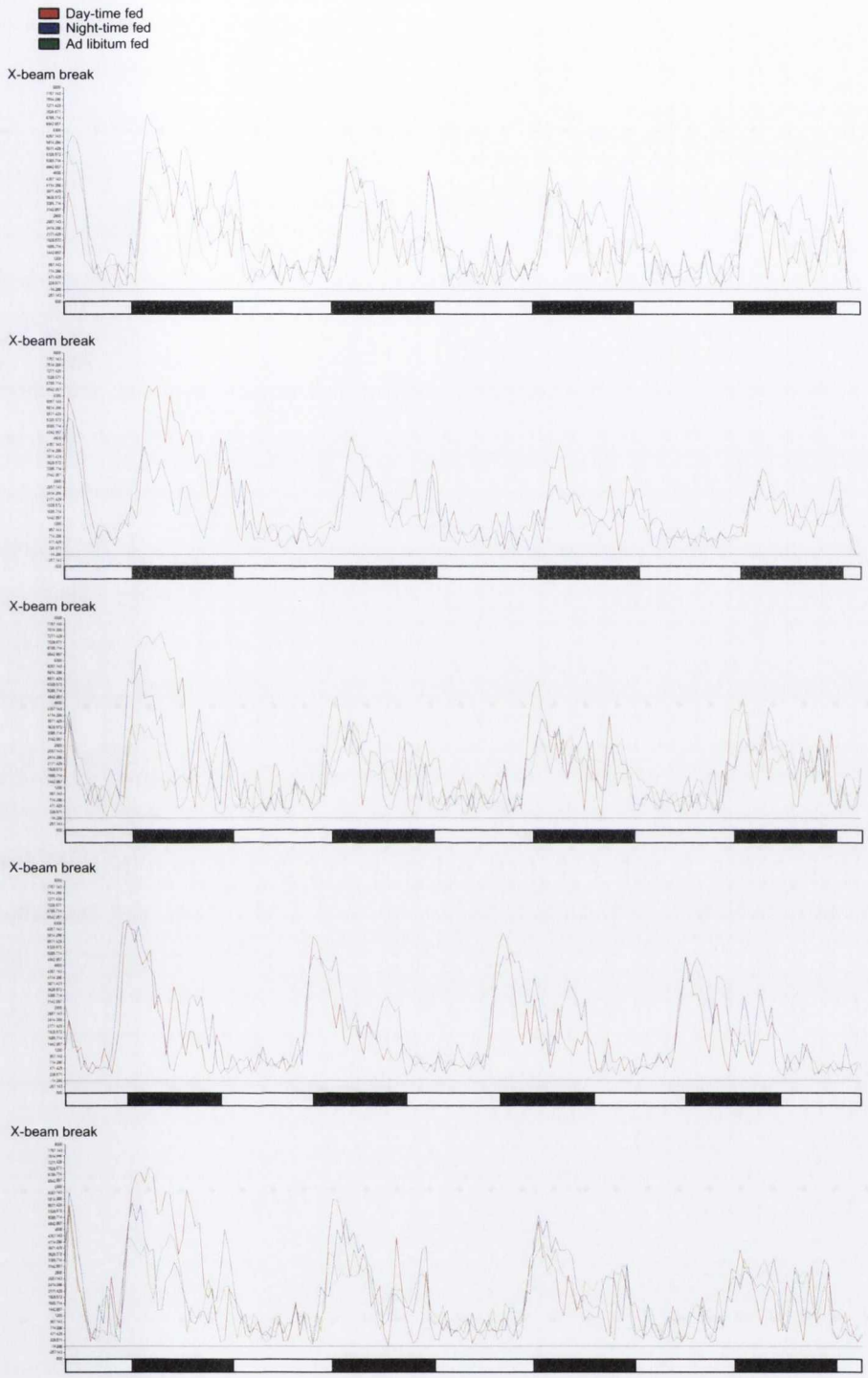


Figure 4.2.5.3: Activity is regulated by the light, not the feeding schedule.
X-beam breaks as a measurement of activity in metabolic cages are displayed as a function of time over 5 days in night-time (blue), day-time (red), or ad libitum (green) fed animals. Light schedule as indicated by black (dark phase) or white (light phase) bars in 5 independent experiments.

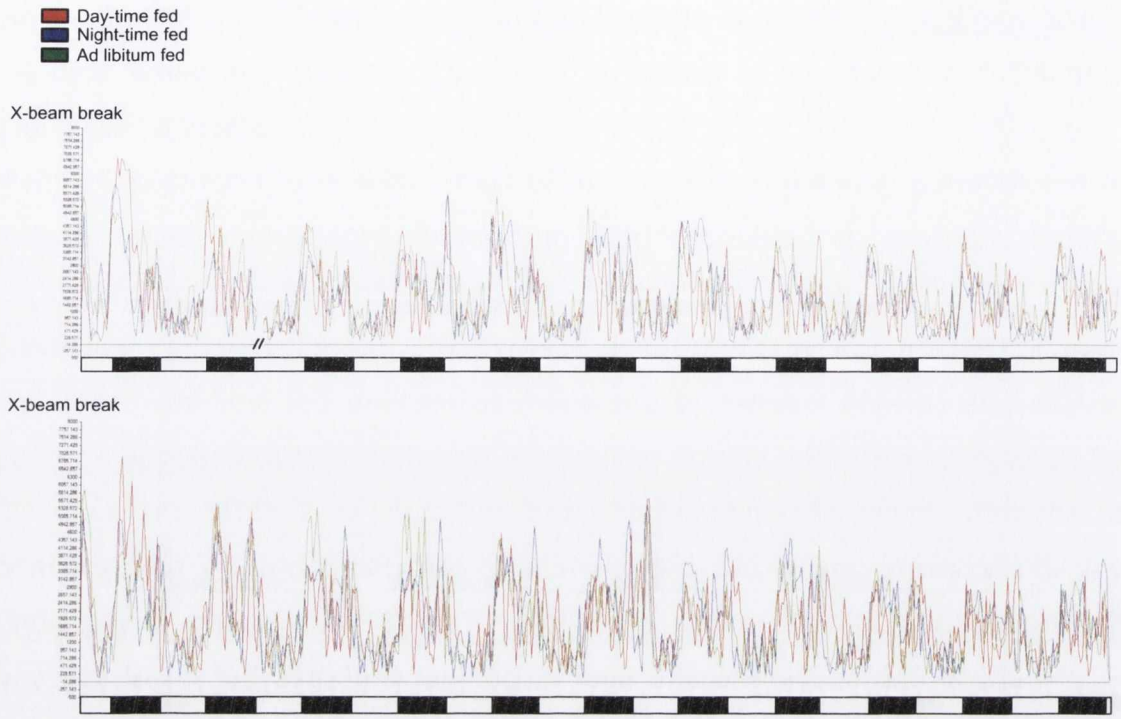


Figure 4.2.5.4: Light dependency of activity patterns is sustained over the course of two weeks.

X-beam breaks as a measurement of activity in metabolic cages are displayed as a function of time over two weeks in night-time (blue), day-time (red), and ad libitum (green) fed animals. Light schedule as indicated by black (dark phase) or white (light phase) bars in two independent experiments.

Because RER presented to be food dependent, while activity patterns appeared food independent, it was of interest to record the amount and timing of food intake in these individuals. As the feeding container opened and closed automatically, this was simultaneously used to control for proper food restriction in the CLAMS. While the feeding curves of day- and night-time fed animals verified functionality of the system, the patterns were slightly different between the distinct TRF groups (Figure 4.2.5.5, Figure 4.2.5.6). Night-time fed animals showed an almost constitutive level of food intake during times of food availability, while day-time fed animals displayed short spikes of food intake where greater amounts were consumed at once. This was not only seen in the beginning of TRF, but was sustain for 12 days (Figure 4.2.5.6). Although this discrepancy had the potential to impact other characteristics of day-time fed animals, it should be noted, that feeding time in these animals was not entirely restricted to a small time window, but was still occurring over the complete 12 h of food availability. Despite differences in the details of food ingestion patterns in day- and night-time fed animals, these discrepancies are unlikely to affect diurnal susceptibility significantly. However, this result should not be neglected and should be reviewed when a more compete picture of the mechanism underlying diurnal susceptibility is present in order to reassess a possible impact.

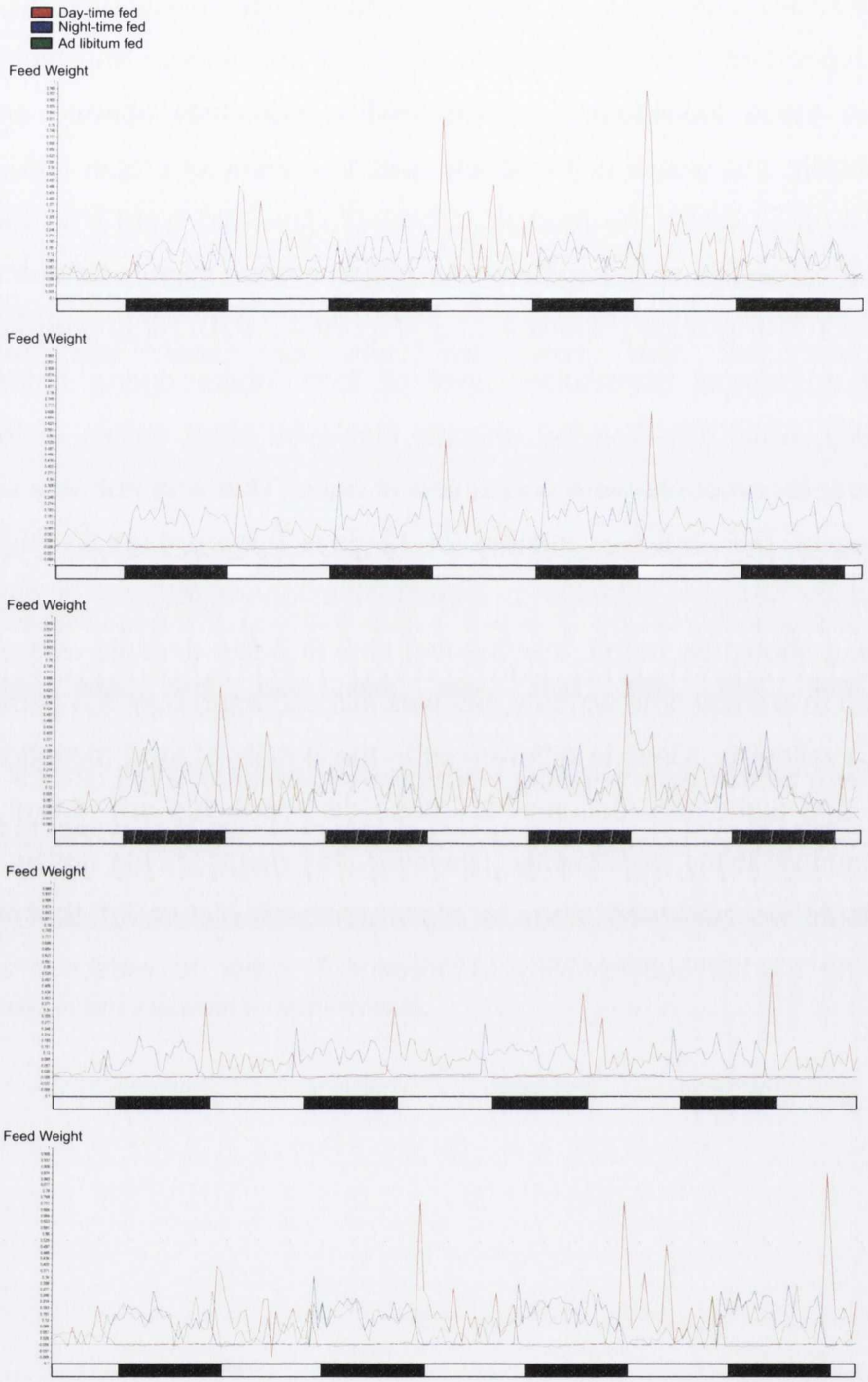


Figure 4.2.5.5: Dietary intake patterns in day and night-time fed animals are comparable.

Amount of ingested food as a function of time over a 5 day period in night-time (blue), day-time (red), and ad libitum (green) fed animals. Light schedule as indicated by black (dark phase) or white (light phase) bars in 5 independent experiments.

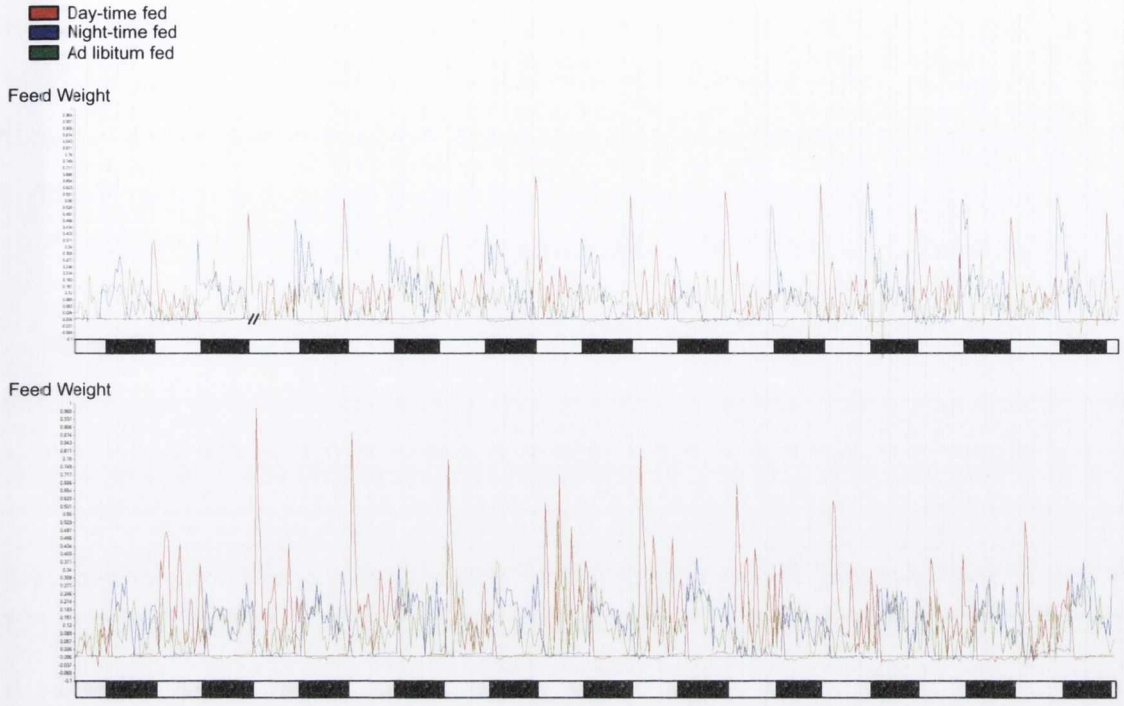


Figure 4.2.5.6: Feeding patterns adjust rapidly and are sustained over the course of two weeks.

Amount of ingested food as a function of time over two weeks in night-time (blue), day-time (red), and ad libitum (green) fed animals. Light schedule as indicated by black (dark phase) or white (light phase) bars in two independent experiments.

Having examined levels of food intake, RER and activity as functions of time over the course of several days on time restricted feeding, overall changes in these parameters were yet to be analysed. To illustrate average values while maintaining information about feeding-phase specific effects, average values from the feeding and food deprivation phases for each subject were graphed. While overall food intake, RER and activity were similar between groups (Figure 4.2.5.7), feeding phase specific differences in RER and food ingestion, as well as feeding phase independent activity patterns that were previously seen in the timed graphs, were also recapitulated.

Body composition, which provides information about the lean and the fat mass as well as total weight of an animal, was also comparable in day- and night-time fed animal (Figure 4.2.5.8). Lean mass in day- compared to night-time fed

animals appeared marginally decreased, but considering the variation in the data, more data points would be necessary to substantiate a genuine effect. Comparable average values across feeding groups did nevertheless provide evidence that differences in the susceptibility to LPS injection were not merely a matter of malnutrition or lethargy and that this system was well controlled.

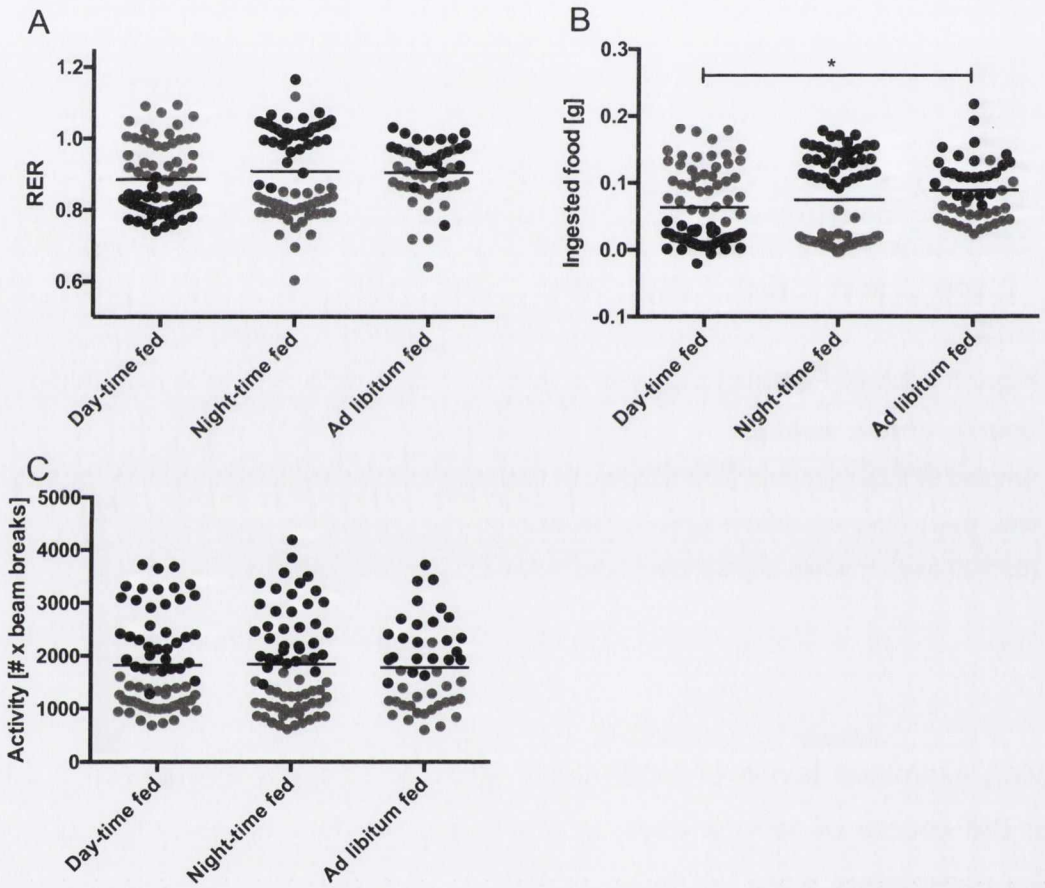


Figure 4.2.5.7: Overall metabolism and activity is unaffected by TRF.

Respiratory exchange ration (RER) **(A)**, amount of food intake **(B)** and activity as measured by X-beam breaks **(C)** in mice that were housed in the CLAMS facility for 5-12 days. Each data point represents the average value from all measurements during the light (grey) or the dark (black) phase for each individual subject. Significance using Kruskal Wallis ANOVA and Dunn's post-hoc multiple comparison (indicated in the graph with *p<0.05). **A)** p=0.2398. **B)** p=0.0278. **C)** p=0.9934.

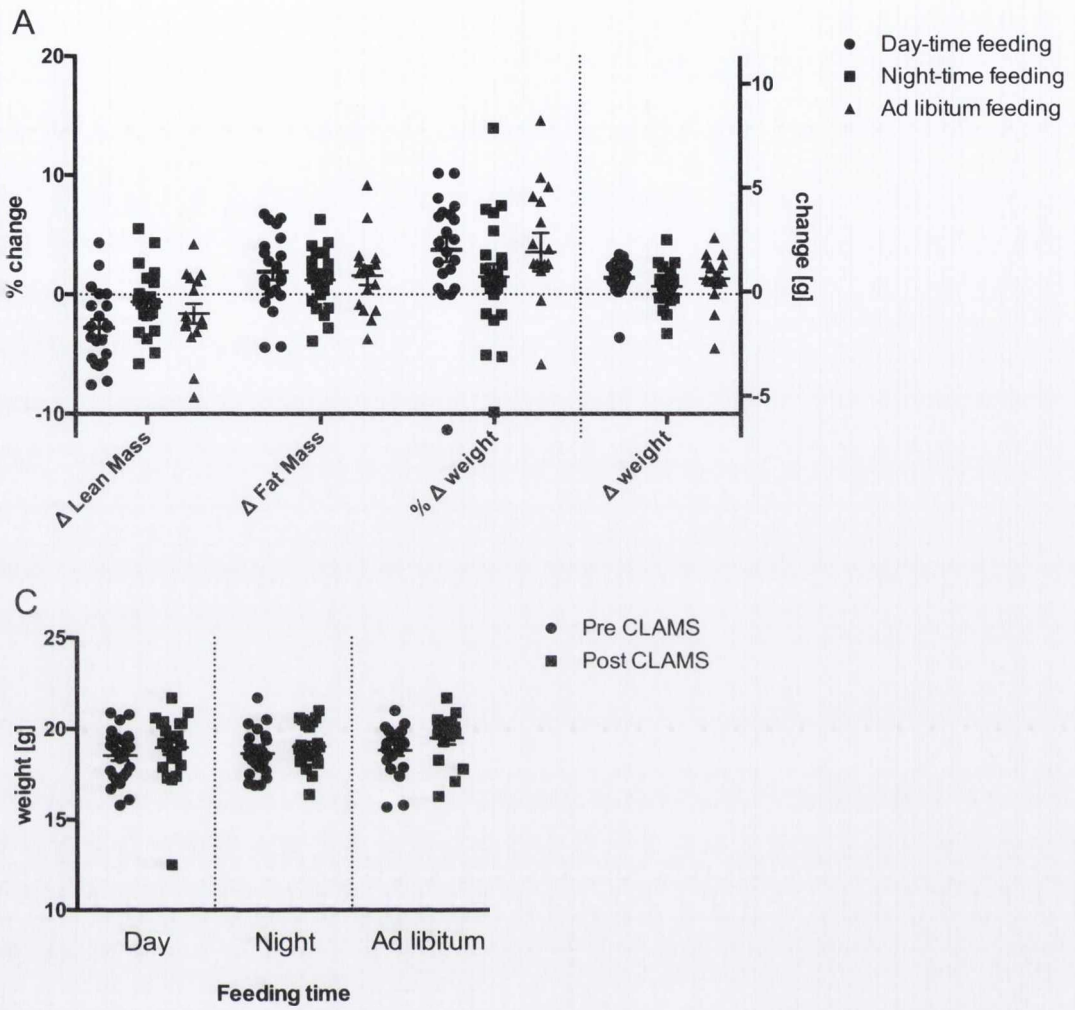


Figure 4.2.5.8: Body composition is unaffected by time restricted feeding up to two weeks.

A) Absolute and percental weight change, and percental change in lean and fat mass as defined by EchoMRI in animals before and after housing in the CLAMS facility for 5-12 days. Statistical analysis using Kruskal Wallis ANOVA and Dunn's post-hoc multiple comparison. ΔLean Mass: p=0.0522. ΔFat Mass: p=0.7755. %Δweight: p=0.0915. Δweight: p=0.107. **B**) Absolute body weight pre and post CLAMS housing. Statistical analysis using two way ANOVA and Sidak's multiple comparisons test. Interaction: DF=2, F=0.1136, p=0.8927. ZT: DF=1, F=3.959, p=0.0488. Feeding: DF=2, F=0.8998, p=0.4092.

4.3 Discussion and Future Studies

Rhythmic susceptibility to LPS has been described in multiple studies (Halberg et al., 1960, Curtis et al., 2015). The present work investigated whether this phenotype was a function of the widely studied solar cycle or rhythmic food ingestion, which normally correlates with light entrained activity and sleep-wake cycles. By artificial restriction of food intake to the day-time - the phase nocturnal animals such as mice are usually inactive -, or the natural feeding time at night, the effect of light and food signals could be experimentally dissociated.

In a study where this food restriction was maintained for 5 consecutive days in a 12 h light and 12 h darkness environment, subsequent LPS stimulation indicated a critical role for food in regulating diurnal mortality. Recapitulating work from others (Halberg et al., 1960, Curtis et al., 2015, Scheiermann et al., 2012), night-time fed control mice were highly susceptible following LPS stimulation at ZT12 compared to ZT0. By contrast, day-time fed animals were highly protected at ZT12 (significantly exceeding the protection of night-time fed animals at ZT0) and displayed lethality rates following ZT0 stimulation similar to the night-time fed animals.

Mortality in day- and night-time fed animals did consequently not occur as a mirror image (Figure 4.2.1.1). The reason for this effect is not entirely clear, but it could be reasoned that this may be due to light entrainment of other peripheral tissues and discrepancies between clock states of different compartments within the animal. To examine this possibility, several models may be deployed. One of them is the model of constant light, which has been shown by some labs to result in desynchronized clock oscillation in various tissues (Hamaguchi et al., 2015) and arrhythmic behaviour in some animals (Polidarova et al., 2011). Reintroduction of food cycles corresponding to the light cycle predating constant light (similar to the TRF model) should then solely synchronize food entrained oscillators, while light entrained clocks remain desynchronized. Following stimulation with LPS at the transition times of food availability and deprivation (corresponding to ZT0 and ZT12 predating constant light) mortality rates could be recorded. In a hypothetical model where a food

entrained oscillator drives rhythmicity in mortality while other peripheral tissues are subordinate, this experimental setting should result in mirror image mortality curves between the groups that received food during the corresponding night- or day-time predating the introduction of constant light.

Validity of this model was supported by analysis of clock states in an assortment of tissues at times of prospective LPS stimulation as part of this study (Figure 4.2.2.9, Figure 4.2.2.11). As such, the liver was indeed synchronized to the feeding schedule, while adipose tissue, spleen, peritoneal macrophages and SCN did not show the expected peak and troughs. However, only two time-points were investigated and considering the often seen prolonged phase in locomotor activity of mice in constant light, the phase of peripheral clock genes may have similarly been phase shifted. Peak and trough times may therefore be simply present at times deviating from sampling time. Constant light further acts as a strong stressor (Abilio et al., 1999), potentially affecting study relevant pathways in a clock independent manner. This, and the variability of phenotypes regarding behaviour as discussed in the introduction (1.5.2 Entrainment) may make this experimental setup less adequate and the interpretation of results difficult. The use of genetic models may therefore be preferable and will be exploited before experimental setups that include constant light.

To quantitate the inflammatory response and test abundance of markers that were shown to correlate with mortality in the setting of sepsis, serum samples from mice injected with a lethal dose of LPS were collected 6 h post stimulation. Cytokines are generally good indicators of the intensity of an immune response, and IL-6 in particular correlates with mortality in humans (Damas et al., 1992). A range of cytokines were significantly induced in LPS, compared to PBS control injected animals; however none of the screened cytokines appeared to be present at different levels in the serum of ZT0 or ZT12 LPS stimulated day- or night-time fed animals 6 h post stimulation (Figure 4.2.3.3). It should be noted that cytokine response and mortality not always appear to correlate. While Marpegan argued a correlation in the setting of LD conditions, their mortality data in DD, which showed a lack of time dependency (Marpegan et al., 2009),

is in contrast to findings by other groups that describe sustained rhythmicity in the intensity of cytokine production upon stimulation in constant darkness (Gibbs et al., 2012, Adams et al., 2013). While greater immune responses often correlate with increased activation, which often directly correlates with the intensity of cytokines released, cytokines themselves may also not be critical in conveying sepsis-induced mortality. Nonetheless, earlier sampling time at two hours post stimulation may be more informative as disease is still rapidly progressing, compared to later time points where disease is almost fully established.

Besides cytokines, liberation of liver enzymes due to liver damage is an indication for disease progression. Considering the time line of mortality and the use of high doses of LPS, mortality in this model may however be a result of severe cytokine storm, rather than excessive liver damage and secondary infections due to immune paralysis, which are often seen in patients in later stages of sepsis (Bone, 1996). This was supported by the absence of increased liver enzyme liberation in LPS vs. PBS control injected animals (Figure 4.2.3.4). Access to a marker which could predict mortality, would greatly facilitate mechanistic studies, as it would allow euthanasia of subjects for tissue harvest while retaining the information of anticipated mortality. Thus far, no reliable marker indicative of mortality in this model could however be found.

A hormone that is often associated with rhythmic susceptibility to infection is cortisol, the predominant glucocorticoid in humans. Cortisol and corticosterone, which is the dominating glucocorticoid in rodents, are known for their rhythmicity and generally anti-inflammatory properties (Petrovsky et al., 1998). Although corticosterones basally peaked at times of increased susceptibility and therefore were unlikely to convey a poised state that would determine mortality, it was of interest to examine food dependency and abundance post LPS stimulation. Diverging to some extent from previous publications that reported an only transient shift in corticosterone levels following TRF (Le Minh et al., 2001), this study identified strong food dependency under regular and constant light conditions (Figure 4.2.4.1). Following LPS stimulation, however,

corticosterone levels were increased to similar levels in all feeding groups, arguing against a possible regulatory role for corticosterones in this model.
A metabolite that sparked interest due to its newly identified role as a NLRP3 inflammasome inhibitor is β-Hydroxybutyrate (Youm et al., 2015). Congruent with this ketone body to be starvation induced, serum abundance increased steadily during the food deprivation phase in the TRF model, and decreased upon food reintroduction. As expected, this was light independent, based on inversed patterns in day- compared to night-time fed animals. Upon LPS stimulation, β-Hydroxybutyrate levels were significantly increased, while the pattern between feeding groups remained similar to the pre-LPS states. Therefore, the anti-inflammatory metabolite β-Hydroxybutyrate positively correlated with mortality (Figure 4.2.4.2 C), arguing against involvement of this ketone body in the regulation of susceptibility to LPS stimulation.

Besides investigating a possible predictor of mortality at baseline or post stimulation, the properties of animals that were subject to TRF were examined more in detail. As diurnal mortality appeared to be food dependent, a central role for metabolism and food entrained clocks was standing to reason. Studies in the CLAMS facility provided a metabolic profile that was consistent across experiments and displayed almost immediate adaptation of whole animal metabolism to food availability, while activity remained similar between the different feeding groups. This very rapid adaptation questions the involvement of the molecular clock rather than a direct food effect in the regulation of metabolism. To investigate this further, a similar CLAMS experiment would be needed in which the animals would be food deprived for an additional 24 h at the end of the study. Sustained fluctuations in RER would then be indicative of clock regulation, while permanently low RER levels would suggest a direct food effect. A similar setting will be used to address the possibility that diurnal mortality could be regulated by food directly, and not by a genuine food entrained oscillator. Considering that the mortality patterns in day- and night-time fed animals did not appear as mirror images, and that stimulation of these mice at ZT0 resulted in similar mortality rates, a direct food effect seems unlikely.

Of note in the here presented work is the absence of food anticipatory behaviour. While this observation is in concordance with Damiola's original study of liver entrainment in conditions were food was also made available for 12 h each day (Damiola et al., 2000), this generally challenges the notion of conventional food entrainment in this experimental setup. Typically, restriction of food to short intervals outside the normal feeding time causes increased wheel running activity, starting around an hour before anticipated food availability (Richter, 1922, Bolles and De Lorge, 1062). The here presented results may therefore be more adequately interpreted as a result of internal desynchrony rather than food entrainment.

Considering that internal desynchrony can be induced by shift work, which pertains roughly 20% of the western work force and has been associated in a multitude of studies to be detrimental to health (Wyse et al., 2017, Esquirol et al., 2011, Pietroiusti et al., 2006, Hedstrom et al., 2011), investigating immune activity in the setting of internal desynchrony is indeed of particular interest. We understand very little about entrainment throughout the circadian network within an organism and what range of misalignment may be tolerable or promote disease (Roenneberg and Merrow, 2016). It is further unclear which outputs are regulated entirely by the SCN or are cell autonomous and if they necessarily follow the same entrainment pattern if they are involved in related pathways. As an example, cytokine production by *ex vivo* stimulated PBMCs upon shift work simulation displays a ~5h phase advance in its oscillation, while the abundance of immune cells in human blood is sustained (Cuesta et al., 2016), underscoring differential regulation of distinct mechanism within the immune system. Having a clearer understanding of how certain environmental settings affect distinct peripheral clocks, and how endogenous zeitgeber, or 'eigen-zeitgeber', consolidate these oscillations will significantly facilitate comprehension as well as strategies of how to prevent and treat diseases that are promoted by, or are direct consequences of internal misalignment (Roenneberg and Merrow, 2016).

Alterations in the sleeping pattern of TRF mice should also be considered in the interpretation of results. Sleep certainly greatly influences the immune system (Bryant et al., 2004), and sleep itself is strongly modulated following immune

activation (Toth and Krueger, 1988). Sleep deprivation, as well as more subtle changes in sleep architecture may therefore consolidate some of the phenotypes that were described in this study. Mice - unlike humans - sleep in short bouts. This may allow mice to sustain their activity patterns, as was seen in the CLAMS data, while still feeding during their rest phase. More sophisticated studies would be necessary to investigate possible differences in sleep properties in detail, and will most likely exceed the scope of this work.

If indeed the molecular clock is critical to convey diurnal susceptibility to LPS, the tissue responsible would then be expected to be similarly coupled to the feeding schedule. Of the screened tissues, only the clock in the liver displayed food entrainment, and given that the liver is an important metabolic and inflammatory organ, a central role in regulating diurnal mortality appears plausible. Using a hepatocyte specific *Bmal1* knockout mouse this will be examined under the standard TRF settings that were used within this study. If the liver clock is critical in this phenotype, mortality in these conditional knockouts is expected to display independence of any feeding regimens.

Finally, several pathways underlying diurnal susceptibility may be hypothesised. Food may directly modulate abundance of metabolites in the system, or entrain tissues to produce a mediator, which can influence the ability of immune cells to respond to an inflammogenic insult. This would imply that the ability of immune cells to mount a response - and therefore the resistance of animals - is regulated. Cytokine production is generally an appropriate readout for changes in the intensity of an immune response, and in the here presented studies, no significant differences in selected cytokines were present 6 h post stimulation with LPS. This may have been caused by an unsuitable sample collection time, which will be addressed by future sampling at two, instead of six hours following LPS injection. There is however the possibility that not resistance - the ability of the organism to clear an infection - but tolerance, such as tissue sensitivity is modulated in a diurnal fashion (Wang et al., 2016, Schneider and Ayres, 2008).

This study provides evidence that diurnal susceptibility to LPS stimulation is influenced by feeding cycles; and while the mechanism is under on-going investigation, a central role for the liver, a tissue that is strongly controlled by the feeding regimen and has previously been implemented in the inflammatory response, is anticipated. Figure 4.2.5.1 graphically outlines our findings and indicates the regulation of selected outputs by the light and the feeding cycle as well as the correlation of feeding time and clock state to LPS induced susceptibility at different times of the day. The tools to investigate this further and bring this project to completion are in place and while the presented data focused primarily on the description of the animals at times of prospective stimulation, subsequent studies will concentrate on inflammatory response pathways following LPS injection.

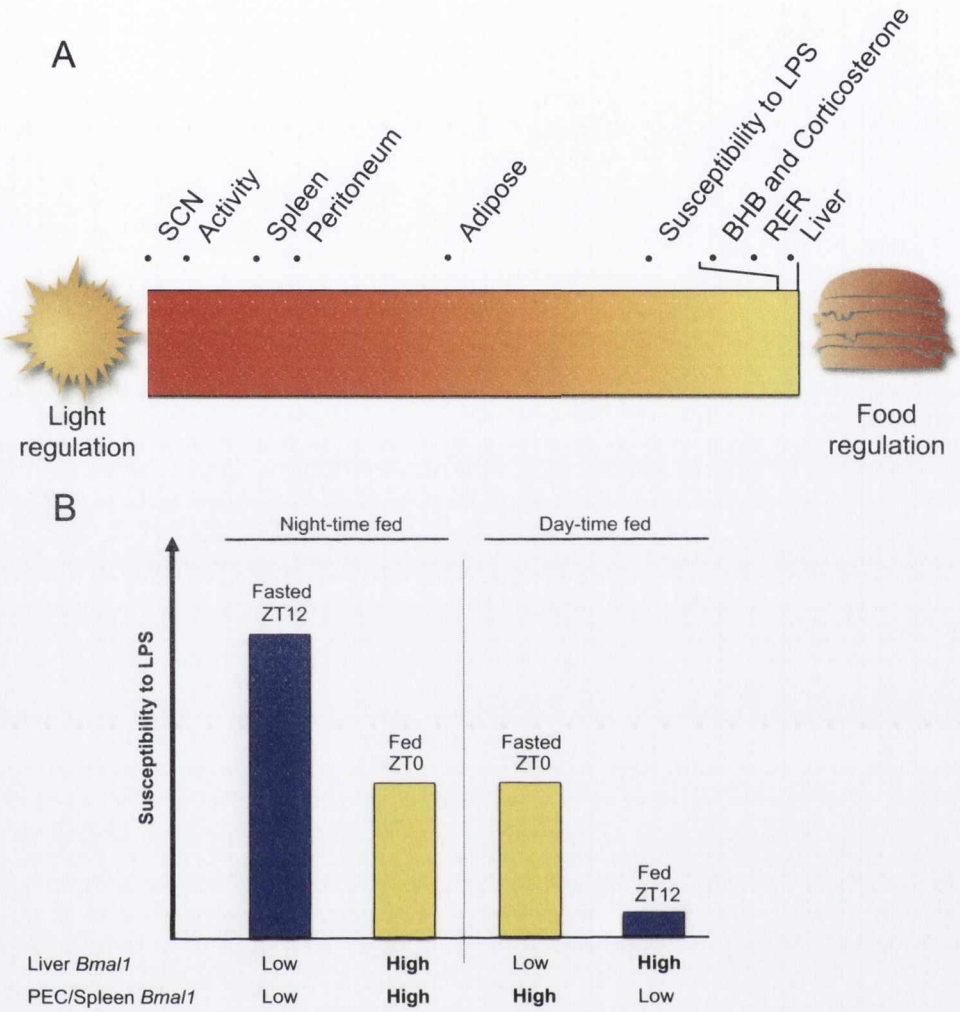


Figure 4.2.5.1: Graphic summary: Food entrainment determines oscillations in the susceptibility to LPS.

A) Feeding time determines the clock phase in the liver, but not in other peripheral organs or the brain. Activity also continues to follow the solar cycle, while respiratory exchange ratio (RER), Corticosterone and β-Hydroxybutyrate (BHB) levels are controlled by the feeding cycle. **B)** Susceptibility to LPS stimulation is strongly, but not solely regulated by the feeding schedule. Feeding state and *Bmal1* levels in liver and spleen/peritoneum at times of stimulation as indicated.

5 Conclusions and Future Work

The interest in chrono-immunological research is continuously growing as the consequences of clock disruption on health become more apparent. Shift work, artificial light at night, and intermittent meals can cause clock dysregulation and are not uncommon features of a lifestyle that is normality to a substantial part of the population. In recent years tremendous progress has been made in understanding more about the interplay of the circadian and the immune system, but a coherent mechanism to explain circadian immunity, or specific immune pathologies has not yet evolved. In the course of the present study, two aspects of chrono-immunology have been examined. The first was to test whether particle uptake in tissue resident macrophages is circadian and how this rhythmicity is regulated. The second aspect addressed a much more fundamental question about the origin of rhythmic susceptibility. What is the critical zeitgeber, and is there a clock in a specific tissue that is central to rhythmic mortality?

In an *in vivo* model we were able to demonstrate that uptake of heat inactivated *S. aureus* is not diurnal and is not regulated by *Bmal1* in a clock oscillation dependent or independent manner. It therefore appears unlikely that uptake of particles may influence the experimental outcome of the inflammatory response to bacterial infection *in vivo*. Treatment of severe infections and sepsis is a balancing act of immune suppression to hinder further tissue damage and jeopardizing subsequent organ failure and possibly death, and promoting clearance of the infection as well as cell corpses from apoptotic cells. This study argues that phagocytic properties are sustained independently of the molecular clock, and together with work from others that define a critical role for the clock in tailoring the pro-inflammatory immune response (Gibbs et al., 2012, Curtis et al., 2015), this presents a strategy to target the clock to inhibit pro-inflammatory action, while maintaining beneficial phagocytic properties.

Surprisingly, *ex vivo* results in preliminary studies presented very different results with increased phagocytic capacity of an assortment of bacterial and inert particles at ZT12. Despite great effort to understand the mechanism, the

pathway explaining this observation could not be identified. The reason of this apparent discrepancy of *in vivo* and *ex vivo* data is unclear, but a number of hypotheses are plausible. Extraction of peritoneal macrophages at different times of the day may pre-activate the cells differently at ZT0 and ZT12, causing a poised state that deviates from the natural properties within the animal. Alternatively, pathways that involve opsonization of particles with serum constituents or pathways that involve humoral, neuronal or other systemic (e.g. temperature) or paracrine signalling cues, may be absent *ex vivo*, but could mask rhythmic uptake *in vivo*. It is challenging to exactly recapitulate *ex vivo* settings in an *in vivo* environment, and it is possible that divergence in experimental properties such as MOS may have resulted in discrepancies. However, the use of multiple time points and concentrations of the bacterial particles argued against this possibility.

As the goal of this study was to investigate the role of the circadian system in the regulation of immunity to better understand *in vivo* observations, this was not further examined. However, it clearly raises a concern about validity of *ex vivo* models. We and others, have shown that cytokine response is indeed affected by (even if not entirely depend on) phagocytic ingestion. Artificially introduced changes in uptake may therefore cause divergence in cytokine and possibly other inflammatory responses that could not be found *in vivo*.

In the second part of this work, we provide evidence that susceptibility to LPS is a function of the feeding, and not as generally assumed, the solar cycle. While the phenotypical observation was robust and could be verified in a total of three independent experiments (one of which was entirely blinded), the mechanism could not be unravelled in the course of this study, but is under on-going, thorough investigation. We were however able to characterize the study subjects in various experimental settings at times where subsequent studies will induce an inflammatory response to further investigate the cascade that is induced. These baseline studies indicated a central role for the liver, as it was the only screened tissue that fully entrained to newly introduced feeding regimens. Genuine circadian rhythmicity, by definition is sustained under free running conditions, an environment that is deprived of the entraining zeitgeber.

Therefore, sustained oscillations in the expression of clock genes in the liver, as well as susceptibility to LPS will be examined in mice that were food restricted for 24 h following a 5 day TRF regimen, to distinguish circadian rhythmicity from direct food control. It will also be of interest to test the animals' metabolism in this setting. RER strictly followed the feeding regimen under TRF, but the fact that RER appeared to adjust almost instantaneously raised the question of this being a genuine circadian effect. A 24 h starvation period will therefore not only define genuine circadian rhythmicity, but may further narrow down the pathways possibly involved in controlling rhythmic susceptibility.

Many studies that investigate food entrainable oscillators utilize a feeding regiment that allows access to food for usually 4 h in the early light phase (Stokkan et al., 2001). However, the first report about food regulation of peripheral tissues, similar to the herein presented data, restricted feeding to the entire light phase (12 h) (Damiola et al., 2000). In concordance with this study, we also did not observe food anticipatory behaviour when mice were monitored in metabolic cages. Although there is no data available that investigates the requirements for animals to display food anticipatory behaviour, it has been reported that elongation of food availability from 4 to 8 h reduced the intensity of food anticipatory behaviour (Stokkan et al., 2001). The maximal time of food availability that still results in food anticipatory locomotor activity would therefore be of interest as it could possibly indicate the nature of this phenotype. Stress certainly contributes to food anticipatory behaviour in the 4 h schedule (Stokkan et al., 2001), however, it's contribution during prolonged food availability is not entirely clear.

Nevertheless, similar to the situation in shift workers, the model of 12 h food restriction during the light phase appears to cause internal desynchrony - the misalignment of elements of the circadian program - making this work applicable to human pathologies. Shift work is associated with a multitude of metabolic and inflammatory diseases as well as cancer (Roenneberg et al., 2012, Wyse et al., 2017, Papagiannakopoulos et al., 2016, Pietroiusti et al., 2006, Angersbach et al., 1980), and considering that 20% of the western workforce are involved in work schedules that deviate from the regular day-centric weekday regime, scientific advances understanding the molecular basis

for some of these pathologies to develop new strategies to prevent and improve disease in those affected, is of great interest. It is known that composition and timing of food intake is greatly affected in night-shift workers (Waterhouse et al., 2003), the contribution of feeding time in the development of disease beyond obesity and type-2 diabetes (Pan et al., 2011, Arble et al., 2009) has however not been investigated. Paralleling reports of sustained caloric intake in night-shift workers, we observed similar food ingestion in day- and night-time fed animals, further underpinning the relevance for the model we deployed in investigating human pathologies observed in shift workers.

An observation that is puzzling, is the fact the day-time restricted mice generally appeared more protected than the night-time fed animals. Considering the data gathered so far, feeding regimens maintained overall metabolic parameters and generally displayed mirror image inversions in oscillations. A noticeable discrepancy between day- and night-time fed animals presented in regard to clock function in peripheral organs excluding the liver. There, clock oscillations were not inverted upon food restriction to the inactive phase. This discrepancy between tissues may therefore be causing an attenuation of the immune system, and thereby an overall protection of day-time fed animals. This may be further investigated in the setting of constant light, where these organs may be rendered arrhythmic. It will also be of great interest to examine the role of rhythmic leukocyte trafficking and myeloid clock ablation. Both of these have been reported to be causal for diurnal susceptibility in the setting of sepsis (Curtis et al., 2015, Scheiermann et al., 2012).
Using Bmal1 floxed LyzMCre mice, in which the clock was dysfunctional in the myeloid compartment, hyper-responsiveness compared to WT mice was previously shown and a central role for peritoneal macrophages was argued (Curtis et al., 2015). In those studies, a small, yet consistent decrease in mortality at ZT0 could still be found, suggesting that there may be diurnal entrainment of mortality independent of clock genes in the myeloid compartment. There is no doubt that myeloid clock ablation renders mice hyper-sensitive, however, mortality studies that result in average mortalities similar to what is seen in the WT, by the use of decreased LPS doses, will determine

whether oscillations in mortality are indeed diminished in this model or may have been undetectable due to rapidly induced lethality in ZT0 and ZT12 stimulated Bmal1 floxed LyzMCre mice.

Our findings argue for a central role of the liver, and it is possible that some of the effects seen in macrophage-specific clock knockout mice may be due to liver resident macrophages (Kupffer cells). Identification of the tissue central to diurnal susceptibility to LPS stimulation will be critical for mechanistic investigations. Although it is likely that this regulation will be very complex and certainly not entirely explainable considering only one tissue, the use of multiple genetic and environmental models will give us the opportunity to test a range of possibilities to pinpoint the cornerstones of food regulated susceptibility to LPS stimulation. Testing the role of the liver and the genuine circadian nature of rhythmic susceptibility to LPS will thereby be priorities.

Using hepatocyte specific deletion of *Bmal1*, we will first investigate the role of the liver in susceptibility in food entrained animals. While multiple outcomes are thinkable, only two shall be discussed here. Mortalities that are similar in the day- and night time fed animals as well as throughout the day (ZT0 vs. ZT12) in these animal, would argue for a central role of the liver clock and contradict the possibility of a clock independent, direct food effect. Survival curves that match the data presented in the course of this study (Figure 4.2.1.1) despite a non-functional clock in hepatocytes, would in contrast suggest a direct food effect or possibly the involvement of a food regulated oscillator other than the liver. To provide evidence for a genuine circadian effect, rather than a clock gene independent or dependent food effect, we will further implement a 24 h food deprivation period in TRF mice prior to LPS stimulation. Susceptibility patterns that recapitulate the observations made under regular TRF conditions will indicate a genuine circadian effect, as rhythmicity is sustained when the entraining zeitgeber is deprived. To examine the role of other peripheral organs in diurnal susceptibility to LPS stimulation, we plan to deploy several models.

As mentioned earlier, macophages have an important role in sensing of innate stimuli, and have the potential to affect mortality following LPS stimulation. In order to test their contribution to the observed phenotype, we will use conditionals knockouts that mediate *Bmal1* deletion under the LyzM promotor,

resulting in a myeloid targeted knockout animal. Similar susceptibility patterns following LPS stimulation between day- and night-time fed animals, would then argue for a central role for macrophages in the initially observed mortality patterns (Figure 4.2.1.1), which did not present mirror images between feeding groups.

A model that allows desynchronization of the body clocks to reintroduce a zeitgeber that will only synchronize food regulated clocks would generally be of interest to broadly investigate the nature or LPS induced mortality patterns that do not entirely present as mirror images. Constant light in some experimental setting appears do convey this state of desynchronization (Hamaguchi et al., 2015), and time restricted feeding could be used to induce synchronization in food dependent tissues (Polidarova et al., 2011). In this model, susceptibility patterns following LPS challenge which display mirror images between mice that were fed anti-phasic, would suggest that food independent oscillators may influence the patterns that were observed in the initial LPS susceptibility studies (which did not present mirror images between feeding groups). While this appears to be an attractive model, it comes with extensive limitations. As such, arrthmicity is not exclusively seen in mice housed in constant light, and phenotypes with prolonged period lengths or a 'split' behaviour have been reported (Pittendrigh, 1960). Although some studies argue arrthymicity in peripheral tissues independently of the individual behaviour of the subjects, interpretation is aggravated when locomotor activity varies significantly between subjects. More extensive data, including locomotor activity and detailed time courses of clock gene expression in peripheral tissues, would be necessary to lay the groundwork for constant light studies, verifying actual desynchronization and re-synchronization of food regulated oscillators upon introduction of restricted feeding. Consideration should also be given to constant light as a strong stressor (Abilio et al., 1999), potentially affecting study relevant pathways in a clock independent manner. Finally, this, and the variability of phenotypes regarding behaviour may make this experimental setup less adequate and the interpretation of results difficult. The use of genetic models may therefore be preferable and will be exploited before experimental setups that include constant light.

Another interesting aspect that is worth testing in the setting of TRF, is the recruitment of leukocytes to sites of inflammation and the circulation. Inflammatory response is significantly restrained when trafficking of leukocytes is attenuated by deletion of *Icam1* for instance, a rhythmic gene that appears to be critical in diurnal mobilization of cells. As leukocyte abundance in the circulation has been associated with nutritional intake (Calder, 1998) and diurnal susceptibility to LPS (Scheiermann et al., 2012), a role for immune cell trafficking is therefore possible.

It should be noted that while outcomes that appear most likely according to the preliminary data were outlined here, many other results are thinkable and could change subsequent experimental setups to get a better understanding of the molecular mechanism.

The immune systems' complexity is astonishing and it will take tremendous effort to fully understand how it is regulated by the circadian system. The present study provides a piece of the puzzle and uncovered a previously unknown level of immune-regulation by restricted feeding. It fills me with excitement to be part of this new lead of food regulation in rhythmic susceptibility to infection, which certainly has the potential to change the way we think about and investigate observations in the field of chrono-immunology.

6 References

ABILIO, V. C., FREITAS, F. M., DOLNIKOFF, M. S., CASTRUCCI, A. M. & FRUSSA-FILHO, R. 1999. Effects of continuous exposure to light on behavioral dopaminergic supersensitivity. *Biol Psychiatry,* 45, 1622-9.

ABRAHAM, D., DALLMANN, R., STEINLECHNER, S., ALBRECHT, U., EICHELE, G. & OSTER, H. 2006. Restoration of circadian rhythmicity in circadian clock-deficient mice in constant light. *J Biol Rhythms,* 21, 169-76.

ADAMS, D. 1996. How the immune system works and why it causes autoimmune diseases. *Immunology Today,* 17, 300-302.

ADAMS, K. L., CASTANON-CERVANTES, O., EVANS, J. A. & DAVIDSON, A. J. 2013. Environmental circadian disruption elevates the IL-6 response to lipopolysaccharide in blood. *Journal of Biological Rhythms,* 28, 272-277.

ADEREM, A. 2003. Phagocytosis and the inflammatory response. *J Infect Dis,* 187 Suppl 2, S340-5.

ALAMILI, M., BENDTZEN, K., LYKKESFELDT, J., ROSENBERG, J. & GOGENUR, I. 2014. Pronounced inflammatory response to endotoxaemia during nighttime: a randomised cross-over trial. *PLoS One,* 9, e87413.

ANDERS, H. J., ROMAGNANI, P. & MANTOVANI, A. 2014. Pathomechanisms: homeostatic chemokines in health, tissue regeneration, and progressive diseases. *Trends Mol Med,* 20, 154-65.

ANDERSON, S. T., COMMINS, S., MOYNAGH, P. N. & COOGAN, A. N. 2015. Lipopolysaccharide-induced sepsis induces long-lasting affective changes in the mouse. *Brain Behav Immun,* 43, 98-109.

ANDREWS, T. & SULLIVAN, K. E. 2003. Infections in patients with inherited defects in phagocytic function. *Clin Microbiol Rev,* 16, 597-621.

ANGERSBACH, D., KNAUTH, P., LOSKANT, H., KARVONEN, M. J., UNDEUTSCH, K. & RUTENFRANZ, J. 1980. A retrospective cohort study comparing complaints and diseases in day and shift workers. *Int Arch Occup Environ Health,* 45, 127-40.

ARANDJELOVIC, S. & RAVICHANDRAN, K. S. 2015. Phagocytosis of apoptotic cells in homeostasis. *Nat Immunol,* 16, 907-17.

ARBLE, D. M., BASS, J., LAPOSKY, A. D., VITATERNA, M. H. & TUREK, F. W. 2009. Circadian timing of food intake contributes to weight gain. *Obesity (Silver Spring),* 17, 2100-2.

ARJONA, A. & SARKAR, D. K. 2005. Circadian oscillations of clock genes, cytolytic factors, and cytokines in rat NK cells. *The Journal of Immunology,* 174, 7618-7624.

ASCHOFF, J. 1951. Die 24-Stunden-Periodik der Maus unter konstanten Umgebungsbedingungen. *Naturwissenschaften,* 38, 506-507.

ASCHOFF, J. 1960. Exogenous and endogenous components in circadian rhythms. *Cold Spring Harbor symposia on quantitative biology,* 25, 11-28.

ASCHOFF, J., FATRANSKA, M., GIEDKE, H., DOERR, P., STAMM, D. & WISSER, H. 1971. Human Circadian Rhythms in Continuous Darkness: Entrainment by Social Cues. *Science,* 171, 213-215.

AUSTYN, J. M. & GORDON, S. 1981. F4/80, a monoclonal antibody directed specifically against the mouse macrophage. *European journal of immunology,* 11, 805-815.

AZEVEDO, E., OLIVEIRA, L. T., CASTRO LIMA, A. K., TERRA, R., DUTRA, P. M. & SALERNO, V. P. 2012. Interactions between Leishmania braziliensis and Macrophages Are Dependent on the Cytoskeleton and Myosin Va. *J Parasitol Res,* 2012, 275436.

AZZI, A., DALLMANN, R., CASSERLY, A., REHRAUER, H., PATRIGNANI, A., MAIER, B., KRAMER, A. & BROWN, S. A. 2014. Circadian behavior is light-reprogrammed by plastic DNA methylation. *Nature neuroscience,* 17, 377-382.

BALSALOBRE, A., BROWN, S. A., MARCACCI, L., TRONCHE, F., KELLENDONK, C., REICHARDT, H. M., SCHUTZ, G. & SCHIBLER, U. 2000. Resetting of circadian time in peripheral tissues by glucocorticoid signaling. *Science,* 289, 2344-7.

BALSALOBRE, A., DAMIOLA, F. & SCHIBLER, U. 1998. A serum shock induces circadian gene expression in mammalian tissue culture cells. *Cell,* 93, 929-37.

BARKHAUSEN, T., TSCHERNIG, T., ROSENSTIEL, P., VAN GRIENSVEN, M., VONBERG, R. P., DORSCH, M., MUELLER-HEINE, A., CHALARIS, A., SCHELLER, J., ROSE-JOHN, S., SEEGERT, D., KRETTEK, C. & WAETZIG, G. H. 2011. Selective blockade of interleukin-6 trans-signaling improves survival in a murine polymicrobial sepsis model. *Crit Care Med,* 39, 1407-13.

BASS, J. & LAZAR, M. A. 2016. Circadian time signatures of fitness and disease. *Science,* 354, 994-999.

BAUMANN, A., GONNENWEIN, S., BISCHOFF, S. C., SHERMAN, H., CHAPNIK, N., FROY, O. & LORENTZ, A. 2013. The circadian clock is functional in eosinophils and mast cells. *Immunology,* 140, 465-74.

BELLET, M. M., DERIU, E., LIU, J. Z., GRIMALDI, B., BLASCHITZ, C., ZELLER, M., EDWARDS, R. A., SAHAR, S., DANDEKAR, S., BALDI, P., GEORGE, M. D., RAFFATELLU, M. & SASSONE-CORSI, P. 2013. Circadian clock regulates the host response to Salmonella. *Proceedings of the National Academy of Sciences of the United States of America,* 110, 9897-9902.

BODE, J. G., ALBRECHT, U., HAUSSINGER, D., HEINRICH, P. C. & SCHAPER, F. 2012. Hepatic acute phase proteins--regulation by IL-6- and IL-1-type cytokines involving STAT3 and its crosstalk with NF-kappaB-dependent signaling. *Eur J Cell Biol,* 91, 496-505.

BOIVIN, D. B., JAMES, F. O., WU, A., CHO-PARK, P. F., XIONG, H. & SUN, Z. S. 2003. Circadian clock genes oscillate in human peripheral blood mononuclear cells. *Blood,* 102, 4143-5.

BOLLES, R. C. & DE LORGE, J. 1062. The rat's adjustment to a-diurnal feeding cycles. *Journal of Comparative and Physiological Psychology,* 55, 760-762.

BONE, R. C. 1996. Sir Isaac Newton, sepsis, SIRS, and CARS. *Crit Care Med,* 24, 1125-8.

BORASCHI, D. & TAGLIABUE, A. 2013. The interleukin-1 receptor family. *Seminars in immunology,* 25, 394-407.

BORBÉLY, A. A., DAAN, S., WIRZ-JUSTICE, A. & DEBOER, T. 2016. The two-process model of sleep regulation: a reappraisal. *Journal of sleep research,* 25, 131-143.

BORN, J., LANGE, T., HANSEN, K., MÖLLE, M. & FEHM, H. L. 1997. Effects of sleep and circadian rhythm on human circulating immune cells. *The Journal of Immunology,* 158, 4454-4464.

BORN, J., RASCH, B. & GAIS, S. 2006. Sleep to remember. *The Neuroscientist : a review journal bringing neurobiology, neurology and psychiatry,* 12, 410-424.

BROWN, R., PANG, G., HUSBAND, A. J. & KING, M. G. 1989. Suppression of immunity to influenza virus infection in the respiratory tract following sleep disturbance. *Regional Immunology,* 2, 321-325.

BROWN, S. A., ZUMBRUNN, G., FLEURY-OLELA, F. & PREITNER, N. 2002a. Rhythms of mammalian body temperature can sustain peripheral circadian clocks. *Current Biology,* 12, 1574-1583.

BROWN, S. A., ZUMBRUNN, G., FLEURY-OLELA, F., PREITNER, N. & SCHIBLER, U. 2002b. Rhythms of mammalian body temperature can sustain peripheral circadian clocks. *Current biology : CB,* 12, 1574-1583.

BRYANT, P. A., TRINDER, J. & CURTIS, N. 2004. Sick and tired: Does sleep have a vital role in the immune system? *Nature reviews. Immunology,* 4, 457-467.

BULTINCK, J., BROUCKAERT, P. & CAUWELS, A. 2006. The in vivo contribution of hematopoietic cells to systemic TNF and IL-6 production during endotoxemia. *Cytokine,* 36, 160-6.

BUNGER, M. K., WILSBACHER, L. D., MORAN, S. M., CLENDENIN, C., RADCLIFFE, L. A., HOGENESCH, J. B., SIMON, M. C., TAKAHASHI, J. S. & BRADFIELD, C. A. 2000. Mop3 is an essential component of the master circadian pacemaker in mammals. *Cell,* 103, 1009-1017.

CALDER, P. C. 1998. Dietary fatty acids and the immune system. *Nutr Rev,* 56, S70-83.

CAMACHO, F., CILIO, M., GUO, Y., VIRSHUP, D. M., PATEL, K., KHORKOVA, O., STYREN, S., MORSE, B., YAO, Z. & KEESLER, G. A. 2001. Human casein kinase Idelta phosphorylation of human circadian clock proteins period 1 and 2. *FEBS letters,* 489, 159-165.

CAMERON-SMITH, D., BURKE, L. M., ANGUS, D. J., TUNSTALL, R. J., COX, G. R., BONEN, A., HAWLEY, J. A. & HARGREAVES, M. 2003. A short-term, high-fat diet up-regulates lipid metabolism and gene expression in human skeletal muscle. *The American journal of clinical nutrition,* 77, 313-318.

CAPRA, J. D. & KINDT, T. J. 1974. Antibody diversity: Can more than one gene encode each variable region? *Immunogenetics,* 1, 417-427.

CARRILLO-VICO, A. & LARDONE, P. J. 2013. Melatonin: buffering the immune system. *International Journal of Molecular Sciences,* 14, 8636-8683.

CERRETTI, D., KOZLOSKY, C., MOSLEY, B., NELSON, N., VAN NESS, K., DRUCK, T., CANNIZZARO, L., HUEBNER, K. & BLACK, R. 1992. Molecular Cloning of the Interleukin-1b Converting Enzyme. 256, 97-100.

CHAWLA, A., NGUYEN, K. D. & GOH, S. Y. P. 2011. Macrophage-mediated inflammation in metabolic disease. *Nature Reviews Immunology,* 11, 738-749.

CHEN, R., SEO, D. O., BELL, E., VON GALL, C. & LEE, C. 2008. Strong resetting of the mammalian clock by constant light followed by constant darkness. *J Neurosci,* 28, 11839-47.

CLARKE, L. L., JESSOP, D. S., HUNT, L. P., STRAUB, R. H., PERRY, M. G. & KIRWAN, J. R. 2011. Alleviation of morning joint stiffness by low-dose prednisone in rheumatoid arthritis is associated with circadian changes in IL-6 and cortisol. *International Journal of Clinical Rheumatology,* 6, 241-249.

COHEN, J. 2002. The immunopathogenesis of sepsis. *Nature,* 420, 885-91.

CRISPE, I. N. 2009. The liver as a lymphoid organ. *Annu Rev Immunol,* 27, 147-63.

CUESTA, M., BOUDREAU, P., DUBEAU-LARAMEE, G., CERMAKIAN, N. & BOIVIN, D. B. 2016. Simulated Night Shift Disrupts Circadian Rhythms of Immune Functions in Humans. *J Immunol,* 196, 2466-75.

CURTIS, A. M., FAGUNDES, C. T., YANG, G., PALSSON-MCDERMOTT, E. M., WOCHAL, P., MCGETTRICK, A. F., FOLEY, N. H., EARLY, J. O., CHEN, L., ZHANG, H., XUE, C., GEIGER, S. S., HOKAMP, K., REILLY, M. P., COOGAN, A. N., VIGORITO, E., FITZGERALD, G. A. & O'NEILL, L. A. 2015. Circadian control of innate immunity in macrophages by miR-155 targeting Bmal1. *Proc Natl Acad Sci U S A,* 112, 7231-6.

DAMAS, P., LEDOUX, D., NYS, M., VRINDTS, Y., DE GROOTE, D., FRANCHIMONT, P. & LAMY, M. 1992. Cytokine serum level during severe sepsis in human IL-6 as a marker of severity. *Annals of surgery,* 215, 356-362.

DAMIOLA, F., LE MINH, N., PREITNER, N., KORNMANN, B., FLEURY-OLELA, F. & SCHIBLER, U. 2000. Restricted feeding uncouples circadian oscillators in peripheral tissues from the central pacemaker in the suprachiasmatic nucleus. *Genes & Development,* 14, 2950-2961.

DAVIES, L. C. & TAYLOR, P. R. 2015. Tissue-resident macrophages: then and now. *Immunology,* 144, 541-548.

DE WAAL MALEFYT, R. 1991. Interleukin 10 (IL-10) and viral IL-10 strongly reduce antigen-specific human T cell proliferation by diminishing the antigen-presenting capacity of monocytes via downregulation of class II major histocompatibility complex expression. *Journal of Experimental Medicine,* 174, 915-924.

DENG, M., SCOTT, M. J., LOUGHRAN, P., GIBSON, G., SODHI, C., WATKINS, S., HACKAM, D. & BILLIAR, T. R. 2013. Lipopolysaccharide clearance, bacterial clearance, and systemic inflammatory responses are regulated by cell type-specific functions of TLR4 during sepsis. *Journal of immunology (Baltimore, Md. : 1950),* 190, 5152-5160.

DIMITROV, S., BENEDICT, C., HEUTLING, D., WESTERMANN, J., BORN, J. & LANGE, T. 2009. Cortisol and epinephrine control opposing circadian rhythms in T cell subsets. *Blood,* 113, 5134-5143.

DIMITROV, S., LANGE, T., BENEDICT, C., NOWELL, M. A. & JONES, S. A. 2006. Sleep enhances IL-6 trans-signaling in humans. *The FASEB journal,* 20, 2174-2176.

DINARELLO, C. A. 1996. Biologic basis for interleukin-1 in disease. *Blood,* 87, 2095-147.

DINARELLO, C. A. 2000. Proinflammatory cytokines. *Chest,* 118, 503-8.

DING, W.-X. X. & YIN, X.-M. M. 2012. Mitophagy: mechanisms, pathophysiological roles, and analysis. *Biological chemistry,* 393, 547-564.

DUMONT, M., BENHABEROU-BRUN, D. & PAQUET, J. 2001. Profile of 24-h light exposure and circadian phase of melatonin secretion in night workers. *J Biol Rhythms,* 16, 502-11.

EDMONDS, S. C. & ADLER, N. T. 1977. Food and light as entrainers of circadian running activity in the rat. *Physiology & Behavior,* 18, 915-919.

ELLA, K., CSEPANYI-KOMI, R. & KALDI, K. 2016. Circadian regulation of human peripheral neutrophils. *Brain Behav Immun,* 57, 209-21.

ELMORE, S. 2007. Apoptosis: a review of programmed cell death. *Toxicologic pathology,* 35, 495-516.

ENDEMANN, G., STANTON, L. W. & MADDEN, K. S. 1993. CD36 is a receptor for oxidized low density lipoprotein. *The Journal of biological chemistry.*

ESQUIROL, Y., PERRET, B., RUIDAVETS, J. B., MARQUIE, J. C., DIENNE, E., NIEZBORALA, M. & FERRIERES, J. 2011. Shift work and cardiovascular risk factors: new knowledge from the past decade. *Arch Cardiovasc Dis,* 104, 636-68.

FADOK, V. A., BRATTON, D. L., KONOWAL, A., FREED, P. W., WESTCOTT, J. Y. & HENSON, P. M. 1998. Macrophages that have ingested apoptotic cells in vitro inhibit proinflammatory cytokine production through autocrine/paracrine mechanisms involving TGF-beta, PGE2, and PAF. *Journal of Clinical Investigation,* 101, 890-898.

FANG, J., WANG, Y. & KRUEGER, J. M. 1997. Mice lacking the TNF 55 kDa receptor fail to sleep more after TNFalpha treatment. *The Journal of Neuroscience : the official journal of the Society for Neuroscience,* 17, 5949-5955.

FANG, J., WANG, Y. & KRUEGER, J. M. 1998. Effects of interleukin-1 beta on sleep are mediated by the type I receptor. *The American Journal of Physiology,* 274, R655-R660.

FEIGIN R. D, M. J. N., REED C. 1972. Circadian Rhythmicity in Susceptibility of Mice to Sublethal Coxsackie B3 Infection. *Nature,* 240, 57-58.

FEIGIN, R. D., SAN JOAQUIN, V. H., HAYMOND, M. W. & WYATT, R. 1996. Daily Periodicity of Susceptibility of Mice to Pneumococcal Infection. *Nature,* 224, 379-380.

FERRARA, J., ABHYANKAR, S. & GILLILAND, D. 1993. Cytokine storm of graft-versus-host disease: a critical effector role for interleukin-1. *Transplantation proceedings,* 25, 2.

FIORENTINO, D. F. 1989. Two types of mouse T helper cell. IV. Th2 clones secrete a factor that inhibits cytokine production by Th1 clones. *Journal of Experimental Medicine,* 170, 2081-2095.

FONKEN, L. K., FRANK, M. G., KITT, M. M., BARRIENTOS, R. M., WATKINS, L. R. & MAIER, S. F. 2015. Microglia inflammatory responses are controlled by an intrinsic circadian clock. *Brain Behav Immun,* 45, 171-9.

FONKEN, L. K., KITT, M. M., GAUDET, A. D., BARRIENTOS, R. M., WATKINS, L. R. & MAIER, S. F. 2016. Diminished circadian rhythms in hippocampal microglia may contribute to age-related neuroinflammatory sensitization. *Neurobiol Aging,* 47, 102-112.

FORTIER, E. E., ROONEY, J. & DARDENTE, H. 2011. Circadian variation of the response of T cells to antigen. *The Journal of Immunology,* 187, 6291-6300.

GALLAND, L. 2010. Diet and inflammation. *Nutr Clin Pract,* 25, 634-40.

GAUTIER, E. L., SHAY, T., MILLER, J., GRETER, M., JAKUBZICK, C., IVANOV, S., HELFT, J., CHOW, A., ELPEK, K. G., GORDONOV, S., MAZLOOM, A. R., MA'AYAN, A., CHUA, W.-J. J., HANSEN, T. H., TURLEY, S. J., MERAD, M., RANDOLPH, G. J. & CONSORTIUM, I. 2012. Gene-expression profiles and transcriptional regulatory pathways that underlie the identity and diversity of mouse tissue macrophages. *Nature immunology,* 13, 1118-1128.

GEKAKIS, N., STAKNIS, D., NGUYEN, H. B., DAVIS, F. C., WILSBACHER, L. D., KING, D. P., TAKAHASHI, J. S. & WEITZ, C. J. 1998. Role of the CLOCK protein in the mammalian circadian mechanism. *Science,* 280, 1564-1569.

GIBBS, J. E., BLAIKLEY, J., BEESLEY, S., MATTHEWS, L., SIMPSON, K. D., BOYCE, S. H., FARROW, S. N., ELSE, K. J., SINGH, D., RAY, D. W. & LOUDON, A. S. 2012. The nuclear receptor REV-ERBα mediates circadian regulation of innate immunity through selective regulation of inflammatory cytokines. *Proceedings of the National Academy of Sciences of the United States of America,* 109, 582-587.

GIGUERE, V., TINI, M., FLOCK, G., ONG, E., EVANS, R. M. & OTULAKOWSKI, G. 1994. Isoform-specific amino-terminal domains dictate DNA-binding properties of ROR alpha, a novel family of orphan hormone nuclear receptors. *Genes & Development,* 8, 538-553.

GLEESON, L. E. & SHEEDY, F. J. 2016. Metabolic reprogramming & inflammation: Fuelling the host response to pathogens. *Semin Immunol,* 28, 450-468.

GLICK, D., BARTH, S. & MACLEOD, K. F. 2010. Autophagy: cellular and molecular mechanisms. *The Journal of pathology,* 221, 3-12.

GORDON, S., PLÜDDEMANN, A. & MARTINEZ ESTRADA, F. 2014. Macrophage heterogeneity in tissues: phenotypic diversity and functions. *Immunological reviews,* 262, 36-55.

GREENWALT, D. E., SCHECK, S. H. & RHINEHART-JONES, T. 1995. Heart CD36 expression is increased in murine models of diabetes and in mice fed a high fat diet. *The Journal of clinical investigation,* 96, 1382-1388.

HACK, C. E., GROOT, D. E. R., FELT-BERSMA, R. J. & NUIJENS, J. H. 1989. Increased plasma levels of interleukin-6 in sepsis. *Blood,* 74, 1704-10.

HALBERG, F., JOHNSON, E., BROWN, B. & BITTNER, J. 1960. Susceptibility Rhythm to E. coli Endotoxin and Bioassay. *Experimental Biology and Medicine,* 103, 142-144.

HAMAGUCHI, Y., TAHARA, Y., HITOSUGI, M. & SHIBATA, S. 2015. Impairment of Circadian Rhythms in Peripheral Clocks by Constant Light Is Partially Reversed by Scheduled Feeding or Exercise. *J Biol Rhythms,* 30, 533-42.

HANAHAN, D. & WEINBERG, R. A. 2011. Hallmarks of cancer: the next generation. *Cell,* 144, 646-674.

HAND, L. E., HOPWOOD, T. W., DICKSON, S. H., WALKER, A. L., LOUDON, A. S., RAY, D. W., BECHTOLD, D. A. & GIBBS, J. E. 2016. The circadian clock regulates inflammatory arthritis. *FASEB journal : official*

publication of the Federation of American Societies for Experimental Biology, 30, 3759-3770.

HAO, H., ALLEN, D. L. & HARDIN, P. E. 1997. A circadian enhancer mediates PER-dependent mRNA cycling in Drosophila melanogaster. *Molecular and Cellular Biology,* 17, 3687-3693.

HARA, R., WAN, K., WAKAMATSU, H., AIDA, R., MORIYA, T., AKIYAMA, M. & SHIBATA, S. 2001. Restricted feeding entrains liver clock without participation of the suprachiasmatic nucleus. *Genes to Cells : devoted to molecular & cellular mechanisms,* 6, 269-278.

HARD, G. C. 1970. Some biochemical aspects of the immune macrophage. *British journal of experimental pathology.*

HARDING, H. P. & LAZAR, M. A. 1993. The orphan receptor Rev-ErbA alpha activates transcription via a novel response element. *Molecular and Cellular Biology,* 13, 3113-3121.

HASTINGS, M., O'NEILL, J. S. & MAYWOOD, E. S. 2007. Circadian clocks: regulators of endocrine and metabolic rhythms. *Journal of Endocrinology,* 195, 187-198.

HATORI, M., VOLLMERS, C., ZARRINPAR, A. & DITACCHIO, L. 2012. Time-restricted feeding without reducing caloric intake prevents metabolic diseases in mice fed a high-fat diet. *Cell Metabolism,* 15, 848-860.

HAUS, E. & SMOLENSKY, M. 2006. Biological clocks and shift work: circadian dysregulation and potential long-term effects. *Cancer Causes Control,* 17, 489-500.

HAUS, E. L. & SMOLENSKY, M. H. 2013. Shift work and cancer risk: potential mechanistic roles of circadian disruption, light at night, and sleep deprivation. *Sleep Med Rev,* 17, 273-84.

HAYASHI, M., SHIMBA, S. & TEZUKA, M. 2007. Characterization of the molecular clock in mouse peritoneal macrophages. *Biological & pharmaceutical bulletin,* 30, 621-626.

HAYASHI, Y., KOYANAGI, S., KUSUNOSE, N., OKADA, R., WU, Z., TOZAKI-SAITOH, H., UKAI, K., KOHSAKA, S., INOUE, K., OHDO, S. & NAKANISHI, H. 2013. The intrinsic microglial molecular clock controls synaptic strength via the circadian expression of cathepsin S. *Sci Rep,* 3, 2744.

HEDSTROM, A. K., AKERSTEDT, T., HILLERT, J., OLSSON, T. & ALFREDSSON, L. 2011. Shift work at young age is associated with increased risk for multiple sclerosis. *Ann Neurol,* 70, 733-41.

HIRAO, A., TAHARA, Y., KIMURA, I. & SHIBATA, S. 2009. A balanced diet is necessary for proper entrainment signals of the mouse liver clock. *PLoS One,* 4, e6909.

HIROTA, T., OKANO, T., KOKAME, K., SHIROTANI-IKEJIMA, H., MIYATA, T. & FUKADA, Y. 2002. Glucose down-regulates Per1 and Per2 mRNA levels and induces circadian gene expression in cultured Rat-1 fibroblasts. *J Biol Chem,* 277, 44244-51.

HOEBE, K., JANSSEN, E. & BEUTLER, B. 2004. The interface between innate and adaptive immunity. *Nat Immunol,* 5, 971-4.

HOFFMAN, A. E., ZHENG, T., STEVENS, R. G., BA, Y. & ZHANG, Y. 2009. Clock-Cancer Connection in Non–Hodgkin's Lymphoma: A Genetic Association Study and Pathway Analysis of the Circadian Gene Cryptochrome 2. *Cancer Research,* 69, 3605-3613.

HOTAMISLIGIL, G. S., SHARGILL, N. S. & SPIEGELMAN, B. M. 1993. Adipose Expression of Tumor Necrosis Factor- : Direct Role in Obesity-Linked Insulin Resistance. *SCIENCE-NEW YORK THEN WASHINGTON-,* 259, 87-87.

HOTCHKISS, R. S., TINSLEY, K. W. & KARL, I. E. 2003. Role of apoptotic cell death in sepsis. *Scand J Infect Dis,* 35, 585-92.

HOUGHTON, S. G., IQBAL, C. W., DUENES, J. A., FATIMA, J., KASPAREK, M. S. & SARR, M. G. 2008. Coordinated, diurnal hexose transporter expression in rat small bowel: implications for small bowel resection. *Surgery,* 143, 79-93.

HOZUMI, N. & TONEGAWA, S. 1976. Evidence for somatic rearrangement of immunoglobulin genes coding for variable and constant regions. *Proc Natl Acad Sci U S A,* 73, 3628-32.

HRISCU, M. L. 2005. Modulatory Factors of Circadian Phagocytic Activity. *Annals of the New York Academy of Sciences,* 1057, 403-430.

HRUSHESKY, W. J., LANGEVIN, T., KIM, Y. & WOOD, P. A. 1994a. Circadian dynamics of tumor necrosis factor alpha (cachectin) lethality. *The Journal of Experimental Medicine,* 180, 1059-1065.

HRUSHESKY, W. J., LANGEVIN, T. & KIM, Y. J. 1994b. Circadian dynamics of tumor necrosis factor alpha (cachectin) lethality. *The Journal of Experimental Medicine,* 180, 1059-1065.

HSU, H., SHU, H. B., PAN, M. G. & GOEDDEL, D. V. 1996. TRADD-TRAF2 and TRADD-FADD interactions define two distinct TNF receptor 1 signal transduction pathways. *Cell,* 84, 299-308.

HUGHES, M. E., HOGENESCH, J. B. & KORNACKER, K. 2010. JTK_CYCLE: an efficient nonparametric algorithm for detecting rhythmic components in genome-scale data sets. *J Biol Rhythms,* 25, 372-80.

HUSSE, J., LELIAVSKI, A., TSANG, A. H., OSTER, H. & EICHELE, G. 2014. The light-dark cycle controls peripheral rhythmicity in mice with a genetically ablated suprachiasmatic nucleus clock. *The FASEB Journal,* 28, 4950-4960.

IMERI, L. & OPP, M. R. 2009. How (and why) the immune system makes us sleep. *Nature Reviews. Neuroscience,* 10, 199-210.

JACOBS, S. R., HERMAN, C. E., MACIVER, N. J., WOFFORD, J. A., WIEMAN, H. L., HAMMEN, J. J. & RATHMELL, J. C. 2008. Glucose uptake is limiting in T cell activation and requires CD28-mediated akt-dependent and independent pathways. *Journal of Immunology,* 180, 4476-4486.

JANCAR, S. & SANCHEZ CRESPO, M. 2005. Immune complex-mediated tissue injury: a multistep paradigm. *Trends Immunol,* 26, 48-55.

JANEWAY, C. A., JR. 1989. Approaching the asymptote? Evolution and revolution in immunology. *Cold Spring Harb Symp Quant Biol,* 54 Pt 1, 1-13.

JAY, A. G., CHEN, A. N., PAZ, M. A., HUNG, J. P. & HAMILTON, J. A. 2015. CD36 Binds Oxidized Low Density Lipoprotein (LDL) in a Mechanism Dependent upon Fatty Acid Binding. *Journal of Biological Chemistry,* 290, 4590-4603.

JOHANNES, L., PARTON, R. G., BASSEREAU, P. & MAYOR, S. 2015. Building endocytic pits without clathrin. *Nat Rev Mol Cell Biol,* 16, 311-21.

KARLSSON, B., KNUTSSON, A. & LINDAHL, B. 2001. Is there an association between shift work and having a metabolic syndrome? Results from a population based study of 27,485 people. *Occupational and Environmental Medicine,* 58, 747-752.

KAWAI, T. & AKIRA, S. 2010. The role of pattern-recognition receptors in innate immunity: update on Toll-like receptors. *Nat Immunol,* 11, 373-84.

KEESLER, G. A., CAMACHO, F., GUO, Y. & VIRSHUP, D. 2000. Phosphorylation and destabilization of human period I clock protein by human casein kinase Iε. *Neuroreport,* 11, 951-955.

KELLER, M., MAZUCH, J., ABRAHAM, U., EOM, G. D., HERZOG, E. D., VOLK, H.-D. D., KRAMER, A. & MAIER, B. 2009. A circadian clock in macrophages controls inflammatory immune responses. *Proceedings of the National Academy of Sciences of the United States of America,* 106, 21407-21412.

KINNE, R. W., BRÄUER, R., STUHLMÜLLER, B., PALOMBO-KINNE, E. & BURMESTER, G. R. 2000. Macrophages in rheumatoid arthritis. *Arthritis research,* 2, 189-202.

KIRCHHAUSEN, T., OWEN, D. & HARRISON, S. C. 2014. Molecular structure, function, and dynamics of clathrin-mediated membrane traffic. *Cold Spring Harb Perspect Biol,* 6, a016725.

KITANI, A., HARA, M., HIROSE, T., HARIGAI, M., SUZUKI, K., KAWAKAMI, M., KAWAGUCHI, Y., HIDAKA, T., KAWAGOE, M. & NAKAMURA, H. 1992. Autostimulatory effects of IL-6 on excessive B cell differentiation in patients with systemic lupus erythematosus: analysis of IL-6 production and IL-6R expression. *Clin Exp Immunol,* 88, 75-83.

KOHSAKA, A., LAPOSKY, A. D., RAMSEY, K., ESTRADA, C., JOSHU, C., KOBAYASHI, Y., TUREK, F. W. & BASS, J. 2007. High-fat diet disrupts behavioral and molecular circadian rhythms in mice. *Cell Metabolism,* 6, 414-421.

KOO, D. J., CHAUDRY, I. H. & WANG, P. 1999. Kupffer cells are responsible for producing inflammatory cytokines and hepatocellular dysfunction during early sepsis. *The Journal of surgical research,* 83, 151-157.

KORNS, D., FRASCH, S. C., FERNANDEZ-BOYANAPALLI, R., HENSON, P. M. & BRATTON, D. L. 2011. Modulation of macrophage efferocytosis in inflammation. *Frontiers in immunology,* 2, 57.

KOWANKO, I. C., KNAPP, M. S. & POWNALL, R. 1982. Domiciliary self-measurement in the rheumatoid arthritis and the demonstration of circadian rhythmicity. *Annals of the Rheumatic Diseases,* 41, 453-455.

KRAWCZYK, C. M., HOLOWKA, T., SUN, J., BLAGIH, J., AMIEL, E., DEBERARDINIS, R. J., CROSS, J. R., JUNG, E., THOMPSON, C. B., JONES, R. G. & PEARCE, E. J. 2010. Toll-like receptor-induced changes in glycolytic metabolism regulate dendritic cell activation. *Blood,* 115, 4742-4749.

KRONENBERG, M. & RUDENSKY, A. 2005. Regulation of immunity by self-reactive T cells. *Nature,* 435, 598-604.

KRUEGER, J. M. 1990. Somnogenic activity of immune response modifiers. *Trends in Pharmacological Sciences,* 11, 122-126.

KRUEGER, J. M., OBÁL, F., FANG, J. & KUBOTA, T. 2001. The role of cytokines in physiological sleep regulation. *Annals of the New York Academy of Sciences,* 933, 211-221.

KUMAR, V. & MCNERNEY, M. E. 2005. A new self: MHC-class-I-independent natural-killer-cell self-tolerance. *Nat Rev Immunol,* 5, 363-74.

KURIHARA, T., WARR, G., LOY, J. & BRAVO, R. 1997. Defects in macrophage recruitment and host defense in mice lacking the CCR2 chemokine receptor. *The Journal of experimental medicine,* 186, 1757-1762.

KURTZ, J. 2004. Memory in the innate and adaptive immune systems. *Microbes Infect,* 6, 1410-7.

KUSANAGI, H., MISHIMA, K., SATOH, K., ECHIZENYA, M., KATOH, T. & SHIMIZU, T. 2004. Similar profiles in human period1 gene expression in peripheral mononuclear and polymorphonuclear cells. *Neurosci Lett,* 365, 124-7.

LAMIA, K. A., STORCH, K. F. & WEITZ, C. J. 2008. Physiological significance of a peripheral tissue circadian clock. *Proc Natl Acad Sci U S A,* 105, 15172-7.

LANGE, T., DIMITROV, S. & BORN, J. 2010. Effects of sleep and circadian rhythm on the human immune system. *Annals of the New York Academy of Sciences,* 1193, 48-59.

LANGE, T., PERRAS, B., FEHM, H. L. & BORN, J. 2003. Sleep enhances the human antibody response to hepatitis A vaccination. *Psychosomatic Medicine,* 65, 831-835.

LE MINH, N., DAMIOLA, F., TRONCHE, F., SCHUTZ, G. & SCHIBLER, U. 2001. Glucocorticoid hormones inhibit food-induced phase-shifting of peripheral circadian oscillators. *EMBO J,* 20, 7128-36.

LEE, J. H. & SANCAR, A. 2011. Regulation of apoptosis by the circadian clock through NF-κB signaling. *Proceedings of the National Academy of Sciences of the United States of America,* 108, 12036-12041.

LEON, L. R., WHITE, A. A. & KLUGER, M. J. 1998. Role of IL-6 and TNF in thermoregulation and survival during sepsis in mice. *Am J Physiol,* 275, R269-77.

LOMEDICO, P., GUBLER, U., HELLMANN, C., DUKOVICH, M., GIRI, J., PAN, Y., COLLIER, K., SEMIONOW, R., CHUA, A. & MIZEL, S. 1984. Cloning and expression of murine interleukin-1 cDNA in Escherichia coli. *Nature,* 312, 458-62.

LONG, J. E., DRAYSON, M. T., TAYLOR, A. E., TOELLNER, K. M. & LORD, J. M. 2016. Morning vaccination enhances antibody response over afternoon vaccination: A cluster-randomised trial. *Vaccine,* 34, 2679-2685.

MADERNA, P. & GODSON, C. 2003. Phagocytosis of apoptotic cells and the resolution of inflammation. *Biochim Biophys Acta,* 1639, 141-51.

MARPEGAN, L., LEONE, M. J., KATZ, M. E., SOBRERO, P. M., BEKINSTEIN, T. A. & GOLOMBEK, D. A. 2009. Diurnal variation in endotoxin-induced mortality in mice: correlation with proinflammatory factors. *Chronobiology international,* 26, 1430-1442.

MARSHALL, J. C., REINHART, K. & FORUM, I. 2009. Biomarkers of sepsis. *Critical care medicine,* 37, 2290-2298.

MARTINO, T. A., OUDIT, G. Y., HERZENBERG, A. M., TATA, N., KOLETAR, M. M., KABIR, G. M., BELSHAM, D. D., BACKX, P. H., RALPH, M. R. & SOLE, M. J. 2008. Circadian rhythm disorganization produces profound cardiovascular and renal disease in hamsters. *Am J Physiol Regul Integr Comp Physiol,* 294, R1675-83.

MATZINGER, P. 1994. Tolerance, danger, and the extended family. *Annual review of immunology,* 12, 991-1045.

MCIVER, K. S., HEATH, A. S. & SCOTT, J. R. 1995. Regulation of virulence by environmental signals in group A streptococci: influence of osmolarity, temperature, gas exchange, and iron limitation on emm transcription. *Infect Immun,* 63, 4540-2.

MENAKER, M. 1968. Extraretinal light perception in the sparrow. I. Entrainment of the biological clock. *Proceedings of the National Academy of Sciences of the United States of America,* 59, 414-421.

METCHNIKOFF, E. 1905. Immunity in infective diseases. *Immunity in infective diseases.*

METSCHNIKOFF, E. 1887. Ueber den Kampf der Zellen gegen Erysipelkokken. *Virchows Archiv.*

METZGER, T. C. & ANDERSON, M. S. 2011. Control of central and peripheral tolerance by Aire. *Immunol Rev,* 241, 89-103.

MICHALEK, R. D., GERRIETS, V. A., JACOBS, S. R., MACINTYRE, A. N., MACIVER, N. J., MASON, E. F., SULLIVAN, S. A., NICHOLS, A. G. & RATHMELL, J. C. 2011. Cutting edge: distinct glycolytic and lipid oxidative metabolic programs are essential for effector and regulatory CD4+ T cell subsets. *J Immunol,* 186, 3299-303.

MINIHANE, A. M., VINOY, S., RUSSELL, W. R., BAKA, A., ROCHE, H. M., TUOHY, K. M., TEELING, J. L., BLAAK, E. E., FENECH, M., VAUZOUR, D., MCARDLE, H. J., KREMER, B. H., STERKMAN, L., VAFEIADOU, K., BENEDETTI, M. M., WILLIAMS, C. M. & CALDER, P. C. 2015. Low-grade inflammation, diet composition and health: current research evidence and its translation. *Br J Nutr,* 114, 999-1012.

MISTLBERGER, R. E. 1994. Circadian food-anticipatory activity: Formal models and physiological mechanisms. *Neuroscience & Biobehavioral Reviews,* 18, 171-195.

MISTLBERGER, R. E. & MARCHANT, E. G. 1995. Computational and entrainment models of circadian food-anticipatory activity: evidence from non-24-hr feeding schedules. *Behavioral Neuroscience,* 109, 790-798.

MIZUSHIMA, N. 2007. Autophagy: process and function. *Genes & development,* 21, 2861-2873.

MOHREN, D. C. L., JANSEN, N. W. H. & KANT, I. J. 2002. Prevalence of common infections among employees in different work schedules. *Journal of Occupational and Environmental Medicine,* 44, 1003-1011.

MOORE, R. Y. & EICHLER, V. B. 1972. Loss of a circadian adrenal corticosterone rhythm following suprachiasmatic lesions in the rat. *Brain Research,* 42, 201-206.

MOSER, B., WOLF, M., WALZ, A. & LOETSCHER, P. 2004. Chemokines: multiple levels of leukocyte migration control. *Trends Immunol,* 25, 75-84.

MUNOZ, M., PEIRSON, S. N., HANKINS, M. W. & FOSTER, R. G. 2005. Long-term constant light induces constitutive elevated expression of mPER2 protein in the murine SCN: a molecular basis for Aschoff's rule? *J Biol Rhythms,* 20, 3-14.

NABI, I. R. & LE, P. U. 2003. Caveolae/raft-dependent endocytosis. *J Cell Biol,* 161, 673-7.

NAGOSHI, E., SAINI, C., BAUER, C., LAROCHE, T., NAEF, F. & SCHIBLER, U. 2004. Circadian gene expression in individual fibroblasts: cell-

autonomous and self-sustained oscillators pass time to daughter cells. *Cell,* 119, 693-705.

NAU, G. J., RICHMOND, J. F., SCHLESINGER, A., JENNINGS, E. G., LANDER, E. S. & YOUNG, R. A. 2002. Human macrophage activation programs induced by bacterial pathogens. *Proceedings of the National Academy of Sciences of the United States of America,* 99, 1503-1508.

NEWSHOLME, P., CURI, R., GORDON, S. & NEWSHOLME, E. A. 1986. Metabolism of glucose, glutamine, long-chain fatty acids and ketone bodies by murine macrophages. *Biochem J,* 239, 121-5.

NGUYEN, K. D., FENTRESS, S. J., QIU, Y., YUN, K., COX, J. S. & CHAWLA, A. 2013. Circadian gene Bmal1 regulates diurnal oscillations of Ly6Chi inflammatory monocytes. *Science,* 341, 1483-1488

NOZAKI, S., KASHIWAGI, H., YAMASHITA, S., NAKAGAWA, T., KOSTNER, B., TOMIYAMA, Y., NAKATA, A., ISHIGAMI, M., MIYAGAWA, J. & KAMEDA-TAKEMURA, K. 1995. Reduced uptake of oxidized low density lipoproteins in monocyte-derived macrophages from CD36-deficient subjects. *The Journal of clinical investigation,* 96, 1859-1865.

O'NEILL, J. S. & REDDY, A. B. 2011. Circadian clocks in human red blood cells. *Nature,* 469, 498-503.

OHTA, H., YAMAZAKI, S. & MCMAHON, D. G. 2005. Constant light desynchronizes mammalian clock neurons. *Nature neuroscience,* 8, 267-269.

OIKE, H. 2017. Modulation of circadian clocks by nutrients and food factors. *Biosci Biotechnol Biochem,* 1-8.

OIKE, H., NAGAI, K., FUKUSHIMA, T., ISHIDA, N. & KOBORI, M. 2010. High-salt diet advances molecular circadian rhythms in mouse peripheral tissues. *Biochem Biophys Res Commun,* 402, 7-13.

OISHI, K., UCHIDA, D., OHKURA, N., DOI, R., ISHIDA, N., KADOTA, K. & HORIE, S. 2009. Ketogenic diet disrupts the circadian clock and increases hypofibrinolytic risk by inducing expression of plasminogen activator inhibitor-1. *Arterioscler Thromb Vasc Biol,* 29, 1571-7.

PAN, A., SCHERNHAMMER, E. S., SUN, Q. & HU, F. B. 2011. Rotating night shift work and risk of type 2 diabetes: two prospective cohort studies in women. *PLoS Medicine,* 8, e1001141.

PAN, X. Y., TERADA, T., OKUDA, M. & INUI, K. I. 2004. The diurnal rhythm of the intestinal transporters SGLT1 and PEPT1 is regulated by the feeding conditions in rats. *Journal of Nutrition,* 134, 2211-2215.

PAPAGIANNAKOPOULOS, T., BAUER, M. R., DAVIDSON, S. M., HEIMANN, M., SUBBARAJ, L., BHUTKAR, A., BARTLEBAUGH, J., VANDER HEIDEN, M. G. & JACKS, T. 2016. Circadian Rhythm Disruption Promotes Lung Tumorigenesis. *Cell metabolism,* 24, 324-331.

PASCHOS, G. K., IBRAHIM, S., SONG, W. L. & KUNIEDA, T. 2012. Obesity in mice with adipocyte-specific deletion of clock component Arntl. *Nature Medicine,* 18, 1768-1777.

PATTON, D. F., KATSUYAMA, Â. M., PAVLOVSKI, I., MICHALIK, M., PATTERSON, Z., PARFYONOV, M., SMIT, A. N., MARCHANT, E. G., CHUNG, J. & ABIZAID, A. 2014. Circadian Mechanisms of Food Anticipatory Rhythms in Rats Fed Once or Twice Daily: Clock Gene and Endocrine Correlates. *PloS One,* 9, e112451.

PEARCE, E. L., WALSH, M. C., CEJAS, P. J., HARMS, G. M., SHEN, H., WANG, L. S., JONES, R. G. & CHOI, Y. 2009. Enhancing CD8 T-cell memory by modulating fatty acid metabolism. *Nature,* 460, 103-7.

PENDERGAST, J. S., NAKAMURA, W., FRIDAY, R. C., HATANAKA, F., TAKUMI, T. & YAMAZAKI, S. 2009. Robust food anticipatory activity in BMAL1-deficient mice. *PLoS One,* 4, e4860.

PETROVSKY, N., MCNAIR, P. & HARRISON, L. C. 1998. Diurnal rhythms of pro-inflammatory cytokines: regulation by plasma cortisol and therapeutic implications. *Cytokine,* 10, 307-12.

PETRZILKA, S., TARABORRELLI, C. & CAVADINI, G. 2009. Clock gene modulation by TNF-α depends on calcium and p38 MAP kinase signaling. *Journal of Biological Rhythms,* 24, 283-294.

PIETROIUSTI, A., FORLINI, A., MAGRINI, A., GALANTE, A., COPPETA, L., GEMMA, G., ROMEO, E. & BERGAMASCHI, A. 2006. Shift work increases the frequency of duodenal ulcer in H pylori infected workers. *Occup Environ Med,* 63, 773-5.

PIRES - LAPA, M. A., TAMURA, E. K., SALUSTIANO, E. M. A. & MARKUS, R. P. 2013. Melatonin synthesis in human colostrum mononuclear cells enhances dectin - 1 - mediated phagocytosis by mononuclear cells. *Journal of Pineal Research,* 55, 240-246.

PITTENDRIGH, C. S. 1960. Circadian rhythms and the circadian organization of living systems. *Cold Spring Harb Symp Quant Biol,* 25, 159-84.

POLIDAROVA, L., SLADEK, M., SOTAK, M., PACHA, J. & SUMOVA, A. 2011. Hepatic, duodenal, and colonic circadian clocks differ in their persistence under conditions of constant light and in their entrainment by restricted feeding. *Chronobiol Int,* 28, 204-15.

POLIDAROVA, L., SOTAK, M., SLADEK, M., PACHA, J. & SUMOVA, A. 2009. Temporal gradient in the clock gene and cell-cycle checkpoint kinase Wee1 expression along the gut. *Chronobiol Int,* 26, 607-20.

POZZI, L. A. M., MACIASZEK, J. W. & ROCK, K. L. 2005. Both dendritic cells and macrophages can stimulate naive CD8 T cells in vivo to proliferate, develop effector function, and differentiate into memory cells. *Journal of Immunology,* 175, 2071-2081.

RAMAKRISHNAN, S. N., LAU, P., BURKE, L. J. & MUSCAT, G. E. 2005. Rev-erbbeta regulates the expression of genes involved in lipid absorption in skeletal muscle cells: evidence for cross-talk between orphan nuclear receptors and myokines. *J Biol Chem,* 280, 8651-9.

REINBERG, A., GERVAIS, P., LEVI, F., SMOLENSKY, M., DEL CERRO, L. & UGOLINI, C. 1988. Circadian and circannual rhythms of allergic rhinitis: an epidemiologic study involving chronobiologic methods. *The Journal of Allergy and Clinical Immunology,* 81, 51-62.

REPPERT, S. M. & WEAVER, D. R. 2002. Coordination of circadian timing in mammals. *Nature,* 418, 935-41.

REUTRAKUL, S. & KNUTSON, K. L. 2015. Consequences of Circadian Disruption on Cardiometabolic Health. *Sleep Med Clin,* 10, 455-68.

RICHARD, C. A., GUDEWICZ, P. W. & LOEGERING, D. J. 1999. IgG-coated erythrocytes augment the lipopolysaccharidestimulated increase in serum tumor necrosis factor-alpha. *Am J Physiol,* 276, R171-7.

RICHTER, C. P. 1922. A behavioristic study of the activity of the rat. *Comp. Psychol. Monogr.,* 1, 1-55.

RIPPERGER, J. A. & SCHIBLER, U. 2006. Rhythmic CLOCK-BMAL1 binding to multiple E-box motifs drives circadian Dbp transcription and chromatin transitions. *Nature Genetics,* 38, 369-374.

RODRÍGUEZ, A. B., MARCHENA, J. M., NOGALES, G., DURÁN, J. & BARRIGA, C. 1999. Correlation between the circadian rhythm of melatonin, phagocytosis, and superoxide anion levels in ring dove heterophils. *Journal of pineal research,* 26, 35-42.

ROENNEBERG, T., ALLEBRANDT, K. V., MERROW, M. & VETTER, C. 2012. Social jetlag and obesity. *Curr Biol,* 22, 939-43.

ROENNEBERG, T. & MERROW, M. 2016. The Circadian Clock and Human Health. *Curr Biol,* 26, R432-43.

ROSEBOOM, P. H., NAMBOODIRI, M. A., ZIMONJIC, D. B., POPESCU, N. C., RODRIGUEZ, I. R., GASTEL, J. A. & KLEIN, D. C. 1998. Natural melatonin 'knockdown' in C57BL/6J mice: rare mechanism truncates serotonin N-acetyltransferase. *Brain research. Molecular brain research,* 63, 189-197.

RUTTER, J., REICK, M., WU, L. C. & MCKNIGHT, S. L. 2001. Regulation of clock and NPAS2 DNA binding by the redox state of NAD cofactors. *Science,* 293, 510-4.

SBARRA, A. J. & KARNOVSKY, M. L. 1959. The biochemical basis of phagocytosis. I. Metabolic changes during the ingestion of particles by polymorphonuclear leukocytes. *J Biol Chem,* 234, 1355-62.

SCHEIERMANN, C., KUNISAKI, Y. & FRENETTE, P. S. 2013. Circadian control of the immune system. *Nature Reviews Immunology,* 13, 190-198.

SCHEIERMANN, C., KUNISAKI, Y., LUCAS, D., CHOW, A., JANG, J. E., ZHANG, D., HASHIMOTO, D., MERAD, M. & FRENETTE, P. S. 2012. Adrenergic nerves govern circadian leukocyte recruitment to tissues. *Immunity,* 37, 290-301.

SCHNEIDER, D. S. & AYRES, J. S. 2008. Two ways to survive infection: what resistance and tolerance can teach us about treating infectious diseases. *Nature reviews. Immunology,* 8, 889-895.

SCOTT, J. T. 1960. Morning stiffness in rheumatoid arthritis. *Annals of the Rheumatic Diseases,* 19, 361-368.

SHEEDY, F. J., GREBE, A., RAYNER, K. J., KALANTARI, P., RAMKHELAWON, B., CARPENTER, S. B., BECKER, C. E., EDIRIWEERA, H. N., MULLICK, A. E., GOLENBOCK, D. T., STUART, L. M., LATZ, E., FITZGERALD, K. A. & MOORE, K. J. 2013. CD36 coordinates NLRP3 inflammasome activation by facilitating intracellular nucleation of soluble ligands into particulate ligands in sterile inflammation. *Nature Immunology,* 14, 812-820.

SILVER, A. C., ARJONA, A., HUGHES, M. E., NITABACH, M. N. & FIKRIG, E. 2012a. Circadian expression of clock genes in mouse macrophages, dendritic cells, and B cells. *Brain Behav Immun,* 36, 407-13.

SILVER, A. C., ARJONA, A., WALKER, W. E. & FIKRIG, E. 2012b. The circadian clock controls toll-like receptor 9-mediated innate and adaptive immunity. *Immunity,* 36, 251-261.

SPÄTH-SCHWALBE, E., HANSEN, K., SCHMIDT, F., SCHREZENMEIER, H., MARSHALL, L., BURGER, K., FEHM, H. L. & BORN, J. 1998. Acute effects of recombinant human interleukin-6 on endocrine and central nervous sleep functions in healthy men. *The Journal of Clinical Endocrinology and Metabolism,* 83, 1573-1579.

SPENGLER, M. L., KUROPATWINSKI, K. K., COMAS, M., GASPARIAN, A. V., FEDTSOVA, N., GLEIBERMAN, A. S., GITLIN, II, ARTEMICHEVA, N. M., DELUCA, K. A., GUDKOV, A. V. & ANTOCH, M. P. 2012. Core circadian protein CLOCK is a positive regulator of NF-kappaB-mediated transcription. *Proc Natl Acad Sci U S A,* 109, E2457-65.

STEIN, M., KESHAV, S., HARRIS, N. & GORDON, S. 1992. Interleukin 4 potently enhances murine macrophage mannose receptor activity: a marker of alternative immunologic macrophage activation. *The Journal of experimental medicine,* 176, 287-292.

STEPHAN, F. K. & ZUCKER, I. 1972. Circadian rhythms in drinking behavior and locomotor activity of rats are eliminated by hypothalamic lesions. *Proceedings of the National Academy of Sciences of the United States of America,* 69, 1583-1586.

STERN, S. T., ADISESHAIAH, P. P. & CRIST, R. M. 2012. Autophagy and lysosomal dysfunction as emerging mechanisms of nanomaterial toxicity. *Particle and Fibre Toxicology,* 9.

STOKKAN, K. A., YAMAZAKI, S., TEI, H., SAKAKI, Y. & MENAKER, M. 2001. Entrainment of the circadian clock in the liver by feeding. *Science,* 291, 490-3.

STUART, L. M., DENG, J., SILVER, J. M., TAKAHASHI, K., TSENG, A. A., HENNESSY, E. J., EZEKOWITZ, R. A. & MOORE, K. J. 2005. Response to Staphylococcus aureus requires CD36-mediated phagocytosis triggered by the COOH-terminal cytoplasmic domain. *J Cell Biol,* 170, 477-85.

STUART, L. M. & EZEKOWITZ, R. A. 2005. Phagocytosis: elegant complexity. *Immunity,* 22, 539-50.

SUKARI, A., NAGASAKA, M., AL-HADIDI, A. & LUM, L. G. 2016. Cancer Immunology and Immunotherapy. *Anticancer research,* 36, 5593-5606.

SUN, E. W. & SHI, Y. F. 2001. Apoptosis: the quiet death silences the immune system. *Pharmacology & therapeutics,* 92, 135-145.

SWANSON, J. A. & WATTS, C. 1995. Macropinocytosis. *Trends in cell biology,* 5, 424-428.

TAHARA, Y. & SHIBATA, S. 2013. Chronobiology and nutrition. *Neuroscience,* 253, 78-88.

TAKAHASHI, J. S. 2016. Transcriptional architecture of the mammalian circadian clock. *Nature Reviews Genetics.*

TAKEUCHI, O. & AKIRA, S. 2010. Pattern recognition receptors and inflammation. *Cell,* 140, 805-20.

TAMARU, T., HATTORI, M., HONDA, K., BENJAMIN, I., OZAWA, T. & TAKAMATSU, K. 2011. Synchronization of circadian Per2 rhythms and HSF1-BMAL1:CLOCK interaction in mouse fibroblasts after short-term heat shock pulse. *PloS one,* 6.

TANNAHILL, G. M., CURTIS, A. M., ADAMIK, J., PALSSON-MCDERMOTT, E. M., MCGETTRICK, A. F., GOEL, G., FREZZA, C., BERNARD, N. J., KELLY, B., FOLEY, N. H., ZHENG, L., GARDET, A., TONG, Z., JANY,

S. S., CORR, S. C., HANEKLAUS, M., CAFFREY, B. E., PIERCE, K., WALMSLEY, S., BEASLEY, F. C., CUMMINS, E., NIZET, V., WHYTE, M., TAYLOR, C. T., LIN, H., MASTERS, S. L., GOTTLIEB, E., KELLY, V. P., CLISH, C., AURON, P. E., XAVIER, R. J. & O'NEILL, L. A. 2013. Succinate is an inflammatory signal that induces IL-1beta through HIF-1alpha. *Nature,* 496, 238-42.

TAVAKKOLIZADEH, A., RAMSANAHIE, A., LEVITSKY, L. L., ZINNER, M. J., WHANG, E. E., ASHLEY, S. W. & RHOADS, D. B. 2005. Differential role of vagus nerve in maintaining diurnal gene expression rhythms in the proximal small intestine. *J Surg Res,* 129, 73-8.

THAISS, C. A., ZEEVI, D., LEVY, M., ZILBERMAN-SCHAPIRA, G., SUEZ, J., TENGELER, A. C., ABRAMSON, L., KATZ, M. N., KOREM, T., ZMORA, N., KUPERMAN, Y., BITON, I., GILAD, S., HARMELIN, A., SHAPIRO, H., HALPERN, Z., SEGAL, E. & ELINAV, E. 2014. Transkingdom control of microbiota diurnal oscillations promotes metabolic homeostasis. *Cell,* 159, 514-29.

TIEGS, G. & LOHSE, A. W. 2010. Immune tolerance: What is unique about the liver. *Journal of Autoimmunity,* 34, 1-6.

TOTH, L. A. & KRUEGER, J. M. 1988. Alteration of sleep in rabbits by Staphylococcus aureus infection. *Infection and Immunity,* 56, 1785-1791.

TRONCHE, F., KELLENDONK, C., REICHARDT, H. M. & SCHUTZ, G. 1998. Genetic dissection of glucocorticoid receptor function in mice. *Curr Opin Genet Dev,* 8, 532-8.

TROUSSEAU, A. 1865. *Clinique medicale de L'Hotel dieu Paris,* 2.

TUREK, F. W. 2016. Circadian clocks: Not your grandfather's clock. *Science (New York, N.Y.),* 354, 992-993.

UEDA, H. R., HAYASHI, S., CHEN, W., SANO, M. & MACHIDA, M. 2005. System-level identification of transcriptional circuits underlying mammalian circadian clocks. *Nature Genetics,* 37, 187-192.

UKAI-TADENUMA, M., KASUKAWA, T. & UEDA, H. R. 2008. Proof-by-synthesis of the transcriptional logic of mammalian circadian clocks. *Nature Cell Biology,* 10, 1154-1163.

UNANUE, E. R. & ALLEN, P. M. 1987. The basis for the immunoregulatory role of macrophages and other accessory cells. *Science,* 236, 551-7.

UNDERHILL, D. M. & GOODRIDGE, H. S. 2012. Information processing during phagocytosis. *Nat Rev Immunol,* 12, 492-502.

UNDERHILL, D. M. & OZINSKY, A. 2002. PHAGOCYTOSIS OF MICROBES: Complexity in Action. *Annual review of immunology,* 20, 825-852.

UNNIKRISHNAN, M., COHEN, J. & SRISKANDAN, S. 1999. Growth-phase-dependent expression of virulence factors in an M1T1 clinical isolate of Streptococcus pyogenes. *Infect Immun,* 67, 5495-9.

VAN DER WINDT, G. J. W., EVERTS, B., CHANG, C. H., CURTIS, J. D., FREITAS, T. C., AMIEL, E., PEARCE, E. J. & PEARCE, E. L. 2012. Mitochondrial Respiratory Capacity Is a Critical Regulator of CD8(+) T Cell Memory Development. *Immunity,* 36, 68-78.

VANDER HEIDEN, M. G., CANTLEY, L. C. & THOMPSON, C. B. 2009. Understanding the Warburg effect: the metabolic requirements of cell proliferation. *Science,* 324, 1029-33.

VARFOLOMEEV, E. E. & ASHKENAZI, A. 2004. Tumor necrosis factor: an apoptosis JuNKie? *Cell,* 116, 491-7.

VATS, D., MUKUNDAN, L., ODEGAARD, J. I., ZHANG, L., SMITH, K. L., MOREL, C. R., WAGNER, R. A., GREAVES, D. R., MURRAY, P. J. & CHAWLA, A. 2006. Oxidative metabolism and PGC-1beta attenuate macrophage-mediated inflammation. *Cell metabolism,* 4, 13-24.

VIDENOVIC, A. & ZEE, P. C. 2015. Consequences of Circadian Disruption on Neurologic Health. *Sleep Med Clin,* 10, 469-80.

VINCENT, J. L., ABRAHAM, E., ANNANE, D., BERNARD, G., RIVERS, E. & VAN DEN BERGHE, G. 2002. Reducing mortality in sepsis: new directions. *Crit Care,* 6 Suppl 3, S1-18.

VLAHOS, R. & BOZINOVSKI, S. 2014. Role of alveolar macrophages in chronic obstructive pulmonary disease. *Frontiers in immunology,* 5, 435.

VOIGT, R. M., FORSYTH, C. B. & KESHAVARZIAN, A. 2013. Circadian disruption: potential implications in inflammatory and metabolic diseases associated with alcohol. *Alcohol research : current reviews,* 35, 87-96.

VYAS, D., JAVADI, P., DIPASCO, P. J., BUCHMAN, T. G., HOTCHKISS, R. S. & COOPERSMITH, C. M. 2005. Early antibiotic administration but not antibody therapy directed against IL-6 improves survival in septic mice predicted to die on basis of high IL-6 levels. *American journal of physiology. Regulatory, integrative and comparative physiology,* 289, 53.

WALLACH, D., KANG, T. B. & KOVALENKO, A. 2014. Concepts of tissue injury and cell death in inflammation: a historical perspective. *Nat Rev Immunol,* 14, 51-9.

WANG, A., HUEN, S. C., LUAN, H. H., YU, S. & ZHANG, C. 2016. Opposing effects of fasting metabolism on tissue tolerance in bacterial and viral inflammation. *Cell.*

WARBURG, O. 1956. On the Origin of Cancer Cells. *Science,* 123, 309-314.

WATERHOUSE, J., BUCKLEY, P., EDWARDS, B. & REILLY, T. 2003. Measurement of, and some reasons for, differences in eating habits between night and day workers. *Chronobiology International,* 20, 1075-1092.

WHITMORE, D., S. FOULKES, N. & SASSONE-CORSI, P. 2000. Light acts directly on organs and cells in culture to set the vertebrate circadian clock. *Nature,* 404, 87-91.

WYNN, T. A., CHAWLA, A. & POLLARD, J. W. 2013. Macrophage biology in development, homeostasis and disease. *Nature,* 496, 445-55.

WYSE, C. A., CELIS MORALES, C. A., GRAHAM, N., FAN, Y., WARD, J., CURTIS, A. M., MACKAY, D., SMITH, D. J., BAILEY, M. E., BIELLO, S., GILL, J. M. & PELL, J. P. 2017. Adverse metabolic and mental health outcomes associated with shiftwork in a population-based study of 277,168 workers in UK biobank. *Ann Med,* 1-10.

YAN, J., LI, S. & LI, S. 2014. The role of the liver in sepsis. *International reviews of immunology,* 33, 498-510.

YOUM, Y. H., NGUYEN, K. Y., GRANT, R. W., GOLDBERG, E. L., BODOGAI, M., KIM, D., D'AGOSTINO, D., PLANAVSKY, N., LUPFER, C., KANNEGANTI, T. D., KANG, S., HORVATH, T. L., FAHMY, T. M., CRAWFORD, P. A., BIRAGYN, A., ALNEMRI, E. & DIXIT, V. D. 2015. The ketone metabolite beta-hydroxybutyrate blocks NLRP3 inflammasome-mediated inflammatory disease. *Nat Med,* 21, 263-9.

YOUNG, M. R. I. & MATTHEWS, J. P. 1995. Circadian rhythmometry of serum interleukin-2, interleukin-10, tumor necrosis factor-α, and granulocyte-

macrophage colony-stimulating factor in men. *Chronobiology International,* 12**,** 19-27.

ZHANG, R., LAHENS, N. F., BALLANCE, H. I., HUGHES, M. E. & HOGENESCH, J. B. 2014. A circadian gene expression atlas in mammals: implications for biology and medicine. *Proceedings of the National Academy of Sciences,* 111**,** 16219-16224.

ZHONG, Z., WEN, Z. & DARNELL, J. E. 1994. Stat3: a STAT family member activated by tyrosine phosphorylation in response to epidermal growth factor and interleukin-6. *Science*.

ZHU, J., XU, Z., CHEN, X., ZHOU, S., ZHANG, W., CHI, Y., LI, W., SONG, X., LIU, F. & SU, C. 2014. Parasitic antigens alter macrophage polarization during Schistosoma japonicum infection in mice. *Parasites & vectors,* 7**,** 122.

7 Appendix

CodeSet Clock1	
Gene	**Accession #**
BMAL1	NM_007489.3
BMAL2	NM_001289679.1
Casp-11	NM_007609.2
CD36	NM_007643.3
CLOCK	NM_001289826.1
CRY1	NM_007771.3
CRY2	NM_001113333.1
CXCL2	NM_009140.2
DBP	NM_016974.3
DECR1	NM_026172.3
Fasn	NM_007988.3
FPGS	NM_010236.2
G6pc	NM_008061.3
HMBS	NM_013551.2
HPRT1	NM_013556.2
IL10	NM_010548.1
IL1b	NM_008361.3
IL6	NM_031168.1
Lipc	NM_008280.2
Nampt	NM_021524.1
NPAS2	NM_008719.2
NR1D1	NM_145434.4
NR1D2	NM_011584.3
PER1	NM_011065.4
PER2	NM_011066.3
PER3	NM_011067.2
PPARg	NM_011146.1
PPIB	NM_011149.2
RORalpha	NM_013646.1
RORgamma	NM_011281.2
Sirt1	NM_019812.2
TK-1	NM_009387.1
TNF	NM_013693.1
UCP2	NM_011671.4

CodeSet Clock2	
Gene	**Accession #**
Apcs	NM_011318.2:148
Arntl	NM_007489.3:1519
Casp4	NM_007609.2:408
Cd36	NM_007643.3:1520
Cdk5r1	NM_009871.2:3280
Clock	NM_001289826.1:1284
Cry1	NM_007771.3:945
Cry2	NM_001113333.1:226
Cxcl2	NM_009140.2:765
Dbp	NM_016974.3:975
Decr1	NM_026172.3:716
Eif4a2	NM_013506.2:1655
Elf1	NM_007920.3:620
Fasn	NM_007988.3:6560
G6pc	NM_008061.3:150
Hk2	NM_013820.3:480
Hmbs	NM_013551.2:464
Hprt	NM_013556.2:30
Ifng	NM_008337.1:95
Il10	NM_010548.1:985
Il1b	NM_008361.3:1120
Il6	NM_031168.1:40
Lipc	NM_008280.2:630
Nampt	NM_021524.1:1205
Npas2	NM_008719.2:770
Nr1d1	NM_145434.4:2001
Nr1d2	NM_011584.3:190
Per1	NM_011065.4:4055
Per2	NM_011066.3:5650
Pparg	NM_011146.1:1060
Ppib	NM_011149.2:103
S100a1	NM_011309.3:170
Sirt1	NM_019812.2:843
Slc2a2	NM_031197.2:690
Tk1	NM_009387.2:172
Tnf	NM_013693.1:1135
Tnfsf15	NM_177371.3:4695
Ucp2	NM_011671.4:950

Appendix 1: NanoString CodeSets

Gene names and associated accession numbers of genes that were included in CodeSet Clock 1 or 2 as indicated. Genes that served as housekeepers for normalization purposes are shown in red.

Oxidative Stress			
Symbol	Refseq	Symbol	Refseq
Alb	NM_009654	Nox1	NM_172203
Als2	NM_028717	Nox4	NM_015760
Aox1	NM_009676	Noxa1	NM_172204
Apc	NM_007462	Noxo1	NM_027988
Apoe	NM_009696	Nqo1	NM_008706
Atr	NM_019864	Park7	NM_020569
Cat	NM_009804	Prdx1	NM_011034
Ccl5	NM_013653	Prdx2	NM_011563
Ccs	NM_016892	Prdx3	NM_007452
Ctsb	NM_007798	Prdx4	NM_016764
Cyba	NM_007806	Prdx5	NM_012021
Cygb	NM_030206	Prdx6	NM_007453
Dnm2	NM_001039520	Prnp	NM_011170
Duox1	NM_001099297	Psmb5	NM_011186
Ehd2	NM_153068	Ptgs1	NM_008969
Epx	NM_007946	Ptgs2	NM_011198
Ercc2	NM_007949	Rag2	NM_009020
Ercc6	NM_001081221	Recql4	NM_058214
Fancc	NM_007985	Scd1	NM_009127
Fmo2	NM_018881	Serpinb1b	NM_173052
Fth1	NM_010239	Slc38a1	NM_134086
Gclc	NM_010295	Sod1	NM_011434
Gclm	NM_008129	Sod2	NM_013671
Gpx1	NM_008160	Sod3	NM_011435
Gpx2	NM_030677	Sqstm1	NM_011018
Gpx3	NM_008161	Srxn1	NM_029688
Gpx4	NM_008162	Tpo	NM_009417
Gpx5	NM_010343	Txn1	NM_011660
Gpx6	NM_145451	Txnip	NM_023719
Gpx7	NM_024198	Txnrd1	NM_015762
Gsr	NM_010344	Txnrd2	NM_013711
Gss	NM_008180	Txnrd3	NM_153162
Gstk1	NM_029555	Ucp2	NM_011671
Gstp1	NM_013541	Ucp3	NM_009464
Hmox1	NM_010442	Vim	NM_011701
Hspa1a	NM_010479	Xpa	NM_011728
Idh1	NM_010497	Actb	NM_007393
Ift172	NM_026298	B2m	NM_009735
Il19	NM_001009940	Gapdh	NM_008084
Il22	NM_016971	Gusb	NM_010368
Krt1	NM_008473	Hsp90ab1	NM_008302
Lpo	NM_080420	MGDC	SA_00106
Mb	NM_013593	RTC	SA_00104
Mpo	NM_010824	RTC	SA_00104
Ncf1	NM_010876	RTC	SA_00104
Ncf2	NM_010877	PPC	SA_00103
Ngb	NM_022414	PPC	SA_00103
Nos2	NM_010927	PPC	SA_00103

Phagocytosis			
Symbol	Refseq	Symbol	Refseq
Adipoq	NM_009605	Pecam1	NM_008816
Ager	NM_007425	Pik3cb	NM_029094
Anxa1	NM_010730	Pip5k1a	NM_008846
Axl	NM_009465	Pla2g4a	NM_008869
C3	NM_009778	Pla2g5	NM_011110
Calr	NM_007591	Pld1	NM_008875
Cd14	NM_009841	Pld2	NM_008876
Cd36	NM_007643	Prkce	NM_011104
Cd44	NM_009851	Pros1	NM_011173
Cd47	NM_010581	Pten	NM_008960
Ceacam3	NM_054059	Rab5a	NM_025887
Clec7a	NM_020008	Rab7	NM_009005
Clic4	NM_013885	Rac1	NM_009007
Cnn2	NM_007725	Rac2	NM_009008
Colec12	NM_130449	Rala	NM_019491
Crk	NM_133656	Ralb	NM_022327
Crp	NM_007768	Rapgef3	NM_144850
Csf1	NM_007778	Rhoa	NM_016802
Csf2	NM_009969	Scarb1	NM_016741
Csk	NM_007783	Serpine1	NM_008871
Cyp2s1	NM_028775	Sftpd	NM_009160
Dock1	NM_001033420	Siglec1	NM_011426
Dock2	NM_033374	Sirpb1a	NM_001002898
Elmo1	NM_198093	Stab2	NM_138673
Fas	NM_007987	Stx18	NM_026959
Fcer1g	NM_010185	Syk	NM_011518
Fcgr1	NM_010186	Tgm2	NM_009373
Fcgr2b	NM_010187	Ticam1	NM_174989
Fcgr3	NM_010188	Tlr3	NM_126166
Fyn	NM_008054	Tlr9	NM_031178
Gulp1	NM_028450	Tnf	NM_013693
Ifng	NM_008337	Tnfsf11	NM_011613
Il1rl1	NM_010743	Vamp7	NM_011515
Iqsec1	NM_001134383	Vav1	NM_011691
Itgam	NM_008401	Was	NM_009515
Itgav	NM_008402	Wnt5a	NM_009524
Itgb2	NM_008404	Actb	NM_007393
Lyn	NM_010747	B2m	NM_009735
Mapk14	NM_011951	Gapdh	NM_008084
Marco	NM_010766	Gusb	NM_010368
Mbl2	NM_010776	Hsp90ab1	NM_008302
Mcoln3	NM_134160	MGDC	SA_00106
Mertk	NM_008587	RTC	SA_00104
Mfge8	NM_008594	RTC	SA_00104
Mif	NM_010798	RTC	SA_00104
Msn	NM_010833	PPC	SA_00103
Myd88	NM_010851	PPC	SA_00103
Nod1	NM_172729	PPC	SA_00103

Appendix 2: RT Profiler Gene Sets

Gene names and accession number of genes that were part of the RT profiler plate "mouse oxidative stress" or "mouse phagocytosis". Housekeeping genes that were used for normalization are marked in red.